# PRODUCTION AND CHARACTERIZATION OF BORON BASED ADDITIVES AND THE EFFECT OF FLAME RETARDANT ADDITIVES ON PET BASED COMPOSITES

A THESIS SUBMITTED TO
THE GRADUATE SCHOOL OF NATURAL AND APPLIED SCIENCES
OF
MIDDLE EAST TECHNICAL UNIVERSITY

BY

MERT KILINÇ

IN PARTIAL FULFILLMENT OF THE REQUIREMENTS
FOR
THE DEGREE OF DOCTOR OF PHILOSOPHY
IN
CHEMICAL ENGINEERING

JUNE 2009

Approval of the thesis:

## "PRODUCTION AND CHARACTERIZATION OF BORON BASED ADDITIVES AND THE EFFECT OF FLAME RETARDANT ADDITIVES ON PET BASED COMPOSITES"

submitted by **MERT KILINÇ** in partial fulfillment of the requirements for the degree of **Doctor of Philosophy in Chemical Engineering Department, Middle East Technical University** by,

Prof. Dr. Canan Özgen
Dean, Graduate School of **Natural and Applied Sciences**

Prof. Dr. Gürkan Karakaş
Head of Department, **Chemical Engineering**

Assoc. Prof. Dr. Göknur Bayram
Supervisor, **Chemical Engineering Dept., METU**

**Examining Committee Members:**

Prof. Dr. Ülkü Yılmazer
Chemical Engineering Dept., METU

Assoc. Prof. Dr. Göknur Bayram
Chemical Engineering Dept., METU

Prof. Dr. Erdoğan Alper
Chemical Engineering Dept., Hacettepe University

Prof. Dr. İnci Eroğlu
Chemical Engineering Dept., METU

Prof. Dr. Leyla Aras
Chemistry Dept., METU

**Date: 15.06.2009**

**I hereby declare that all information in this document has been obtained and presented in accordance with academic rules and ethical conduct. I also declare that, as required by these rules and conduct, I have fully cited and referenced all material and results that are not original to this work.**

Name, Last Name : Mert Kılınç

Signature :

# ABSTRACT

## PRODUCTION AND CHARACTERIZATION OF BORON-BASED ADDITIVES AND THE EFFECT OF FLAME RETARDANT ADDITIVES ON PET-BASED COMPOSITES

Kılınç, Mert
Ph.D, Department of Chemical Engineering
Supervisor: Assoc. Prof. Dr. Göknur Bayram

June 2009, 292 pages

For the aim of production of poly(ethylene terephthalate), PET based flame retardant composites; boron based flame retardant additives, 3.5 mole hydrated zinc borate and boron phosphate were synthesized. Zinc borate was synthesized with the reaction of boric acid and zinc oxide in both laboratory and pilot scale reactors. Effects of reaction parameters on kinetics of reaction and final product particle size were evaluated. Boron phosphate was synthesized via dry, wet and microwave methods. In addition to the synthesized flame retardant additives, several non-halogenated flame retardant additives, which were commercially available, were also used. Composites were prepared using twin screw extruder and molded by injection molding, followed by characterization in terms of flame retardancy behavior, mechanical and thermal properties, and morphologies. Based on the results of first stage experiments, aiming to determine effective additives, different amounts and combinations of triphenyl phosphate, triphenyl phosphine oxide, zinc borate and microwave produced boron phosphate were chosen and used in PET matrix. Flame retardancy of the composites were determined by conducting horizontal burning rate and limiting oxygen index (LOI) tests. Smoke emissions during fire were also measured. According to the LOI test results, LOI of neat PET was determined as 21%, and with the addition of 5% boron phosphate and 5% triphenyl phosphate together, LOI was increased up to 36%.

The smoke density analysis results implied that, boron phosphate was a successful smoke suppressant for PET matrix. In addition to flammability properties, tensile and impact properties of the composites were also improved with flame retardant additives and expecially with the addition of triphenyl phosphate.

Keywords: Borates, reaction engineering, poly(ethylene terephthalate), extrusion, flame retardants, limiting oxygen index, mechanical properties

# ÖZ

## “BORON BAZLI KATKI MADDELERİNİN ÜRETİMİ, KARAKTERİZASYONU VE ALEV GECİKTİRİCİ KATKI MADDELERİNİN PET BAZLI KOMPOZİTLERDEKİ ETKİLERİ”

Kılınç, Mert
Doktora, Kimya Mühendisliği Bölümü
Tez Yöneticisi: Doç. Dr. Göknur Bayram

Haziran 2009, 292 sayfa

Poli(etilen tereftalat), PET bazlı yanması geciktirilmiş kompozitlerin üretilmesi maksadıyla, yanmayı geciktirici bor esaslı katkı maddeleri, 3.5 mol kristal sulu çinko borat ve bor fosfat sentezlenmişlerdir. Çinko borat laboratuvar ölçekte ve pilot ölçekte borik asit ve çinko oksidin reaksiyonu ile sulu ortamda sentezlenmiştir. Değişik reaksiyon parametrelerinin reaksiyon kinetiğine ve son ürünün ortalama parçacık boyutuna etkileri incelenmiştir. Bor fosfat kuru, ıslak ve mikrodalga olmak üzere üç farklı yöntemle sentezlenmiştir. Sentezlenen bu iki alev geciktirici yanında, piyasada bulunan, halojen içermeyen alev geciktiriciler de kullanılmıştır. Kompozitler çift vidalı ekstrüder kullanılarak üretilmiş ve enjeksiyonlu kalıplama ile kalıplanmışlardır. Kalıplama işleminin ardından kompozitler yanma davranışları açısından, mekanik ve termal özellikleri, ve morfolojileri açısından karakterize edilmişlerdir. Uygun alev geciktiricilerin belirlenmesini amaçlayan ilk aşama denemelerin sonuçları esas alınarak değişik miktarlarda ve değişik kombinasyonlarda trifenilfosfat, trifenilfosfin oksit, 3.5 mol kristal sulu çinko borat ve mikrodalga yöntemi ile sentezlenmiş bor fosfat alev geciktirici olarak seçilmiş ve PET matrikste kullanılmıştır. Kompozitlerin yanma özellikleri yatay yanma hızı testi ve sınırlayıcı oksijen indeksi testleri ile belirlenmişlerdir. Malzemelerin yanma anında açığa çıkardıkları dumanın yoğunluğu da ölçülmüştür. Sınırlayıcı oksijen indeksi test sonuçlarına göre, saf PET’ın sınırlayıcı oksijen indeks değeri %21 olarak belirlenmiş, matriks malzemesine %5 bor fosfat ve %5 trifenil fosfat ilavesi ile bu değer %36'ya yükselmiştir. Duman yoğunluğu analizleri sonuçları, bor fosfatın PET matriks için başarılı bir duman bastırıcı olduğunu göstermiştir. PET matriksin yanmasının gecikmesinin yanında çekme dayanımı ve darbe dayanımı özellikleri de alev geciktirici katkı maddeleri ilavesi ve de özellikle trifenil fosfat ilavesi ile artış göstermiştir.

Anahtar Kelimeler: Boratlar, reaksiyon mühendisliği, poli(etilen tereftalat), ekstrüzyon, alev geciktiriciler, sınırlayıcı oksijen indeksi, mekanik özellikler

To Mum, and my sister Burçak...

“By three methods we may learn wisdom: First, by reflection, which is noblest; second, by imitation, which is easiest; and third by experience, which is the bitterest.”

**Confucius**

# ACKNOWLEDGEMENTS

I would like to express my deepest gratitude to my thesis supervisor Assoc. Prof. Dr. Göknur Bayram for advising and encouraging me, being such a dedicated, ardent, and causative individual throughout my thesis. Above all and the most needed, she provided me unflinching encouragement and support in various ways. I appreciate her valuable guidance, encouraging advice and discussions.

I would sincerely like to thank Prof. Dr. Ülkü Yılmazer and Prof. Dr. Leyla Aras for so open-heartedly sharing their knowledge, contributions and experiences with me, Prof. Dr. İnci Eroğlu, Prof. Dr. Saim Özkar, and especially Dr. Gaye Çakal, for their contributions in the synthesis and characterization of zinc borate. I would appreciate to Assoc. Prof. Dr. Ayşen Yılmaz and Prof. Dr Jale Hacaloğlu for opening their laboratories for me to perform boron phosphate synthesis and performing Py-MS analysis.

I gratefully thank to Semih Seyyidoğlu for boron phosphate synthesis and characterization, Mihrican Açıkgöz from Chemical Engineering Department for the DSC and TGA analysis, Kerime Günay from Chemical Engineering Department for the chemical analysis of zinc borate, Cengiz Tan from Metallurgical and Materials Engineering Department for the SEM analysis, Yusuf Nur for the Py-MS analysis, Osman Yassıtaş from the Chemistry Department for the molecular weight determination analysis and Hande Durgun and Dr. Göktuğ Günkaya from Chemical Engineering and Metallurgical and Materials Engineering Department of Anadolu University for the SEM analysis. Without the support of the METU Chemical Engineering Department's machine shop staff, this work could not be done. Many thanks go in particular to Dr. Cevdet Öztin.

I would like to also thank to the National Boron Research Institute (BOREN) and The Scientific and Technological Research Council of Turkey (TUBITAK) for the financial support during my thesis for my research.

The friendly and helpful contributions of the polymer group encouraged me during my studies. The polymer group including Assist. Prof. Dr. Güralp Özkoç, Dr. Işıl Işık Gülsaç, Sertan Yeşil, Dr. Özcan Köysüren, Damla Eroğlu, Canan Yeniova, Tijen Seyidoğlu, İlknur Çakar, Fatma Işık, Saniye Yayla, Ceren Çamlıyurt Kurtuluş deserve my gratitude. Thanks folks. I convey special acknowledgement to Dr. Belma Soydaş, Dr. Funda Erol, Güneş Ünal.

This thesis could not be done without the patience, support and understanding of Ebru Acar. I express my sincerest thanks to her for support, patience and help in every single step of this study.

Words fail me to express my appreciation to my soul mate and love Canan Gücüyener whose dedication, love and persistent confidence in me, has helped me incredibly. I owe her being unselfishly let her intelligence, energy, cheerfulness and help collide with mine. This work could not be completed without her support in the thesis writing period and so on.

Where would I be without my family? Finally, I want to thank my family Tülay Ege, Burçak Kılınç, Gülnur Toker, and Cihat Toker for their support for the completion of my education and every part of my life. It would not have been possible without their love and support to complete this study.

# TABLE OF CONTENTS

CHAPTER

APPENDICES

# LIST OF TABLES

**TABLES**

# LIST OF FIGURES

**FIGURES**

# CHAPTER 1

# INTRODUCTION

Having both mineral and synthetic forms, metal borates in which boron is bond only to oxygen are numerous and find widespread industrial use. Many synthetic metal borates resemble minerals in structure, containing isolated polyborate anions or complex polyborate rings, chains, sheets, or networks. Metal borates can be divided into two categories, hydrated and anhydrous. Well known hydrated borates, which account for the majority of known boron-containing minerals and synthetic borates consumed by industry, have structures containing B-OH groups (hydroxyl hydrated borates) and may also, contain hydrated water. Zinc borate is also a member of hydrated metal borates. There are several works and evidence for the existence of at least eight unique crystalline hydrated zinc borates. These have compositions; $4ZnO{\cdot}B_2O_3{\cdot}H_2O$ [1], $ZnO{\cdot}B_2O_3{\cdot}1.12H_2O$ [2], $ZnO{\cdot}B_2O_3{\cdot}2H_2O$ [2], $6ZnO{\cdot}5B_2O_3{\cdot}3H_2O$) [3], $2ZnO{\cdot}3B_2O_3{\cdot}7H_2O$ [4], $2ZnO{\cdot}3B_2O_3{\cdot}3H_2O$, $3ZnO{\cdot}5B_2O_3.14H_2O$ [5], and $ZnO{\cdot}5B_2O_3{\cdot}4.5H_2O$ [3], have a range of $B_2O_3$:ZnO mole ratios from 0.25 to 5.0.

Zinc borate is primarily used as a multifunctional polymer additive and as a preservative in wood composites. As a polymer additive, it serves as a fire retardant synergist, char promoter, ant drip agent, smoke and afterglow suppressant, and modifier of electrical and optical properties. In many fireproofing applications, zinc borate has greater flame retardancy than other borates used alone. The most commonly used ones are $3ZnO{\cdot}2B_2O_3{\cdot}3.5H_2O$, $2ZnO{\cdot}3B_2O_3{\cdot}3H_2O$, and anhydrous $2ZnO{\cdot}3B_2O_3$. The zinc borate does not affect the color of plastics, and is only slowly affected by high temperatures. When heated, zinc borate promotes the formation of char and inhibits the release of combustible material [6]. The addition of aluminum trihydrate to the zinc borate forms a synergistic mixture more effective than either material alone, particularly in reducing the fire's smoke. Previous studies have demonstrated that they are commonly used as flame-retardant filler in polyvinyl chloride (PVC), polypropylene (PP), polyamides, epoxy resins, etc. Moreover, their action as smoke suppressants, afterglow suppressants, corrosion inhibitors, and synergistic agent has been pointed out [7-11].

Various attempts were performed to produce 3.5 hydrated zinc borate. Nies et al. [12] investigated different methods to obtain zinc borate. In the first example, a solution was prepared containing borax pentahydrate, boric acid and water. A second solution with zinc oxide, sulfuric acid, and water was also provided. A seed of zinc borate with chemical formula of $2ZnO\cdot3B_2O_3\cdot9H_2O$ was blended. The mixtures were stirred and filtrated. The formulas of the zinc borates obtained were $2.06ZnO\cdot3B_2O_3.3.59H_2O$ and $2.07ZnO\cdot3B_2O_3\cdot3.71H_2O$, respectively. Shete et al. [13] presented a comprehensive set of experimental results on the influence of process variables on the size distribution of a product made in a batch heterogeneous reaction. In this work, the effect of speed of agitation, mean initial particle size of zinc oxide, temperature, boric acid concentration in the solution on conversion of zinc oxide and mean particle size of zinc borate were investigated. The controlling mechanism, mixing effects and reaction kinetics were also studied. It is proposed that the zinc borate formation reaction takes place on the surface of ZnO with the diffusion of boric acid to the surface of ZnO. Eltepe et al. [14] examined the temperature and time effects on zinc borate synthesis. It was concluded that a powerful mixer, good temperature control and preventing the vapor evaporation during the reaction were essential for a successful synthesis reaction.

Zinc borate ($2ZnO\cdot3B_2O_3\cdot3.5H_2O$) in general is produced with the reaction of zinc oxide and boric acid. Boric acid is dissolved in water and reaction is carried out at 85°C. After complete dissolution of boric acid, zinc oxide and seed crystals of $2ZnO\cdot3B_2O_3\cdot3.5H_2O$ are added to this solution at a certain stoichiometric ratio. The reaction continues for a while by mixing, and the zinc borate formed is filtered, washed with hot water-ethanol mixture in order to get rid of residual boric acid, dried, and ground [15]. Schubert et al. [16] found out that $2ZnO\cdot3B_2O_3\cdot3.5H_2O$ was actually $Zn[B_3O_4(OH)_3]$ ($ZnO\cdot3B_2O_3\cdot3H_2O$ written in oxide form). The structure of $Zn[B_3O_4(OH)_3]$ was determined for the first time by single-crystal X-ray diffraction and

H magic angle spinning (MAS) NMR, revealing it to be a complex network consisting of infinite polytriborate chains crosslinked by coordination with zinc and further integrated by hydrogen bonding.

Almost all works in the published literature dealt with the successful synthesis of 3.5 hydrated zinc borate and characterization of the final product. Practically very few work has been published, that could describe the effects of important reaction parameters on the synthesis [13-15].

The aim of the first part of this study is to present a set of experimental results on the influence of process variables on both the zinc borate synthesis reaction and final product properties in terms of batch type laboratory scale production followed by scale-up process, batch type pilot scale production of $2ZnO \cdot 3B_2O_3 \cdot 3.5H_2O$. Thus, the effects of stirring rate and presence of baffle in the reactor, seed amount used in the reaction, zinc oxide average particle size, zinc oxide purity, $B_2O_3$:ZnO mol ratio on the reaction and final product were determined at both laboratory and pilot scale reactor capacities. Results of the kinetic parameters on zinc borate synthesis reaction was tried to be fit to the logistic model in order to determine a kinetic model for the 3.5 hydrated zinc borate synthesis.

In addition to zinc borate synthesis, another boron based flame retardant additive, boron phosphate was in the scope of this study. Boron phosphate was synthesized with three different techniques; dry, wet, and microwave techniques. Boron phosphate is an inorganic material which has a melting point above 1000°C, and it can be used with polyester based polymers as flame retardant.

After synthesis of the two flame retardant additives and their characterization, they were combined with other commercially available flame retardant additives, which were suitable for the polyesters, and flame retardant composites were produced.

Polymers are widely used in many applications. However, most polymers, like the majority of other organic compounds, will burn readily in air or oxygen. The flammability of polymers is a serious issue and severely limits their applications [17, 18]. Recent fire-safety concerns put even more stringent requirements for the materials used in enclosed and inescapable areas, such as electronic enclosures, high-rise buildings, submarines, ships and aircraft cabins [19]. Light-weight, high-performance polymeric materials offer many advantages in these applications over conventional metal and ceramic materials, but they greatly increase the fire risk because of their flammability and possible release of toxic by-products.

In the plastic flame retardant additive field, the most common active flame retardant chemicals involve the use of halogen compounds, phosphorus, or additives that produce water to extinguish the flames. In many cases "synergists" are used to enhance the flame retardant capabilities of these primary flame retardant species. Examples of these flame retardant enhancers are antimony, zinc and other metal salts [20, 21].

Halogenated flame retardant additives lost popularity due to the strict governmental regulations to forbid usage as the toxic gases evolved during the fire (like HCl evolution during the burning of PVC) caused by the halogens.

During burning, when the material is exposed to a sufficiently large heat flux radiated from a fire, the polymer matrix and organic fibers will thermally decompose to yield volatile gases, solid carbonaceous char and airborne soot particles. The volatiles consist of a variety of vapors and gases, both flammable (e.g. carbon monoxide, methane, and low molecular organics) and non-flammable (carbon dioxide, water) [22]. These diffuse from the decomposing composite into the flame zone, where the flammable volatiles react with oxygen in the fire atmosphere leading to the formation of the final combustion products (usually carbon dioxide, water, smoke particles and a small amount of carbon monoxide) accompanied by the liberation of heat.

Phosphorus acts as a flame retardant in the gas and/or condensed phase, depending on the chemical nature and thermal stability of the host polymer. The gas phase mechanism dominates in most thermoplastics and non-oxygenated thermoset polymers. This mechanism involves the release of phosphorus radicals from the polymer at elevated temperature; although to be effective, the volatilization process must occur below 350-400°C or otherwise the polymer itself will decompose [23]. A variety of phosphorus radicals can be released into the flame, depending on the temperature and composition of the phosphorus-containing flame retardant. For example, the decomposition of triphenylphosphate [$(C_6H_5)_3PO$] results in the release of $PO^\bullet$ radicals and smaller amounts of $P^\bullet$, $HPO_2$ and $P_2$ volatile compounds [24]. $PO^\bullet$ has a strong affinity to $H^\bullet$ and $OH^\bullet$ radicals. The HPO produced in this reaction sequence is inherently less reactive than the $H^\bullet$ and $OH^\bullet$ radicals it replaces, and thereby flaming combustion is suppressed.

It has been also reported that triphenyl phosphate generates phosphoric acid during thermal degradation and reaction takes place between phosphoric acid to yield pyrophosphoric acid, which acts as a heat transfer barrier in the condensed phase [25, 26].

When phosphorus compounds are used in oxygenated and hydroxylated organic polymers they also act as a flame retardant in the condensed phase. Phosphorus in these polymer systems promotes the formation of char that reduces the amount of flammable volatiles released into the flame. Phosphorus can also accelerate heat loss in some thermoplastics by promoting melting and dripping. As mentioned, the efficacy of phosphorus as a flame retardant is strongly dependent on the chemical nature of the polymer. As a rule, the flame retardant efficiency of phosphorus increases with the oxygen content of the polymer. The effect of phosphorus content on the flame retardant behavior of polymers has been extensively studied, and it is often found that flammability resistance usually improves with increasing phosphorus content.

During burning, the oxygen released from the structure could combine with the carbon monoxide and would form carbon dioxide. Unlike carbon monoxide, which has black, sooty smoke, carbon dioxide has colorless smoke.

While the boron containing flame retardant additives have a smoke suppressant effect, phosphate based flame retardants that have aromatic groups in the structure, due to high carbon content produce more smoke.

In the second part of the study, it is desired to produce flame retardant PET composites with the help of non-halogenated flame retardant additives. Two different sets of flame retardant composites were formulated. In the first stage, flame retardant additives; 3.5 hydrated zinc borate, three different boron phosphates, which were produced in wet, dry and microwave method, anhydrous borax, complex of metal oxide powder (Smokebloc AZ-12), Cloisite 30B organically modified clay, phosphorus based intumescent flame retardant additive (Reogard 2000), calcium sulfate dihydride, triphenyl phosphate, triphenyl phosphine oxide, were added to PET at 5 weight percent except the anhydrous borax. Due to process limitations, anhydrous borax was added to the matrix at 10 weight percent. Then, the composites were characterized in terms of flammability, mechanical and thermal properties. Starting from the flammability and mechanical test results of the first stage, second stage flame retardant composites were formulated by choosing the four successful flame retardant additives of the first stage in terms of increase in limiting oxygen index (LOI) test results, tensile and mechanical properties characterization, and they were compounded in different amounts and then characterized. The PET based composites were aimed to be not only flame retardant, but also to have high mechanical properties, transparency and low UV transmittance to be used in various fields of applications.

# CHAPTER 2

# BACKGROUND

## 2.1 General Information about Boron

### 2.1.1 Boron in the World

Boron was discovered by Joseph Gay-Lussac and Louis Thénard, French chemists, and independently by Sir Humphry Davy, a British chemist, in 1808. Boron is a hard, brittle semi-metallic element [27]. Boron has a chemical symbol of B and atomic number of 5. Its atomic weight is 10.81. Melting point and boiling point of boron are 2074°C and 4000°C, respectively.

### 2.1.2 Boron Minerals

Boron does not occur in nature as a free element, crude borax occurs in nature as a mineral with associated clay and other impurities. There are over 200 naturally occurring boron containing minerals but the most commercially important and frequently used minerals (salts, known as borates) are tincal, colemanite, ulexite and kernite. These ores can be refined into a pure chemical compounds. The ones that have the commercial importance are [28]; boric acid ($H_3BO_3$), anhydrous boric acid ($B_2O_3$), anhydrous borax ($Na_2B_4O_7$), borax pentahydrate ($Na_2B_4O_7 \cdot 10H_2O$), borax decahydrate ($Na_2B_4O_7 \cdot 5H_2O$), sodium perborate ($Na_2B_4O_7 \cdot 5H_2O$).

Some commercially important boron minerals are [28]; tincal ($Na_2B_4O_7 \cdot 10H_2O$), kernite ($Na_2B_4O_7 \cdot 4H_2O$), colemanite ($Ca_2B_6O_{11} \cdot 5H_2O$), ulexite ($NaCaB_5O_9 \cdot 8H_2O$), datolite ($Ca_2B_2O_5 \cdot Si_2O_5 \cdot H_2O$), hydroboracite ($CaMgB_6O_{11} \cdot 6H_2O$).

Turkey is the largest producer of boron ore in the world. Important boron minerals of Turkey's are tincal, colemanite and ulexite. The important factor for industrial application of boron minerals are their $B_2O_3$ content. Boron minerals can be used in some fields in the industry as crude minerals. In general, their applications after refining and end-products are wider than crude ones. Borates find use in different field of applications, however the principal markets are: Agriculture, detergents and soaps, flame retardants, glass, glazes, frits, enamels and insulation.

### 2.1.3 Metal Borates

It is possible to produce borate salts or complexes of virtually every metal. For most metals, a series of hydrated anhydrous compounds may be obtained by varying the starting materials and/or reaction conditions. Some have achieved commercial importance. In general, hydrated borates of heavy metals are prepared by mixing aqueous solutions or suspensions of the metal oxides, sulfates, or halides and boric acid or alkali metal borates such as borax. The precipitates formed from basic solutions are often sparingly-soluble amorphous solids having variable compositions. Crystalline products are generally obtained from slightly acidic solutions. Anhydrous metal borates may be prepared by heating the hydrated salts to 300-500°C, or by direct fusion of the metal oxide with boric acid or $B_2O_3$. Many binary or tertiary anhydrous systems containing $B_2O_3$ form vitreous phases over certain ranges of composition, like anhydrous borax, borax pentahydrate, etc. [29].

## 2.2 Zinc Borate

### 2.2.1 Zinc Borate Properties and Usage

Zinc borate is a boron-based inorganic fire retardant with a chemical composition of $xZnO \cdot yB_2O_3 \cdot zH_2O$. The most commonly used grade has following structure $2ZnO \cdot 3B_2O_3 \cdot 3.5H_2O$. There are different types of zinc borate; $ZnO \cdot B_2O_3 \cdot H_2O$,

$ZnO \cdot 3B_2O_3 \cdot 7\text{-}7.5H_2O$, $2ZnO \cdot 3B_2O_3 \cdot 9H_2O$, $3ZnO \cdot 2B_2O_3 \cdot 5H_2O$, $ZnO \cdot B_2O_3 \cdot 2H_2O$, $4ZnO \cdot B_2O_3 \cdot H_2O$ and $2ZnO \cdot 3B_2O_3$.

Zinc borate, $2ZnO \cdot 3B_2O_3 \cdot 7H_2O$, is formed when borax is added to aqueous solutions of soluble zinc salts at temperatures below about 70°C. An x-ray structure determination has indicated that this compound is orthorhombic and has a zinc triborate monohydrate structure, $Zn[B_3O_3(OH)_5] \cdot H_2O$ [30]. Zinc borates $2ZnO \cdot 3B_2O_3 \cdot 7H_2O$ and $ZnO \cdot B_2O_3 \cdot 2H_2O$ lose water of hydration when heated from 130 to 250°C [31]. Zinc borate can be used as a fire retardant in PVC, polyolefins, elastomers, polyamides, epoxy resins. In halogen-containing systems, it is also used in conjunction with antimony oxide, while in halogen-free systems; it is normally used in conjunction with alumina trihydrate, magnesium hydroxide, or red phosphorus [31] and in some particular application zinc borate can be used alone.

Zinc borate acts through [29]:

- zinc halide or zinc oxyhalide that accelerate the decomposition of halogen sources and promote char formation.
- by the $B_2O_3$ moiety released, a low melting glass, that can stabilize the char. $B_2O_3$ released can also promote the formation of ceramic formation in systems containing ATH or magnesium hydroxide.
- the endothermic, stepwise release of water that can promote the formation of foamy char.

Table 2.1 shows the usage of zinc borate in different polymer matrices and the benefits of its usage as a flame retardant additive. Zinc borate is of special commercial importance. Its water of hydration is retained up to about 290°C.

**Table 2.1** Mechanisms of action of zinc borate on different polymer matrices

| **Polymer** | **Benefits** |
|---|---|
| PVC | Smoke suppressant<br>Flame retardant<br>Synergist of antimony oxide<br>Lowers total fire retardant cost<br>Char promoter |
| Polyolefins | Smoke suppressant/char promoter<br>Afterglow suppressant<br>Improves elongation properties<br>Anti-arcing agent |
| Polyamides | Anti-tracking agent<br>Synergist of halogen sources<br>Afterglow suppressant<br>Used in both halogen containing and halogen-free nylons |
| Elastomers | Smoke suppressant<br>Afterglow suppressant<br>Char promoter<br>Anti-arcing and anti-tracking agent |
| Epoxy resins | Smoke suppressant<br>Char promoter<br>Partial or complete replacement of antimony oxide |

Zinc borate is noted for the following attributes as it is the synergist of halogen sources, can either partially or completely replace antimony oxide, can function as a smoke suppressant, can function as an afterglow suppressant, can promote char formation and prevent dripping in most polymers, can function as an anti-tracking agent and its refractive index is similar to that of most polymers, which results in the retention of considerable translucency and allows the use of low pigment loading.

Recent research at Borax and published literature [10, 16, 19] reported the following newly discovered benefits with the use of zinc borate; as it reduces rate of heat release in PVC and engineering plastics, improves aged elongation property of polyolefins, improves thermal stability of bromine/antimony oxide systems, improves corrosion resistance of processing equipment, promotes ceramic formation with aluminum trihydrate, can function as a flame retardant in certain halogen-free systems.

### 2.2.2 Zinc Borate Manufacturers around the World

Zinc borate is marketed by the United States Borax & Chemical Corp. under the trademark Firebrake ZB, Borogard ZB, and under Greatlakes, Inc. as ZB-467. Its thermal stability makes it attractive as a fire-retardant additive for plastics and rubbers that require high processing temperatures. It is also used as an anticorrosive pigment in coatings. The 2000 selling price for Firebrake ZB ranged from 2.40 $/kg to 2.90 $/kg [32]. Zinc borates are also manufactured by Storey (UK) and Waardals (Norway). Besides these, the general producers are tabulated in Table 2.2.

**Table 2.2** Zinc borate manufacturers and capacities [32]

| Country | Producer | Place | Capacity (ton/year) |
|---|---|---|---|
| China | Hainan Zhongxin Chemical | Haiko | 1000 |
|  | Shanghai Jinghua Chemical | Wujing | --- |
|  | Wuxi Daxhong Chemical | Wuxi | --- |
|  | Zhenjiang Sulphuric Acid Plant | Zhenjiang | 1000 |
| India | C-Tech | Mumbai | --- |
| Norway | Waardals | Skalevik | --- |
| USA | Anzon | Laredo | --- |
|  | U.S Borax | Wilmington | 12 000 |

### 2.2.3 Zinc Borate Market Share

The most zinc borate consuming countries in the world are from the US and West Europe [32]. The consumption of the zinc borate material according to regions are given in Table 2.3.

**Table 2.3** Consumption of zinc borate in 1998 [32]

| Regions | Percent Consumption (%) |
|---|---|
| North America | 45 |
| West Europe | 32 |
| Japan | 13 |
| Asian Countries | 8 |
| Others | 2 |

### 2.2.4 Future Market of Zinc Borate

The increase in the use of synergistic mixture of zinc borate together with aluminum trihydrate has also increased the consumption of zinc borate. The reason for this usage is that the synergistic mixture of these two compounds promotes a non-halogen char formation. All around the world the consumption of halogeneous flame retardants are decreasing and due to governmental and environmental regulations their usage is shifting towards the compounds which are not halogeneous. Also when zinc borate is used with aluminum trihydrate they have a smoke suppressant effect. The price of zinc borate is lower than the bromine based flame retardants which will affect the consumption of zinc borate in favor of this compound.

### 2.3 Synthesis of 3.5 Hydrated Zinc Borate

#### 2.3.1 Synthesis Technique for Zinc Borate

Zinc borate ($2ZnO{\cdot}3B_2O_3{\cdot}3.5H_2O$) in general is produced with the reaction between zinc oxide and boric acid. Boric acid is solved in water between temperatures 80°C and 95°C and zinc oxide and seed crystal of $2ZnO{\cdot}3B_2O_3{\cdot}3.5H_2O$ are added to this solution at a certain stoichiometric ratio related to the reaction equation. Seed crystal amount was determined to the results of previous studies [13, 15]. The reaction continues for a while by mixing and the zinc borate formed is filtered, dried and ground. The synthesis of $2ZnO{\cdot}3B_2O_3{\cdot}3.5H_2O$ was done in accordance with the given reaction in Reaction 2.1.

$$6B(OH)_3\ (aq.) + 2ZnO\ (s) \rightarrow 2ZnO{\cdot}3B_2O_3{\cdot}3.5H_2O\ (s) + 5.5H_2O\ (l) \qquad (2.1)$$

#### 2.3.2 Previous Studies on Zinc Borate Synthesis

Nies et al. [33] investigated different methods to produce zinc borate. In the first example a solution was prepared containing borax pentahydrate, boric acid and water. A second solution with zinc oxide, sulfuric acid, and water was also prepared. A seed of zinc borate with chemical formula of $2ZnO{\cdot}3B_2O_3{\cdot}9H_2O$ was added and then mixtures were stirred and filtrated. The formula of the zinc borate obtained was $2.06ZnO{\cdot}3B_2O_3{\cdot}3.59H_2O$. In the second example, a solution containing borax, boric acid and water was prepared. A second solution containing zinc chloride and water was also prepared. The solutions were mixed and seeded with the crystal ($2.06ZnO{\cdot}3B_2O_3{\cdot}3.59H_2O$) obtained from previous example. The mixture was stirred and filtered. The analysis of the resulting zinc borate was $2.07ZnO{\cdot}3B_2O_3{\cdot}3.71H_2O$. In the third example, boric acid added to water. Previously prepared crystals of $2ZnO{\cdot}3B_2O_3{\cdot}3.5H_2O$ were added as seed. A mixture of boric acid and zinc oxide was then added. The mixture was stirred, filtrated, washed and dried. The formula of the zinc borate obtained was $2.07ZnO{\cdot}3B_2O_3{\cdot}3.66H_2O$.

Dong and Hu [34] studied the synthesis of nanometer sized zinc borate using ethanol supercritical fluid drying technique. To prepare the zinc borate; zinc nitrate was added to borax aqueous solution with stirring. After filtering, and washing with distilled water and ethyl alcohol the precipitate was added to ethyl alcohol and stirred into slurry. The slurry was added to enough absolute ethyl alcohol in an autoclave. The ethanol and the nitrogen along with the remaining alcohol were removed very slowly. It was possible to synthesize nanometer sized zinc borate with an average particle size of 20-50 nm.

Ting et al. [35] produced a new netlike nano zinc borate with a chemical formula of $ZnO.yB_2O_3.zH_2O$ ($y=0.3–0.4$, $z=1.0–1.4$), which was in amorphous phase, was prepared via coordination homogeneous precipitation method. A solution containing zinc oxide, concentrated ammonia and boric acid was prepared. Solution was then stirred at room temperature and separated by centrifuge and rinsed with distilled water to remove adsorbed ions, then for 12 hours precipitate was dried in a vacuum oven at 70°C. The samples obtained were composed of fibers with a diameter about 15 nm and length about hundreds of nanometers.

Yumei et al. [36] synthesized, zinc borate nanoplatelets with chemical formula of $Zn_2B_6O_{11}\cdot3H_2O$, which have a polycrystalline and hydrophobic structure, were in situ synthesized via one-step precipitation reaction in aqueous solution of $Na_2B_4O_7\cdot10H_2O$ and $ZnSO_4\cdot7H_2O$ with oleic acid as the modifying agent. Experiment was done in a 500 ml three-neck round-bottomed flask with a thermometer, reflux condenser and mechanical stirrer. Flask was charged with $Na_2B_4O_7\cdot10H_2O$, absolute ethanol and oleic acid and heated to 70°C. $ZnSO_4\cdot7H_2O$ was then added drop wise with continuous stirring. The final solution was filtered and washed with absolute ethanol and distilled water. The precipitate was dried at 80°C in an oven. The nanoplatelets obtained were with the average diameters of 100–500 nm and thickness of 30±5 nm.

Shete et al. [13] presented a comprehensive set of experimental results on the influence of process variables on the size distribution of a product made in a batch heterogeneous reaction. In this work, the effect of speed of agitation, mean initial particle size of zinc oxide, temperature, boric acid concentration in the solution on conversion of zinc oxide and mean particle size of zinc borate were investigated. The controlling mechanism, mixing effects and reaction kinetics were also studied.

Gürhan et al. [15] studied the effect of some reaction parameters on the synthesis of $2ZnO{\cdot}3B_2O_3{\cdot}3.5H_2O$ via the reaction of zinc oxide and boric acid with the presence of seed crystals at 1.5 liter batch reactor. The reaction rate, reaction completion time, composition and particle size distribution of zinc borate product were determined. The examined reaction parameters were the boric acid to zinc oxide ratio, the particle size of zinc oxide, stirring rate, and temperature, and the size of seed crystals. It was concluded that the reaction rate increases with the increase in $H_3BO_3$:ZnO ratio, particle size of zinc oxide, stirring rate and reaction temperature. The reaction completion time was decreased by increasing the $H_3BO_3$:ZnO ratio, stirring rate and temperature. The products were also analyzed in terms of average particle size distribution of the final products.

As could be seen from the contents of the works in literature, there is few studies that were focused on the characterization of the zinc borate product at the end of the experiments, observing the effects of the experimental parameters on reaction rate and final zinc borate product size and reducing the reaction completion time. Furthermore, all the studies involved in the synthesis of zinc borate at small laboratory scale batch reactors.

### 2.4 Polymers

Polymers are everywhere in our everyday environment, from proteins to DNA, synthetic polymers, from leather to the latest microfibers. Time, technologies and end uses for polymers have drastically changed since the first polymer chemists. Examples of applications now are the clothing industry in fabrics; the construction industry in paints, films, insulation; the automotive and transportation industry in vehicle bodies, interior accessories, windows; and the food industry in packaging [37]. The wide variety of polymeric materials offers an extensive pool of properties to choose from for almost any application, and companies are in perpetual competition to produce the strongest fiber or the clearest plastic.

As a result of this high volume of polymer present and used in our modern society, two main issues have arisen:

- handling of such materials after use
- behavior at extreme conditions.

In 2003, the United States generated more than 236 million tons of municipal solid waste, also called garbage, which represents about 4.5 pounds per person per day. Paper and wood accounted for 41.0% of that amount, plastics for 11.3%, leather, rubber and textiles for 7.4% [38]. In total, polymeric materials formed more than 140 million tons of waste in the United States alone. They are usually disposed of by either burying them in landfills or burning them in combustion facilities. Both processes are highly harmful to the environment and do not provide any economical advantage. Therefore, recycling is highly encouraged, and items such as poly(ethylene terephthalate) (PET) bottles are commonly recycled into various products, such as fabric or pavement. Unfortunately, this trend is not widespread, and most plastics still end up in landfills or combustion facilities. The former is often preferred over the latter, since many common polymers release toxic gases when burned, such as hydrogen chloride in the case of poly(vinyl chloride) or PVC. The second issue concerns the conditions of use of polymeric materials. Pressure, temperature, and UV light are parameters that can affect polymers, modifying their physical and chemical properties. Nowadays, polymers have been synthesized that can sustain very high pressures (Arkema Group Plexiglas® for aircraft windows), U.V. light (General Electric Lexan® film instead of paint), or even provide impact resistance (General Electric Xenoy® resin for car body panels).

However, most commercial polymers still cannot retain their physical properties when exposed to high temperatures. Fire-safe polymers are scarce and their cost is relatively high compared to widely used polymers such as PET or polystyrene (PS). Examples of these materials are Nomex®, Kevlar®, Kapton® from DuPont, or Ultem® from General Electric. The transportation industry and the Federal Aviation Administration (F.A.A.) in particular, are very sensitive to this problem [39-41]. The F.A.A. requires that all polymers used in aircrafts satisfy strict fire safety requirements [42]. Indeed, a substantial number of fatalities in airplane crashes are not caused by the crash itself, but by the post-crash fire. The goal of the F.A.A. is to increase safety and save lives by delaying the spread of fire to the entire cabin. Increasing the evacuation time from its present test value of 3 to 4 minutes to its goal value of 10 to 15 minutes can only be achieved through the use of ultra-fire-safe materials.

## 2.5 Flame Retardants

Flame retardants are additives that can be added to or applied as a treatment to materials such as plastics, textiles, foams, timber. Alternatively they can be used during the production process as a chemical modification of some plastic materials. In all cases, effective fire safety will only be achieved if flame retardants specifically adapted to the material to be treated are used appropriately. Their effect is to reduce the chances of a fire starting by providing increased resistance to ignition. Even if ignition does occur, flame retardants will act to delay the spread of flame, providing extra time in the early stages when the fire can be extinguished or an escape can be made.

Flame retardants save lives and property and protect the environment by helping to prevent fires from starting or from spreading. It is possible to treat most potentially flammable materials in the modern world with special additives to make them more difficult to ignite and to significantly reduce the spread of fire. Use of flame retardants plays a major role in fire safety, saving lives and preventing injuries and property damage. The general consumption percentages of flame retardant additives in 2002 are given in Table 2.4.

**Table 2.4** Flame retardants usage in the USA and West Europe [32]

| Flame Retardants | USA | West Europe |
|---|---|---|
| | Consumption Percentage (%) | |
| $Al(OH)_3$ | 39 | 47 |
| Bromine Based | 27 | 13 |
| Phosphorus Based | 12 | 23 |
| Chlorine Based | 11 | 3 |
| Antimony Oxides | 8 | 7 |
| $Mg(OH)_2$ | 1 | 2 |
| Zinc Borates | 2 | 5 |

## 2.6 Flame Retardancy Background

Flame retardants and methods for making flammable materials resistant to fires have been tried since the beginning of recorded history. Vinegar and alum (potassium aluminum sulfate ($KAl(SO_4)_2 \cdot 12H_2O$) or an ammonium aluminum sulfate ($NH_4Al(SO_4)_2 \cdot 12H_2O$) were used as paints or coatings for wood to help impart some flame resistance. Over time, different types of clays, gypsum, borax, and asbestos have been used to make canvas and clothing resistant to flames. Inorganic salts and materials have been the staple of flame retardants and are still used today. It was not until the early part of the 20th Century that William Henry Perkins [43] developed the basic work for the flame retardant theory. He was the first person to study the mechanism of flame retardancy on wood, cotton, paper and plastics [43]. Inorganic salts, acids and clays were the main ingredients of his flame retardant mixtures. World War II was another dominant milestone in the creation of flame retardants. Troops slept in canvas tents made flame retardant and waterproof by the use of chlorinated paraffin, antimony oxide and a binding agent [44]. In the 1950's, the polymer industry was starting to grow into a big market. During this period, the majorities of commodity plastics (e.g. polystyrene, polyurethane, polyethylene) were developed on a widespread and economically favorable scale and were preferred over other materials such as wood and metal alloys. It was not until the mid-1960’s before the

U.S. government created federal laws to mandate that plastics be made less flammable. The government also established guidelines for fire safe materials in fabrics and transportation materials, particularly airplanes [44].

## 2.7 Polymer Combustion Process

Many polymers, if subjected to some suitable ignition sources, will undergo self-sustained combustion in air or oxygen [45]. In general, non-polymeric materials (e.g. matches, cigarettes, torches or electric arcs) are the main sources of ignition, but polymers are most frequently responsible for the propagation of a fire. A burning polymer constitutes a highly complex combustion system. Chemical reactions may take place in three interdependent regions: within the condensed phase, at the interface between the condensed phase and gas phase, and in the gas phase. Polymer combustion occurs as a cycle of coupled events [46]:

(l) heating of the polymer,
(2) decomposition,
(3) ignition,
(4) combustion.

The polymer first is heated to a temperature at which it starts to decompose and gives out gaseous products which are usually combustible. These products then diffuse into the flame zone above the burning polymer. If there is an ignition source, they will undergo combustion in the gas phase and liberate more heat. Under steady-state burning conditions, some of the heat is transferred back to the polymer surface, producing more volatile polymer fragments to sustain the combustion cycle. This process is summarized in Figure 2.1.

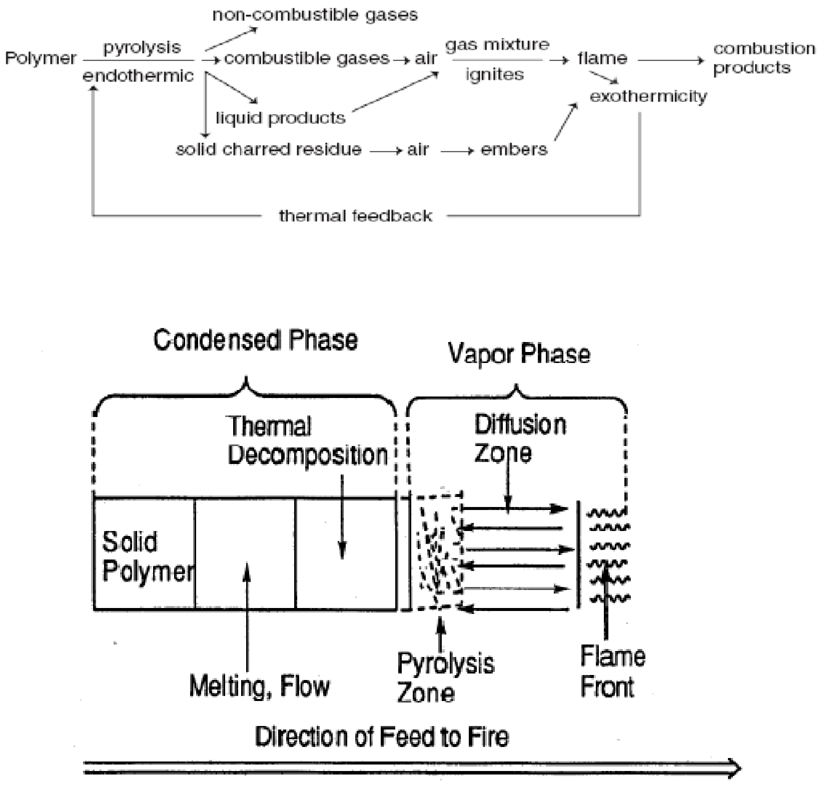

**Figure 2.1** Combustion of polymers [47]

There are two types of combustion involved when polymers are burned: flaming combustion and non-flaming combustion [48]. Flames are self-propagating combustion reactions in which both the fuel and the oxidant are present in the gas phase. Since most polymers are hydrocarbon-based, the flame above burning polymers is usually a hydrocarbon flame. The principal reactions in the flames are free-radical reactions. The most important radicals in hydrocarbon flames are simple species such as $H^{\bullet}$, $O^{\bullet}$, $OH^{\bullet}$, and a small amount of $HO_2^{\bullet}$, $HCO^{\bullet}$, and $CH_3^{\bullet}$. Chain-branching reactions in the combustion process, for example $H^{\bullet} + O_2 \rightarrow HO^{\bullet} + O^{\bullet}$, can accelerate the burning of polymers by generating more radicals. Smoke formation in flames is highly dependent on the structure of the gaseous fuel and on the fuel-to-oxidant ratio. Normally, polymers containing purely aliphatic structural units produce relatively little smoke, while polymers with aromatic groups in the main chain produce intermediate amounts of smoke.

Non-flaming combustion, including smoldering and glowing combustion, propagates through the polymer by a thermal front or wave involving the surface oxidation of the pyrolysis products [46]. Glowing combustion differs from smoldering combustion in that it is accompanied by pale flames of carbon burning to form carbon monoxide. Smoldering combustion usually occurs with polymeric materials of high surface area which can form a residual carbonaceous char. It is generally accompanied by the generation of smoke due to pyrolysis at or near the surface. Glowing combustion occurs after the initial charring of the material. From a practical point of view, it is also important to consider the associated fire hazards. The effects resulting from polymer combustion which can threaten human life include oxygen depletion, flame, heat, smoke, hot and toxic combustion gases, and structural failure. The two major causes of fire-related deaths are inhalation of toxic gases and burns [49, 50].

## 2.8 Thermal Decomposition of Polymers

Although there is still considerable disagreement about the precise role of oxygen in the initial breakdown of hydrocarbon polymers, it is clear that both thermal and oxidative processes may be involved in the decomposition of the polymer; the process depends on the nature of the polymer itself [46]. For instance, the decomposition of polypropylene is considerably affected by the presence of oxygen. In the presence of oxygen the products are mainly ketones in contrast to the alkanes and alkenes formed in the absence of oxygen [51, 52]. On the other hand, the decomposition of the polydienes is very little affected by oxygen [53]. A physical model was proposed for the candle-like burning of polymers by Fenimore and Martin [54] in which heal is transferred from the flame to the polymer surface where pyrolysis takes place and more gaseous fuel is produced. It was suggested that the oxygen from the surrounding atmosphere is usually completely consumed in the flame zone so that the pyrolysis of the condensed phase polymer takes place in the absence of oxygen. In terms of the thermal decomposition of organic polymers, four general mechanisms can be identified as shown in Table 2.5.

**Table 2.5** Decomposition routes of some polymers

| Mechanism | Polymer | Products |
|---|---|---|
| Random-chain | Polyethylene | Alkanes, alkene |
| | Polypropylene | Monomer |
| | Polystyrene | Styrene monomer, dimer and trimer |
| | General | Monomers and oligomers |
| Depolymerization | PMMA | 90-100% Monomer |
| | Polymethacrylonitrile | |
| | Polyformaldehyde | |
| | PTFE | |
| | General | Monomer |
| Chain-stripping | Poly(vinyl chloride) | HCl, aromatic hydrocarbons, char |
| | Poly(vinylidine chloride) | HCl, char |
| | Poly(vinyl alcohol) | Water, char |
| | General | Small molecules, char |
| Cross-linking | Polyacrylonitrile | Char |
| | General | Much char, few volatile products |

While some polymers undergo reactions which fall almost exclusively into one of the four classes shown, others exhibit mixed behavior. For example, poly(methyl acrylate), which gives a variety of oligomer fragments as well as carbon dioxide and methanol but hardly any monomer, breaks down by a combination of random-chain scission and chain stripping [55]. In the random-chain scission process, polymers break down to give fragments of various molecular weights which are lower than that of the "mother" molecule. Chain scission occurs at random points along the chain. This process can be either by a free radical process or some molecular rearrangement mechanism. Such random scissions may lead to a complex degradation pathway, cross-linking, small fragments from secondary reactions, a change in repeating unit functionality, or other complex chemical changes.

Depolymerization, also called the unzipping process, leads to the release of monomer units. Such a process can be viewed as the opposite of the propagation step in addition polymerization. This process is encountered most prevalently with vinyl polymers in which free radical reactions are predominantly involved.

Another type of polymer breakdown is chain-stripping which involves interaction of the substituent [56]. When the substituent are halogen atoms (other than fluorine) or hydroxyl or acetate groups, decomposition tends to involve the loss of small molecules such as hydrogen chloride, water, or acetic acid and subsequently the formation of polyene. Decomposition continues until the polymer chain has been stripped entirely of its substituent groups. Cyclization and cross-linking of the unsaturated chain lead to char formation. Cross-linking reactions leading to char formation are not clarified enough with current studies. Here the polymers structures are usually complicated and the reactions occur in the solid phase so that they are not readily accessible to the normal techniques of chemical investigation.

### 2.9 Chemical Reactions in Flame

Since the majority of common polymers are hydrocarbon-based, the flames above burning polymers are usually hydrocarbon flames [46]. The combustion gas-phase reactions of hydrocarbon flames have been studied in some detail [57], and many of the processes have been quantitatively defined and shown to be predominantly free radical in nature. An example of the chain reactions involved in the oxidation of methane is indicated in Reactions 2.2-2.15.

$$CH_4 + OH^- \leftrightarrow CH_3^- + H_2O \qquad (2.2)$$

$$CH_4 + H^+ \leftrightarrow CH_3^- + H_2 \qquad (2.3)$$

$$CH_4 + O^{2-} \leftrightarrow CH_3^- + OH^- \qquad (2.4)$$

$$CH_3^- + O_2 \leftrightarrow HCHO + OH^- \qquad (2.5)$$

$$HCHO + 2OH^- \leftrightarrow CO + 2H_2O \qquad (2.6)$$

$$CO + OH^- \leftrightarrow CO_2 + H^+ \qquad (2.7)$$

$$H^+ + O_2 \leftrightarrow OH^- + O^{2-} \qquad (2.8)$$

$$O^{2-} + H_2O \leftrightarrow OH^- + OH^- \qquad (2.9)$$

$O^{2-} + H_2 \leftrightarrow OH^- + H^+$ (2.10)

$H^+ + H_2O \leftrightarrow H_2 + OH^-$ (2.11)

$H^+ + H^+ + M \leftrightarrow H_2 + M$ (2.12)

$O^{2-} + O^{2-} + M \leftrightarrow O_2 + M$ (2.13)

$H^+ + O^{2-} + M \leftrightarrow OH^- + M$ (2.14)

$H^+ + OH^- + M \leftrightarrow H_2O + M$ (2.15)

The complete oxidation of the hydrocarbons involves a complicated series of free radical reactions. The most important radicals in all hydrocarbon flames are simple species such as $H^+$, $O^{2-}$, and $OH^-$. Chain branching reactions lead to an exponential increase in the concentration of these radicals. In most organic polymers, the large hydrocarbon radicals, which are produced in the initial step, breakdown rapidly to give smaller species such as $CH_3^-$. Thus the flame propagating species are largely independent of the initial fuel. In other words, the combustion of a polymer can viewed as a chemical reaction which yields a hydrocarbon flame. In terms of chemical composition, flames above different burning organic polymers do not differ greatly from one polymer to another. In contrast to the situation with flames of gaseous fuel, in which the fuel is supplied to the flame front at an arbitrary rate, a burning polymer generates its own fuel. Because fuel generation in the condensed phase is followed by the fuel consumption in the gas phase, the rate of these processes must be in equilibrium in order to maintain a steady state of combustion. Acceleration or deceleration of either process will tend to collapse or blow-off the flame.

## 2.10 Inherently Flame Retardant Polymers

The market for flame retardant polymers is considerably smaller than for additives. Most of the products that fit the criteria for being a flame retardant polymer are usually marketed as heat-resistant materials, meaning these polymers do not bum but rather decompose at elevated temperatures. There are five main principles that have to be considered while developing heat resistant polymers [46]:

- Compounds with strong covalent bonds should be used.
- There should be no easy pathway for the molecular rearrangements.

- Resonance stabilization of aromatic polymer rings should be used to maximize the bonding energy.
- All of the rings in the structure should have normal bond angles, i.e. no bond strain or weak points.
- Multiple bonding to several centers should be utilized, i.e. ladder polymer would be the most stable.

These are idealized goals for heat resistant polymers and no material utilizes all of these qualities to their maximum efficiency. Rather, they are guidelines to be used when designing a polymer. In reviewing the several types of polymer made with these heat-resistant properties, key observations can be made about what makes a good material. Polymer chains that use para-linkages between rings have shown to be the most stable, unfortunately this also results in poor processibility and insolubility in most solvents [46]. Adding aliphatic branching only provides additional fuel for a fire and makes the polymer more prone to oxidation. Flexible linker groups that have worked the best and have negligible impact on the polymer's stability include: -CO-, -COO-, -CONH-, -S-, $-SO_2-$, -O-, $-[CF_2]-$, $-[C(CF_3)_2]-$.

There have been many polymers that have been developed over the years as heat resistant or flame retardant polymers, but few have ever achieved commercial success. A few polymers have emerged as economically feasible, most notably Kevlar, polyether imides, polyetheretherketone (PEEK), and Teflon (Figure 2.2).

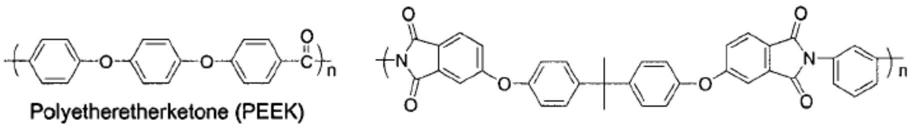

Polyetheretherketone (PEEK)

Polyetherimide

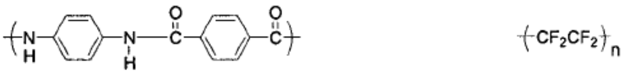

Poly(1,4-phenylene terepthalamide) Kevlar

Polytetrafluorethylene (Teflon)

**Figure 2.2** Inherently flame retardant polymers

Polymers such as Kevlar and Teflon are common place in today's market but still command a high price tag due to the cost of making them and their low sales volume. While these materials are non-combustible, they are not flame extinguishing. The decomposition by-products from these types of polymers are important indicators as to how well they will perform when exposed to a flame. Some of these by-products are quite harmful and toxic. The decomposition of Teflon in air, under 650°C produces carbonyl difluoride ($O=CF_2$), carbon monoxide and carbon dioxide. These non-flammable decomposition products help to increase heat-resistance and in some cases flame retardancy. Another important feature in some of these polymers is having unsaturation in the polymer backbone or various leaving groups, which will crosslink in a fire to form char, i.e. poly(styryl pyridine) or PSP (Figure 2.3).

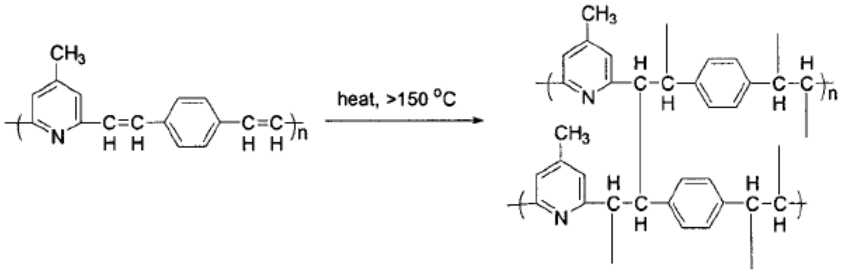

**Figure 2.3** Crosslinking mechanism of poly(styryl pyridine) [58]

The final way in which these polymers can form char during the burning process is to form additional rings either by Claisen-Cope or Diels Alder rearrangement. The following polyamide, similar to Dupont's Nomex, forms a more stable benzoxazole structure on heating (Figure 2.4).

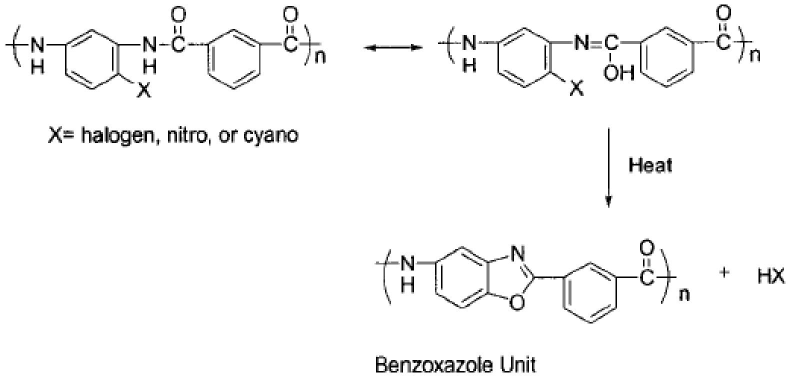

**Figure 2.4** Formation of additional rings of polyamide [59]

Heat-resistant polymers are a growing market. These products are becoming more common every day. Research in this area is ongoing and the goal of a low cost, easily processible, flame retardant polymer is well within reach.

### 2.11 Flame Retardant Additives

From the manufacturing point of view, the introduction of flame retardant additives undoubtedly constitutes the easiest way of making a polymer less flammable. There are two main types of additives: reactive and additive flame retardants [44]. The reactive flame retardants are the compounds containing heteroatoms known to confer some degree of flame retardance, and they are built chemically into the polymer molecule. Alternatively, the additive flame retardant can be physically mixed with existing polymers. In this case, the compounds do not react chemically with the polymers. The flame retardants most abundantly used at the present time are based largely on six elements: boron, aluminum, phosphorus, antimony, chlorine, and bromine. In addition, nitrogen and silicon can also confer some degree of flame retardance. Other elements and their compounds have proved to be less effective. Combinations of flame retardants often have synergistic or antagonistic effects. Sometimes a hetero atom already present in the polymer backbone may interact with a flame retardant and thus exhibit synergism or antagonism.

Although additive flame retardants are widely used in polymers, there are some limitations such as poor compatibility, high volatility effects on the properties of polymers and increase of the production of carbon monoxide (CO) and smoke [60].

Flame-retardant additives can act by a variety of mechanisms in either the condensed phase or the gas phase [44]. They can terminate the free-radical reactions in the condensed phase, act as heat sinks due to their heat capacity, form a non-flammable protective coating or char to insulate the flammable polymer from the source of the heat and oxidant, and interrupt the flame combustion in the gas phase. It is difficult, however, to unequivocally attribute a single mode of action to a particular additive or class of additives. Many flame retardants appear to be capable of functioning simultaneously by several different mechanisms, often depending on the nature of the organic polymers.

### 2.11.1 Inorganic Hydroxide Flame Retardants

Inorganic hydroxides are a very important class of flame retardants due to their relatively low cost, easy of handling and low toxicity [61]. Aluminium oxide trihydrate is used in the largest quantities by far as an inorganic flame retardant for polymers [62]. It is normally introduced into polymers in large quantities (>50% by weight) in order to attain a significant flame-retardant effect. This addition reduces the amount of combustible materials available for decomposition. During decomposition, this compound acts as a heat sink and thus delays the polymer from reaching its decomposition temperature [63]. When heated, it decomposes to form anhydrous alumina and releases water, which is an endothermic reaction. This energy consumption can remove the heat from the substrate, slow the decomposition of the substrate, and keep it below its ignition temperature. Also, water released into the vapor phase dilutes the concentration of the combustible gases. The oxide residue generated during decomposition has a relatively high heat capacity, which can reduce the heat transfer to the substrates. Another advantage of using inorganic hydroxides is that they can reduce the amount of smoke generated on combustion [64]. Due to its low thermal stability, aluminum oxide trihydrate should be used below 200°C. Other inorganic hydroxides and hydroxycarbonates [65] also have some flame-retardant action. For example, magnesium hydroxide is more thermally stable and can be used above 300°C.

### 2.11.2 Antimony Compounds

Antimony trioxide is not a flame retardant alone, but it is used as a synergist. It is utilized in plastics, rubbers, textiles, paper and paints, typically 2-10% by weight.

Antimony oxides and antimonates must be converted to volatile species. This is usually accomplished by release of halogen acids at fire temperatures. The halogen acids react with the antimony containing materials to form antimony trihalide and/or antimony halide oxide. These materials act both in the substrate (condensed phase) and in the flame to suppress flame propagation. In the condensed phase, they promote char formation, which acts as a physical barrier to flame and inhibits the volatilization of flammable materials. In the flame, the antimony halides and halide oxides, generated in sufficient volume, provide an inert gas blanket over the substrate, thus excluding oxygen and preventing flame spread. These compounds alter the chemical reactions occurring at fire temperatures in the flame, thus reducing the ease with which oxygen can combine with the volatile products. It is also suggested that antimony oxychloride or trichloride reduces the rate at which the halogen leaves the flame zone, thus increasing the probability of reaction with the reactive species. Antimony trichloride probably evolves heavy vapors which form a layer over the condensed phase, stop oxygen attack and thus choke the flame. It is also assumed that the liquid and solid antimony trichloride particles contained in the gas phase reduce the energy content of the flames by wall or surface effects [43].

Other antimony compounds include antimony pentoxide, available primarily as a stable colloid or as a redispersible powder. It is designed primarily for highly specialized applications, although manufacturers suggest it has potential use in fiber and fabric treatment.

Sodium antimonate ($Na_2OSb_2O_5 \cdot nH_2O$) is recommended for formulations in which deep tone colors are required or where antimony trioxide may promote unwanted chemical reactions.

### 2.11.3 Halogenated Flame Retardants

Halogen-containing flame retardants make up one of the largest groups of additives in the plastic industry. As reactive flame retardants, halogen-containing alkenes, cycloalkanes and styrene can be copolymerized directly with the corresponding non-halogenated monomers. As additive flame retardants, these organic halogenated compounds are most commonly used in conjunction with phosphorus compounds or with metal oxides, especially antimony oxide. The stability of the halogen compounds go as F>Cl>Br>I. Iodine compounds are not sufficiently stable to be used commercially, whereas, the fluorine compounds are too stable to be generally useful. Bromine and chlorine compounds are the most generally used halogen-containing flame retardants. Bromine compounds are more effective than chlorine compounds on a weight basis, but they are considerably more expensive. Halogen-containing flame retardants may function either in the vapor phase or in the condensed phase [66]. The action of the flame retardant depends on the structure of the additive and of the polymer. Generally, the radicals produced by thermal decomposition of a halogenated flame retardant can interact with the polymer to form hydrogen halide (HX). Hydrogen halides inhibit the radical propagation reactions which take place in the flame by reacting with the most active radicals, R and OR. It also should be noted that aromatic brominated compounds can produce large amounts of char. Although halogen compounds are quite widely used on their own in flame retardants, their effectiveness is sometimes considerably increased by a free-radical initiator and antimony trioxide. Antimony-halogen systems can affect the combustion of polymers by their ability to act both in the gas phase and the condensed phase. Although there is an increasing legislation against the use of halogenated compounds in disposable items that must be recycled or land filled, brominated and chlorinated flame retardants still occupy the largest share of the flame-retardant market.

The effectiveness of halogenated flame retardants depends on the type of halogen. Fluorine and iodine-based compounds are not used because they do not interfere with the polymer combustion process. Fluorinated compounds are more thermally stable than most polymers and do not release halogen radicals at the same temperature range or below the decomposition temperature of the polymers. Iodinated compounds are less thermally stable than most commercial polymers and therefore release halogenated species during polymer processing. Bromine and chlorine, because of their low bonding energy with carbon atoms, can readily be released and take part in the combustion process, especially with the previously discussed free-radical mechanism occurring in the gas phase.

As stated above, thermally induced polymer decomposition releases very reactive free-radical species such as $H^{\bullet}$ and $OH^{\bullet}$, which maintain combustion by a cascade chain mechanism in the gas phase. Halogenated flame retardants are able to react with these species, stopping the chain decomposition and therefore the combustion of the polymer. As seen in Reaction 2.16, RX denotes the flame retardant additive (where X denotes Br or Cl) and in Reactions 2.18 and 2.19 inhibition step could be seen:

$$RX \rightarrow R^{\bullet} + X^{\bullet} \tag{2.16}$$

$$X^{\bullet} + R'H \rightarrow R'^{\bullet} + HX \tag{2.17}$$

$$HX + H^{\bullet} \rightarrow H_2 + X^{\bullet} \tag{2.18}$$

$$HX + OH^{\bullet} \rightarrow H_2O + X^{\bullet} \tag{2.19}$$

### 2.11.4 Phosphorus-based Flame Retardants

Both inorganic and organic phosphorus compounds are useful for imparting flame retardance to many polymers. Phosphorus flame retardants include elemental red phosphorus, water-soluble inorganic phosphates, insoluble ammonium polyphosphate, organophosphates and phosphonates, phosphine oxides, and chloroaliphatic and bromoaromatic phosphates [67]. Both additive and reactive flame retardants are commercially available. Additive compounds, especially phosphates, are widely used for highly hydroxylated polymers such as cellulose. The most extensively employed reactive flame retardants are phosphorus-containing polyols used in the polyurethane foams [68]. Other reactive flame retardants include vinyl and allyl phosphonates [69]. The flame retardance mechanisms of these phosphorus compounds include the formation of a surface glass to protect the substrate from oxygen and flame, promoting of charring, and free-radical inhibition generally proposed for halogens. The flame retardant mechanism for phosphorus depends on the type of phosphorus compound and the chemical structure of the polymer. Phosphorus flame retardants containing halogens or nitrogen are often stated to exhibit synergistic behavior due to the formation of phosphorus halides or oxyhalides or P-N bonds on decomposition [70, 71]. Recently, there is an increased interest in intumescent systems, which can develop a foamed char on the surface of the polymeric materials during burning. The combination of ammonium polyphosphate, dipentaerythritol and melamine is the most commonly used intumescent flame-retardant system [72]. Generally intumescence requires a carbonific (char former) such as a polyol, a catalyst or acid source such as a phosphate, and a spumific (gas generator) such as a nitrogen source. The mechanism involves decomposition of the phosphate to phosphoric acid, esterification of the polyol, and subsequently, decomposition and regeneration of the phosphoric acid. Ammonium polyphosphate with a high ammonia content helps blow the forming char to a porous product. This surface char insulates the substrate from flame, heat, and oxygen. There are also some self-intumescing compounds which contain all three required functions in a single molecule (Figure 2.5). Such intumescent coatings can satisfy environmental and toxicity issues because the coatings are halogen-free and the decomposition gases are water and ammonia.

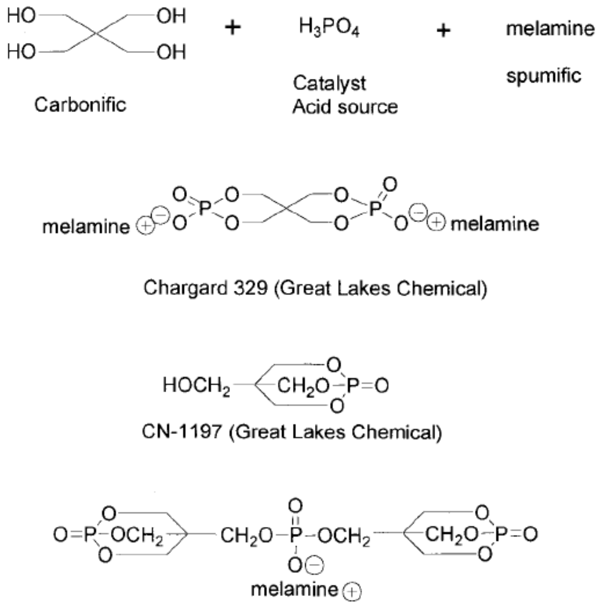

**Figure 2.5** Intumescent phosphorus compounds

### 2.11.5 Nitrogen-based Flame Retardants

The presence of nitrogen in natural polymers appears to exert some degree of flame retardance as shown by the relatively low flammability of wool, silk, and leather [73]. Synthetic polymers which contain nitrogen are not so resistant to combustion. A number of nitrogen-containing organic compounds are used as reactive flame retardants for certain polymers. These include triazines, isocyanates, urea, guanidine, and cyanuric acid derivatives [74]. Some of these compounds are also employed as additive flame retardants, often in conjunction with phosphorus compounds, to reduce the flammability of cellulosic textiles. In the latter cases, the nitrogen appears to act to a considerable extent by strengthening the attachment of phosphorus to the polymer, but nothing is yet certain about the mechanisms of action. One possible explanation is that the release of nitrogen or ammonia dilutes the volatile polymer decomposition products and hence makes them less flammable. Ammonium salts and metal-amine complexes have also been quite widely used as flame retardants for certain applications, such as ammonium phosphates for wood [73].

Melamine is a thermally stable crystalline product characterized by a melting point as high as 345°C that contains 67 weight percent nitrogen atoms. Melamine sublimates at about 350°C. Upon sublimation, a significant amount of energy is absorbed, decreasing the temperature. At high temperature, melamine decomposes with the elimination of ammonia, which dilutes oxygen and combustible gases and leads to the formation of thermally stable condensates.

These melamine decomposition reactions compete with melamine volatilization reactions and are more pronounced if melamine volatilization is hindered, e.g. by the formation of a protective layer. The formation of thermally stable condensates generates residues in the condensed phase and results in endothermic processes, also effective for flame retardancy. In addition, melamine can form thermally stable salts with strong acids: melamine cyanurate, melamine phosphate, and melamine pyrophosphate. Melamine and melamine salts are characterized by various flame retardant mechanisms. Upon heating, melamine based salts dissociate and the re-formed melamine volatilizes, like neat melamine, but a large proportion of the melamine undergoes more progressive condensation than in the case of pure melamine. The action of salts in the condensed phase is therefore significantly higher.

The thermal decomposition of melamine phosphate leads to the formation of melamine polyphosphate, with the release of melamine and phosphoric acid. The phosphoric acid released is known to phosphorylate (addition of a phosphate group to an organic molecule) many polymers and produce flame retardant effects similar to phosphorus-based flame retardant additives.

The thermal decomposition of melamine polyphosphate leads to the formation of ammonium polyphosphate, with the release of melamine. However, the melamine in the gaseous phase competes with the formation of its condensation products. The condensation of melamine is thus accompanied by the formation of polyphosphoric structures. The melamine pyrophosphate transforms into melamine during thermal decomposition but its thermal performances are different from those of melamine and its other salts; the formation of carbonaceous structures is more significant here and its action mode is similar to that of ammonium polyphosphate.

### 2.11.6 Silicon-containing Flame Retardants

There is a renewed interest in using silicon-based flame retardants as substitutes for the halogens or phosphorus [75]. Almost all forms of silicon have been explored: silicones, silicas, organosilanes, silsesquioxanes, and silicates. The most common flame retardant based on silicon is in the form of polyorganosiloxane, in particular, polydimethylsiloxane (PDMS). The flammabilities of the block copolymers of various types of polycarbonate (PC) and poly(ether imide) (PEI) with PDMS [76] show significant decreases. Silicon can also be incorporated into the branches of the polymer chains [77]. Under certain cases, the addition of silica can also affect the flammability properties of materials [78]. The formation of a silicon-based protective surface layer appears to be the flame-retardant mechanism for silicone and silica systems. Polycarbosilane (PCS), polysilastyrene (PSS), and polysilsesquioxane preceramic polymers are also used to blend with various thermoplastics. Studies show [79, 80] that, they are all effective flame retardants. They can reduce the peak heat release rate (HRR) and average HRR, but the total heat released remains unchanged. The primary reason for the lower HRR for the blends is the reduced mass loss rate; i.e., the rate at which fuel is released into the gas phase is slowed by the presence of the ceramic char. Recently, there is a great interest in the flammability properties of polymer layered-silicate (clay) nanocomposites. Cone calorimetry data show that both the peak and average heat release rate are reduced significantly for intercalated and delaminated nanocomposites with low silicate mass fraction (3-5%), but there is little improvement in the char yield. Polymer clay nanocomposites are materials that may fulfill the requirements for a high-performance, additive-type flame-retardant system. In general, a condensed-phase mechanism, which involves a protective surface layer, is proposed for silicon-based flame retardants.

### 2.11.7 Boron-based Flame Retardants

Borate treatments were the first to be extensively applied to cotton and then to wool. Boric acid and borax are frequently used together [81]. On evaporation of the water of hydration, the polymers swell and an intumescent coating is formed on the surface which insulates the bulk of the polymer from the heat source. The enhancement of the char formation, the endothermic dehydration process and the dilution of the gaseous breakdown products by the water released could be the reasons for the flame retardance of boron-containing additives. Cyclic borate esters have been used as durable additives for cellulose, and boric acid and polyols have been incorporated into rigid polyurethane foams.

Among them, zinc borates such as $2ZnO{\cdot}3B_2O_3{\cdot}3.5H_2O$ are the most frequently used. Their endothermic decomposition (503 kJ/kg) between 290 and 450°C liberates water, boric acid and boron oxide ($B_2O_3$). The $B_2O_3$ formed softens at 350°C and flows above 500°C leading to the formation of a protective vitreous layer. In the case of polymers containing oxygen atoms, the presence of boric acid causes dehydration, leading to the formation of a carbonized layer. This layer protects the polymer from heat and oxygen. The release of combustible gases is thus reduced.

### 2.11.8 Polymeric Flame Retardants

Polymeric flame retardants have been much less studied than their small molecule counterparts even though they have many advantages. By the incorporation of a polymeric flame retardant, the physical and mechanical properties of the polymer are less affected. It can also avoid the outward diffusion in the system and consequent risk of environmental contamination. Polydibromostyrene and polyphosphazenes are among some of these flame retardants [82, 83]. In a broad sense, all the fire-resistant polymers can be used as polymeric flame retardants to be blended with some other polymers to enhance fire retardancy. As a matter of fact, this is a very convenient way to adjust polymer flammability by composition.

### 2.11.9 Nanometric Particles

Nanometric particles when individualized and properly dispersed in polymer matrices are known to contribute to the enhancement of properties such as thermal, mechanical or fire resistance. They enable a considerable reduction of the loading rate as the interfacial area between the polymer and the nanofiller is greatly increased. More precisely, the contribution of each type of nanoparticle to flame retardancy varies and strictly depends on its chemical structure and geometry. The flame retardant effects and flame retardant mechanisms of three widely investigated nanoparticles are:

- layered materials, such as nanoclays (e.g., montmorillonite: MMT), which are characterized by one nanometric dimension, referred to as 2D nanoparticles;

- fibrous materials, such as carbon nanotubes and sepiolite, which are characterized by elongated structures with two nanometric dimensions and referred to as 1D nanoparticles;

- particulate materials, such as polyhedral oligosilsesquioxane (POSS) and spherical silica nanoparticles, which are characterized by three nanometric dimensions and sometimes referred to as 0D nanoparticles.

### 2.12 Mechanisms of Action of Flame Retardant Additives

Flame retardant systems are intended to inhibit or to stop the polymer combustion process. In function of their nature, flame retardant systems can either act physically (by cooling, formation of a protective layer or fuel dilution) or chemically (reaction in the condensed or gas phase). They can interfere with the various processes involved in polymer combustion (heating, pyrolysis, ignition, propagation of thermal degradation).

### 2.12.1 Physical Act of Flame Retardant Additives

The endothermic decomposition of some flame retardant additives induces a temperature decrease by heat consumption. This involves some cooling of the reaction medium to below the polymer combustion temperature. In this category hydrated tri-alumina or magnesium hydroxide can be mentioned, which start liberating water vapor at approximately 200 and 300°C, respectively. Such a marked endothermic reaction is known to act as a heat sink.

When the flame retardants decompose, with the formation of inert gases ($H_2O$, $CO_2$, $NH_3$, etc.), the combustible gas mixture is diluted, which limits the concentration of reagents and the possibility of ignition. In addition, some flame retardant additives lead to the formation of a protective solid or gaseous layer between the gaseous phase where combustion occurs and the solid phase where thermal degradation takes place. Such a protective layer limits the transfer of matter such as combustible volatile gases and oxygen. As a result, the amount of decomposition gases produced is significantly decreased. Moreover, the fuel gases can be physically separated from the oxygen, which prevents the combustion process being sustained.

#### 2.12.1.1 Water Formation of Flame Retardant Material

Some flame retardants used today; act by cooling down the combustion process. As these water forming materials decompose, they evolve water that cools the process and due to the endothermic nature the process absorbs much of the energy from the system. Therefore the heat that is generated is not returned to the polymer to perpetuate the combustion cycle; rather it is used to burn the water off as steam. Aluminium trihydrate, $Al_2O_3 \cdot 3H_2O$, is the most common water evolving flame retardant for thermoplastics. As this material starts to break down, it gives off nearly 35% of its weight as water. The usual breakdown temperature that results in the release of water vapor is around 180°C to 200°C [84]. Some of the main advantages of this compound are that it is relatively inexpensive; it does not produce additional toxic gases, while at the same time it decreases smoke generation, and it is also non-volatile. The main disadvantages of this material are that it requires relatively high loadings to achieve substantial flame retardant capabilities. It also has a low degradation temperature, which can be a problem when processing higher melt temperature polymer formulations. Its use can dramatically affect the end properties of the final product due primarily to the high loading levels. Magnesium hydroxide, $Mg(OH)_2$, works in much the same way as aluminium trihydrate, by forming water to cool the combustion process. This compound has the advantage that it does not decompose until temperatures around 340°C are reached. This opens up its use for a wider spectrum of plastics that are processed at higher temperatures above 200°C. When this material decomposes, it gives off 31% water by weight. Relatively high loadings in the range of 40-60% are still required to reach sufficient flame retardancy [84].

#### 2.12.1.2 Intumescent Coating Formation of Flame Retardant Material

Intumescent systems work by producing a char like foam that protects the substrate to which it is applied from the heat of the flame. Historically these systems have been used on wood, and plastic that burn without the aid of a flame retardant compound. For several years, these types of agents have been available as protective coatings for plastics. In recent times they have been used as flame-retardants in plastics, actually being incorporated into the polymer formulations rather than just a surface treatment. Intumescents use phosphorous based compounds to produce a char. The thing that differentiates them from the char forming phosphorus FR systems is the fact that there is no oxygen needed in the backbone of the polymer. The oxygen is supplied through additives [43]. The main components necessary for all intumescent systems are as follows:

1. An acid source: The most common ones are the salts of an inorganic non-volatile acid such as boric, sulphuric or phosphoric acid. The salts, such as ammonium phosphate, release phosphoric acid at temperatures above 150°C. This acid then initiates the series of events, which begins with the dehydration of the carbonific compound.

2. Carbonific compounds: These polyhydroxy compounds which when dehydrated produce a char because of the acid attack.

3. Blowing agents: Materials such as chloroparaffins, melamine and guanidine are commonly used for this aspect of the intumescent flame retardant. With the onset of high temperatures these compounds will release quantities of non-combustible gases like HCl, $NH_3$, and $CO_2$. These gases ensure a good layer of charred foam, which acts as a protective barrier for the inner plastic.

4. Binder: A resin binder is used to cover the foam, which is produced by the blowing agent so as not to release the gases formed. This material should not harden but should remain somewhat molten in order to have the optimum effect.

### 2.12.2 Chemical Act of Flame Retardant Additives

Flame retardancy through chemical modification of the fire process can occur in either the gaseous or the condensed phase. The free-radical mechanism of the combustion process can be stopped by the incorporation of flame retardant additives that preferentially release specific radicals (e.g. $Cl^{\bullet}$ and $Br^{\bullet}$) in the gas phase. These radicals can react with highly reactive species (such as $H^{\bullet}$ and $OH^{\bullet}$) to form less reactive or even inert molecules. This modification of the combustion reaction pathway leads to a marked decrease in the exothermicity of the reaction, leading to a decrease in temperature and therefore a reduction in the fuel produced.

In the condensed phase, two types of chemical reactions triggered by flame retardants are possible: first, the flame retardants can accelerate the rupture of the polymer chains. In this case, the polymer drips and thus moves away from the flame action zone. Alternatively, the flame retardant can cause the formation of a carbonized (perhaps also expanded) or vitreous layer at the surface of the polymer by chemical transformation of the degrading polymer chains. This char or vitrified layer acts as a physical insulating layer between the gas phase and the condensed phase.

#### 2.12.2.1 Char Forming Reactions (Phosphorous Compounds)

While the halogenated flame retardants act primarily in the gas phase of the burn zone, the phosphorous based compounds work mostly in the condensed phase to form a char layer. The characteristics of an effective char layer are [85]:

- difficult to ignite,
- insulate the polymer beneath from the thermal degradation,
- block oxygen access, and the release of degradation products.

Phosphorous-based systems are the most effective char forming flame retardants, and can be divided into two main categories. The two types are (i) organophosphorus compounds and (ii) inorganic phosphorus compounds. The organophosphorus compounds are typically phosphate esters. Triaryl phosphate esters are the most common of the non-halogenated phosphate esters. These triaryl phosphates are generally used in to flame retard engineering thermoplastics. The inorganic phosphorous flame retardants most commonly used for plastics materials are ammonium phosphates, and red phosphorous.

These flame retardants have been shown to work most effectively with plastics that have oxygen in their structural backbone. Examples of oxygen containing polymers are cellulose, polyesters, acetals, and polyurethanes. In polymers with primary hydrocarbon structure, such as polyolefins, it is common to find phosphorous compounds in conjunction with other flame retardant additives.

The basic mechanism of the phosphorous compounds is the formation of a char that protects the polymer substrate by cutting off the fuel for the fire. This is accomplished by converting the flame retardant compound into phosphoric acid by a decomposition process brought on by the heat from the flames. This phosphoric acid reaction extracts water from the burning substrate, which causes it to char. This char is made up of a glassy coating which protects the inner plastic from oxygen and the radiant heat of the fire [43].

Advantages of phosphorous fire retardants are easily incorporated into the polymer formulation during processing, the low concentrations needed for suitable flame retardancy, they have little effect to the physical properties of the product, and moderately low costs. The disadvantages of these systems are the hygroscopic nature of the materials in some environments, and the possible release of toxic gases as some of the organic materials burn.

### 2.12.2.2 Char Forming Reactions

Inorganic and organic phosphorus compounds are useful as flame retardants for many polymers. Both additive and reactive flame retardants are commercially available.

The mode of action of phosphorus compounds are different from one to another and depend upon the nature of the additives and the polymers. In general, the volatile phosphorus compounds are efficient gas-phase inhibitors. An example is triphenyl phosphine oxide. It is found that this compound is subject to vaporization at 900°C [87]. When triphenyl phosphine oxide is used in conjunction with polyester, a significant proportion of the phosphorus compound is lost prior to decomposition of the polymer [88]. In the flame zone, triphenyl phosphine oxide decomposes to give intermediates such as PO, $PO_2$ .and $P_2$ (Reaction 2.20). Hastie [87, 89] has suggested that the gas phase inhibition involves the destruction of hydrogen radicals in which the radical PO catalyzes the recombination (Reactions 2.21-2.23, where M is a third body e.g. $H_2O{\cdot}N_2$).

$$(C_6H_5)_3PO \rightarrow PO^{\bullet} + P^{\bullet} + P_2 \qquad (2.20)$$

$$H\cdot + PO^{\bullet} + M \rightarrow HPO + M \qquad (2.21)$$

$$OH^{\bullet} + PO^{\bullet} \rightarrow HPO + O^{\bullet\bullet} \qquad (2.22)$$

$$HPO + H^{\bullet} \rightarrow H_2 + PO^{\bullet} \qquad (2.23)$$

Some typical phosphorus based flame retardants are shown in Table 2.6 [46].

**Table 2.6** Typical phosphorus containing flame retardants

| Type | Flame Retardant | Polymer |
|---|---|---|
| Inorganic Additive | Red Phosphorus | Polyolefins, polystyrene, polyesters, epoxy |
| | Ammonium Phosphate | Cellulosics, acrylics |
| Organic Additive | Triethyl-Trioctyl Phosphate | Cellulosics, polyesters |
| | Triphenyl Phosphate | Cellulosics, thermoplastics |
| | Diphosphates | Polyurathane, acrylics, epoxy |
| | Triphenyl Phosphine Oxide | Polyester |
| | Tris(2,3-dibromopropyl) Phosphate | Cellulosics, acrylics, polystyrene, polyurathanes |
| Organic Reactive | Tetarakis Hydroxymethyl Phosphonium Salts | Cellulosics, thermosets |
| | Allyl Phosphates and Phosphonates | Polyolefins |
| | Oligomeric Vinyl Phosphonates | Cellulosics, polyester |

## 2.13 Flame Retardant Synergy

In general, flame retardant additives are used to limit the risk of fire and its propagation. They are incorporated in the polymer matrix to increase the time to ignition, improve the self-extinguishability of the polymer, decrease the heat release rate during combustion and prevent the formation of flammable drops. In order to achieve high fire performance levels, it is necessary to develop a flame retardant system based on a combination of different flame retardant agents. The concept of synergism is used to optimize flame retardant formulations and enhance the performance of mixtures of two or more additives. Synergism is achieved when the performance level due to a mixture of additives xA + yB (x + y = 1) for a given property (P) is greater than that predicted for the linear combination (xPA + yPB) of the single effects of each additive (PA and PB). Conversely, opposite effects can be detected. As discussed above, polymer flame retardancy can be achieved through one or more chemical and/or physical mechanisms taking place in either the gas or the condensed phase. Synergistic phenomena can be obtained either by a combination of flame retardancy mechanisms, such as char formation by a phosphorated flame retardant combined with a gas phase action by a halogenated flame retardant, or by a combination of flame retardant agents reinforcing the same mechanism, e.g. nanoclays and phosphorated flame retardant agents, both acting in the condensed phase.

For example, the gas-phase flame retardant action of halogenated additives can be improved by the incorporation of antimony oxide ($Sb_2O_3$). Antimony oxide reacts with the hydracids (HCl or HBr) generated by the halogenated flame retardants to form antimony oxyhalides, which are much heavier than the native hydracids, thus prolonging their residence time in the flame. All these oxyhalides lead to the formation of $SbCl_3$ or $SbBr_3$, which act as scavengers of radicals such as $H^\bullet$:

$$SbCl_3 + H^\bullet \rightarrow HCl + SbCl_2 \quad (2.24)$$

$$SbCl_2 + H^\bullet \rightarrow HCl + SbCl^\bullet \quad (2.25)$$

$$SbCl + H^\bullet \rightarrow HCl + Sb^\bullet \quad (2.26)$$

Moreover, antimony oxide and $Sb^\bullet$ can also react by a parallel oxidation mechanism and participate in the scavenging of radicals [44]:

$$Sb + OH^\bullet \rightarrow SbOH \quad (2.27)$$

$$SbOH^\bullet + H^\bullet \rightarrow SbO^\bullet + H_2 \quad (2.28)$$

$$SbO^\bullet + H^\bullet \rightarrow SbOH \quad (2.29)$$

Synergistic effects can also be obtained by combining the gas phase action of halogen species with the condensed-phase action of phosphorus-based compounds. Improved fire performances can thus be achieved by the use of mixtures of halogenated and phosphorated flame retardant compounds, or by incorporation of substances containing both phosphorus and halogen groups in their molecular structure. Indeed, phosphorus halides or oxyhalides are excellent free-radical scavengers, better than hydrogen halides (HX), and can release more halogen-based radicals due to the P–X bond being weaker than the C–X bond. In addition, the phosphorus contained in phosphorus halides or oxyhalides can also act in the condensed phase to promote the formation of a protective char layer.

However, due to toxicological and environmental concerns, halogen flame retardant additives are currently being phased out and replaced, and the latest research trends mostly focus on the development of new halogen-free flame retardant systems together with combinations of traditional flame retardant additives exhibiting enhanced efficiency when combined together [67].

For instance, the use of nitrogenated additives combined with phosphorus flame retardants can produce interesting synergistic effects [73]. The formation of phosphorus–nitrogen intermediates can accelerate the in situ production of phosphoric acid and therefore polymer phosphorylation. P–N bonds are more reactive than P–O bonds in the phosphorylation process. They maintain phosphorus in the condensed phase, yielding crosslinked networks that promote more intensive char formation. Phosphorus–nitrogen synergism is not a general phenomenon but depends on the nature of the phosphorus and nitrogen flame retardants, as well as the chemical structure of the polymer.

Other types of synergism can be considered. For example, in order to preserve the flame retardant effect beyond 400°C and decrease the total filler loading rate, the endothermic effect of metallic hydroxides can be improved by the use of other flame retardant systems. Metal borates and particularly zinc borates have frequently been used as synergistic agents for metal hydroxides in polyolefin matrices. Partial substitution of 3 wt% of MDH by zinc borate ($2ZnO{\cdot}3B_2O_3{\cdot}H_2O$) in EVA (8 wt% vinyl acetate at a global filler percentage of 40 wt%) [89] increase the LOI value from 38.5 to 43% and decreases the peak heat release rate (HRR) recorded by cone calorimetry. In this system, the thermal decomposition of MDH catalyzes the decomposition of zinc borate, generating boron oxide at lower temperature. A vitreous layer is then formed in combination with MgO located at the material surface [89]. Moreover, the combination of both fillers triggers a physical effect corresponding to the formation of an expanded vitreous layer more mechanically resistant than the crust formed with magnesium dihydroxide alone. The physical barrier effect of the protective layer formed can be improved by the addition of lamellar talc particles to magnesium dihydroxide and zinc borate in ternary systems [90]. The combination of a small fraction of organomodified montmorillonite and talc together with magnesium hydroxide also considerably reduces the pHRR value and generates a cohesive residue.

The action in the polymer of nanoparticles alone proves to be insufficient for ensuring adequate fire resistance to meet the required standards. However, their association with other flame retardant systems such as phosphorated compounds could potentially be a very interesting approach. Several recent works have focused on such methods. For example, Laachachi et al. [91] combined the flame retardant action of nanometric metallic oxides ($TiO_2$, $Al_2O_3$) with the char formation induced by phosphorated flame retardant systems (ammonium polyphosphates and phosphinates) in PMMA. In the case of aluminium phosphinate supplied by Clariant under the trade name Exolit OP930 (phosphinate), cone calorimeter results showed that partial substitution of phosphinate by alumina nanoparticles promoted synergistic effects, with a marked decrease in peak HRR. However, no significant effect could be achieved with $TiO_2$ nanoparticles.

## 2.14 Smoke Evolution

Most of the work done on smoke generation during polymer burning has taken place over the last 20 years or so beginning with the development of test methods for measuring smoke density from burning materials. Even now, no single smoke test is universally recognized for its predictive ability or high correlation with real fire situations. The term smoke has a vague definition. In general use, smoke is considered to be a cloud of particles, individually invisible, which is opaque as a result of scattering and/or absorption of visible light. Fumes are considered to be less opaque forms of smoke.

Among the combustion gases, carbon monoxide, CO, is of chief concern [92]. Other toxic gases can be formed in fires include hydrogen cyanide, nitrogen oxides, hydrogen chloride, sulphur oxides and some very toxic organics. In certain fire situations both aspects can be of comparable concern, since the loss of visibility due to heavy smoke can hinder escape until toxic gas concentrations and temperatures become critical. Presumably, reductions in the rate or intensity of visible smoke development will help to increase escape time, hence the need to develop effective smoke suppressants for polymers.

Visible smoke from burning polymers is generally a result of incomplete combustion. Since polymer flames are diffusion flames, proper mixing for complete burning does not readily occur.

Recent investigations using pyrolysis-gas chromatography/mass spectroscopy and special kinetic methods, have shown that within a flame, unsaturated hydrocarbon molecules formed by thermal cracking of the fuel will polymerize and dehydrogenate to form carbon, or soot. During these processes intermediate molecules can form unsaturated species or they can cyclises to form polybenzenoid structures, both of which will lead to soot formation. These polybenzenoid structures take on more importance as intermediates when they are formed directly from aromatic fuels. More detailed reviews of the chemistry of flames and soot formation have been published [93, 94].

In the presence of a sufficiently intense heat source a polymer will pyrolyze, breaking down to low molecular weight species. These species diffuse from the solid phase into the gas phase, where they form the smoke observed in the absence of flame. At high heating rates and with ignition, these low molecular weight species fuel the polymer flame. Aliphatic fuels are cracked to smaller alkyl radicals which, in the absence of oxygen grow to form conjugated polyenes or polybenzenoids which may be radical, ionic, or neutral. Ultimately the intermediates, which are highly reactive, react with other unsaturated species and condense to form soot. Aromatic fuels are thought to proceed directly to polybenzenoid intermediates. In these cases, heavy soot formation occurs rapidly. Since oxidation to oxides of carbon is competitive with soot formation, oxygen containing fuels generally show a decreased tendency for soot formation. On the other hand, halogens may promote soot formation through dehydrohalogenation, assisting ring closure and the formation of olefins and polyenes [95].

The nature of the cracked species and pyrolyzates generated is thus a major factor in determining smoke formation, given similar conditions of polymer combustion. Pyrolyzates of some common polymers are listed below:

- polyethylene – ethylene, propylene, higher olefins
- poly(methyl methacrylate) – methyl methacrylate (monomer)
- polystyrene – styrene, styrene oligomers, aromatics
- polyurethanes – aromatic isocyanates and amines, aldehydes
- poly(vinyl chloride) – HCl, benzene, other aromatics and low molecular weight alkenes and alkanes
- poly(ethylene terephthalate) – acetaldehyde, unsaturated esters, carboxylated aromatics

The relative distribution of pyrolysis products from an individual polymer is dependent on the pyrolysis temperature, the heating rate and the pyrolysis atmosphere. For example, it has been shown in a series of polyesters that yields of styrene and toluene pass through maxima at 600-700°C [96] and naphthalene is found among the pyrolyzates at 700°C and above. The amount of smoke generated in a nitrogen atmosphere passes through maxima with increasing temperature in several of the polyesters whereas from others the smoke increases steadily with temperature. A study of the variation of smoke intensity with temperature for a group of 8 natural and 12 synthetic polymers showed that smoke density passes through a maximum in the region of 400-600°C apart from poly(methyl methacrylate) [97].

### 2.14.1 Effect of Polymer Structure on Smoke Formation

The structure of a polymer influences both flammability and smoke formation [98]. Polymers with aliphatic backbones, or those that are largely aliphatic and oxygenated, have a tendency toward low smoke generation, while polyenic polymers and those with pendant aromatic groups generally produce more smoke. There are two important exceptions to this simple rule, the saturated polymers poly(vinylchloride) and poly(vinylidene chloride). In poly(vinylchloride), dehydrohalogenation gives a polyenic structure which cyclises to form aromatic products, while poly(vinylidene chloride) forms more char and gives different volatile pyrolyzates. Polymers with high thermal stability or which form small amounts of flammable pyrolyzates generally produce little visible smoke. Increasing char formation is one way of minimizing the yield of pyrolyzates and hence smoke reduction. Structural factors in smoke generation are thus important, as they contribute to the inherent stability of the polymer and largely determine the nature of the pyrolyzates which form the combustion fuels. The following much simplified generalizations about structural factors can be made:

- Aromatic and polyenic polymers have greater tendencies to produce smoke than aliphatic or oxygenated polymers.

- Polymers with aromatic units in the backbone have lower tendencies to reduce smoke than polymers with pendant aromatic groups.

- Halogenation to low or intermediate levels tends to increase the amount of smoke formed, but highly halogenated polymers have reduced smoking tendencies.

- The amount of smoke produced is related to the types of fuels formed on degradation and to the degree of thermal stability of the polymers.

Many other factors such as sample size, sample orientation, ventilation, heat flux etc. also contribute to the amount of smoke formed.

### 2.14.2 Smoke Suppressant Technology

The combustion of polymers involves a variety of processes (both physical and chemical) occurring in several phases. Thus, polymer melting and degradation, heat transfer in both solid and liquid phases and diffusion of the breakdown products through the degrading polymer into the gas phase accompany the various combustion reactions which occur. As a result, polymers and polymer formulations can be modified so that additive smoke suppressing compounds are effective in reducing smoke during burning. Several of the smoke suppressant additives known to be effective in burner fuels are also effective in polymers. Approaches used for reducing smoke during burning have included the use of fillers, additives, surface treatments, and structural modification of the polymers themselves. Certain chemical reactions occurring during combustion processes affect the generation of visible smoke.

Gas phase act of smoke suppressants are; oxidation and hindered nucleation of soot, flocculation and growth of soot particles, dilution of the fuel, modification of the type and composition of pyrolyzates and modification of flame temperatures.

Solid and liquid phase performance of smoke suppressants are; dilution of combustible polymer content, dissipation of heat, surface insulation and protection of combustible substrate, promotion of char formation, alteration of pyrolysis reactions and energy flow, reduction of polymer mass burning rate.

### 2.14.3 Smoke Suppressants for Polymers

#### 2.14.3.1 Fillers

Fillers are non-polymeric compounding materials used at concentrations greater than about 20% of the polymer mass and often at concentrations as high as 40%. Two classes of fillers, based on their apparent smoke suppressant functions are known: they are inert and active smoke suppressant fillers.

Inert fillers reduce the amount of smoke generated from a given mass or volume of a polymer simply by diluting or reducing the amount of combustible substrate present and also by absorbing heat to reduce the burning rate. Examples of such fillers are silica ($SiO_2$), clays, $CaCO_3$, and carbon black. It is possible that filler may be inert in one polymer system, but active in another. For example, $CaCO_3$ often remains unchanged during the combustion of polypropylene, but will react with HCl formed during combustion of chlorinated polymers. Inert fillers usually give only marginal improvements in flame retardancy, unless present in very high concentrations.

Active fillers promote the same diluents and heat absorption functions as inert fillers, but they absorb more heat per unit weight by endothermic processes. Gases such as water, carbon dioxide, or ammonia, released during heating may also dilute the fuel volatiles and modify flame reactions. Examples of currently used active fillers include

$Al(OH)_3$ [99, 100], basic magnesium carbonate, $Mg(OH)_2$ [101, 102] and talcs. In these the water of hydration and/or carbon dioxide is released at temperatures approximating to those of polymer decomposition, producing both flame-retardant and smoke suppressant effects.

The physical properties of polymers are often badly affected by the addition of fillers. Loss of impact and tensile properties in other polymers can be somewhat reduced by the addition of impact modifiers.

#### 2.14.3.2 Additive Compounds

Additives are generally non-polymeric compounding substances used at levels below about 20% of the polymer resin. A number of different types of additives have been shown or are claimed to have smoke suppressant properties. By far the largest class of smoke suppressants are metal compounds (mainly oxides or hydroxides) used in poly(vinylchloride) (PVC) and other halogen containing polymers. Non-metallic additives include some dicarboxylic acids, sulphur, and various plasticizers and surfactants.

A brief discussion of some of the more effective, and most frequently used metal based additives were given in the following section:

Antimony oxides, e.g. $Sb_2O_3$ and $Sb_2O_5$, although widely used flame retarding additives in halogen containing polymers such as PVC, are not considered as smoke suppressants because their effect on smoke production is variable. Some commercial modified antimony oxides have been introduced which claim to reduce smoke generation in PVC. Antimony (V) oxide is more effective in reducing smoke than antimony (III) oxide [103].

Ferrocene (dicyclopentadienyl iron) was one of the early additives for which synergistic flame retardancy and smoke suppression was claimed [104, 105]. Other, less volatile, organo-iron compounds have been investigated as potential smoke suppressants for PVC (rigid and plasticized). Basic iron (III) oxide (FeOOH) is especially effective and has been shown to have excellent smoke suppressing effects in a wide range of chlorine containing polymers and blends of these with other polymers, especially ABS. Recently FeOCl has been identified as the active char forming, smoke suppressing compound formed by reaction of FeOOH with HCl at low temperatures, while iron (III) oxide and iron (III) chloride are formed at higher temperatures. Iron (III) and ferricenium chlorides have also been shown to suppress the formation of benzene and smoke in PVC and CPVC.

Zinc compounds have also been shown to impart smoke suppressant characteristics, largely in chlorinated polymers. Smoke suppressant effects appear to be optimum at 1 phr or lower. Synergistic flame retardant and smoke suppressant effects are found in PVC formulations when used in combination with antimony oxide. Some examples of synergistic effects on flammability and smoke generation have also been recognized with other zinc compounds such as zinc borate in chlorine containing polymers.

Metal compounds (mainly oxides) are added alone or in combination with antimony oxide or alumina trihydrate. However, strong smoke suppressant effects have been achieved in a number of cases by combining two or more metal oxides in an additive system. Kroenke has reviewed the smoke suppressing activity of a wide range of metal compounds (mainly oxides) separately and in combination [106]. The first examples of this were in patents claiming the use of iron powder in combination with copper (I) oxide or molybdenum trioxide [107].

## 2.15 Laboratory Techniques for Flammability Characterization of Polymers

### 2.15.1 Underwriters Laboratory UL 94 Test

The UL 94 test is commonly used to determine the ignition resistance of materials used in the electrical industry. The test results are giving in flammability ratings V-0, V-I, or V-2. The V-0 rating is the best flammability rating, which a material can receive. The criteria for which the materials are rated are based on the time it takes for the burning material to extinguish after the flame source is removed from a vertical specimen, and also if drips fall from the burning specimen. The specifications for the size of the test specimen are either, 12.7 x 1.27 x 0.16 cm or 12.7 x 1.27 x 0.32 cm. Either one of these two samples is mounted into a clamp vertically so that the lower end is 30.5 cm above a 0.6 cm thick layer of a specified surgical cotton. The test specimen is exposed from a flame source from below for duration often seconds.

**Table 2.7** UL 94 rating scale

| Rating | Criteria |
|---|---|
| Class 94 V-0 | Having a series of five specimens with ten ignitions, the sum of the after flame times should not exceed 50 sec and no specimen should burn longer than 10 seconds. During ignition and combustion the cotton layer should not be set on fire by dripping material |
| Class 94 V-I | Having a series of five specimens, which are ignited twice, the sum of after flame times should not exceed 250 seconds, no specimen should burn longer than 30 second, the dripping material should not ignite the cotton layer. |
| Class 94 V-2 | Same as V-I, except that the cotton layer is ignited by burning drops. |

The flame source is then removed. If the specimen extinguishes, the specimen is exposed to the flame for an additional ten seconds. Table 2.7 shown below outlines the criteria for each UL 94 rating.

### 2.15.2 Vertical Burn Test (ASTM D-568 and D-3801)

The sample is suspended vertically, so that it can be ignited at the bottom. After ignition, the ignition source (usually a bunsen burner) is withdrawn and the length of burn of the sample in a set period of time (10 seconds) is measured. If the sample does not burn for the entire time, the time to extinguish is noted. Materials which burn while the ignition source is in contact but go out quickly when it is removed are termed self extinguishing. This test is most useful in measuring the burning characteristics of similar materials. Dripping of the resin should be noted.

### 2.15.3 Horizontal Burning Rate Test (ASTM D-635)

This test is similar to the vertical burn test except that the sample is supported horizontally. This test is less stringent and is used when the vertical test cannot distinguish between materials. Only self supporting materials should be tested in the horizontal test.

### 2.15.4 Limiting Oxygen Index Test (LOI) (ASTM D-2863)

This test is probably the most accurate of the lab tests. In the LOI test a sample is suspended vertically so inside a closed chamber (usually a glass or clear plastic enclosure). The chamber is equipped with oxygen and nitrogen gas inlets so that the atmosphere in the chamber that it can be controlled. The sample is ignited from the bottom and the atmosphere is adjusted to determine the minimum amount of oxygen to just sustain burning. This minimum oxygen content, expressed as a percentage of the oxygen/nitrogen atmosphere, is called the oxygen index. Higher numbers are associated with decreased flammability.

LOI value is calculated according to the equation given below:

$$\text{LOI} = \frac{[O_2]}{[O_2]+[N_2]} x100 \qquad (2.30)$$

### 2.15.5 The Cone Calorimeter Test (ISO 5660)

The cone calorimeter test is a bench-scale test used to determine the reaction to fire for surface lining materials used in buildings. The test apparatus consist basically of an electric heater, an ignition source and a gas collection system, as shown in Figure 2.6.

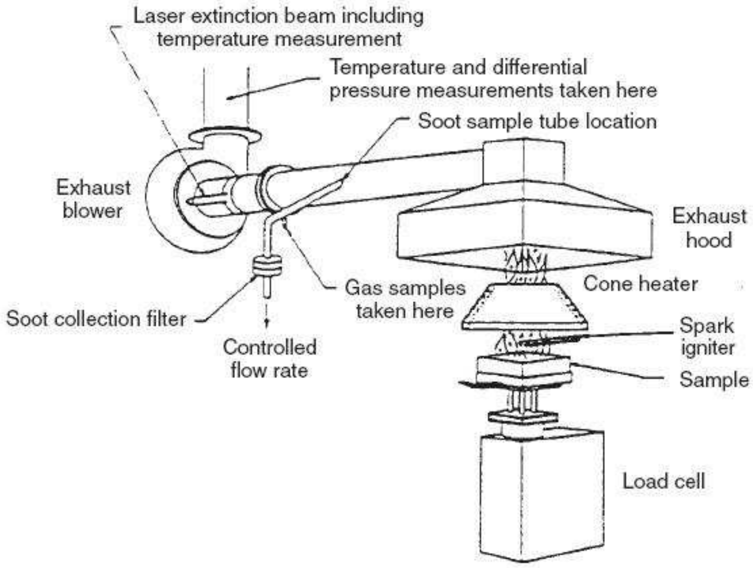

**Figure 2.6** Cone calorimeter test set-up [108]

The test specimen measures 100 x 100 mm and has a thickness between 6 mm and 50 mm. During the test the specimen is mounted horizontally on a low heat loss insulating ceramic material. The orientation of the specimen can also be vertical, but this position is mainly used for exploratory studies.

After the test specimen has been mounted and placed in the right position, it is exposed to a heat flux from the electric heater. The output from the heater can be chosen in the range of 0-100 kW/m$^2$, but usually the heat output is in the range of 25-75 kW/m$^2$. When the mixture of gases above the test specimen is higher than the lower flammability limit, it is ignited by an electric spark source. The duration of the test is normally 10 minutes but is not fixed and can vary, depending on the material. Many variables are measured but the main results from each test are:

- Time to ignition (TTI)
- Mass loss rate (MLR)
- Heat release rate (HRR)

If a gas analyzer is added to the test equipment it is also possible to take the production of smoke and toxic gases into account.

### 2.15.6 Radiant Panel Test (ASTM E-162)

A commonly used laboratory scale flame spread test for engineering thermoplastics in the United States is the ASTM E162 Radiant Panel Test. A sample is placed in the test apparatus that exposes the test specimen to a radiant panel and a small pilot flame. The specimen is 15.24 cm wide by 45.72 cm long and is inclined at an angle of 30 to a radiant panel held at a temperature of 680°C. The thickness of the specimen that is tested is determined by the final product dimensional thickness. A small flame is positioned at the top of the test sample to ignite any volatile gases that have been given off. The rate at which the sample is burning is measured ($F_s$) and the heat that rises off the plaque is also measured (Q) in a flue stack above the test piece. These combined values determine the index of flame spread (I) for the burning substrate. This calculation is given in Equation 2.31.

$$I_s = F_s \times Q \qquad (2.31)$$

### 2.15.7 Smoke Chamber Test (ASTM E-662)

Combustion research has shown that many fire fatalities occur in rooms where the flames never reach. Hence, the nature of the smoke generated in a fire is very important. This test is designed to measure the density of the smoke generated as a function of time, under both flaming and smoldering conditions. Because this test was originally developed by the National Bureau of Standards (NBS), the test is sometimes referred to as the NBS smoke density test. The test apparatus is a closed box (smoke chamber), approximately 3 x 3 x 2 feet which contains an optical light source and detector to measure the reduction of optical density from the smoke generated by the burning of a sample placed inside the chamber. The sample is small (3 x 3 x 1/4 inches, usually). Results are usually expressed as a smoke density, $D_s$, after a 1.5 or 3.0 minutes.

### 2.15.8 Steiner Tunnel Test (ASTM E-84)

This test measures the flame spread and smoke generated by the burning of a sample within a large (25 x 2 foot) chamber. The principal use of the test is for building materials. The sample is attached to the top of the chamber and a fire is started at one end. The rate and extent of burning are reported. The cost of performing this test is relatively high, as is the cost of the materials because of the large sample size.

### 2.15.9 Thermogravimetric Analysis (TGA)

The thermogravimetric analysis (TGA) technique uses heat to cause physical and chemical reactions to take place in the materials being tested. TGA provides a quantitative measure of the mass change of a polymer material when placed in an increasing temperature environment. These changes in mass can be caused by dehydration, decomposition, or oxidation.

TGA can provide some indication of the flame retardancy of polymers by measuring the amounts of residual char. With increasing amounts of residual char, a correlation has been found to an increasing resistance to burning of the polymer material. The TGA of non-flame retardant materials can be compared to those that have flame retardants in them to determine when and how the flame retardant mechanism is being activated. This can be an indicator if the flame retardant mechanism is occurring in the vapor or condensed phase.

TGA can also be used to determine the flame retardant mechanism will occur before the polymer degrades. This is the optimum reaction temperature for the flame retardant so that it will react and interfere with the plastics combustion process before the plastic starts to burn.

Experiments involve both isothermal weight-loss measurements and nonisothermal techniques. The isothermal technique requires almost instantaneous heating of the polymer sample to the desired temperature. The non-isothermal technique involves a programmed linear increase of sample temperature as a function of time. It is also very convenient for getting the mass loss rate versus time (DTG curve) by differentiating the TGA curve. DTG is a good procedure to identify the temperature range at which the various stages of thermal decomposition take place and the order in which they occur. In addition to the rate of decomposition, the heat involved in the decomposition process is also of interest.

### 2.15.10 Pyrolysis GC/MS Spectroscopy

In electron impact-mass spectrometry organic compounds are evaporated into the gas phase and usually ionized by interaction with an electron beam and abstraction of an electron from the molecule. As this ionization process is not a real electron impact the energy transmitted to the molecule cannot be controlled. Experiments have shown that cations (molecular ions or parent ions) are produced, if the electron beam energy exceeds the appearance potential of organic compounds (about 9-13 eV [109]). With increasing electron voltage, additional energy can be transferred to the molecular ion, which together with the thermal excitation from evaporation is used to stabilize the primary radical-ions by further fragmentation reactions. The intensity of fragment ions increases up to 40 eV more than the intensity of the molecular ions, whereas between 40 and 100 eV a nearly constant ratio is found. The mechanisms of electron-impact induced fragmentation reactions are characteristic for functional groups or classes of organic compounds and can be used to identify unknown molecular ions. If polymers are brought into a mass spectrometer, they neither can be evaporated nor ionized. Upon heating the polymer samples, the temperature of initial thermal decomposition can be detected very sensitively, since the produced volatile pyrolysis products are ionized and registered as total ion current before leaving the ion source. As the sensitivity of a mass spectrometer is in the range of $10^{-9}$ g, a sufficient amount of pyrolysis products is evaporated at degradation rates of about % weight loss of polymer/mm). Low degradation rates mean low pyrolysis temperatures and selective degradation mechanisms, which would preserve characteristic structural elements in the pyrolysis products and correspond to the assumption that diagnostic fragments allow the elucidation of degradation mechanisms.

The schematic drawing of a typical mass spectrophotometer is given in Figure 2.7.

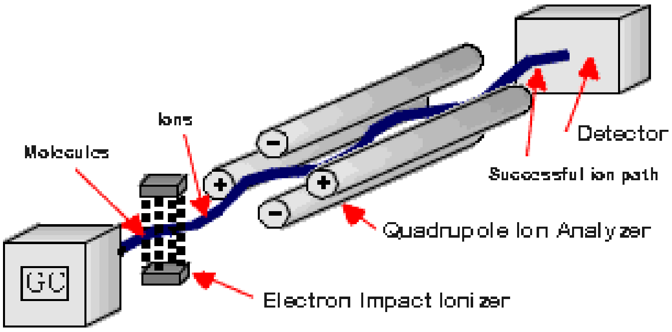

**Figure 2.7** Parts of a mass spectrophotometer [110].

All mass spectrometers consist of three distinct regions: Ionizer, ion analyzer, detector

Ionizer: In the GC-MS, the charged particles (ions) required for mass analysis are formed by Electron Impact (EI) Ionization. The gas molecules exiting the GC are bombarded by a high-energy electron beam (70 eV). An electron which strikes a molecule may impart enough energy to remove another electron from that molecule. Methanol, for example, would undergo the following reaction in the ionizing region:

$$CH_3OH + 1\ \text{electron} \rightarrow CH_3OH^{+\cdot} + 2\ \text{electrons} \qquad (2.32)$$

Ion Analyzer: Molecular ions and fragment ions are accelerated by manipulation of the charged particles through the mass spectrometer. Uncharged molecules and fragments are pumped away. The quadrupole mass analyzer in this example uses positive (+) and negative (-) voltages to control the path of the ions. Ions travel down the path based on their mass to charge ratio (m/z). EI ionization produces singly charged particles, so the charge (z) is one. Therefore an ion's path will depend on its mass.

Detector: There are many types of detectors, but most work by producing an electronic signal when struck by an ion. Timing mechanisms which integrate those signals with the scanning voltages allow the instrument to report which m/z strikes the detector. The mass analyzer sorts the ions according to m/z and the detector records the abundance of each m/z.

### 2.15.11 Other Techniques

Common differential scanning calorimetry (DSC) cannot be used for thermal decomposition process due to its low applicable temperature (below 600°C). Simultaneous thermal analysis (STA) with TGA and DSC performed at the same time to a high temperature of 1200°C, is very useful in measuring the heat evolved or absorbed during decomposition. In addition to the kinetics and thermodynamics of the thermal decomposition process, there are also concerns with the nature of the decomposition process. There are also some other methods which can be used to characterize volatiles, such as infrared spectroscopy (IR) and thermal volatilization analysis (TVA). Chars are complex materials which are usually insoluble. This limits their characterization to the tools used in solid-state chemistry and physics. The chemical structure of the char is usually characterized by elemental analysis. Other properties are characterized through microscopy, various spectroscopies, X-ray diffraction, and thermal conductivity. In all, it is not easy to evaluate the fire behavior of polymers because the thermal decomposition processes of polymers are varied and complex and the fire performance of polymers are also dependent on the test methods and experimental conditions used.

## 2.16 Poly(ethylene terephthalate) PET

Poly(ethylene terephthalate), PET, is one of the most commercially used thermoplastic. PET is a linear condensation polymer that has been used in applications that have seen rapid growth especially as packaging material for carbonated beverages since it was introduced as a container resin. Prior to this surge in use, PET was used as food packaging film, including boil-in-bags for frozen vegetables, and most commonly for the production of fiber for clothing and other applications. The structure of PET is as follows:

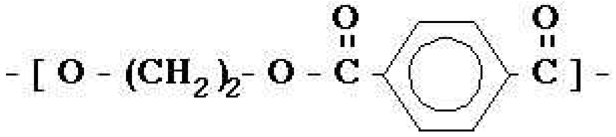

**Figure 2.8** Chemical structure of PET

PET is a step-growth (condensation) polymer derived from terephthalic acid (TPA) or dimethyl terephthalate (DMT) and ethylene glycol (EG) PET is a linear molecule that exists either in an amorphous or a crystalline state. In the crystalline state, the molecules are highly organized and form crystallites, which are crystalline regions that extend no more than a few hundred angstrom units. The maximum crystallinity level that can be achieved is probably no more than 55% [111].

### 2.16.1 Flammability of PET

Poly(ethylene terephthalate), PET, has substantial commercial value in the form of fibers (Dacron) and flexible film (Mylar) due to its good mechanical strength and resistance toward solvents. PET is prepared commercially by the polycondensation of dimethyl terephthalate and ethylene glycol. It has a glass transition temperature, $T_g$ of about 80°C, and a melting point of 260°C [111]. The flammability and retardation of PET are important because of the use of this polymer in clothing and electrical circuits.

In order to be burned, a polymer must first undergo thermal degradation, followed by vaporization and diffusion of the lighter species into the gas phase and hence the flame. Pyrolysis of a polymer involves the cleavage of polymer molecules into two daughter molecules. These undergo further sequential degradative reactions until low molecular weight volatile products are formed. This process should take place at or below the surface temperature of a burning polymer.

It is well established that during the burning process, the concentration of oxygen at the surface of the polymer is so low that the degradation of the polymer can be assumed to take place in the absence of oxygen. In other words, thermooxidative degradation is not significant and the degradation is considered to be purely pyrolytic in nature [55, 112].

The thermal degradation of PET has been studied extensively by several investigators in recent years. Under burning conditions, Granzow [112] reports the limiting oxygen index (LOI) is 20.4% for PET and the surface temperature of the burning polymer is 380°C; dynamic thermogravimetric analysis showed substantial weight loss at about 400°C which implies that the volatile products which act as the fuel for the flame are significantly generated at this point. Under low heating rates (0.1-10°C per min), Cooney et al. [113] and Vijayakumar et al. [114] reported that the degradation of PET takes place in at least four distinct stages; only two stages are distinguishable at higher heating rates, which are combustion conditions. This indicates that thermal degradation of PET is a complex process.

Kinetic studies of the degradation have also been reported [115], but the data obtained differ widely depending on many factors such as the method of determination, atmosphere, temperature, sample mass, sample shape, heating rate, gas flow rate, mathematical treatment used to calculate kinetic parameters, etc. Most investigators do agree that PET decomposes by random chain scission which is the rate determining step and the rate of decomposition follows first-order kinetics.

Most of the earlier investigations on the pyrolysis reactions of PET are based on the analysis of the gas phase, volatile species. These establish that PET decomposes by random chain scission at the ester linkages. On the basis of the identities of the volatile products, two decomposition pathways have been invoked to explain the primary chain-scission. Marshell and Todd [116] proposed the homolytic clevage of a C-O bond followed by the transfer of hydrogen to form a hydroxyl group and an unstable radical.

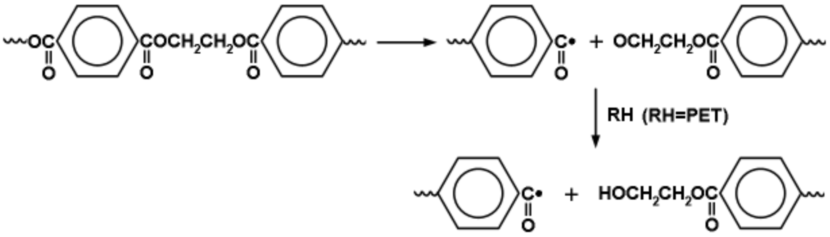

**Figure 2.9** Chain cleavage of PET

However, Goodings [117] reported that the primary chain scission reactions are unaffected by radical scavengers and none of the other investigators have found evidence to substantiate such a free radical mechanism.

Another decomposition pathway proposed for the primary chain scission of PET is a typical ester degradation which involves a cyclic transition state and produces an acid and a vinyl ester [118].

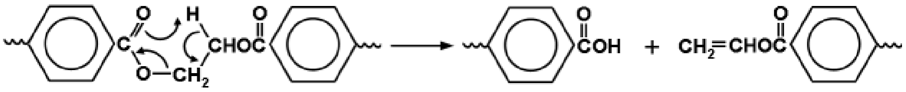

**Figure 2.10** Ester degradation of PET

This mechanism has been confirmed by Bednas et al. [119] and Sugimura [120] with flash pyrolysis, coupled with gas chromatography and mass spectrometry. Divinyl terephthalate, vinyl benzoate derivatives and benzoic acid derivatives were detected in the gas phase.

The three major volatile products of PET, i.e. carbon dioxide, carbon monoxide and acetaldehyde and a large number of minor products [121, 122] are considered to arise from the secondary reactions of the products of chain scission. The proposed decomposition mechanism of PET is summarized in Figure 2.11.

Very little is known about the chemical structure of the char and the reactions involved in its formation. The characterization of this involatile residue is essential to give a comprehensive view of the thermal degradation of PET. Some of the major products found in the nonvolatile residue are terephthalic acid, acidic oligomers, and terphthalic anhydride; nonetheless previous investigations indicate that crosslinking reactions do take place in the solid phase and the result is the formation of char residue. The char is reported to have a high aromatic content [122]. The type of cross-linking and the identity of the crosslinked products are, however, still ambiguous. Goodings [117] reported the appearance of a number of compounds, mainly derivatives of substituted benzoic acids and biphenyl di-carboxylic and mono-carboxylic acids.

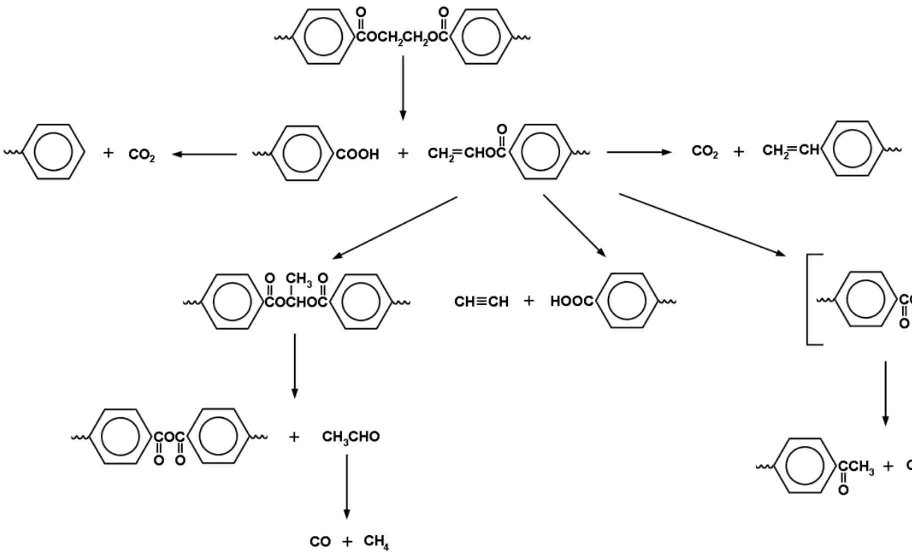

**Figure 2.11** Thermal decomposition pathway of PET that gives volatile products

These compounds were found in very low concentration (0.005-0.09 wt%). Polyene groups also appeared to be present. The formation of these products is presumed to arise from subsequent reactions following the chain scission. Zimmermann [123, 124] reported that crosslinking take place via repolymerization of the vinyl ester. Subsequent reactions generate polyene incorporated into the polymer network as shown in Figure 2.12.

Under thermooxidative conditions, in which the air is drawn through the surface of the degrading PET, a radical chain mechanism is initiated by the formation of peroxide and hydroperoxides radicals, which then decompose differently from that stated in Figure 2.12. Yoda et al. [125] proposed a mechanism similar to Zimmermann, but suggests an interaction between the vinyl ester and methylene radical on the polymer chain instead of repolymerization, as shown in Figure 2.13.

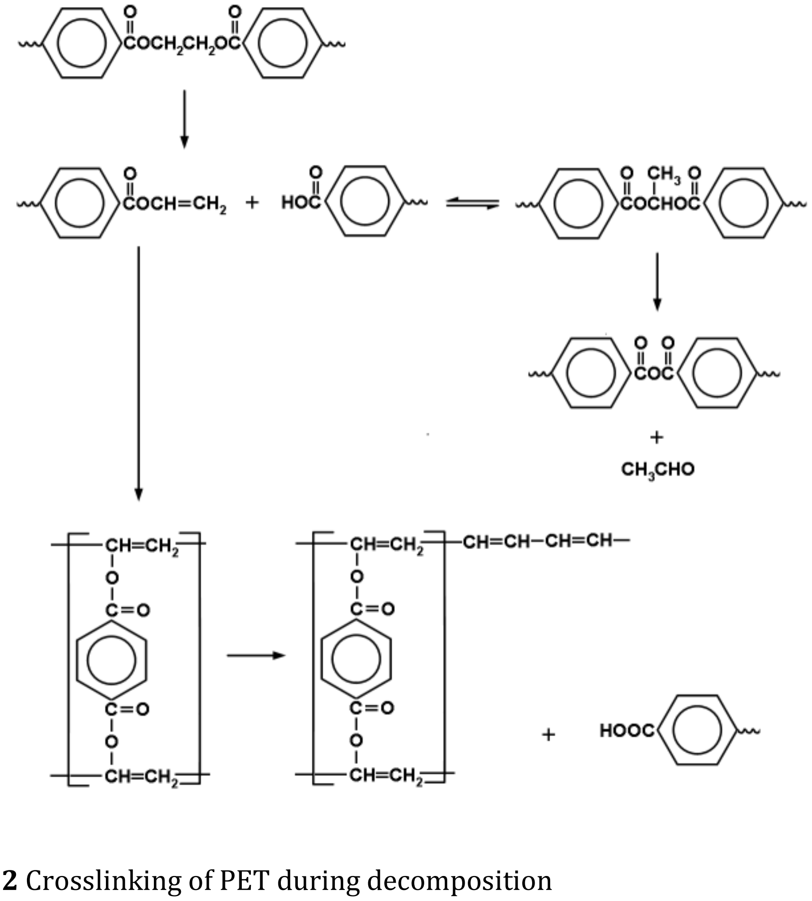

**Figure 2.12** Crosslinking of PET during decomposition

Avondo et al. [122] suggested crosslinking between two aromatic rings by an ethylene moiety produced from the decarboxylation of PET. On the other hand, Nealy and Adams [126] reported the formation of a diphenyl derivative ester, 2,4,5-biphenyltricarboxylate ester, which indicated crosslinking between the aromatic rings.

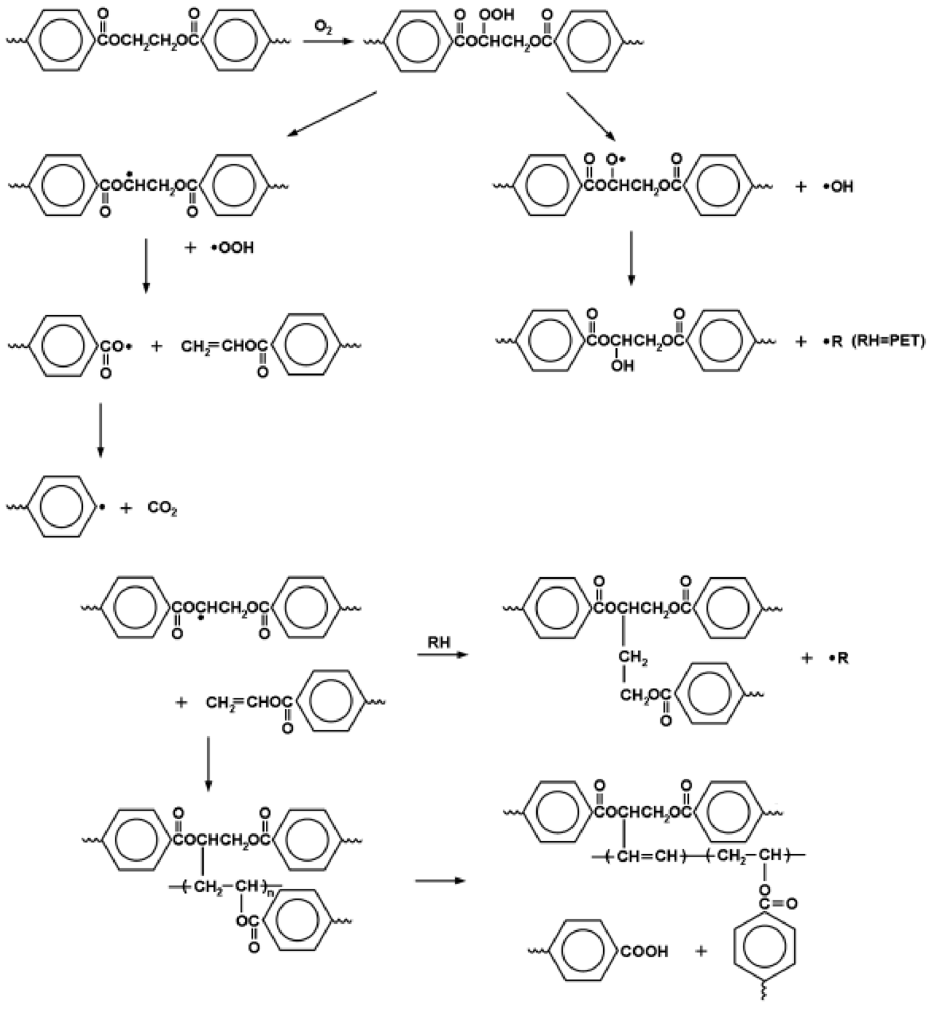

Figure 2.13 Repolymerization of PET during decomposition

In addition, Spinninger [127] reports that 2,4,5-diphenyl ketone tricarboxylate ester was also formed. The thermooxidative degradation mechanism of PET proposed by Nealy and Spinninger is summarized in Figure 2.14.

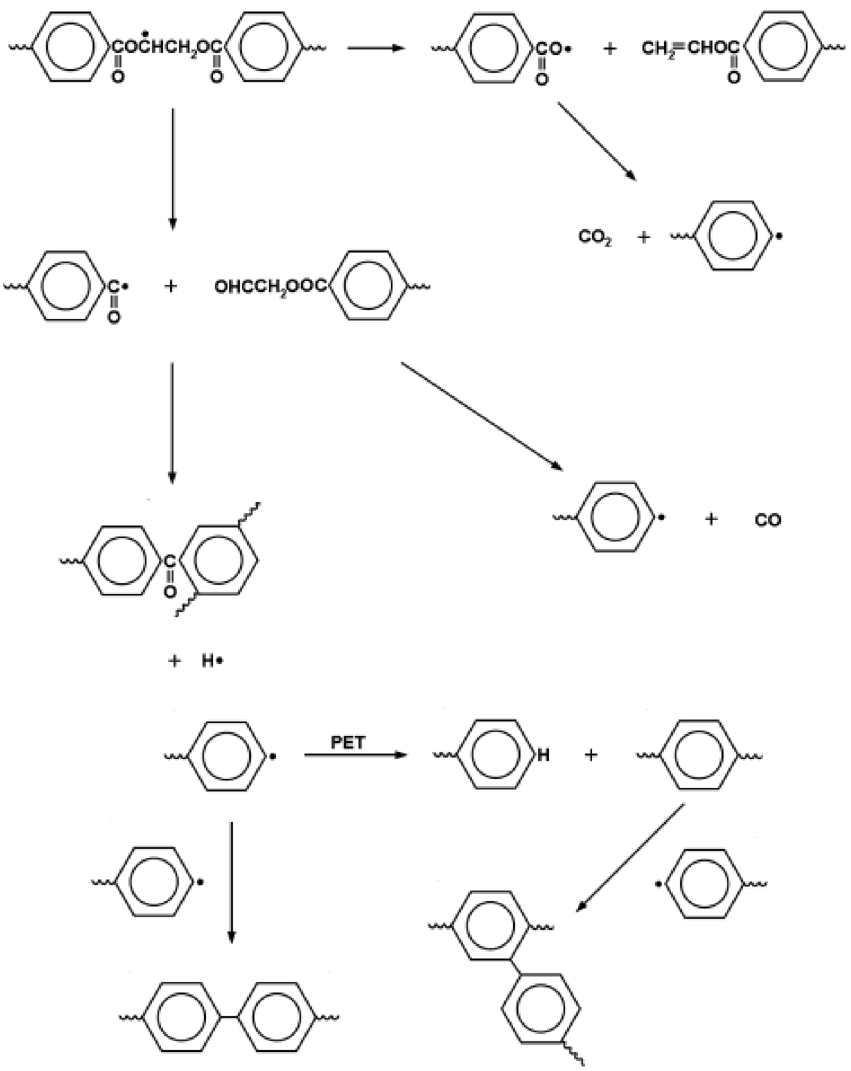

**Figure 2.14** Thermo-oxidative degradation of PET

It should be re-emphasized here that in the thermooxidative process, oxygen in the air plays an important role in the degradation of the polymer. Thermal oxidation of PET has been studied in order to obtain a better understanding of the degradation of PET during the manufacturing process. In the combustion process, PET is considered to degrade in the absence of oxygen.

### 2.16.2 Pyrolysis MS Analysis of PET

The pyrolysis mass spectrum of PET is given in Figure 2.15.

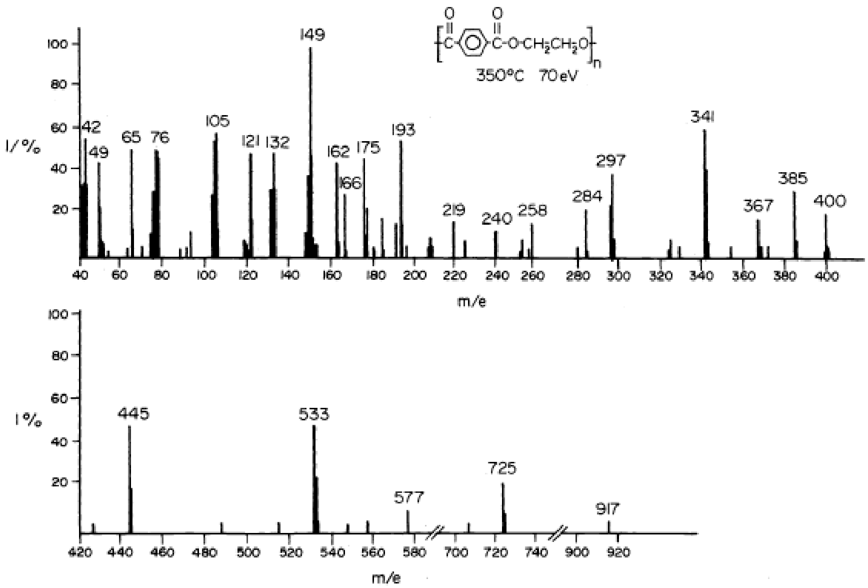

**Figure 2.15** Pyrolysis mass spectrum of PET at 350°C [128]

The molecular weight of the structural unit is 192 and the differences of 192 mass units between the peaks at 917, 725, 533, 341 and 149 indicate that a mixture of oligomeric ions is formed which originate by the same pyrolysis and fragmentation mechanisms [128].

The fragment m/e or m/z 149 is assigned as the carboxonium ion of terephthalic acid. Since in previous studies terephthalic acid was identified as one pyrolysis product of PET, it can be deduced that the series of m/z 149-917 corresponds to oligomers with a thermally formed carboxyl end group.

Applied to a polyester like poly(ethylene terephthalate) the Figure 2.16 implies that thermal degradation should yield a mixture of oligomeric esters.

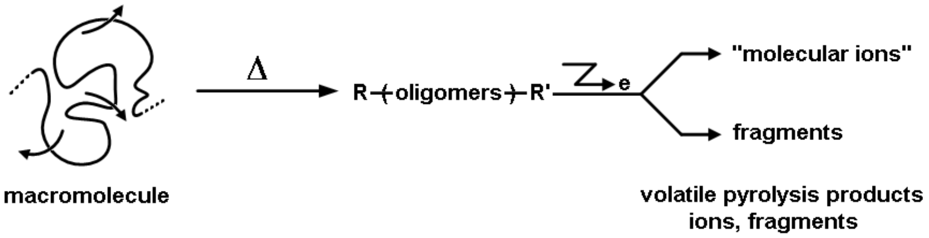

**Figure 2.16** Thermal degradation routes of polymers

$$-\!\left(\mathrm{CO{-}Ph{-}CO{-}O{-}CH_2{-}CH_2{-}O}\right)\!- \xrightarrow{\Delta} \mathrm{R}-\!\left(\mathrm{CO{-}Ph{-}CO{-}O{-}CH_2{-}CH_2{-}O}\right)_{1,2,3\ldots}\!-\mathrm{R'}$$

**Figure 2.17** Formation of terephthalic esters

Low molecular weight esters of terephthalic acid are known to undergo an α-cleavage into carboxonium ions as a characteristic fragmentation reaction followed by a partial elimination of carbon monoxide [129].

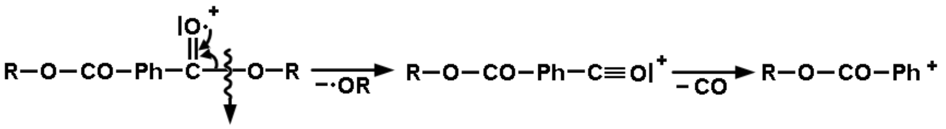

**Figure 2.18** Further fragmentations of terephthalic esters

Therefore, if a mixture of thermally formed terephthalic esters (Figure 2.17) is further fragmented into the ions shown in Figure 2.18, their masses allow the identification of the structure of the end group R and the corresponding pyrolysis mechanism.

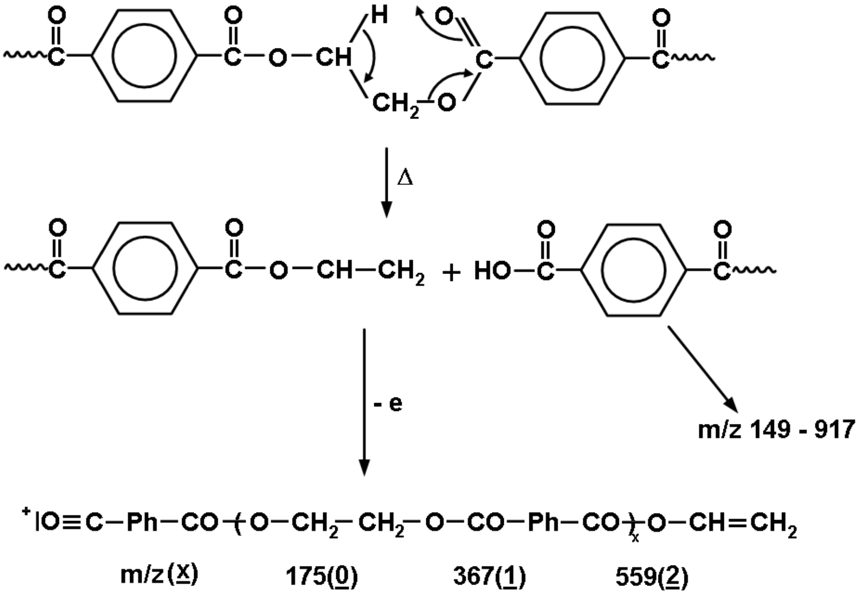

**Figure 2.19** Final pyrolysis mechanism of PET

The supposed pyrolysis mechanism is the thermal cis-elimination which must simultaneously yield carboxonium ions with a thermally formed vinyl ester end group (Figure 2.19).

### 2.16.3 Previous Flammability Studies for PET

A number of studies on the flame retardant capability of compounds based on polyethylene terephthalate (PET) have been performed in recent years, only a few were found to be relevant to this study. The most relevant studies utilized flam-retardant compounds that have either phosphorus or nitrogen (melamine) based additives. Other flame retardant studies for PET have looked at boron type additives [130] , silicone powders [131], and even polymers with flame retardants grafted onto the polymer backbone [132, 133] Studies have been performed using intumescent systems, which are based on phosphorus additives [134].

Koch et al. [135] studied the effects of hexabromobenzene (HBB), triphenyl phosphate (TPP), tricresyl phosphate, pentabromotoluene, and octabromobiphenyl on the oxygen index. The effects that the additives had on thermal and viscosity changes were also studied. The weight percentage for the bromine containing flame retardants varied from 2-10%. For those flame retardants containing phosphorus the concentration range was 0.10-0.50%. The findings of this study showed that concentrations of the bromine additive required could be decreased if a small amount of the phosphorous containing compounds were added.

A study done by Bar-Yaacov et al. [136] looked at the effects of a brominated polymeric additive (BPA) and brominated polystyrene (BPS) on the processing characteristics of PET. The BPA and the BPS varied from 15-18% by weight concentration for all of the tested formulations. They also studied formulations that contained 15% concentration of the primary flame retardant and either antimony trioxide or sodium antimonate added at 3% concentration by weight. It was found that both flame retardants are compatible additives for PET, due to their high degradation temperatures. This is important because PET is processed at high temperatures which if to high can cause some flame retardants to degrade.

Cusack et al. [137] studied the effects of different synergists, in order to replace the usage of antimony trioxide. Zinc hydroxystannate was found to be a successive alternative for the polyester matrix. It is reported that while antimony oxide acts as a flame retardant in the vapor phase, zinc hydroxstannate acts both in the vapor and the condensed phase.

Maspoch et al. [138] investigated the effect of glass fiber and bisphenol A bis-(diphenylphosphate) combinations on recycled PET. Glass fiber was concluded to be a suitable anti dripping agent for PET and with the addition of 1.26% phosphorus additive and 3.5% glass fiber V-0 UL-94 rating could be obtained.

Wang et al. [139] examined the effect of nano layered hydrotalcite (LDH) and brominated styrene (PBS) in the PET matrix. Dispersions of LDH particles were influenced by the LDH concentration, composition of flame-retardant compound and the intrinsic viscosity of PET. The concentration of LDH had an influence on the average size of agglomerates. Oxygen index tests of flame-retardant PET showed that LDH/PBS compound with the nano-dispersion of LDH, i.e., companying lower amount of PBS than PBS only, was an effective flame retardant. Additionally, the mechanical properties of the flame-retardant PET composites had no obvious decrease with the addition of LDH/PBS compound.

Swoboda et al. [140] worked on flame retardant recycled PET blends containing PC and triphenyl phosphite (TPP). PET and PC are first melt blended with a catalyst of transesterification allowing the compatibilization of the blend, before adding TPP. The presence of this last component was shown to stop the transesterification reaction between PET and PC, avoiding chain breaking. In addition, TPP acts as a chain extender of PET, allowing to increase the average chain length. TPP was also shown to be able to act as a flame retardant in pure PET, pure PC and their blends In addition, the blends obtained present enhanced mechanical properties compared to recycled PET, with an increase of flexural modulus of 30%.

# CHAPTER 3

# EXPERIMENTAL

## 3.1 Experimental of Synthesis of 3.5 Hydrated Zinc Borate

### 3.1.1 Materials

Throughout the synthesis of 3.5 mole hydrated zinc borate, different types of zinc oxides were used in order to examine the effects of different parameters. Properties and the suppliers of the zinc oxides are given in Table 3.1.

**Table 3.1** Properties of zinc oxides used in zinc borate synthesis

| ZnO | Manufacturer | Average Particle Size (μm) | Purity (%) |
|---|---|---|---|
| Type 1 | Kartal Oksit, Ankara, Turkey | 25 μm | 99.5 |
| Type 2 | Kartal Oksit, Ankara, Turkey | 25 μm | 98.0 |
| Type 3 | Atlas Oksit, Ankara, Turkey | 20 μm | 96.0 |
| Type 4 | Aldrich | < 1 μm | 99.9 |
| Type 5 | Aldrich | 50-70 nm | 99.9 |

Other chemicals used for the zinc borate synthesis were as follows. The boric acid was supplied by ETI Mine Works with a molecular weight 61.83 and a molecular formula of $B(OH)_3$ with 99.9% purity. Commercial 3.5 mole hydrated zinc borates, called Firebrake ZB and Firebrake ZB Fine obtained from U.S Borax, with contents of 37.5% ZnO and 48% $B_2O_3$ and average particle diameter of 9 μm and 3 μm respectively, were used as seed crystals.

### 3.1.2 Synthesis of 3.5 Hydrated Zinc Borate on Laboratory Scale

The synthesis of $2ZnO\cdot 3B_2O_3\cdot 3.5H_2O$ was done in accordance with the reaction given in Reaction 3.1.

$$6B(OH)_3\,(aq.) + 2\,ZnO\,(s) \rightarrow 2ZnO\cdot 3B_2O_3\cdot 3.5H_2O\,(s) + 5.5H_2O\,(l) \qquad (3.1)$$

In this study, zinc borate was synthesized in 4 liter stainless steel batch reactor. Reactor was equipped with a mechanical stirrer, heat controlling unit and sample taking hole (Figure 3.1).

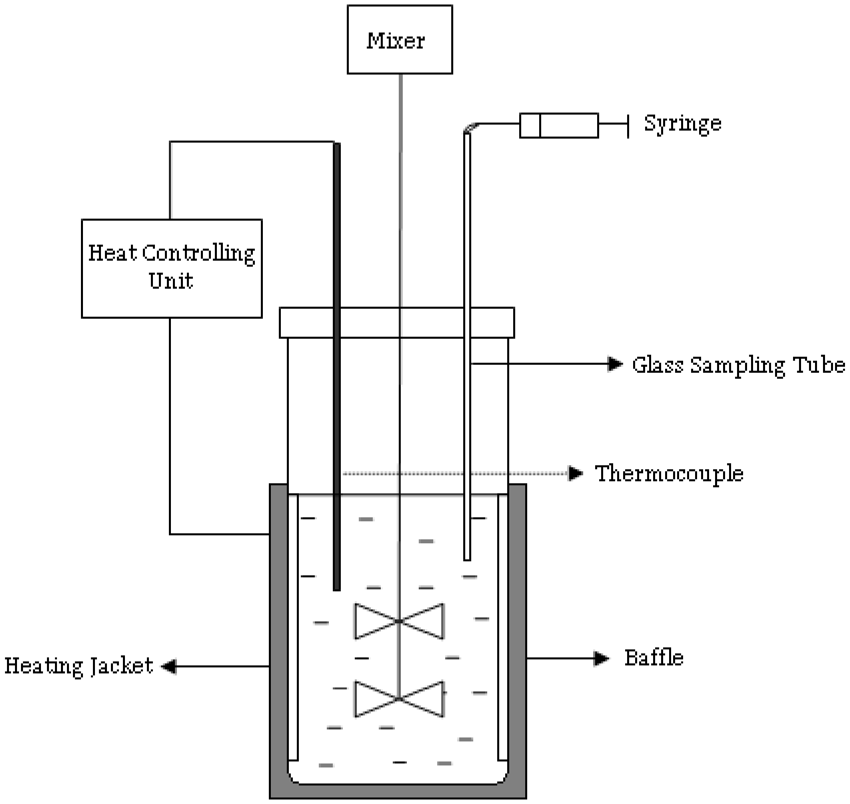

**Figure 3.1** Schematic of laboratory scale batch zinc borate production reactor

During the reaction, reactor was sealed as good as possible to prevent evaporation of water from the system. The experiments were carried out by first dissolving the required amount of boric acid in the reactor. Boric acid amount was calculated as to be at saturation concentration at 85°C. 2.5 liter distilled water, was fed to the reactor initially. Reactor was heated to 85°C. For the laboratory scale production $B_2O_3$:ZnO mole ratio was kept constant as 5:1 in all cases. After boric acid was completely dissolved in water, zinc oxide was added to make the molar ratio of $B_2O_3$ to ZnO be 5. An excess amount of boric acid was used to ensure the formation of $2ZnO{\cdot}3B_2O_3{\cdot}3.5H_2O$. Desired amount of Firebrake ZB and/or Firebrake ZB Fine were used as seed crystals in reactor. This mixture was reacted with stirring at 85°C for 4 hours. To examine the effect of baffle presence to the reaction, in some sets of experiments laboratory scale reactor was equipped with four baffles placed like a crosshair. Baffles were 18 cm long, 17 mm wide rectangular stainless steel plates with a thickness of 0.5 cm. They were placed 5 cm above the reactor bottom. Including the initiation of the reaction, samples were taken at a time interval of every 30 minutes from reactor to perform chemical analysis to determine ZnO and $B_2O_3$ amounts in the solids filtered from the sample mixture. After 4 hours, slurry in the reactor was filtered and washed with hot distilled water-ethanol mixture to get rid of excess boric acid in the system. After filtration process, final product was dried on filter papers for 24 hours at room temperature.

### 3.1.3 Effect of Reaction Parameters on Synthesis of 3.5 Hydrated Zinc Borate on Laboratory Scale

In order to optimize the zinc borate production in terms of final product average particle size and reaction time, effects of different reaction parameters on the synthesis were evaluated in a set of experiment series (Table 3.2).

**Table 3.2** Reaction parameters examined on laboratory scale zinc borate production

| Sample | Seed Amount (wt.%) | Temperature (°C) | Stirring Rate (rpm) | Baffle | ZnO Particle Size |
|---|---|---|---|---|---|
| ZB1 | 1.5 | 85 | 400 | No | 25 μm |
| ZB2 | 0.75 | 85 | 580 | Yes | 25 μm |
| ZB3 | 1.5 | 85 | 580 | Yes | 25 μm |
| ZB4 | 1.5 | 85 | 320 | Yes | < 1 μm |
| ZB5 | 1.5 | 85 | 450 | Yes | < 1 μm |
| ZB6 | 1.5 | 85 | 580 | Yes | < 1 μm |
| ZB7 | 1.5 | 85 | 580 | Yes | 50 – 70 nm |

Effect of seed amount (which is calculated as the weight percentage of boric acid), stirring rate, presence of baffle and ZnO average particle size were examined.

### 3.1.4 Synthesis of 3.5 Hydrated Zinc Borate on Pilot Scale

In order to scale up 3.5 hydrated zinc borate production, pilot scale production was made and also the effects of reaction parameters on synthesis were studied. Reaction scheme and procedure were same as in the laboratory scale. 85 liter stainless steel batch pilot scale reactor was used for the pilot scale zinc borate synthesis. This reactor also has the same hardware in terms of heating, mixing, stirring and sampling as the small scale reactor. For pilot scale reactor, 65 liter distilled water was used for each synthesis. Effect of baffle presence was not examined in pilot scale reactor.

### 3.1.5 Effect of Reaction Parameters on Synthesis of 3.5 Hydrated Zinc Borate on Pilot Scale

Reaction parameters; stirring rate, ZnO average particle size, ZnO purity, and $B_2O_3$:ZnO mole ratio (Table 3.3) were examined in a series of six different reactions.

**Table 3.3** Reaction parameters examined on pilot scale zinc borate production

| Sample | Stirring Rate (rpm) | ZnO Average Particle Size (μm) | ZnO Purity (%) | Temperature (°C) | $B_2O_3$:ZnO Mole Ratio |
|---|---|---|---|---|---|
| ZBP1 | 96 | 25 | 98.0 | 85 | 5:1 |
| ZBP2 | 150 | 25 | 98.0 | 85 | 5:1 |
| ZBP3 | 271 | 25 | 98.0 | 85 | 5:1 |
| ZBP4 | 271 | < 1 | 99.9 | 85 | 5:1 |
| ZBP5 | 271 | 20 | 96.0 | 85 | 3.5:1 |
| ZBP6 | 271 | 20 | 96.0 | 85 | 5:1 |

## 3.2 Experimental of Synthesis of Boron Phosphate

Boron phosphate was synthesized by three different techniques; dry, wet (aqueous) technique and microwave technique.

### 3.2.1 Synthesis of Boron Phosphate via Dry Technique

Boron phosphate was produced at METU Chemistry Department and prepared by dehydrating mixtures of boric acid and phosphoric acid at temperature of 950°C. Reaction scheme is given in Reaction 3.2. Boric acid and phosphoric acid were obtained from Merck. Boric acid has a purity of 99%.

$$B(OH)_3(s) + H_3PO_4(s) \rightarrow BPO_4(s) + 3H_2O(g) \qquad (3.2)$$

Complete dehydration requires temperatures above 700°C.

### 3.2.2 Synthesis of Boron Phosphate via Wet Technique

Synthesis of boron phosphate was carried out by a hydrothermal method starting from mixtures of $H_3BO_3$ and $P_2O_5$ in a 6:1 molar ratio at METU Chemistry Department. The reactants were mixed in 10 ml distilled water and treated while stirring with 25 ml concentrated $HNO_3$ until the components dissolved completely. The clear solution was heated without boiling and concentrated to 15 ml and then transferred to a Teflon-coated steel autoclave (65% filling) and heated at 160°C for 2 days. The crystalline products were filtered of in vacuo, washed with distilled water and dried at 60°C. Boron phosphate was produced according to the reaction given in Reaction 3.3. Dry and wet technique produced boron phosphates were used in the production of first stage flame retardant PET based composites.

$$B_2O_3(aq) + P_2O_5(aq) \rightarrow 2BPO_4(aq) \qquad (3.3)$$

### 3.2.3 Synthesis of Boron Phosphate via Microwave Technique

Boric acid and diammonium hydrogen phosphate which were Merck grade were mixed in stoichiometric amounts. To initiate the synthesis reaction, urea which was 40 weight percent of diammonium hydrogen phosphate was added as microwave activator to the reactants. They were mixed to achieve a homogeneous mixture in a ceramic crucible and then placed in microwave at 10 minutes 650 watts microwave energy (Reaction 3.4). After that, produced boron phosphate was ground and put in an oven which was heated from room temperature to 600°C and kept in the oven for four hours when 600°C was reached. Finally, boron phosphate was ground again after the removal of residual urea in the oven.

$$H_3BO_3(s)+NH_4H_2PO_4(s)+CH_4N_2O(s) \rightarrow BPO_4(s)+3NH_3(g)+2H_2O(g)+CO_2(g) \qquad (3.4)$$

As a representative data, some properties of the microwave technique produced boron phosphate properties are given in Table 3.4. Microwave technique produced boron phosphate was used both in the production of first and second stage PET based flame retardant additives.

**Table 3.4** Properties of microwave produced boron phosphate

| **Property** | |
|---|---|
| Chemical Structure | 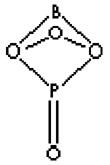 |
| Chemical Formula | $BPO_4$ |
| Melting Point (°C) | ≈ 1400 |
| Specific Gravity (@ 25 °C, g/ml) | 2.67 |

## 3.3 Characterization Experiments for Synthesized Boron Based Flame Retardant Additives

### 3.3.1 Chemical Analysis

One of the major characterization for the zinc borate is performing chemical analyses in order to determine the amount of zinc and boron content of zinc borate. With the help of this analysis, crystalline water content of zinc borate can also be determined indirectly. In terms of chemical analyses, zinc analysis and boron analysis in the solid samples, taken from the reactor during synthesis in equal time intervals, were performed.

#### 3.3.1.1 Zinc Analysis

Zinc analyses were performed on the samples taken during the reaction from the reactor at 30 minutes time interval and on the final product. In this analysis, ammonia buffer solution, EDTA and erichrome black T indicator were used.

Preparation of Ammonia Buffer Solution: The solution was prepared by dissolving 33.75 grams of ammonium chlororide in 460 ml of ammonia solution.

Preparation of 0.05M EDTA : The solution was prepared by dissolving 18.613 grams of A.R disodium dihydrogen ethylene diamine tetra–acetate dihydrate, accurately weighed in distilled water and diluted to 1 liter in a standard volumetric flask with distilled water [16].

Preparation of Erichrome Black T Indicator: The indicator was prepared by dissolving 0.2 grams of the dyestuff in 15 ml of triethanolamine and 5 ml of absolute ethanol [16].

This analysis was applied to the solid part of the sample. 0.2-0.3 gram of the sample was weighed and dissolved by using 1 ml of hydrochloric acid (with purity of 37%). 15-20 ml of ammonia buffer solution was added to set the pH around 9.5. The final solution was titrated with 0.05M EDTA solution by adding few drops of Erichrome Black T indicator. Titration was performed with the help of micropipettes (Finpipette, Thermo Labsystems) and continued until the color changed from purple to blue. The volume of EDTA used in the titration step was recorded [15]. Zinc oxide percentage in the solid phase was calculated from Equation 3.5:

$$P_{ZnO} = V_{EDTA} . (a) / n \tag{3.5}$$

where $P_{ZnO}$, $V_{EDTA}$ and "n" are the weight percentage of ZnO in the taken sample, volume of the EDTA used and amount of sample, respectively. In Equation 3.5, the constant "a" is the weight of ZnO in the sample resulting from the addition of 1 ml of 0.05M EDTA. The value of the "a" is 0.004069 g/l. It was calculated from the basic EDTA analyses principles.

Volume of EDTA used(ml) x Molarity of EDTA (0.05M EDTA used through the study) x Atomic weight of the metal ion ($Zn^{+2}$ ions were detected in the analyses but since it was in the form of ZnO for simplicity the atomic weight of ZnO was taken as 81.37) **=** weight of metal complex [18].

#### 3.3.1.2 Boron Analysis

The determination of boric acid in the solid sample was performed as follows: 0.2-0.3 gram solid sample was weighed and dissolved with 1 ml of hydrochloric acid (with purity of 37%). Before titration begins, necessary EDTA solution (10 ml excess of EDTA determined in zinc analysis) should be added to prevent any mistakes that might be caused by the existence of Zn ions. After EDTA addition, the solution was titrated with 1 N NaOH until a pH of 7 was obtained. At this step an automatic titrator (Mettler Toledo LD 50) involving a magnetic stirrer and pH-meter was used to get accurate results. After reaching the pH of 7, 10-15 gram mannitol was added to the solution. Finally, solution was again titrated with 1 N NaOH until the pH of the solution became 7. The volume of NaOH used in the second titration step was recorded [15]. Boric acid percentage in the liquid phase was calculated from Equation 3.6.

$$\begin{aligned} P_{B_2O_3} &= (V_{NaOH} * F_{NaOH} * 0.1) / n * (69.6202/2) * (100/1000) \qquad (3.6) \\ &= 0.348101 * (V_{NaOH} * F_{NaOH}) / n \end{aligned}$$

where $P_{B_2O_3}$, $V_{NaOH}$, $F_{NaOH}$ and “n” are the weight percentage of $B_2O_3$ in the taken sample, volume of the NaOH used, factor of NaOH solution and amount of sample, respectively

### 3.3.2 XRD Analysis

All of the samples of zinc borate and boron phosphate were characterized by X-ray diffractometer (Rigaku RINT 2100 PC) to analyze the crystal structures with Cu Kα radiation at 40 kV and 40 mA. XRD analysis can provide vital information to determine whether the synthesized zinc borate or boron phosphate is in desired form as each crystal form has its unique XRD pattern. The analyses were performed in the 1-80° 2θ range.

### 3.3.3 TGA Analysis

Thermal gravimetric analyses (TGA) were done with Perkin Elmer Pyris 1 and Shimadzu DTG-60A equipment. Zinc borate samples were heated from 30 to 700°C at 10°C/min under $N_2$ flow (100 ml/min) and boron phosphate samples were heated from 30 to 1200°C at 10°C/min under $N_2$ flow (100 ml/min). TGA analyses are used to determine the thermal stability of the compounds, in addition to indicate the crystal water loss temperature of the zinc borates.

### 3.3.4 Particle Size Distribution Analysis

The particle size distributions of the solid samples were determined by a particle size analyzer (Malvern Instruments, Mastersizer 2000), which is capable to detect 0.02-2000 μm range. Analyses were performed in dry state.

### 3.3.5 BET Analysis

In order to check the particle size distribution, BET analysis were also performed for selected zinc borate and boron phosphate samples. BET surface areas of the zinc borate and boron phosphate particles were determined by nitrogen adsorption at 77 K by Micrometrics Gemini V BET surface area analyzer.

### 3.3.6 SEM Analysis

Microstructure characterizations and also the average particle size distribution of the zinc borate and boron phosphate samples were analyzed by scanning electron microscopy using a Carl Zeiss Supra 55VP SEM instrument (Anadolu University, Metallurgical Engineering Department, Eskişehir). Prior to analysis, samples were coated with Pd-Au mixture by spin coater to impart conductivity.

## 3.4 Experimental of Production of Flame Retardant PET Composites

### 3.4.1 Materials

#### 3.4.1.1 Recycled PET

In this study, two different kinds of poly(ethylene terephthalate) (PET) were used as matrix material. In the first stage of the experiments, recycled PET was used as matrix material and its properties are given in Table 3.5. It was obtained from PET soft drink bottles in the form of flakes from AdvanSA Company, Adana, Turkey.

**Table 3.5** Properties of recycled PET

| **Property** | |
|---|---|
| PVC Content (ppm) | 60 |
| Polyethylene Content (ppm) | 5 |
| Glue Content (ppm) | 10 |
| Paper Content (ppm) | 3 |
| Intrinsic Viscosity (dl/g) | 0.75 |
| Glass Transition Temperature (°C) | 60 |
| Melting Temperature (°C) | 255 – 260 |

### 3.4.1.2 Crystalline PET

For the second stage of flame retardant composites, crystalline PET was used (Table 3.6). Crystalline PET was obtained from AdvanSA Company, Adana, Turkey with a trade name of Melinar.

**Table 3.6** Properties of crystalline PET

| **Property** | |
|---|---|
| Appearance | Opaque Pellet |
| Trade Name | Melinar |
| Intrinsic Viscosity (dl/g) | 0.65 |
| Glass Transition Temperature (°C) | 79 |
| Melting Temperature (°C) | 250 |

### 3.4.1.3 Flame Retardant Additives

In the first stage of flame retardant composites, various flame retardant additives were tried. Pilot scale produced 3.5 hydrated zinc borate is used which was produced in National Boron Institute Research Laboratory in METU Chemical Engineering Department. Boron phosphate which was synthesized by three different methods; dry method, wet method and microwave method were used as flame retardant additive. Flame retardants Greatlakes Reogard 2000, which is intumescent phosphorus based additive and Greatlakes Smokebloc AZ-12, which is a synergist and complex of metal oxides were supplied by Üçgen Boya A.Ş., İstanbul, Turkey Properties of the additives are given in Tables 3.7 and 3.8.

**Table 3.7** Properties of Reogard 2000 phosphorus based flame retardant [141]

| **Property** | |
|---|---|
| Appearance | White Powder |
| Trade Name | Great Lakes Reogard 2000 |
| Specific Gravity (@ 25°C, g/ml) | 0.70 |
| Solubility in Water (g/100 g water @20°C) | 3 |

**Table 3.8** Properties of Smokebloc AZ-12 synergist flame retardant [141]

| **Property** | |
|---|---|
| Appearance | White Powder |
| Trade Name | Smokebloc AZ-12 |
| Particle Size (average, μm) | 1.5 |
| Specific Gravity (@ 25°C, g/ml) | 4.4 |
| Chemical Composition | Antimony 41 min. %<br>Arsenic 0.13 max. % |

Another additive, which is mainly used to produce nanocomposites and mechanical property modification is Cloisite 30 B. It is an organically modified clay obtained from Southern Clay Products, USA (Table 3.9). Other flame retardant additive; anhydrous borax was supplied by Etibor A.Ş., Bandırma, Turkey (Table 3.10).

**Table 3.9** Properties of Cloisite 30B clay [142]

| **Property** | |
|---|---|
| Appearance | Fine White Powder |
| Trade Name | Cloisite 30B |
| Organic Modifier | MT2EtOH |
| Specific Gravity (@ 25°C, g/ml) | 1.98 |
| Average Particle Size (μ) | 6 |
| d-spacing (X-ray) (Å) | 18.5 |

**Table 3.10** Properties of anhydrous borax [143]

| **Property** | |
|---|---|
| Appearance | Crystalline Pellet |
| Trade Name | Etibor-68 |
| Specific Gravity (@ 25°C, g/ml) | 2.30 |
| Chemical Composition (%) | 68.9 $B_2O_3$ ; 30.6 $Na_2O$ |

Triphenyl phosphate, triphenyl phosphine oxide and calcium sulfate dihydrate were purchased from Acros Organics (Tables 3.11-13).

**Table 3.11** Properties of triphenyl phosphate [144]

| **Property** | |
|---|---|
| Chemical Structure | 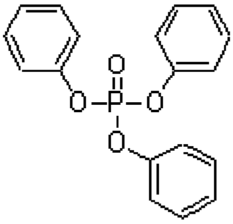 |
| Chemical Formula | $C_{18}H_{15}O_4P$ |
| Melting Point (°C) | 47-53 |
| Boiling Point (°C) | 370 |
| Purity (%) | 98 |

**Table 3.12** Properties of triphenyl phosphine oxide [144]

| **Property** | |
|---|---|
| Chemical Structure | 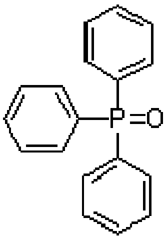 |
| Chemical Formula | $C_{18}H_{15}OP$ |
| Melting Point (°C) | 154-158 |
| Boiling Point (°C) | 360 |
| Purity (%) | 98 |

**Table 3.13** Properties of calcium sulfate dihydrate [144]

| **Property** | |
|---|---|
| Appearance | Fine White Powder |
| Chemical Structure | 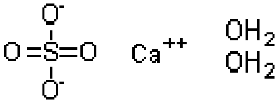 $O=\overset{O^-}{\underset{O^-}{S}}=O \quad Ca^{++} \quad \begin{matrix}OH_2\\OH_2\end{matrix}$ |
| Chemical Formula | $CaO_4S.2H_2O$ |
| Purity (%) | 98 |

During the thesis study, for the sake of simplicity the abbreviations given in Table 3.14 were used for the flame retardant additives.

**Table 3.14** Abbreviations used for the flame retardant additives used in composite production

| **Material** | **Abbreviation** |
|---|---|
| Poly(ethylene terephthalate) (Polymer Matrix) | PET |
| 3.5 Hydrated Zinc Borate | ZB |
| Anhydrated Borax | AnB |
| Boron Phosphate (Dry Method) | BoP |
| Cloisite 30 B Clay | Clay |
| Reogard 2000 | R2000 |
| Smokebloc AZ-12 | SAZ12 |
| Boron Phosphate (Wet Method) | BoP MW |
| Boron Phosphate (Microwave Produced) | BoP Wet |
| Calcium Sulfate Dihydrate | CSDH |
| Triphenyl Phosphate | TPP |
| Triphenyl Phosphine Oxide | TPP Ox |

### 3.4.2 Flame Retardant Formulations

In the scope of this study, firstly suitable flame retardant additives for the PET were determined according to the results of the literature survey. Selected flame retardant additives were used to prepare first stage flame retardant additives. Composites were characterized in terms of flame retardancy, mechanical and thermal properties; through the results of the analysis, four of the additives were chosen as the best ones in terms of flammability, mechanical properties and in the second stage flame retardant composites, combinations and various amounts have been formulated.

#### 3.4.2.1 Formulations of PET Based First Stage Flame Retardant Composites

Formulations of the first stage PET based flame retardant composites are given in Table 3.15 and all percentages of the additives are in weight percent.

**Table 3.15** Formulations of PET based first stage flame retardant composites

| **Sample** | ZB | BoP | AnB | Clay | R2000 | SAZ12 | PET |
|---|---|---|---|---|---|---|---|
| PET1 | **5** | **---** | **---** | **---** | **---** | **---** | **95** |
| PET2 | **---** | **5** | **---** | **---** | **---** | **---** | **95** |
| PET3 | **---** | **---** | **10** | **---** | **---** | **---** | **90** |
| PET4 | **---** | **---** | **---** | **5** | **---** | **---** | **95** |
| PET5 | **---** | **---** | **---** | **---** | **5** | **---** | **95** |
| PET6 | **---** | **---** | **---** | **---** | **---** | **5** | **95** |
| **Sample** | BoP MW | BoP + ZB | BoP Wet | CSDH | TPP | TPP Ox | PET |
| PET7 | **5** | **---** | **---** | **---** | **---** | **---** | **95** |
| PET8 | **---** | **2.5 + 2.5** | **---** | **---** | **---** | **---** | **95** |
| PET9 | **---** | **---** | **5** | **---** | **---** | **---** | **95** |
| PET10 | **---** | **---** | **---** | **5** | **---** | **---** | **95** |
| PET11 | **---** | **---** | **---** | **---** | **5** | **---** | **95** |
| PET 12 | **---** | **---** | **---** | **---** | **---** | **5** | **95** |

The procedure followed in determination of first stage flame retardant composites was to determine the effect of each flame retardant additive, thus equal amount of additive was used in each formulation except for anhydrous borax due to the process limitations. During processing PET feed rate was kept constant to the extruder. The feed rates of the additives were arranged relative to the PET feed rate. As PET feed rate was kept constant, the side feeder screw could not transfer anhydrous borax at 5 weight percent, thus it could be fed at 10 weight percent.

#### 3.4.2.2 Formulations of PET Based Second Stage Flame Retardant Composites

After the characterization of the first stage PET based flame retardant composites in terms of flame retardancy, mechanical properties and thermal properties, triphenyl phosphate, triphenyl phosphine oxide, microwave technique produced boron phosphate and 3.5 hydrated zinc borate were found to be successful additives for PET matrix according to the results of limiting oxygen index tests, smoke density measurements, tensile tests and impact tests. As the aim of the study is to produce not only flame retardant composites, but also composites which have high mechanical properties, relatively higher transparency and generate less smoke during burning. In addition, composites hardness values and UV transmittance properties are important to achieve versatility to the end usage of composites. Thus the results of all these tests were considered to select successive additives for the second stage of the experiments. In the second stage it was planned to perform and further investigate the effect of those flame retardant additives so the formulations given in Table 3.16 was planned and followed.

**Table 3.16** Formulations of PET based second stage flame retardant composites

| **Sample** | ZB | BoP MW | TPP | TPP Ox | PET |
|---|---|---|---|---|---|
| PT1 | **---** | **---** | **2** | **---** | **98** |
| PT2 | **---** | **---** | **10** | **---** | **90** |
| PT3 | **---** | **---** | **15** | **---** | **85** |
| PT4 | **---** | **---** | **5** | **5** | **90** |
| PT5 | **---** | **---** | **10** | **10** | **80** |
| PT6 | **---** | **5** | **5** | **---** | **90** |
| PT7 | **---** | **10** | **10** | **---** | **80** |
| PT8 | **---** | **5** | **2** | **---** | **93** |
| PT9 | **5** | **---** | **5** | **---** | **90** |
| PT10 | **5** | **5** | **5** | **---** | **85** |
| PT11 | **8** | **---** | **---** | **---** | **92** |
| PT12 | **---** | **8** | **---** | **---** | **92** |
| PT13 | **5** | **5** | **---** | **---** | **90** |

### 3.4.3 Preparation of Flame Retardant Composites

#### 3.4.3.1 Twin Screw Extrusion

In this study, Thermo Prism TSE 16 TC twin screw extruder was used for the preparation and melt mixing of all the flame retardant composites. Before each run of the experiments, the matrix material PET was dried in order to prevent the hydrolytic degradation during extrusion. Drying procedure is summarized in Table 3.17.

**Table 3.17** Drying procedure of PET

| **Material Type** | **Drying Temperature (°C)** | **Drying Time (h)** |
|---|---|---|
| Recycled PET | 140 | 5 |
| Crystalline PET | 130 | 5 |

The specifications of the extruder are given in Table 3.18.

**Table 3.18** Specifications of the twin screw extruder

| **Property** | |
|---|---|
| Model | Thermo Prism TSE 16 TC |
| Type | Twin Screw |
| Screw Type | Co-rotating |
| Twin Bore Diameter | 16 mm |
| Screw Diameter | 15.6 mm |
| Maximum Screw Speed | 500 rpm |
| Barrel Length | 384 mm (24 D) |
| Die Length | 16 mm (1 D) |
| Maximum Torque | 12 Nm |

Figure 3.2 represents the schematic drawing of the twin screw extruder which was used during the composite preparation.

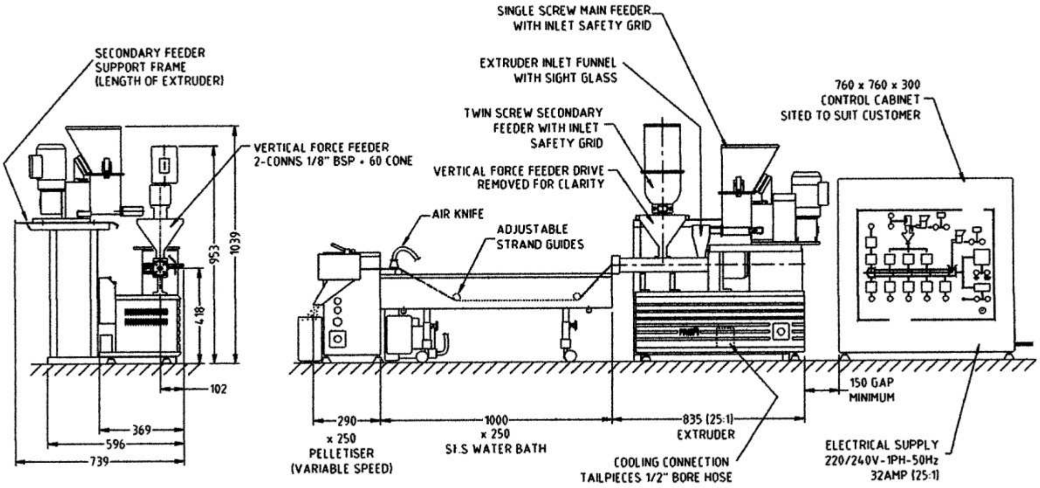

**Figure 3.2** Thermo Prism TSE 16 TC twin screw extruder

### 3.4.3.2 Injection Molding

A laboratory scale micro injection molding machine (DSM Xplore, 12 ml Micro Injection Molding Machine) shown in Figure 3.3 was used to mold flame retardant composites in order to prepare samples for the characterization experiments. Molding parameters given in Table 3.19 were kept constant throughout the molding process. Water was used as a coolant for the mold temperature controller, which was connected to the mold in order to maintain a constant and specific mold temperature.

**Table 3.19** Molding parameters for injection molding

| Parameters | |
|---|---|
| Mold Temperature (°C) | 25 |
| Melt Temperature (°C) | 255 |
| Waiting Time (min.) | 3 |

**Figure 3.3** DSM Xplore Micro Injection molding machine

### 3.2.3 Compression Molding

In order to prepare samples for the UV transmittance tests, compression molding technique was preferred to make very thin films for UV transmittance analysis. During compression molding, selected mold parameters were kept constant. The parameters are given in Table 3.20 and a drawing of the machine is shown in Figure 3.4.

**Table 3.20** Molding parameters for compression molding

| Compression Molding Parameters | Value |
|---|---|
| Molding Temperature (°C) | 270 |
| Oil Pressure (bar) | 150 |
| Mold Pressure (bar) | 7.2 |
| Pre-heating Time (min.) | 5 |
| Heating Time (min.) | 8 |
| Cooling Method | Quenching |

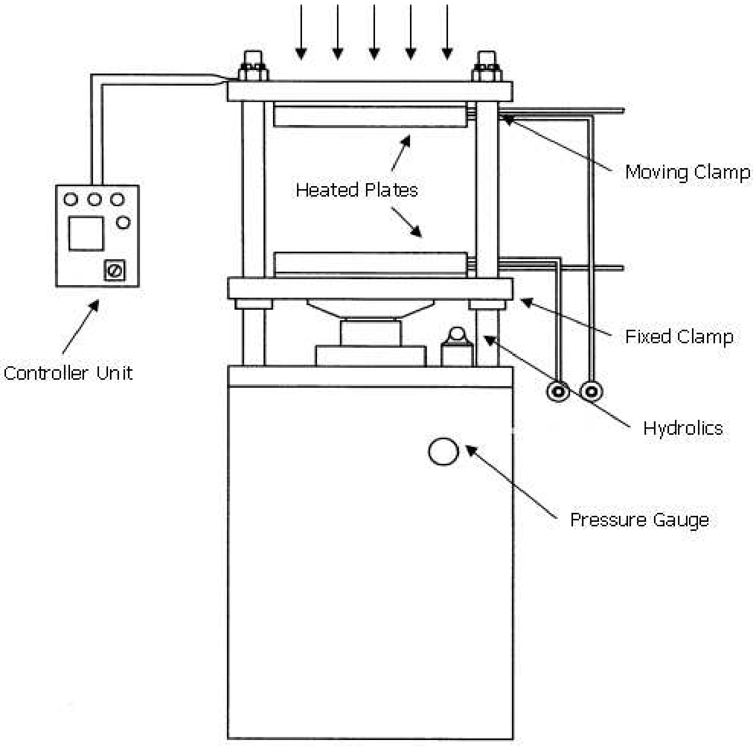

**Figure 3.4** Compression molding machine

### 3.4.4 Experimental Procedure

The general experimental procedure is given in Figure 3.5.

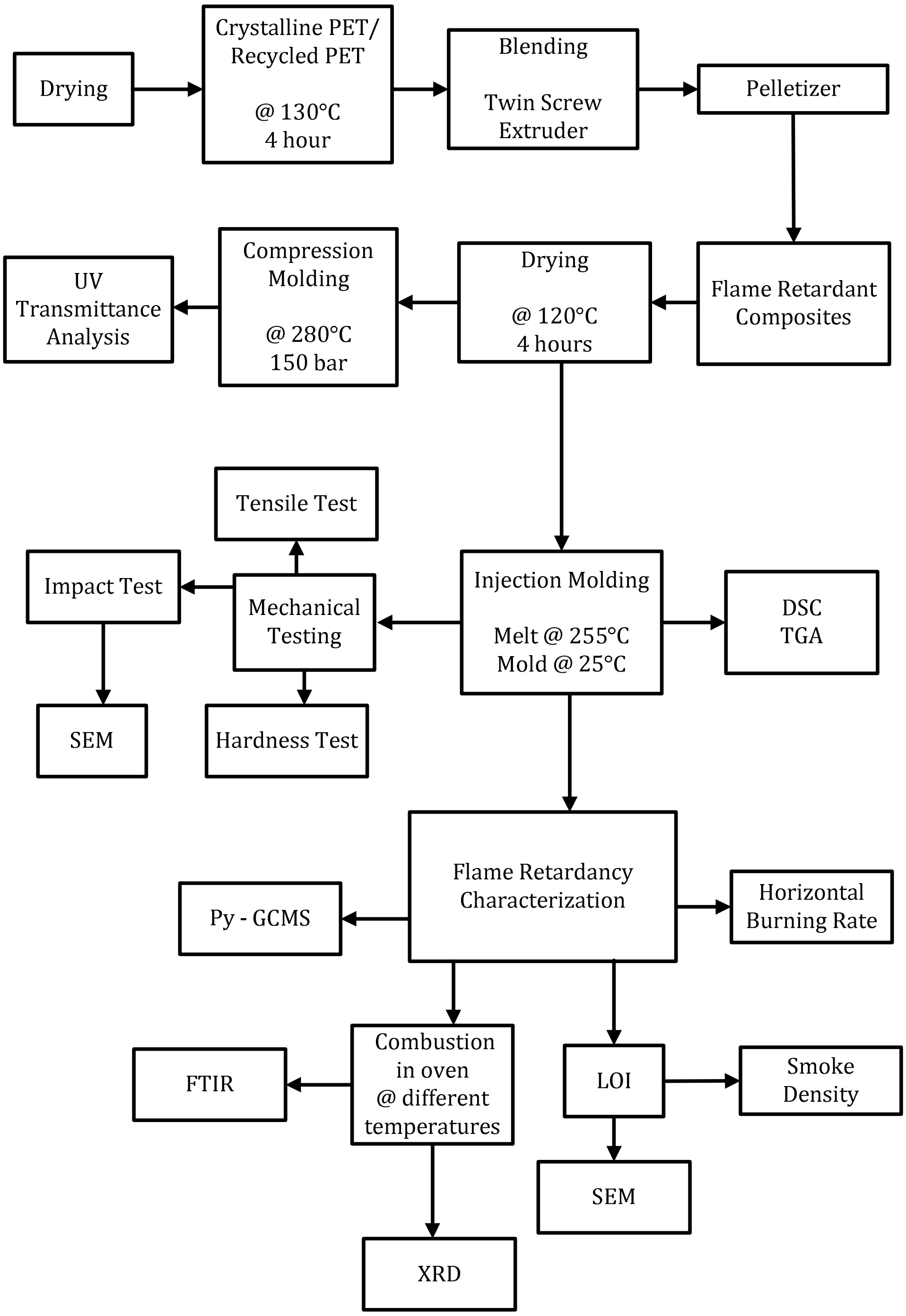

**Figure 3.5** General experimental procedure

In this study, in all sets of experiments samples were dried prior to mixing in extrusion. Then they were mixed in a twin screw extruder and pelletized. During extrusion, polymer matrix PET, was fed from the main feeder and the powder and pellet formed flame retardant additives were fed from the side feeder. Extrusion process parameters are given in Table 3.21.

**Table 3.21** Extrusion process parameters

| Parameters | Temperature Profile | | | | |
|---|---|---|---|---|---|
| | Hopper | 2. Zone | 3. Zone | 4. Zone | Die |
| Temperature (°C) | 230 | 240 | 240 | 250 | 255 |
| Screw Speed (rpm) | 200 | | | | |
| PET Feed Rate (g/min) | 20 | | | | |

Before molding, all samples were dried at 120°C for 4 hours. Samples were injection molded in order to prepare specimens for mechanical testing, thermal and morphological characterization and compression molded for UV transmittance analysis.

### 3.4.5 Characterization Experiments

#### 3.4.5.1 Flammability Tests

In order to determine the flame retardancy of the composites, horizontal burning rate and limiting oxygen index tests were performed. Furthermore, smoke density measurements were performed to evaluate the density of the smoke formed during fire and Pyrolysis-Mass Spectroscopy (Py-MS) analyses were conducted to analyze the act of the flame retardants in the second stage PET based flame retardant additives. Horizontal burning rate, limiting oxygen index, smoke density measurements were performed in METU Chemical Engineering Department and Py-MS analyses were performed in METU Chemistry Department.

### 3.4.5.1.1 Horizontal Burning Rate Test

Horizontal burning rate test was performed according to the ASTM D 635 standard. The rate of burn test is set up to determine the burning time and extent of burning for plastics materials in the horizontal position. The specimen size for this test is 12.5 cm long x 1.25 cm wide x 0.3 to 0.12 cm thick. Ten specimens are marked at a point 10 cm from the free end of the specimen. These are then fixed horizontally in the longitudinal axis at a 45° angle in the transverse axis 1 cm above a wire gauge. The samples are then ignited for a time of 30 seconds by a Bunsen-burner flame that has been calibrated to a flame height of 2.5 cm. There are two variables measured in this test:

1. Burn rate is recorded in mm/min, if the 10 cm mark is reached by the flame front.
2. If the specimen self-extinguished before the 10 cm mark is reached. After ignition, the first the average time of burning (ATB) is recorded in seconds. This is followed by the extent of burning (AEB) in mm which is tabulated and recorded. Schematic of horizontal burning rate test is given in Figure 3.6. Results were reported as average of 5 test specimens.

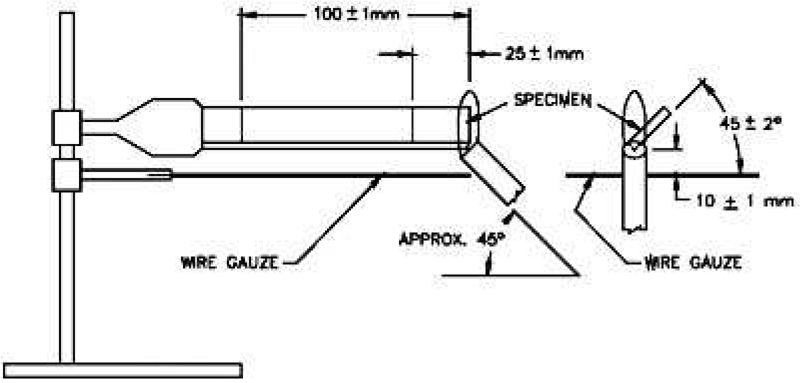

**Figure 3.6** Schematic of horizontal burning rate test [43]

### 3.4.5.1.2 Limiting Oxygen Index Test (LOI)

Limiting oxygen index test was performed according to the ASTM D 2863 standard. The oxygen index test relates flammability to the amount of $O_2$ in an atmosphere required to sustain combustion. Specifically, the minimum concentration of oxygen, expressed as volume percent, in a mixture of oxygen and nitrogen that will just support combustion of a material under the conditions specified in the test method. The apparatus consists of a glass column that is filled with a known concentration of an oxygen-nitrogen mixture. The test sample is mounted vertically with the ignition point at its upper end. A concentration of $O_2$ greater than that required to sustain combustion is first determined; from that point on, the oxygen is lowered at a slow rate until the flame is extinguished. The concentrations of oxygen and nitrogen are then put into Equation 3.7 and the oxygen index is determined and expressed as percent oxygen.

$$\text{LOI} = \frac{[O_2]}{[O_2]+[N_2]} x100 \qquad (3.7)$$

Values that are greater than 21% are desirable since this is the amount of oxygen present in the atmosphere. Therefore a sample with a higher oxygen index than this would not readily burn in our atmosphere. The specimen size for this experiment is 0.65 cm wide by 0.3 cm thick, with a length of 7 to 15 cm.

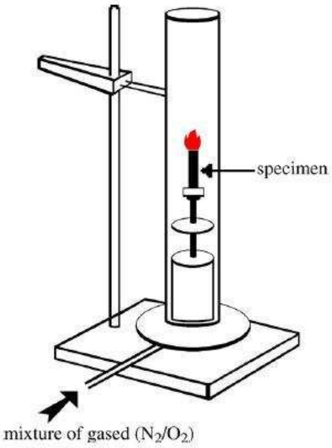

**Figure 3.7** Schematic of LOI device [43]

Experiments were performed by using Dynisco Limiting Oxygen Index equipment. Schematic of the LOI set-up is given in Figure 3.7 and picture of LOI set-up device is given in Figure 3.8.

#### 3.4.5.1.3 Smoke Density Measurement Test

Smoke density measurements were performed by using Dynisco optical smoke detector. This device consists of a measuring unit which is mounted to the top of the Dynisco LOI chamber. Measuring unit consists of a light source and an optical sensor which measures the light coming from the light source. Light emitted by the light source passes through the gases evolved from the burning sample in the LOI chamber and the transmitted light falls on the sensor. Device transforms this data to the recorder unit and recorder records the smoke density of the samples in terms of percent light transmittance. Picture of the smoke detector is given in Figure 3.8.

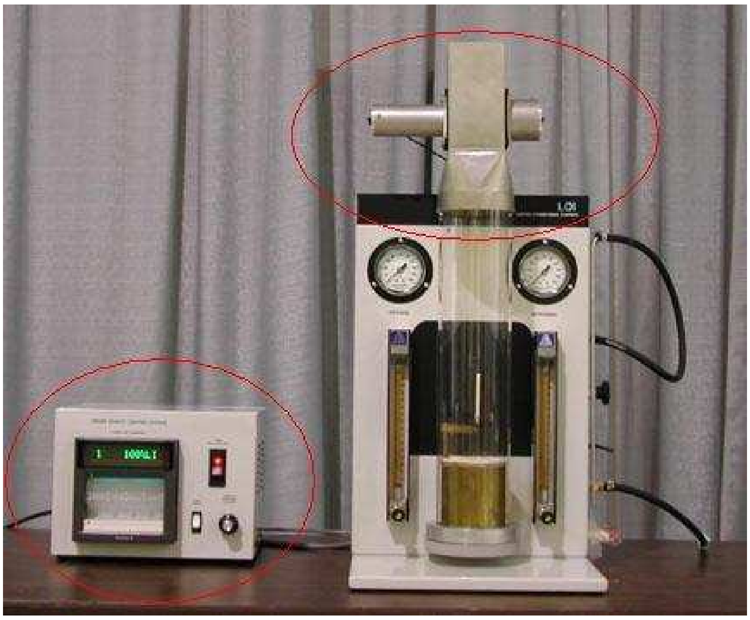

**Figure 3.8** Picture of the smoke detector (red circled parts; left recorder, right measuring unit)

#### 3.4.5.1.4 Py-MS Analysis

Py-MS analysis were performed at METU Chemistry Department with a direct pyrolysis mass spectrometry (DPMS) system consisting of a 5973 HP quadrupole mass spectrometer with a mass range of 10-800 Da coupled to a JHP SIS direct insertion probe ($T_{max}$=450°C). In each experiment, the temperature was increased up to 450°C at a heating rate of 10°C/min, and kept constant for an additional 10 min at 450°C. Samples (0.010 mg) were pyrolyzed in the flared glass sample vials. Pyrolysis mass spectra were recorded using 70 and 19 eV electrons to differentiate the extent of dissociative ionization in the ion source. Detection of identical peaks showed that the effect of dissociative ionization was negligible. Pyrolysis experiments were repeated at least twice to ensure reproducibility.

### 3.4.5.2 Mechanical Tests

All mechanical tests were performed at room temperature. For each type of flame retardant composite, average results from seven specimens with standard deviations were reported.

#### 3.4.5.2.1 Tensile Tests

Tensile tests were performed according to ASTM D638M-91a (Standard Test Method for Tensile Properties of Plastics) by a Shimadzu AG100 KN Universal Testing Machine. The shape and the dimensions of the specimens were specified according to Type-A ISO527 standard which are given in Figure 3.9 and Table 3.22 [26]. The crosshead speed was 20 mm/min. After stress versus strain diagrams from the measurements were obtained, tensile strength, tensile modulus and elongation at break values were calculated. Averages of 5 specimens were reported.

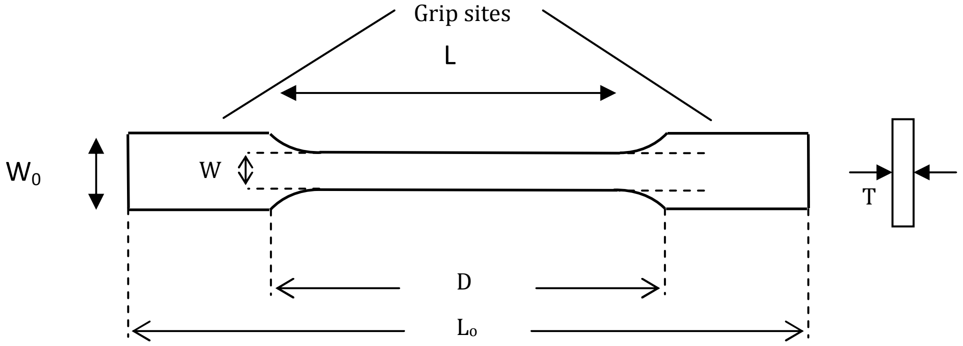

**Figure 3.9** Tensile test specimen

**Table 3.22** Tensile test specimen dimensions

| Dimensions | Specimen Dimensions (mm) |
|---|---|
| **$L_0$** – overall length | 75 |
| **W** – width of narrow section | 5 |
| **L** – length of narrow section | 30 |
| **$W_0$** – width of overall | 10 |
| **D** – distance between grips | 50 |
| **T** – thickness | 2.1 |

### 3.4.5.2.2 Impact Tests

Charpy Impact tests were performed by using a Ceast Resil Impact Test Device, according to the Test Method-I Procedure A in ASTM D256-91a (Standard Test Method for Impact Resistance of Plastics) [43]. Dimensions of the unnotched samples were 60x12x4 mm, respectively. A schematic drawing of the charpy type impact machine is illustrated in Figure 3.10. Averages of 5 specimens were reported.

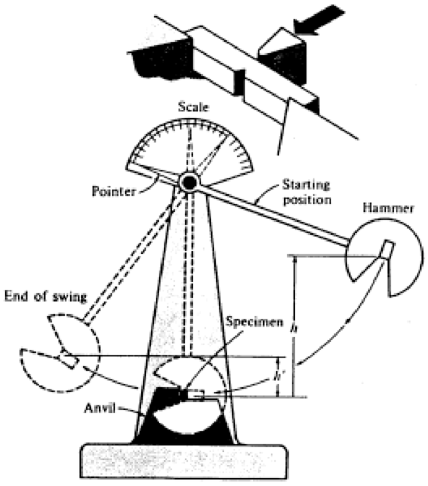

**Figure 3.10** Charpy-type impact machine

### 3.4.5.2.3 Hardness Tests

Hardness values of the composites polymers were determined with a Shore D hardness tester, TH210. A representative picture of hardness test is given in Figure 3.11.

**Figure 3.11** Shore D Hardness test device

### 3.4.5.3 Thermal Analysis

#### 3.4.5.3.1 Differential Scanning Calorimetry (DSC) Analysis

DSC analyses were carried out from 25°C to 500°C with a 5°C/min heating rate under nitrogen atmosphere by using a Shimadzu DSC-60A differential scanning calorimeter. Samples were investigated after first run by performing second run in order to clear the previous thermal history.

#### 3.4.5.3.2 Thermogravimetric (TGA) and Differential Thermal Analysis (DTA)

Thermal gravimetric analyses (TGA) and differential thermal analyses (DTA) were done with Shimadzu DTG-50 equipment. Composite samples were heated from 25°C to 900°C at 10°C/min under $N_2$ flow (100 ml/min).

### 3.4.5.4 FTIR Analysis

Shimadzu IR Prestige-21 was used to determine the structural changes of the flame retardant additives in the range of 400-4000 $cm^{-1}$ wave number. Typical sample preparations for boron phosphate analysis contained 150 mg KBr and 0.8 mg $BPO_4$.

### 3.4.5.5 Morphological Analysis

To characterize the morphologies of the flame retardant composites before and after burning the samples were analyzed by SEM and XRD analysis.

#### 3.4.5.5.1 Scanning Electron Microscopy (SEM) Analysis

A low voltage SEM (JEOL JSM-6400) was used to analyze the samples burnt in the LOI test. Samples were fractured after LOI test and the cross-sections were analyzed to determine the char formation and the structural changes of the flame retardant additive and the polymer matrix. The fracture surfaces were coated by a sputter coater within a thin layer of gold prior to fractographic examination.

### 3.4.5.5.2 X-ray Diffraction (XRD) Analysis

Specimens of flame retardant composites were characterized by X-ray diffractometer (Rigaku RINT 2100 PC) to analyze the crystal structures with Cu Kα radiation at 40 kV and 40 mA. XRD analysis could provide vital information to determine the changes of the crystal structure of the flame retardant additive after exposing to the similar temperatures during burning that simulates their behavior in the polymer matrix when a flame retardant composite sample is burnt. The analyses were performed in the 1-80° 2θ range.

### 3.4.5.6 Molecular Weight Determination

Molecular weight determination of the PET based composites containing triphenyl phosphate were determined by intrinsic viscosity measurements with the help of Ubbelohde Viscometer. Trifloro acetic acid was used as the solvent for PET based composites. To dissolve the samples completely in trifloro acetic acid, firstly trifloro acetic acid was heated up to 120°C. Samples were added and stirred until complete homogeneous dissolvation was obtained. After that, samples taken into the water bed at 25°C where measurements were performed. With this method intrinsic viscosities of the samples were determined. Followed by this determination, viscosity average molecular weights were calculated by using Equation 3.8 which is Mark-Houwink-Sakurada Equation.

$$\eta = K.M^a \tag{3.8}$$

where $\eta$ is intrinsic viscosity, M is viscosity average molecular weight and K and a are Mark-Houwink constants depend upon the type of polymer, solvent, and the temperature of the viscosity determinations.

After intrinsic viscosities were determined an estimation was made to get viscosity average molecular weights by using the K and a values for PET ($K = 14 \times 10^{-4}$, $\alpha = 0.65$, at 25°C for trifloro acetic acid) as it is difficult to find the K and a values for PET including different amounts of triphenyl phosphate.

### 3.4.5.7 UV Transmittance Analysis

Prior to UV transmittance analysis, composites were compression molded in order to obtain very thin films, about 20 μm thick. After obtaining thin films, composites were analyzed by Shimadzu UV 2450 Spectrorophotometer in the range of 280-400 nm wavelength at METU Chemistry Department.

### 3.4.5.8 Transparency Analysis

Transparency of the flame retardant composites is a huge problem due to the different refractive indexes of the polymer and the flame retardant additives and as a result of the high particle size that scatters the light passing through the composite. To visualize the transparency of the composites, photographs were taken by a digital camera on a written manuscript and then their transparencies were compared in terms of the readability of the letters behind the specimens.

# CHAPTER 4

# RESULTS and DISCUSSION

## 4.1 Synthesis and Characterization of 3.5 Hydrated Zinc Borate

### 4.1.1 Zinc and Boron Analyses of Lab Scale Produced 3.5 Hydrated Zinc Borate

In order to determine the completion of the reaction and also to evaluate the $B_2O_3$ and ZnO percents in the final product, $B_2O_3$ analysis by EDTA titration and ZnO analysis by NaOH titration were performed on the solids obtained from the samples taken from the lab scale reactor in every 30 minutes time interval. The results of the chemical analysis for the small scale reactor at the final products are given in Table 4.1.

**Table 4.1** Chemical analyses results of laboratory scale synthesized zinc borates

| Sample | ZnO % | $B_2O_3$ % | Chemical Formula |
|---|---|---|---|
| Firebrake ZB | 37.5 | 48.0 | $2ZnO{\cdot}3B_2O_3{\cdot}3.5H_2O$ |
| ZB1 | 38.3 | 45.7 | $2ZnO{\cdot}3B_2O_3{\cdot}3.5H_2O$ |
| ZB2 | 39.2 | 45.3 | $2ZnO{\cdot}3B_2O_3{\cdot}3.4H_2O$ |
| ZB3 | 40.8 | 45.9 | $2ZnO{\cdot}3B_2O_3{\cdot}3.6H_2O$ |
| ZB4 | 38.5 | 47.1 | $2ZnO{\cdot}3B_2O_3{\cdot}3.5H_2O$ |
| ZB5 | 37.8 | 47.3 | $2ZnO{\cdot}3B_2O_3{\cdot}3.3H_2O$ |
| ZB6 | 39.9 | 45.7 | $2ZnO{\cdot}3B_2O_3{\cdot}3.4H_2O$ |
| ZB7 | 39.4 | 48.2 | $2ZnO{\cdot}3B_2O_3{\cdot}3.5H_2O$ |

Chemical formulas of the products were determined by using the stoichiometry of the reaction and the amount of water in the structure was determined by the ZnO and $B_2O_3$ content. When compared with the commercial product, Firebrake ZB, all products have similar $B_2O_3$ and ZnO content. The similar content of the synthesized zinc borates and commercial product is a support of successful synthesis.

### 4.1.2 Zinc and Boron Analyses of Pilot Scale Produced 3.5 Hydrated Zinc Borate

When scale-up was performed in pilot scale similar results were obtained (Table 4.2). Thus, scale up of zinc borate was successfully achieved according to the results of the chemical analysis in terms $B_2O_3$ and ZnO content in the final products. The crystalline water content of the products varies between 3.1 to 3.8. According to the literature [16] the 3.5 hydrated zinc borate was claimed to have 3 mole crystalline water, thus the variation between 3.1 to 3.8 is normal and the increase in crystalline water content is an advantage in flame retardancy applications. Although there are more types of zinc borate which have different amounts of crystalline water like 7 mole [16]; the most thermally stable one is the one containing 3.5 hydrated zinc borate.

**Table 4.2** Chemical analyses results of pilot scale synthesized zinc borates

| Sample | ZnO % | $B_2O_3$ % | Chemical Formula |
|---|---|---|---|
| ZBP1 | 39.2 | 45.9 | $2ZnO \cdot 3B_2O_3 \cdot 3.6H_2O$ |
| ZBP2 | 39.1 | 46.2 | $2ZnO \cdot 3B_2O_3 \cdot 3.5H_2O$ |
| ZBP3 | 38.8 | 46.3 | $2ZnO \cdot 3B_2O_3 \cdot 3.6H_2O$ |
| ZBP4 | 38.2 | 48.7 | $2ZnO \cdot 3B_2O_3 \cdot 3.1H_2O$ |
| ZBP5 | 41.6 | 42.6 | $2ZnO \cdot 3B_2O_3 \cdot 3.8H_2O$ |
| ZBP6 | 40.5 | 45.2 | $2ZnO \cdot 3B_2O_3 \cdot 3.4H_2O$ |

The theoretical estimated amont of zinc borate production for both and pilot scale production is predicted from the reaction stoichiometry and it was 0.566 kg for laboratory scale and 17.55 kg for pilot scale. The realized zinc borate production for each production was measured by weighing the dried zinc borate after production and  was reported in Appendix B. According to the results 72-82% zinc borate was produced for laboratory scale and 75-80% for the pilot scale. This difference in reality is the result of losses related to mainly evaporation and filtration losses and minor losses due to conversion.

### 4.1.3 XRD Analysis of Lab Scale Produced 3.5 Hydrated Zinc Borate

X-ray diffraction is a powerful technique to characterize the inorganic materials, as each inorganic compound has its unique XRD pattern which can be an advantage to characterize the synthesized products. XRD plot of the commercial zinc borate, Firebrake ZB is given in Figure 4.1. It is clear that characteristic peaks of 3.5 hydrated zinc borate are between 15-70° 2θ ranges. In Figure 4.2, X-ray diffraction diagrams of laboratory scale produced zinc borates are given. It is obvious that the peaks are matching with the XRD peaks of commercial zinc borate, supporting that the 3.5 hydrated zinc borate was successfully synthesized.

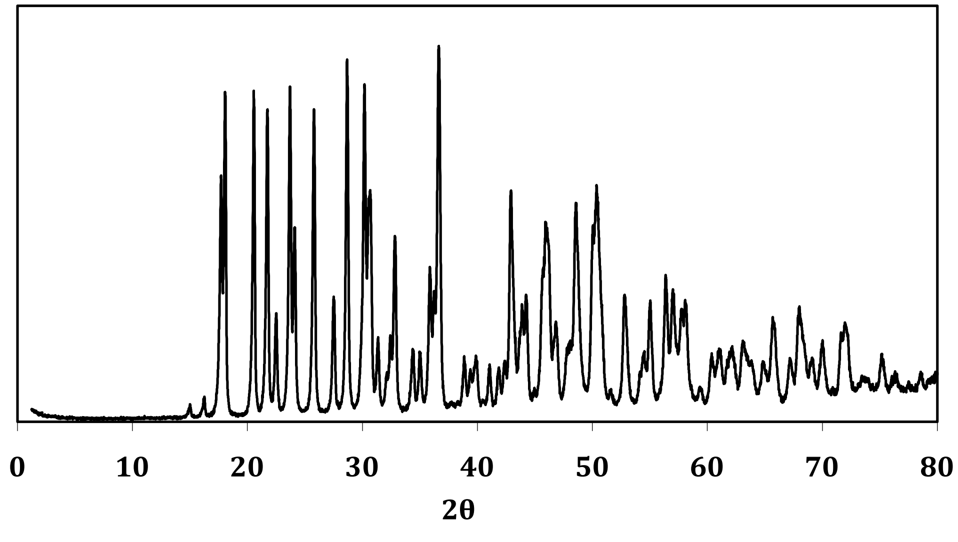

**Figure 4.1** XRD pattern of Firebrake ZB commercial 3.5 hydrated zinc borate

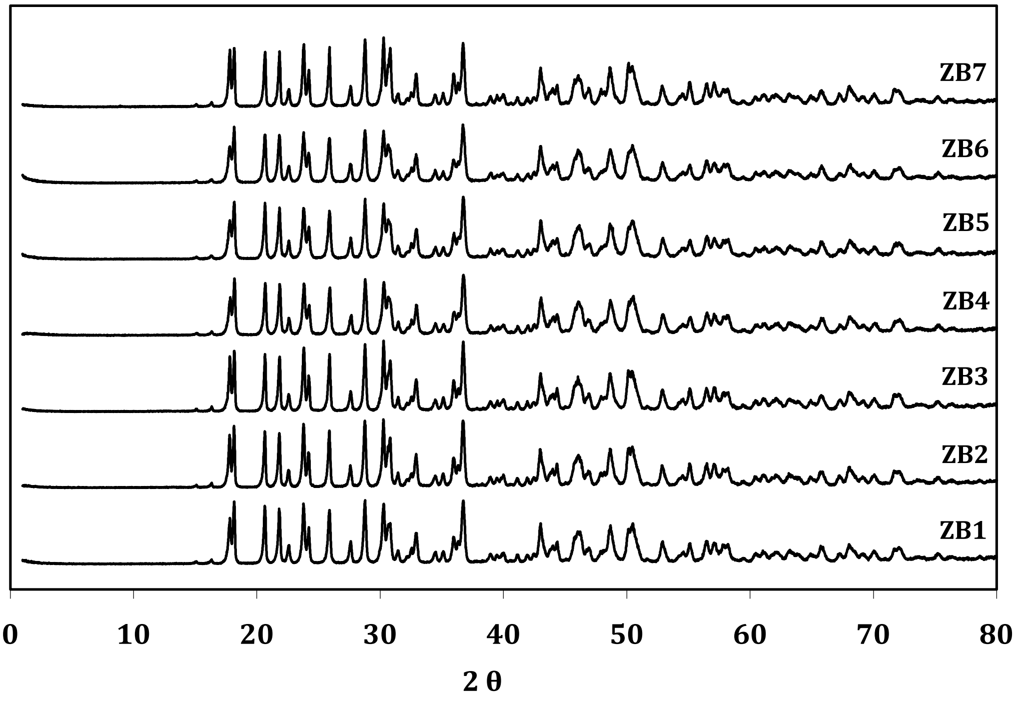

**Figure 4.2** XRD patterns of laboratory scale synthesized zinc borates

### 4.1.4 XRD Analysis of Pilot Scale Produced 3.5 Hydrated Zinc Borate

When Figure 4.3 is considered, XRD plots of all samples match up with each other and also with the commercial product Firebrake ZB, except the product ZBP5 that indicates that its crystal structure did not match with the commercial product. ZBP5 synthesis was performed with a $B_2O_3$:ZnO ratio of 3.5:1 which is near to the stoichiometric amount required to synthesize 3.5 hydrated zinc borate. During reaction due to the leaks from the reactor via evaporation, this amount could drop below the stoichiometrically required amount, thus without excess boric acid the synthesis of zinc borate could not be achieved. If the boric acid amount would get below the desired stoichiometric ratio, another zinc borate compound could be synthesized which could have different crystalline water content than the 3.5 hydrated zinc borate. Remaining plots were also identical with the $2ZnO{\cdot}3B_2O_3{\cdot}3.5H_2O$ reported by Igarashi et al. [145].

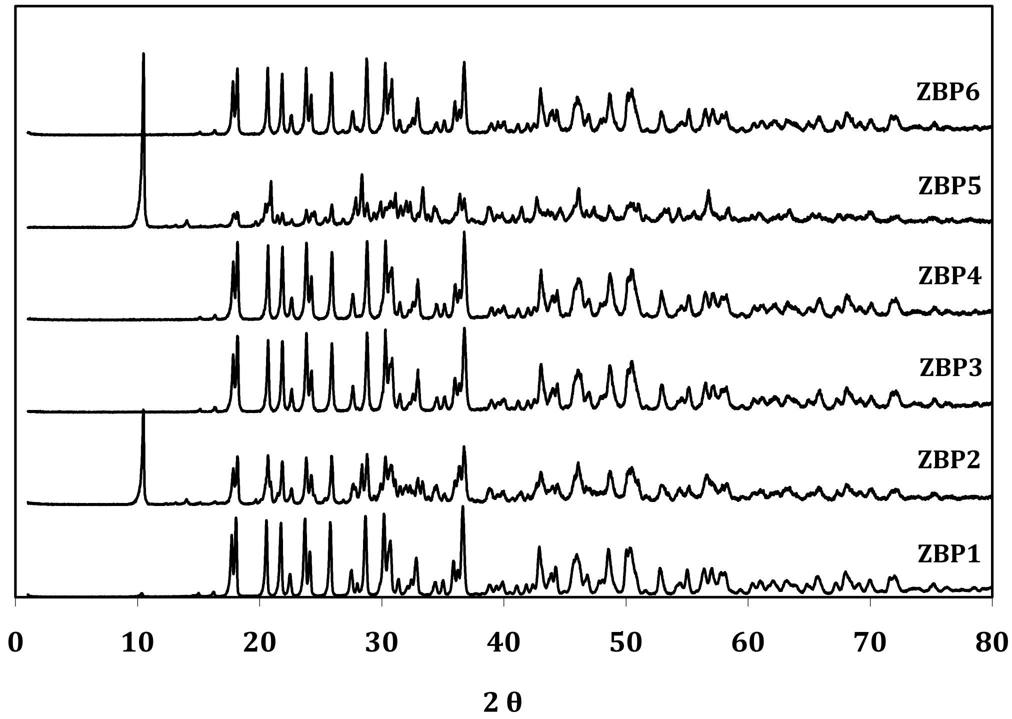

**Figure 4.3** XRD patterns of pilot scale synthesized zinc borates

### 4.1.5 Particle Size Distribution of Lab Scale Produced 3.5 Hydrated Zinc Borates

One of the major points that affect the end usage of zinc borate as filler is the particle size distribution. The smaller the average particle size, the more homogeneous distribution occurs when zinc borate is added to wood or polymeric composites. On the other hand, smaller particle size requires less usage of zinc borate as desired filler, such as the usage of nano fillers in nanocomposites. Particle size distributions of lab scale reactor are given in Table 4.3. The commercial zinc borate has an average particle diameter of 7.5 μm. Zinc borates produced in laboratory scale reactor had smaller particle size distribution in contrast with the commercial product.

**Table 4.3** Particle size distribution results of laboratory scale synthesized zinc borates

| Sample | Average Particle Size (μm) |
|---|---|
| Firebrake ZB | 7.5 |
| ZB1 | 4.1 |
| ZB2 | 2.8 |
| ZB3 | 2.7 |
| ZB4 | 5.0 |
| ZB5 | 4.6 |
| ZB6 | 3.8 |
| ZB7 | 2.7 |

### 4.1.6 Particle Size Distribution of Pilot Scale Produced 3.5 Hydrated Zinc Borates

Products from pilot scale reactor had higher average particle size diameter when compared to laboratory scale reactor (Table 4.4). The pilot scale reactor was scaled up based on the small scale reactor and the stirrer was also scaled up. Due to the reactor design, the formation of dead zones in the reactor is inevitable. These dead zones possibly could occupy more volume on pilot scale reactor and thus the stirring in these regions would be inadequate and non-homogeneous. As a result, due to lower degree of stirring, the final product average particle size could be bigger. The more homogeneous and efficient the stirring is, the more collisions of the zinc borate crystals would take place, thus the possibility of formation of agglomerates would decrease. And the formed agglomerates could break up due to the effective stirring in laboratory scale reactor.

**Table 4.4** Particle size distribution results of pilot scale synthesized zinc borates

| Sample | Average Particle Size (μm) |
|---|---|
| ZBP1 | 8.7 |
| ZBP2 | 4.2 |
| ZBP3 | 3.8 |
| ZBP4 | 3.4 |
| ZBP5 | 5.0 |
| ZBP6 | 3.8 |

### 4.1.7 Effects of Reaction Parameters on Reaction Kinetics and Particle Size Distribution of Laboratory Scale Produced 3.5 Hydrated Zinc Borates

After successive synthesis of zinc borate in laboratory scale, further experiments were performed to characterize the most important parameters on the reaction rate and the final product average particle size. Effects of seed amount used during synthesis, presence of baffles in the reactor, stirring rate, and zinc oxide average particle size distribution were evaluated.

#### 4.1.7.1 Effect of Seed Amount on Laboratory Scale Production of Zinc Borate

Firebrake ZB, commercial $2ZnO{\cdot}3B_2O_3{\cdot}3.5H_2O$ zinc borate, is used as seed crystals during the zinc borate synthesis. Seed initiates the zinc borate synthesis reaction and also catalyzes the reaction. By using 1.5 weight percent of total amount of boric acid which was fed to the reactor as seed, the desired zinc borate could be synthesized within 4 hours (Figure 4.4). It is given in the literature that, without seed usage, the reaction was completed over 24 hours, so it is crucial to use seed during synthesis [146]. In order to examine the effect of seed amount on the reaction, an experiment at the same conditions with 0.75% of boric acid was also performed (ZB2). From Figure 4.4, it can be concluded that the change of seed amount did not affect the reaction and the reaction completion time significantly. Seed, which is 3.5 hydrated zinc borate, acts as an initiator for the reaction and without its presence succesful synthesis could not be achieved [15]. As it acts like an initiator small amount of addition is enough and initiates the reaction and further increase of seed usage is unnecessary as seen from Figure 4.4.

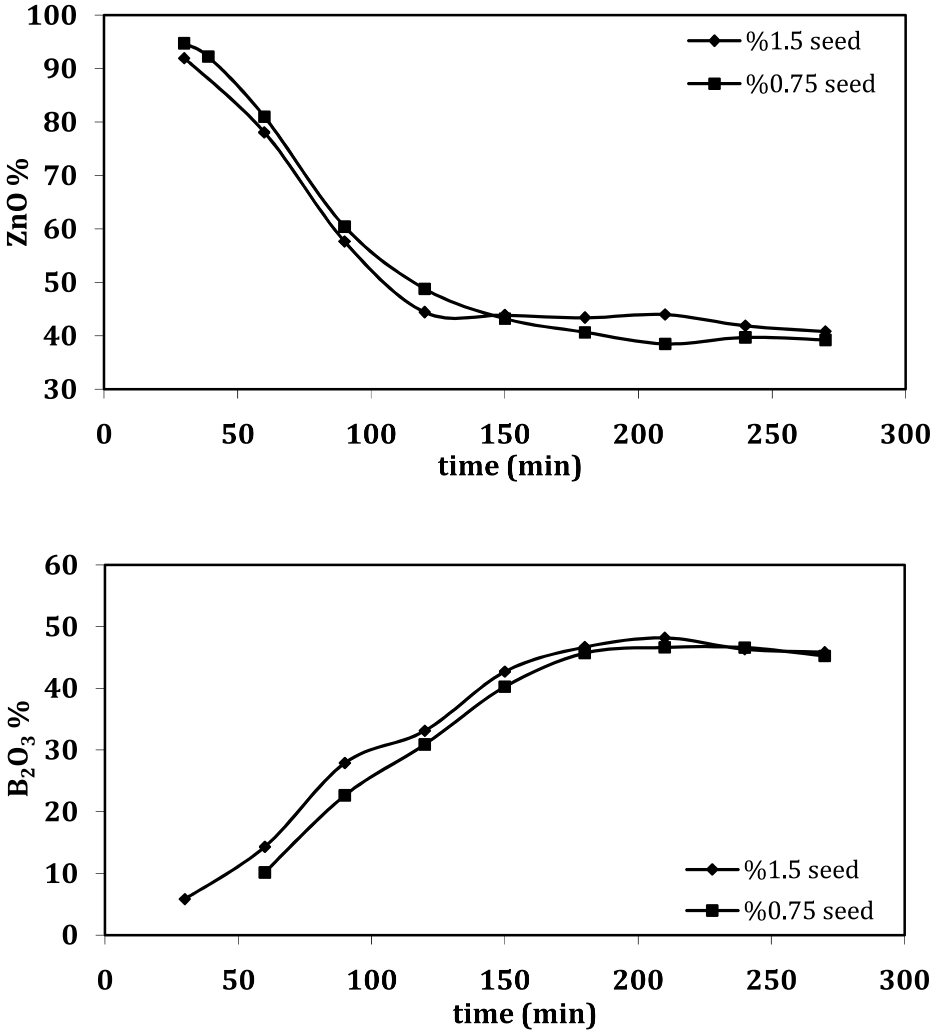

**Figure 4.4** Effect of seed amount on zinc borate production reaction in laboratory scale zinc borate synthesis (temperature (85°C), initial reactants mole ratio ($H_3BO_3$:ZnO ratio of 5:1), stirring rate (580 rpm), and average particle size of zinc oxide particles (25 μm) were constant)

Also the average particle size distribution for the final zinc borate product did not change significantly, which was 2.7 μm for ZB2 and 2.8 μm for ZB3 (Figure 4.5). These results imply that the usage of seed is important, but the amount is not noticeably important for the reaction and the final product.

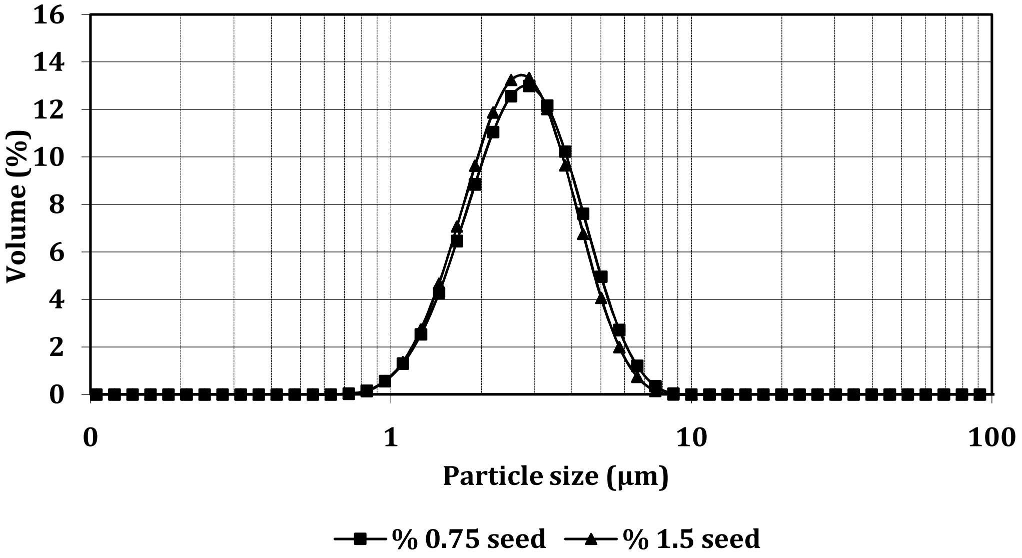

**Figure 4.5** Effect of seed amount on final products average particle size distribution in laboratory scale zinc borate production

### 4.1.7.2 Effect of Presence of Baffle on Laboratory Scale Production of Zinc Borate

In various reaction systems, baffles are integrated to the reactors in order to increase the effectiveness of stirring and to have a rougher mixing in the reactor. Different types of baffles can be used. Although baffles have advantage to increase the mixing and the dispersion in the reactor, one drawback of using baffles is the dead zones that could possibly occur in the reactor at the connection points of the baffle and the reactor. To determine the effect of baffles on zinc borate production in small scale production, samples ZB1 and ZB2 were produced. In the production of ZB2 sample, the reactor was equipped with four baffles placed like a crosshair. Baffles were 18 cm long, 17 mm wide rectangular stainless steel plates with a thickness of 0.5 cm. The rest of the process parameters were kept constant, instead of the seed amount which does not affect the reaction. $B_2O_3$ and ZnO analysis performed during the synthesis was given in Figure 4.6. When baffle was used, ZnO in the reaction medium was depleted more quickly when compared to the case where baffles are not used. When $B_2O_3$ content change was examined, a slight increase was observed in the formation rate of $B_2O_3$.

It is concluded that the usage of baffle did not shorten the reaction time as it is expected. Baffles are needed to stop the swirl in a mixing reactor. Almost all impellers rotate in the clockwise or counter-clockwise direction. Without baffles, the tangential velocities coming from any impellers cause the entire fluid mass to spin. It may look good from the surface seeing that vortex all the way down to the impeller, but this is the worst kind of mixing. There is very little shear and the particles go around and around. This is more like a centrifuge than a mixer. In order to disrupt this, baffles are placed in the reactor and the effect of mixing and homogeneity of mixing in the reactor rises, thus the reaction completion shortens as possibility of collusion of reactants increases. One of the main drawbacks of baffle usage is the increase of dead zones in the reactor, which could decrease the efficiency of the reactor. When ZB2 sample was considered, there is not any significant increase in the reaction completion time, thus in this case the presence of baffle is effectiveness in the zinc borate production in terms of reaction rate case. This could be the result of the dead zones formed related to the baffles and dead zone formation hinders the effect of more effective mixing.

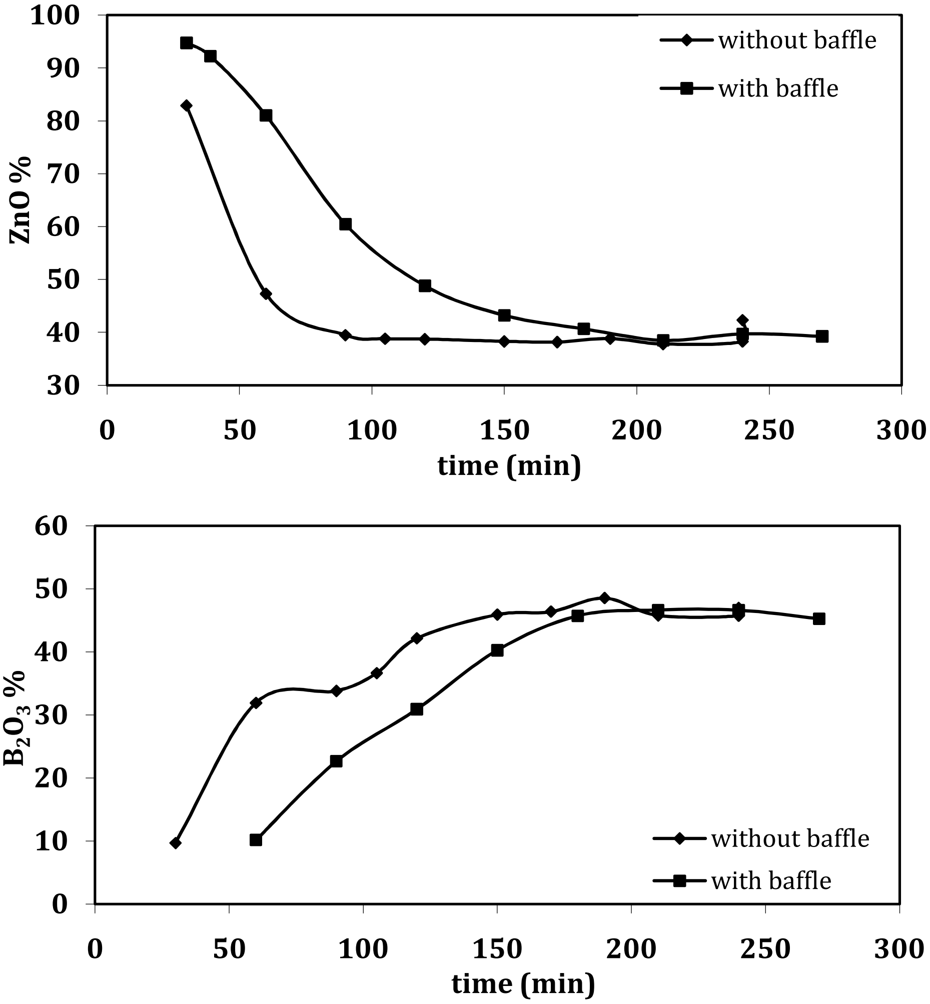

**Figure 4.6** Effect of presence of baffle on zinc borate production reaction in laboratory scale zinc borate synthesis (temperature (85°C), seed amount (1.5%), initial reactants mole ratio ($H_3BO_3$:ZnO ratio of 5:1), and average particle size of zinc oxide particles (25 µm) were constant)

The average particle size of the final product was decreased from 4.1 µm (ZB1) to 2.8 µm (ZB2) (Figure 4.7). Due to the rougher and complex mixing in the reaction medium related to the presence of baffles, the agglomerates of the zinc borate and bigger zinc borate crystals could be broken more effectively and they could not settle down in the reactor, so the average particle size tend to decrease.

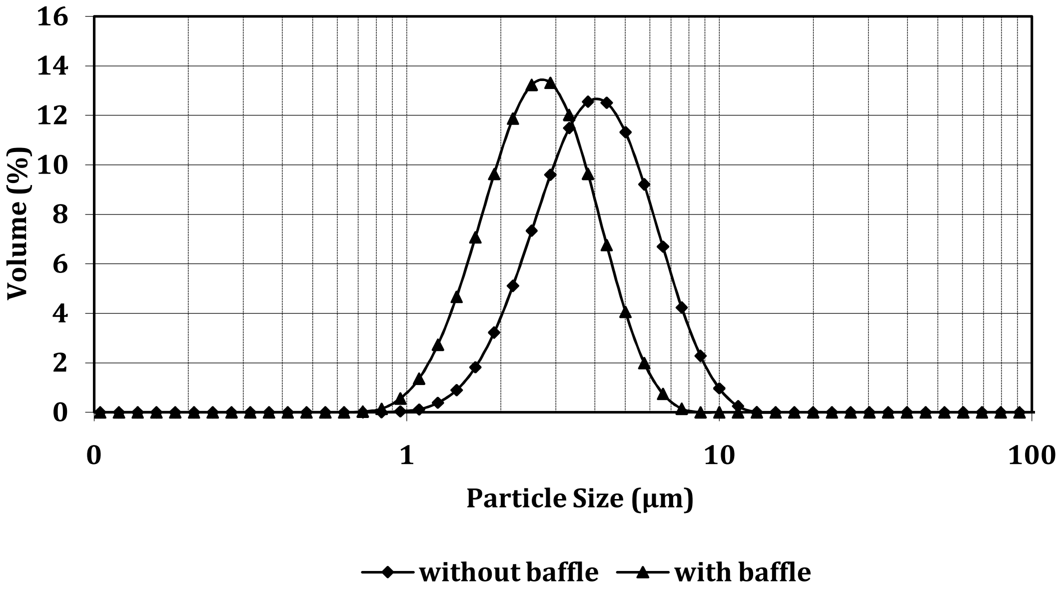

**Figure 4.7** Effect of baffle presence on final product's average particle size distribution in laboratory scale zinc borate production

### 4.1.7.3 Effect of Stirring Rate on Laboratory Scale Production of Zinc Borate

In order to examine the effect of stirring rate both on reaction and final product, three different stirring rates; 320, 450, 580 rpm were chosen. The impellers of the stirrer have a diameter equal to one-third of the vessel. The change of ZnO and $B_2O_3$ content in the reactor with respect to the stirring rate are given in Figure 4.8. In all three cases the reaction was completed nearly in 3 hours. The increase in the stirring rate could be possibly increased by the mass transfer of borate ions coming from the dissolved boric acid to the reaction sites which are ZnO particles. The highest $B_2O_3$ content was obtained when stirring rate was selected as 580 rpm.

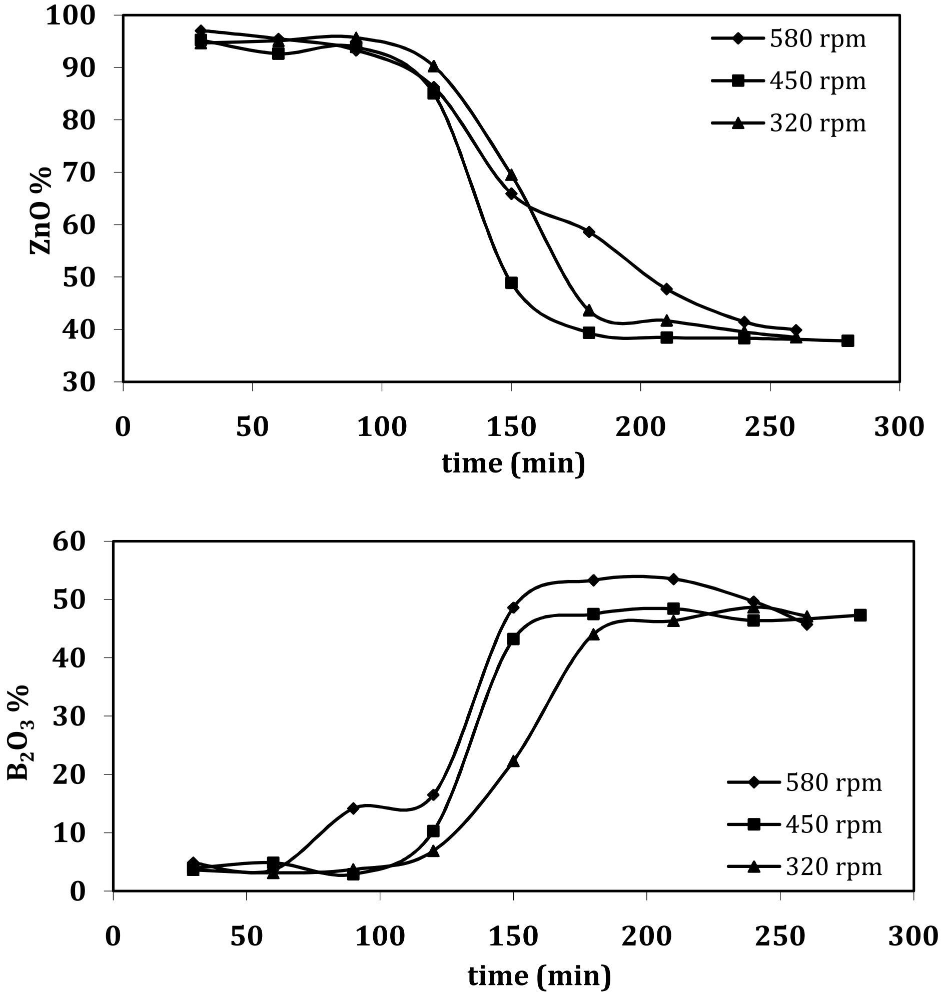

**Figure 4.8** Effect of stirring rate on zinc borate production reaction in laboratory scale zinc borate synthesis (temperature (85°C), seed amount (1.5%), initial reactants mole ratio ($H_3BO_3$:ZnO ratio of 5:1), and average particle size of zinc oxide particles (< 1 μm) were constant)

The particle sizes of the final products (Figure 4.9) decreased with the increase of stirring rate, which is 5.0 μm for 320 rpm (ZB4), 4.6 μm for 450 rpm (ZB5), and 3.8 μm for 580 rpm (ZB6). Average particle size decreased, due to the increase of number of collisions of zinc borate crystals in the reactor and also their impacts became more energetic due to their high velocities to break up the agglomerates in higher stirring rates. Thus, as a result with the increase of stirring rate, the average particle size gets smaller.

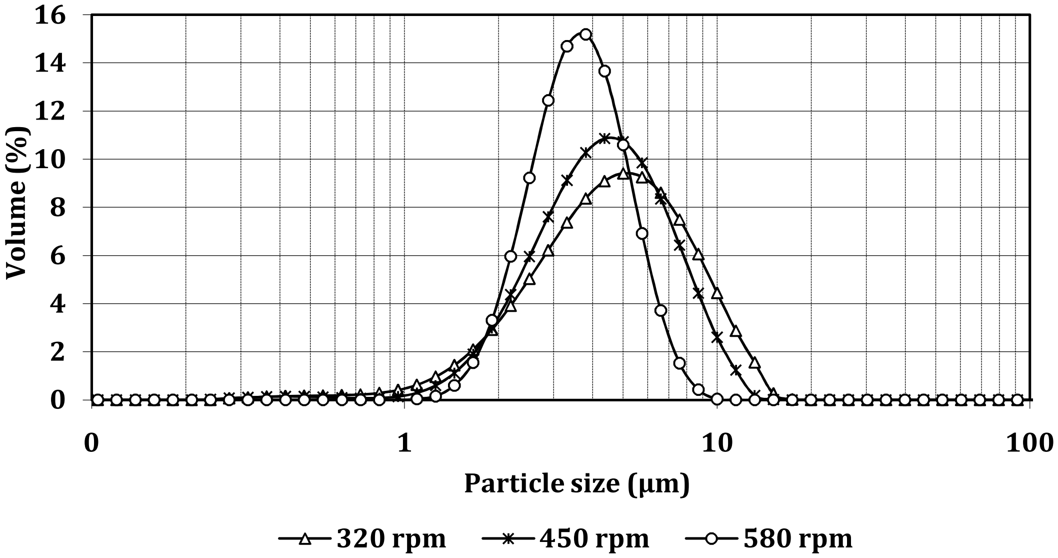

**Figure 4.9** Effect of stirring rate on final product's average particle size distribution in laboratory scale zinc borate production

#### 4.1.7.4 Effect of Zinc Oxide Average Particle Size on Laboratory Scale Production of Zinc Borate

Zinc oxide average particle size diameter is directly related to the final zinc borate product's mean particle size. It was proposed by the proposed adopted logistic model which will be mentioned in the coming sections, the reaction was carried on the surface of zinc oxide. It is expected to have smaller mean particle size for the final product if smaller particle size ZnO was used. In fact this is not true for this case since when 25 μm average particle sized ZnO was used, the reaction was significantly faster and high conversion of ZnO was obtained at the beginning of the reaction. This phenomenon will be explained later in the proposed kinetic model for the zinc borate formation reaction which will be defined as the “logistic model”.

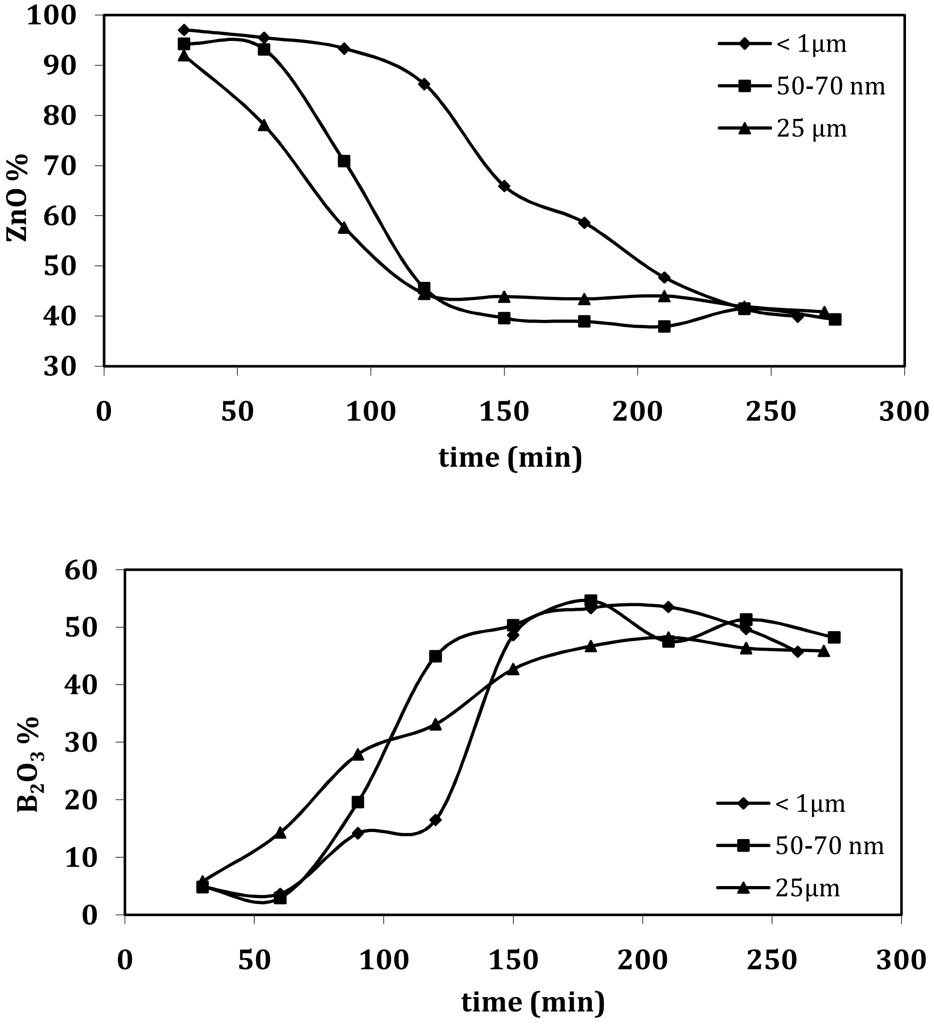

**Figure 4.10** Effect of zinc oxide average particle size on zinc borate production reaction in small scale zinc borate synthesis (temperature (85°C), seed amount (1.5%), initial reactants mole ratio ($H_3BO_3$:ZnO ratio of 5:1), and stirring rate (580 rpm) were constant)

From particle size distribution results (Figure 4.11) it can be pointed out that while the ZnO decreased from 25 µm to 50-70 nm; particle size decreased from 2.9 µm to 2.7 µm. So the decrease in the average particle size of ZnO does not significantly affect the zinc borate average particle size distribution.

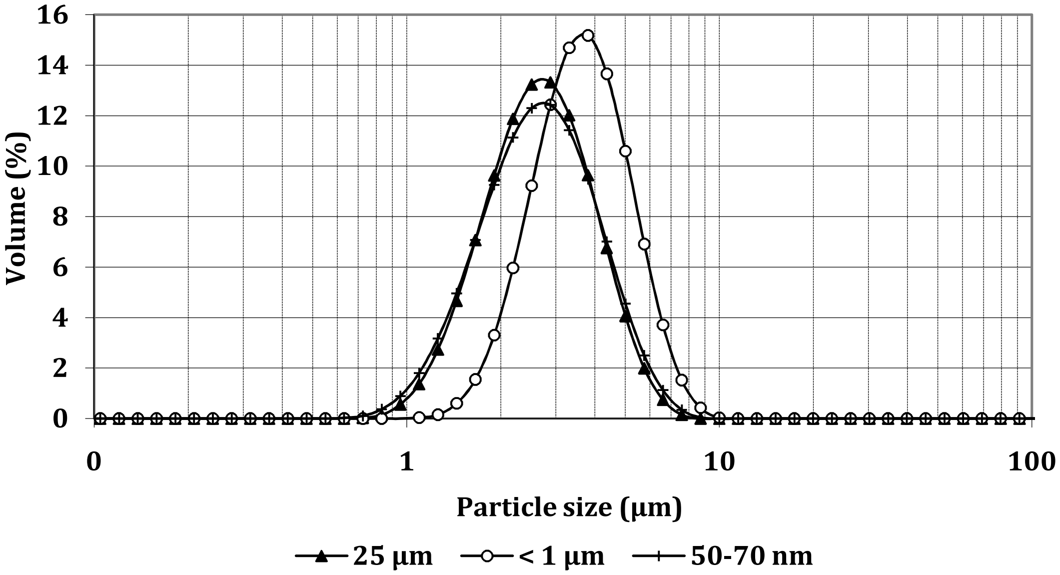

**Figure 4.11** Effect of zinc oxide average particle size on final product's average particle size distribution in laboratory scale zinc borate production

### 4.1.8 Effects of Reaction Parameters on Reaction Kinetics and Particle Size Distribution of Pilot Scale Produced 3.5 Hydrated Zinc Borates

Similar to the laboratory scale production of zinc borate, after a successive synthesis, reaction parameters such as stirring rate, zinc oxide average particle size, zinc oxide purity, $B_2O_3$:ZnO mole ratio were investigated.

### 4.1.8.1 Effect of Stirring Rate on Pilot Scale Production of Zinc Borate

Effect of mixing rate on 80 liter pilot scale, which was fed with 65 liter distilled water initially and operated for the reaction of $2ZnO\cdot 3B_2O_3\cdot 3.5H_2O$ is given in Figure 4.12. Stirring rates were chosen as 150 rpm and 271 rpm which are equivalent to the stirring rates of 320 rpm and 580 rpm in 4 liter reactor.

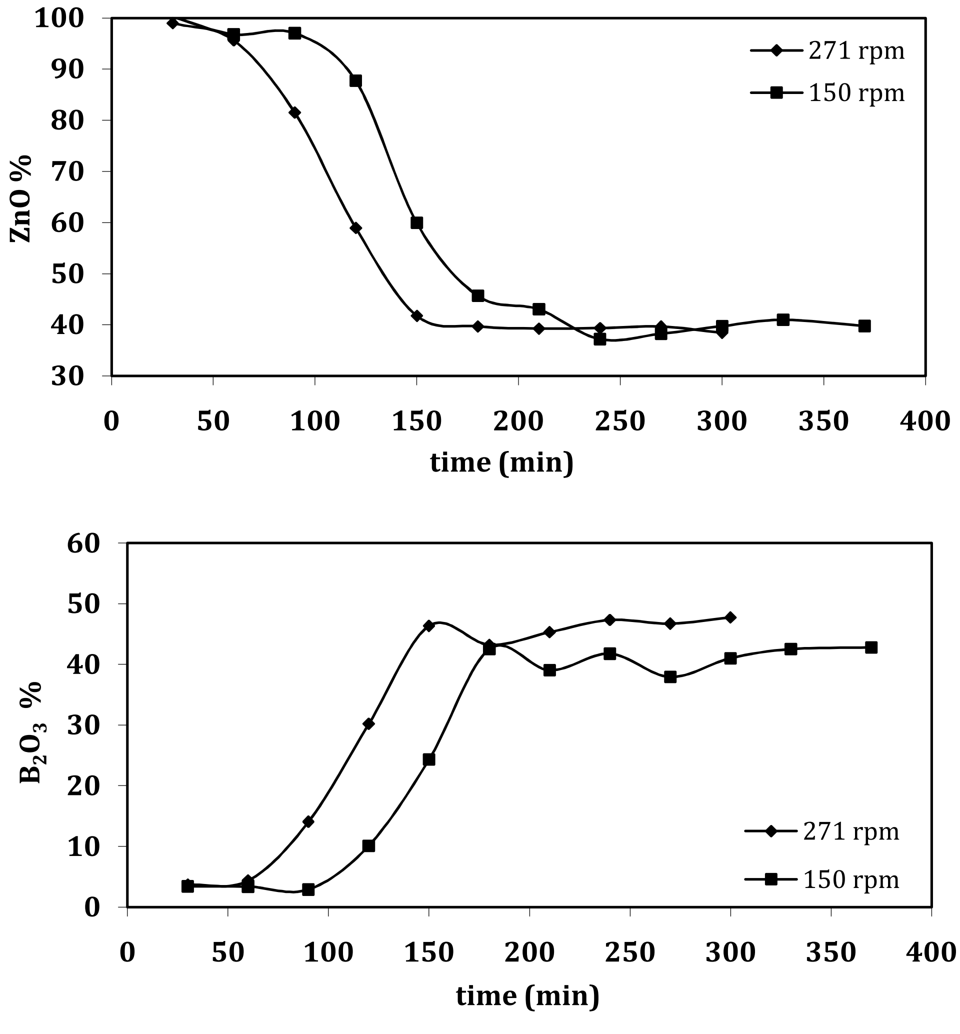

**Figure 4.12** Effect of stirring rate on zinc borate production reaction in pilot scale zinc borate synthesis. (temperature (85°C), seed amount (1.5%), initial reactants mole ratio ($H_3BO_3$:ZnO ratio of 5:1), ZnO purity (98%), and average particle size of zinc oxide particles (25 μm) were constant)

The reaction proceeded in a similar way as in the small scale production and with the increase of mixing rate the reaction was completed quickly.

Mean particle diameter decreased from 4.2 μm to 3.8 μm (Figure 4.13) with the increase of stirring rate which is similar to the laboratory scale production analysis. Increase in stirring rate causes the breakdown of the agglomerates and the removal of zinc borates crystal buds formed on the zinc oxide surface.

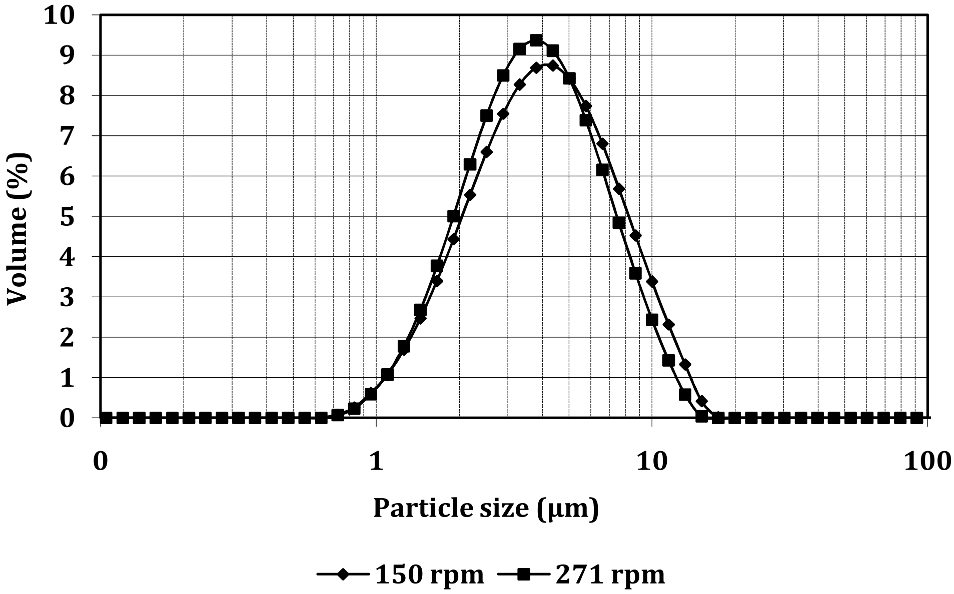

**Figure 4.13** Effect of stirring rate on final product's average particle size distribution in pilot scale zinc borate production

### 4.1.8.2 Effect of Zinc Oxide Average Particle Size on Pilot Scale Production of Zinc Borate

Reaction was completed in 2.4 hours regarding to the chemical analysis and smaller particle sized ZnO was depleted much more quickly than the bigger particle sized zinc oxide (Figure 4.14). This trend is the reverse of the laboratory scale zinc borate synthesis. This might be due to the result of more effective stirring occurred in the pilot scale reactor.

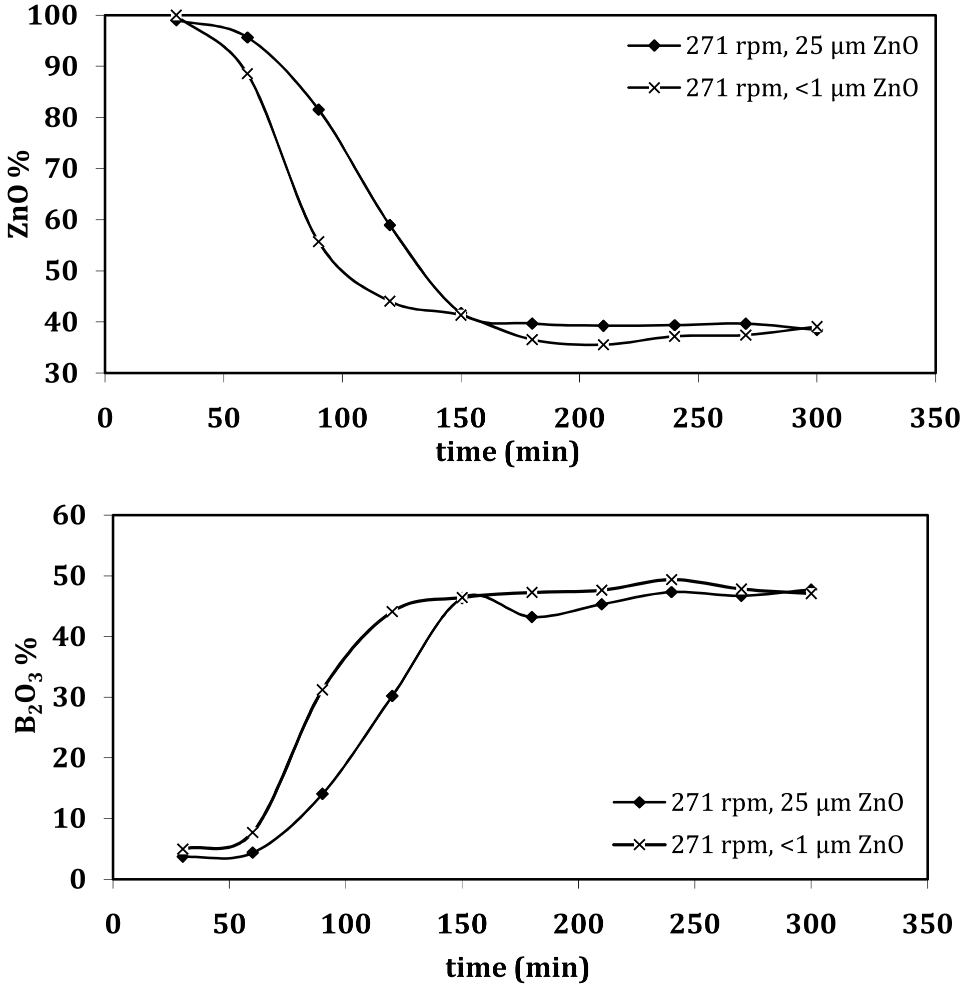

**Figure 4.14** Effect of zinc oxide average particle size on zinc borate production reaction at pilot scale zinc borate synthesis (temperature (85°C), seed amount (1.5%), and initial reactants mole ratio ($H_3BO_3$:ZnO ratio of 5:1) were constant)

Intermediate particle size diameter of the final zinc borate product was decreased from 3.8 μm (ZBP3) to 3.4 μm (ZBP4) as the zinc oxide particle diameter was decreased from 25 μm to < 1 μm (Figure 4.15).

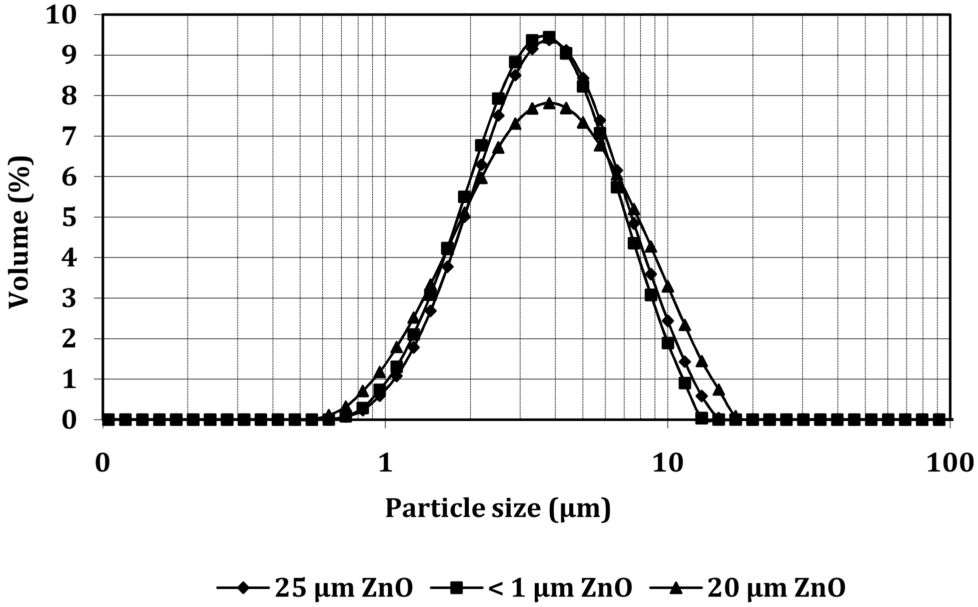

**Figure 4.15** Effect of zinc oxide average particle size on final product's average particle size distribution on pilot scale zinc borate production

#### 4.1.8.3 Effect of Boric Acid:Zinc Oxide Mole Ratio on Pilot Scale Production of Zinc Borate

$B_2O_3$:ZnO mole ratio is an important parameter for the zinc borate production reaction. From the stoichiometry of the reaction, this ratio must be at least 3.5:1. Although the reactors were sealed as good as possible, due to the structure of reactors and sample taking procedure, there would be material loss owing to the high temperature during the reaction which would be water evaporating from the system. As the boric acid was also dissolved in the water, with water loss, boric acid loss would be inevitable. So, by time, the amount of boric acid would decrease below the stoichiometric amount and also the borate ions diffusing to zinc oxide would decrease. In order to prevent this; initially excess amount of boric acid was fed to the system which was in this case 5:1 ratio. In Figure 4.16, $B_2O_3$ and ZnO analyses of the samples are given and according to the results reaction completion took nearly 5 hours when 96% purity ZnO was used.

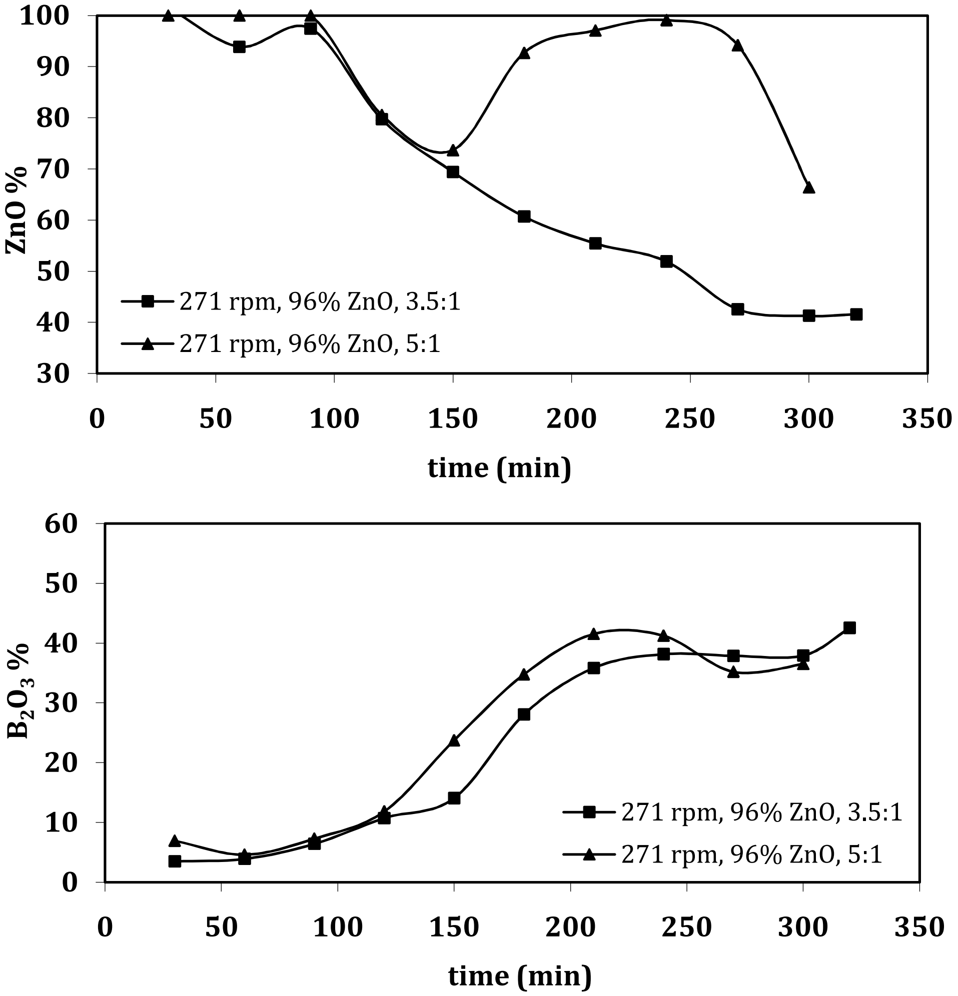

**Figure 4.16** Effect of $B_2O_3$:ZnO mole ratio on zinc borate production reaction at pilot scale zinc borate synthesis (temperature (85°C), seed amount (1.5%), stirring rate (271 rpm), ZnO purity (96%), and average particle size of zinc oxide particles (20 μm) were constant)

From X-ray results (Figure 4.3) it is clear that ZBP5 sample which had a $B_2O_3$:ZnO ratio of 3.5:1 did not match with the X-ray pattern of $2ZnO{\cdot}3B_2O_3{\cdot}3.5H_2O$, which concludes that it is another form of zinc borate. Also samples had mean particle diameter of 5.0 μm, which was relatively high when compared with the other productions in pilot scale.

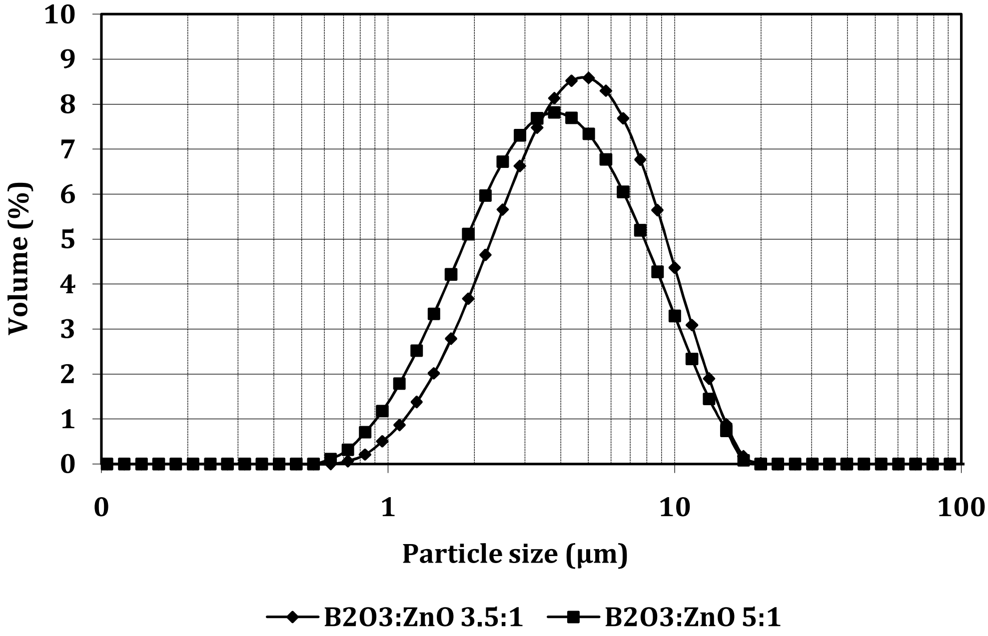

**Figure 4.17** Effect of zinc oxide average particle size on final product's average particle size distribution in pilot scale zinc borate production

### 4.1.8.4 Effect of Zinc Oxide Purity on Pilot Scale Production of Zinc Borate

As the zinc oxide is the key reactant in the 3.5 hydrated zinc borate syntheses, its purity was also evaluated for a successful synthesis. The comparison of three different types of zinc oxides which have purities of 96%, 98% and 99.9% are given in Figure 4.18. It is clear that with the increase of the purity of the zinc oxide, the reaction completed much earlier and more successful products were synthesized. The free impurities coming from the zinc oxide could be an effect as forming resistance to the borate ion's diffusion process and the impurities on the surface of the zinc oxide also decreases the active sites on the zinc oxide at which the conversion of zinc oxide to zinc borate took place.

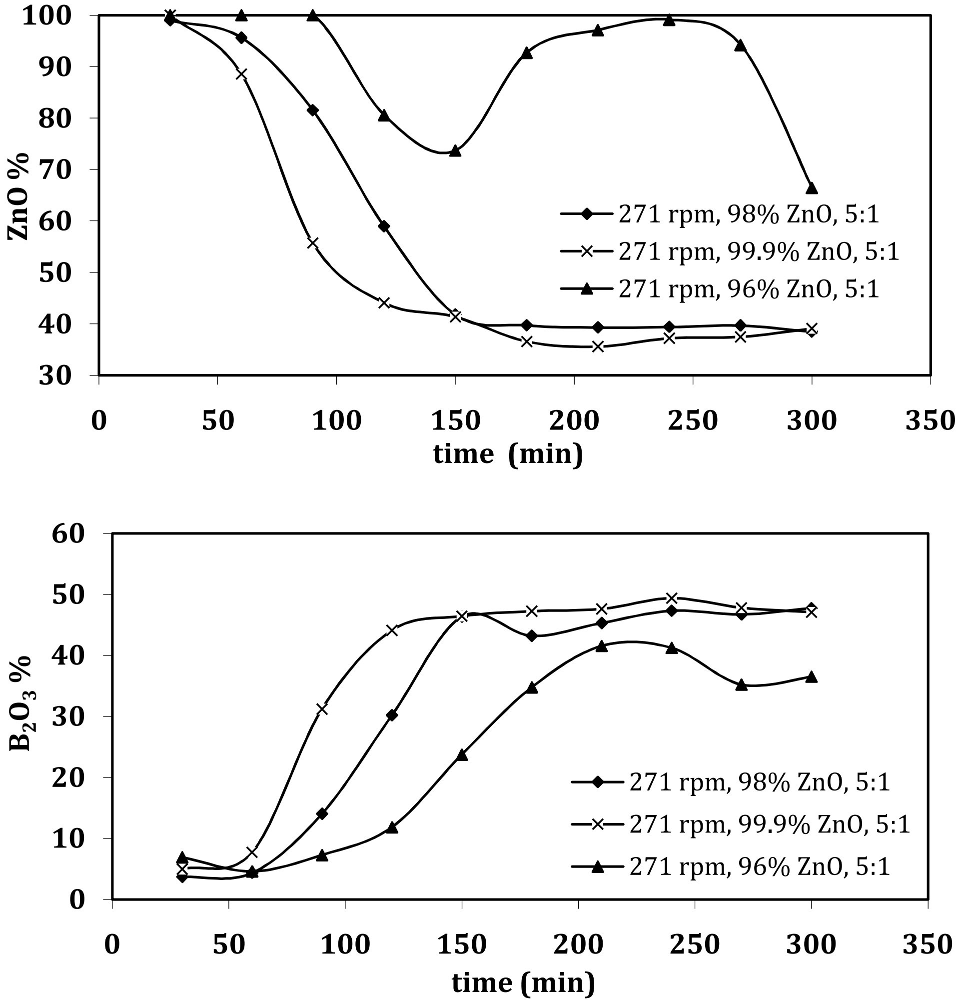

**Figure 4.18** Effect of ZnO purity on zinc borate production reaction in pilot scale zinc borate synthesis (temperature (85°C), seed amount (1.5%), initial reactants mole ratio ($H_3BO_3$:ZnO ratio of 5:1), and stirring rate (271 rpm), were constant)

The fluctuations in Figure 4.18 in $B_2O_3$ and ZnO content could be the result of the impurities in the ZnO, which possibly interferes with the ZnO chemical analysis used to determine ZnO content.

### 4.1.9 Conversion Calculations and Application of Logistic Model to the 3.5 Hydrated Zinc Borate Production on Laboratory and Pilot Scale Production

The formation of zinc borate is a heterogeneous reaction occurring in aqueous medium. During the reaction, zinc oxide is assumed to be insoluble in water and boric acid is assumed to be completely dissolved in water. The reaction scheme is given in Reaction 4.1.

$$6B(OH)_3\ (aq.) + 2\ ZnO\ (s) \rightarrow 2ZnO{\cdot}3B_2O_3{\cdot}3.5H_2O\ (s) + 5.5H_2O\ (l) \qquad (4.1)$$

In this case, unreacted core model is appropriate for this kind of reactions [147]. Steps for these kinds of reactions were proposed by Levenspiel [147]. In the first step, borate ions from the bulk of boric acid solution diffuse to the surface of the zinc oxide particles. Zinc oxide particles were assumed to be spherical. After that, diffusion of borate ions through the ash layer covering the unreacted core over the zinc oxide particles takes place. Followed by this penetration, reaction of borate ions with zinc oxide particles takes place at the reaction surface. The reaction is completed by the formation of zinc borate and diffusion of co-product water molecule through the ash layer covering the unreacted core back to the bulk phase. Beyond this point, the formed zinc borate crystals start to grow up and after some point start to precipitate. This information implies that the average particle size of the zinc borate is directly related to the average particle size of the zinc oxide used as reactant and also for the time utilized for the crystal growth of zinc borate. The analysis performed till here is in contradiction with the unreacted core model as with the decrease of ZnO average particle size, the mean particle size of zinc borate did not decrease. Thus, another model should be proposed to explain the reaction scheme and kinetics which is more appropriate.

The crystal growth of zinc borate from the reaction of zinc oxide and boric acid can be modeled by adopting the logistic model, which has been used for growth in biological system [15, 148]. In contrast to the biological system, the extent of reaction in crystallization is limited to the complete conversion of reactant to the product. Data for the conversion of zinc oxide versus time were fit to the logistic model. In this model, the rate law is given by Equation 4.2 where the rate of crystal growth for zinc borate

$$\text{rate} = \frac{dX}{dt} = k\left(1-\frac{X}{X^*}\right)X \tag{4.2}$$

in M/min is equal to dX/dt in the case of batch reactor, X is the zinc borate concentration (M) in the slurry reactor, X* is the maximum zinc borate concentration (M), k is the specific growth rate (1/min). When X is equal to the X*, the crystal growth rate is zero. The integrated form of the rate law is where $X_0$ is the critical initial

$$X = \frac{X^*}{1+(\frac{X^*}{X_o}-1)e^{-kt}} \tag{4.3}$$

concentration of zinc borate. Using the normalized concentrations ($\chi = X/X^*$ and $\chi_o = X_o/X^*$) will reduce the number of parameters to two, k and $\chi_o$, in the integrated form of rate equation:

$$\chi = \frac{1}{1+(\frac{1}{\chi_o}-1)e^{-kt}} \tag{4.4}$$

This equation can be rearranged into linear form:

$$\ln\left(\frac{1}{\chi}-1\right) = -kt+\ln\left(\frac{1}{\chi_o}-1\right) \tag{4.5}$$

Either using the curve fitting software, Microsoft Excel, the experimental data were fit to the integrated rate law (Eq. 4.3) or the linear regression of the data with Equation

4.5, the values of two model parameters k and $\chi_o$ were obtained and listed in Table 4.5 for laboratory scale zinc borate production and in Table 4.6 for pilot scale zinc borate production. It is worth to mention that the normalized concentration is nothing else than the conversion of zinc oxide, since the X* is the maximum concentration of zinc borate at complete conversion. $X_o$ values are related to the seed concentration added to the solution at the beginning of reaction. Since zinc borate is initially added as seed to the solution, the initial normalized concentration $\chi_o$ is nonzero in all experiments but smaller than the experimental value $\chi_o(\text{exp}) = 0.0213$.

**Table 4.5** Logistic model parameters for the laboratory scale production of zinc borate

| **Sample** | **$\chi_o = X_o/X^*$** | **k, min$^{-1}$** | **$R^2$** |
|---|---|---|---|
| ZB1 | 0.0339 | 0.0502 | 0.954 |
| ZB2 | 0.0255 | 0.0454 | 0.973 |
| ZB3 | 0.0134 | 0.0448 | 0.987 |
| ZB4 | 0.0028 | 0.0366 | 0.857 |
| ZB5 | 0.0014 | 0.0516 | 0.751 |
| ZB6 | 0.0014 | 0.0535 | 0.898 |
| ZB7 | 0.0028 | 0.0550 | 0.797 |

The $R^2$ values for the model for laboratory scale production were in between 0.751-0.987. Those results show that the logistic model fits this reaction kinetics suitably.

**Table 4.6** Logistic model parameters for the pilot scale production of zinc borate

| Sample | $\chi_o = X_o/X^*$ | k, min$^{-1}$ | R$^2$ |
|---|---|---|---|
| ZBP1 | 0.0036 | 0.0341 | 0.939 |
| ZBP2 | 0.0031 | 0.0374 | 0.931 |
| ZBP3 | 0.0052 | 0.0431 | 0.958 |
| ZBP4 | 0.0095 | 0.0444 | 0.983 |
| ZBP5 | 0.0118 | 0.0276 | 0.916 |
| ZBP6 | 0.0335 | 0.0280 | 0.841 |

The R$^2$ values for the model for pilot scale production were in between 0.841-0.983, which implies that logistic model represents the pilot scale production much more accurate.

Figure 4.19 shows the conversion comparison of the effect of seed amount on zinc borate production in laboratory scale. As seen from the figure, the ZnO conversion does not change significantly with the seed amount. Also, the rate constants did not change noticeably. This observation indicates that the particle size of seed crystals has no effect on the reaction. This might be explained by the assumption that the zinc borate added to the solution as seed is dissolved and provides a saturation concentration for zinc borate in solution during the reaction, so that the zinc borate formed from the reaction can precipitate on the zinc oxide surface. The formation of zinc borate on the surface of zinc oxide particles may be considered as nucleation followed by the autocatalytic growth of zinc borate crystals.

When the results of logistic model are compared with the results of Gürhan et al.'s study [15], similar conclusions can be seen. In that study, it is also confirmed that the increase of stirring rate increases the specific growth rate. In addition excess boric acid at the beginning of the reaction and presence of seed are essential for a successful synthesis. In contradiction it is claimed that the increase of stirring rate does not affect the final product's average particle size.

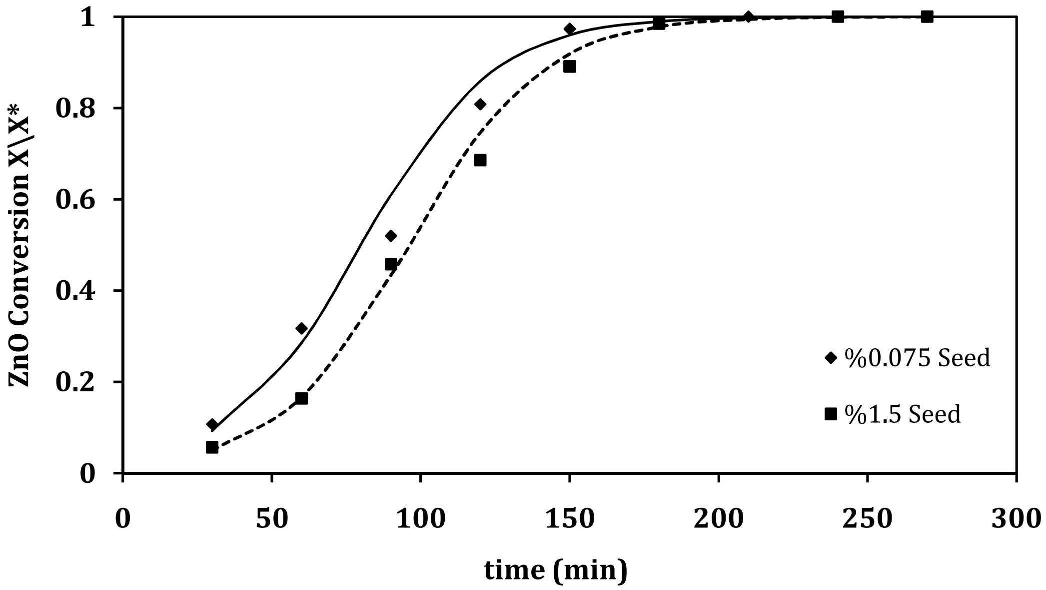

**Figure 4.19** ZnO conversion vs. time graph to observe the effect of seed amount (temperature (85°C), initial reactants mole ratio ($H_3BO_3$:ZnO ratio of 5:1), stirring rate (580 rpm), and average particle size of zinc oxide (25 μm) were constant) Curves denote the logistic model

The effect of presence of baffle presence on ZnO conversion is given in Figure 4.20. While presence of baffles increases the effectiveness of mixing, they could possibly form dead zones in the reactor. Without baffle, consumption of ZnO is much quicker and the specific growth rate constant is higher. These results imply the increase in reaction rate. Unlike the effect on reaction rate, without baffle usage, average particle size of zinc borate decreases significantly when compared to the case where baffles were present.

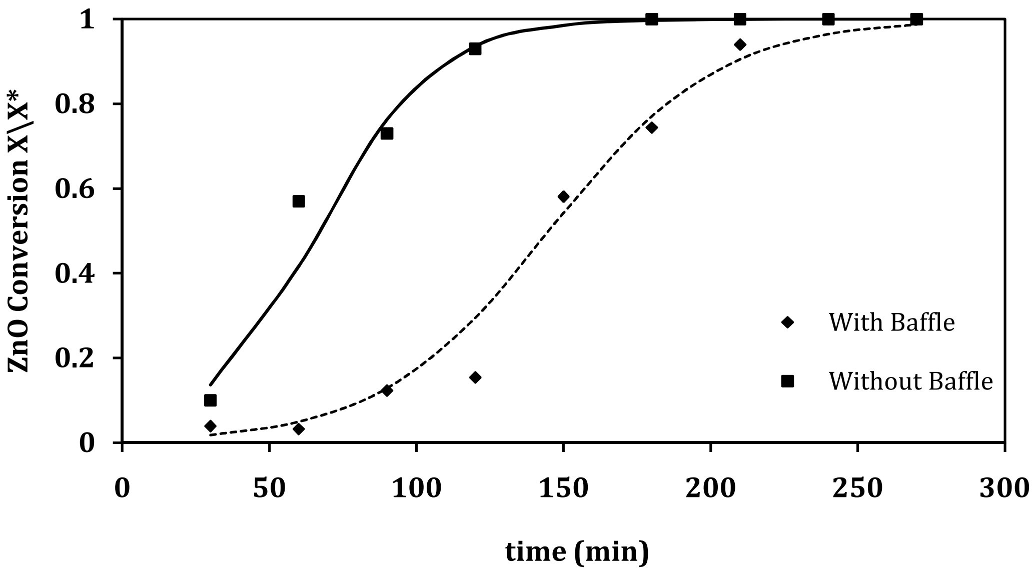

**Figure 4.20** ZnO conversion vs. time graph to observe the effect of presence of baffle (temperature (85°C), seed amount (1.5%), initial reactants mole ratio ($H_3BO_3$:ZnO ratio of 5:1), and average particle size of zinc oxide particles(25 μm) were constant) Curves denote the logistic model

Figure 4.21, shows the effect of stirring rate on zinc oxide conversion during zinc borate synthesis in laboratory scale. As the stirring rate increases one observes a decrease in the induction time (the initial part of the curves). Although the complete conversion of zinc oxide to zinc borate is achieved within a period of time less than 200 min at 450 and 580 rpm stirring rates, at 320 rpm the reaction is much slower. In general, it can be concluded that the stirring rate has a pronounced effect on the reaction rate and reaction completion time. The change of reaction rate with the stirring rate shows clearly that the reaction is mass transfer limited in terms of diffusion of dissolved borate ions coming from boric acid to the zinc oxide particles.

The effect of stirring rate can be appreciated much better in terms of model parameters, $\chi_o$ and k. As seen in Table 4.5, $\chi_o$ shows an abrupt decrease on passing from 320 to 580 rpm. The specific growth rate, k, increases with the stirring rate.

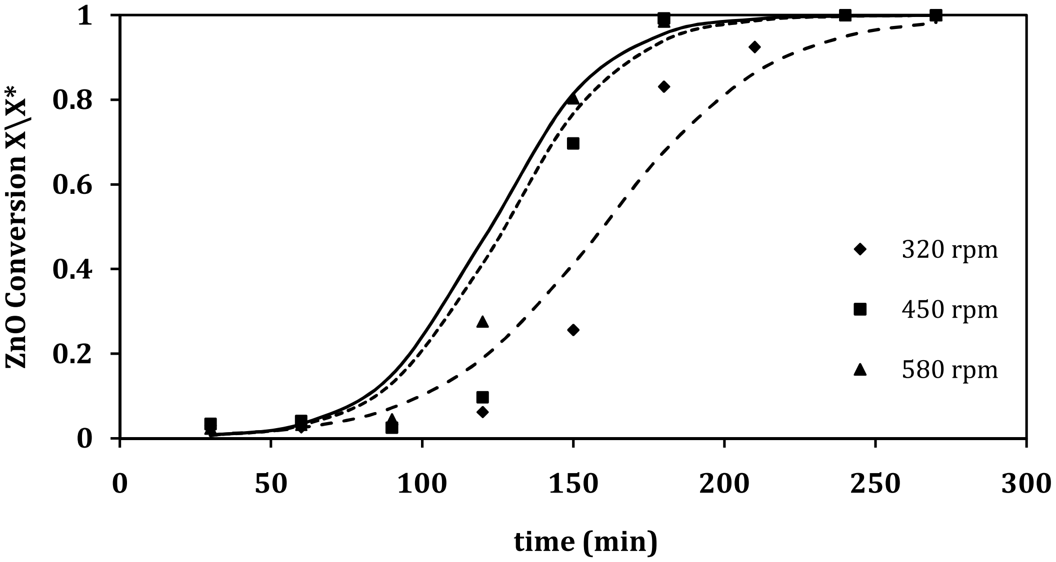

**Figure 4.21** ZnO conversion vs. time graph to observe the effect of stirring rate (temperature (85°C,) seed amount (1.5%), initial reactants mole ratio ($H_3BO_3$:ZnO ratio of 5:1), and average particle size of zinc oxide particles (< 1 µm) were constant) Curves denote the logistic model

The comparison of different average particle sized zinc oxides on the conversion of ZnO during the zinc borate synthesis is given in Figure 4.22. The reaction carried on with larger zinc oxide particles, was found to have a smaller value of specific growth rate (k = 0.0448 $min^{-1}$) than the one with smaller size zinc oxide (k = 0.550 $min^{-1}$). By increasing the particle size of zinc oxide, the surface area of zinc oxide particles increases. Hence, the growth of the zinc borate particles is initiated in larger numbers of active sites on the surface of each zinc oxide crystal. The zinc borate crystals formed on these sites after the formation were detached from the surface of zinc oxide crystals which could be seen in the SEM analysis in the forecoming sections of the characterization experimental results.

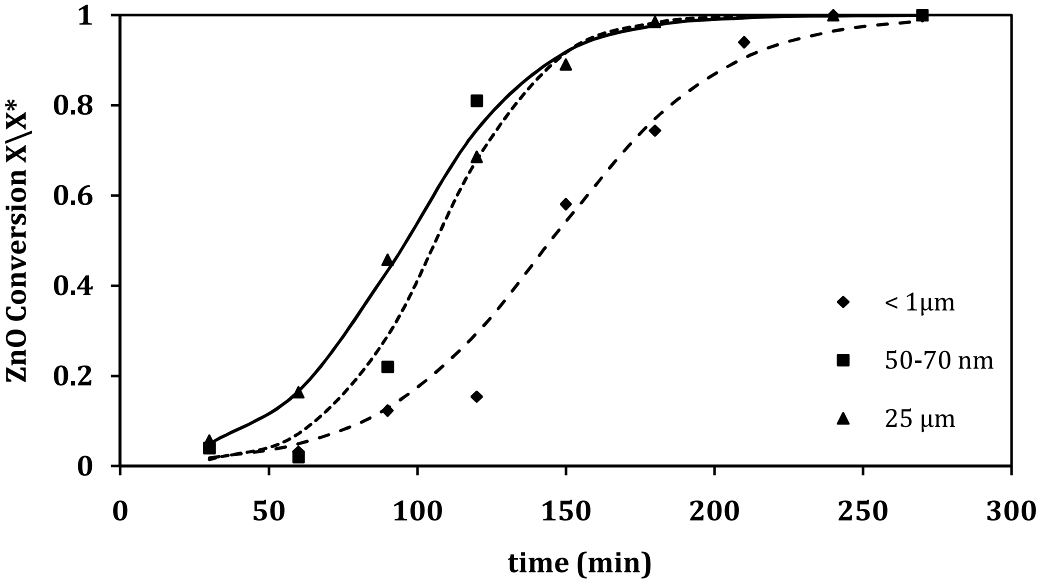

**Figure 4.22** ZnO conversion vs. time graph to observe the effect of average particle size of ZnO (temperature (85°C), seed amount (1.5%), initial reactants mole ratio ($H_3BO_3$:ZnO ratio of 5:1), and stirring rate (580 rpm) were constant) Curves donate the logistic model

In Figure 4.23, effect of stirring rate on zinc oxide conversion on pilot scale zinc production is given. It can be concluded that the specific growth rate is higher at high stirring rates similar to the laboratory scale productions. The zinc oxide conversion was completed before 240 minutes in both cases. Increase in the stirring rate facilitates the diffusion of borate ions to the zinc oxide particles and as a result increases the reaction rate.

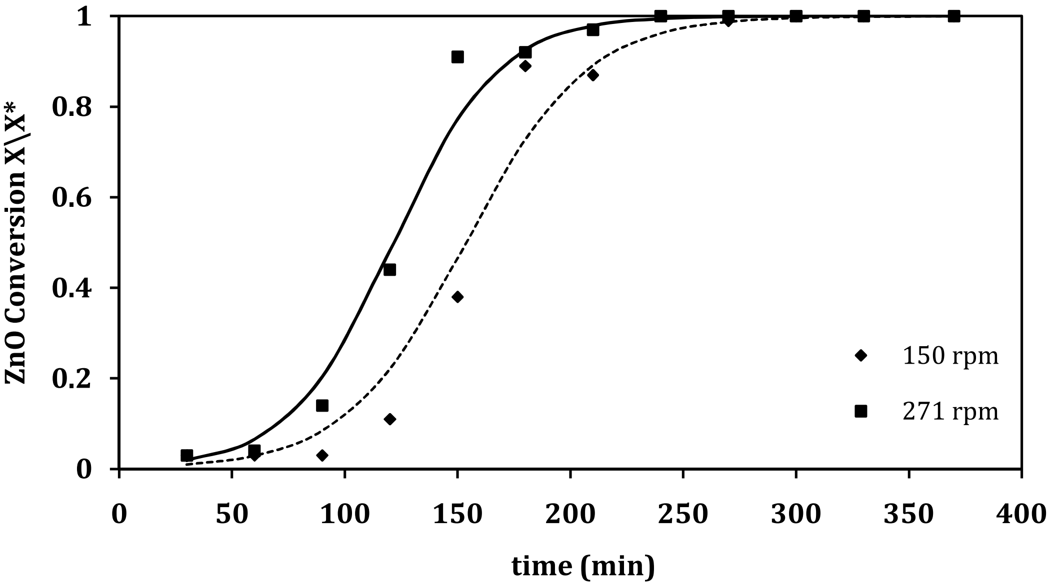

**Figure 4.23** ZnO conversion vs. time graph to observe the effect of stirring rate (temperature (85°C), seed amount (1.5%), initial reactants mole ratio ($H_3BO_3$:ZnO ratio of 5:1), ZnO purity (98%), and average particle size of zinc oxide particles (25 μm) were constant) Curves denote the logistic model

Effect of zinc oxide average particle size on zinc oxide conversion is given in Figure 4.24. The differences between the zinc oxide conversions were not significant when either < 1 μm or 25 μm zinc oxide was used, but the specific growth rate is higher in comparison. As a result, usage of < 1 μm ZnO is beneficial in the production of zinc borate in pilot scale production.

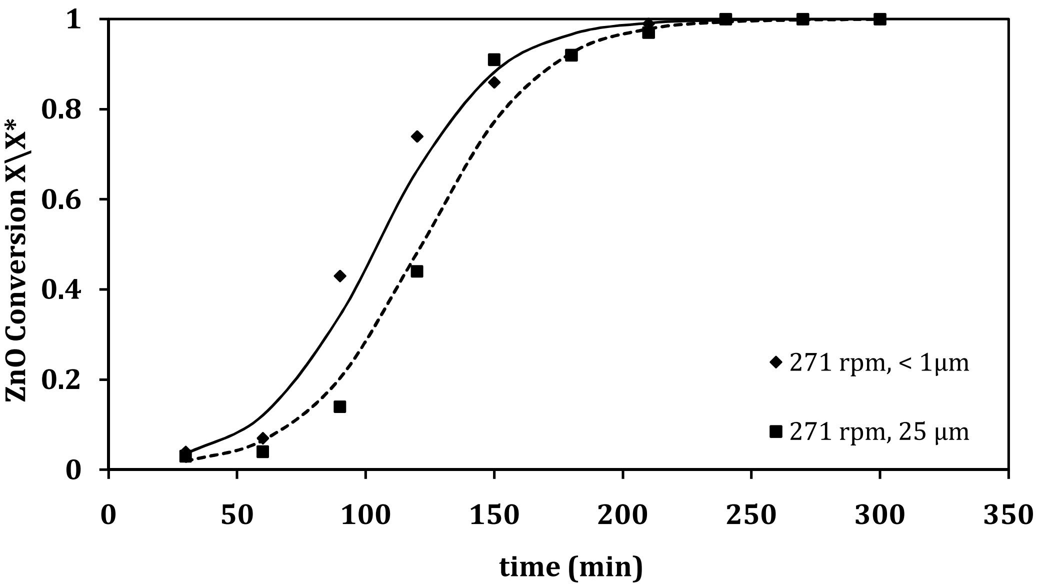

**Figure 4.24** ZnO conversion vs. time graph to observe the effect of average particle size of ZnO (temperature (85°C), seed amount (1.5%), and initial reactants mole ratio ($H_3BO_3$:ZnO ratio of 5:1) were constant). Curves denote the logistic model

The zinc borate, $2ZnO{\cdot}3B_2O_3{\cdot}3.5H_2O$, was not formed when the reactants mole ratio of $H_3BO_3$:ZnO of 3.5:1 was used. One can conclude that, conversion of zinc oxide increases with the increasing concentration of boric acid (Figure 4.25), and boric acid needs to be used in excess to convert all zinc oxide to zinc borate. This is in accordance with the results reported previously by Shete and coworkers and Gürhan et al., as they also mentioned the usage of excess boric acid at the beginning of the reaction[13, 15].

As seen from Table 4.6, the higher the reactants molar ratio, the larger is the specific growth rate (k) and the higher is the critical initial concentration of zinc borate ($\chi_o$).

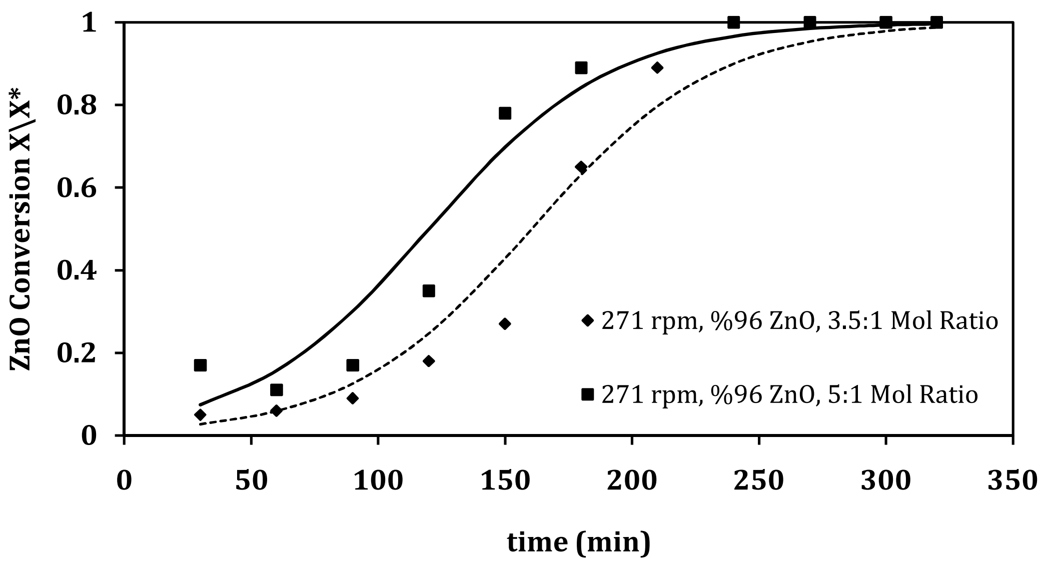

**Figure 4.25** ZnO conversion vs. time graph to observe the effect of initial reactants ratio (temperature (85°C), seed amount (1.5%), stirring rate (271 rpm), ZnO purity (96%), and average particle size of zinc oxide particles (20 µm) were constant) Curves denote the logistic model

Figure 4.26 shows the ZnO conversion related to the purity of zinc oxide and there is not a significant change in terms of conversion. Specific growth rate of ZnO increases from 0.276 min$^{-1}$ (96% purity) to 0.444 min$^{-1}$ (99.9% purity) with the increase of zinc oxide purity. Thus, it can be concluded that the reaction rate increased with the increase of zinc oxide purity. The impurities initially found in the ZnO could form a resistance to the mass transfer case and as the reaction is mass transfer controlled the reaction could slow down with the presence of impurities.

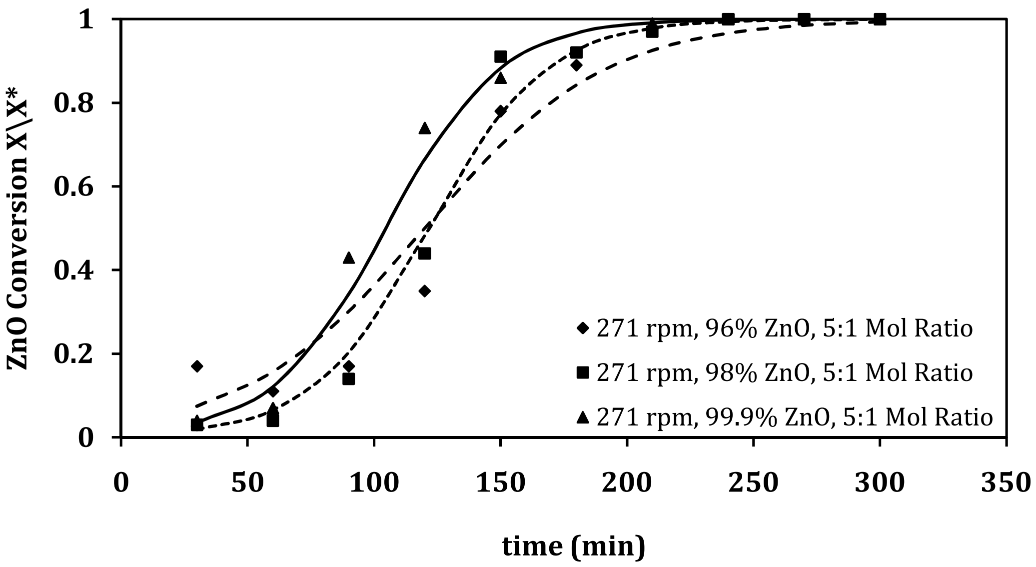

**Figure 4.26** ZnO conversion vs. time graph to observe the effect of ZnO purity (temperature (85°C), seed amount (1.5%), initial reactants mole ratio ($H_3BO_3$:ZnO ratio of 5:1), and stirring rate (271 rpm) were constant) Curves denote the logistic model

### 4.1.10 TGA Analysis of Laboratory Scale Produced 3.5 Hydrated Zinc Borate

Thermal gravimetric analyses (TGA) of the samples were done by heating the samples from 30 to 600°C at 10°C/min under $N_2$. TGA analysis gave ideas about the thermal stability of the zinc borate samples. 3.5 hydrated zinc borate is widely used as flame retardant filler in plastics. It is desired that, hydrated water of the samples should be released at a temperature that could be as high as possible. Especially, the hydrated water must be released above the processing temperature of the plastics in order to preserve its effect when zinc borate is used as flame retardant filler. Most of the plastics are processed between 150 to 250°C, so it is important to achieve the protection of hydrated water in the structure up to those temperatures. TGA analysis of laboratory scale reactor produced zinc borates are given in Figure 4.27. All samples lost the hydrated water around 300°C (the energy required to break the crystalline water from the structure is achieved at this temperature), except for the sample ZB3 that contains 1.5% seed crystal, stirred at 580 rpm and initiated with 25μm ZnO. At

600°C, this sample lost its 21% initial weight, while the other samples lost 8-12% of initial weight. This implies that, this sample has more crystalline water which is also proven by chemical analysis as this sample was found to have the chemical formula of $2ZnO{\cdot}3B_2O_3{\cdot}3.6H_2O$.

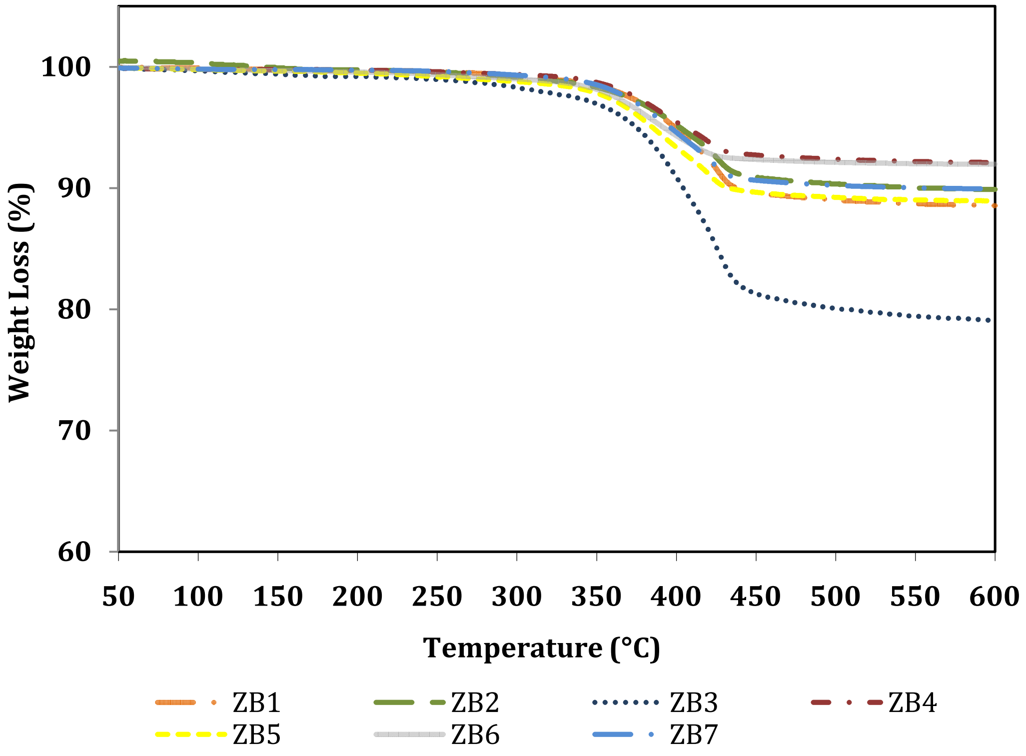

**Figure 4.27** TGA curves of laboratory scale produced zinc borates

TGA curves indicate that the zinc borates lost the crystal water in their structure above the processing temperatures of the most polymer matrices. It was reported by the producer of the commercially available Firebrake ZB, 3.5 hydrated zinc borate, loses its crystal water around 290°C. So there is a slight improvement in the thermal stabilities of the produced zinc borates compared to the commercial zinc borate. The differences between the thermal stabilities of the samples and the commercial product could be due to the result of differences between the exact crystalline water amount in their structures. Different crystalline water amounts require different energies to detach from the zinc borate.

### 4.1.11 TGA Analysis of Pilot Scale Produced 3.5 Hydrated Zinc Borate

In a similar manner when Figure 4.28 was examined, it is clear that ZBP3, ZBP4, ZBP6 had similar trend and start to lose weight at 330°C and lost 18% of initial weight. ZBP2 and ZBP5 released the hydrated water starting at 240°C. ZBP2 lost 18% of its initial weight and ZBP5 lost 30%. ZBP5 has a $B_2O_3$:ZnO ratio of 3.5:1 which is equal to the stoichiometric ratio. In order to achieve a successful reaction, it is suggested to use excess amount of boric acid, so ZBP5 could be considered as an unsuccessful synthesis, which could also be seen in X-ray plots.

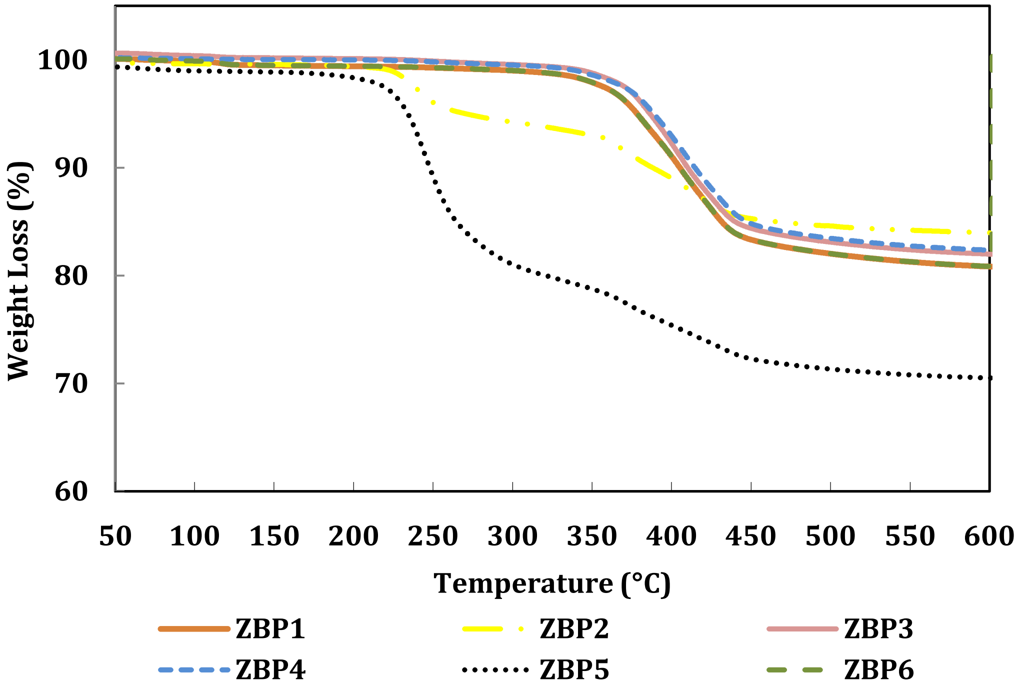

**Figure 4.28** TGA curves of pilot scale produced zinc borates

### 4.1.12 SEM Analysis of Laboratory Scale Produced 3.5 Hydrated Zinc Borate

In addition to the particle size distribution analysis, scanning electron microscopy (SEM) analyses were also performed to characterize the morphology and crystal structure and particle size distribution of synthesized 3.5 hydrated zinc borate. Zinc borate was synthesized with the reaction of boric acid and zinc oxide. Boric acid was dissolved in water, while zinc oxide was dispersed in the water as it is hydrophobic. The kinetics of the reaction was proposed as in the logistic model, in which dissolved boric acid were transferred to the zinc oxide particles and zinc borate formation reaction occurred on the zinc oxide surface. Then the formed crystal buds were detached from the zinc oxide surface and the crystal growth occurs. So the reaction is assumed to happen first by the formation of zinc borate crystals, and then crystal growth of the zinc borate crystals took place.

In Figure 4.29, SEM micrographs of zinc oxide which has an average particle size less than 1 µm are given. It can be seen that the zinc oxide crystals are in the form of agglomerates.

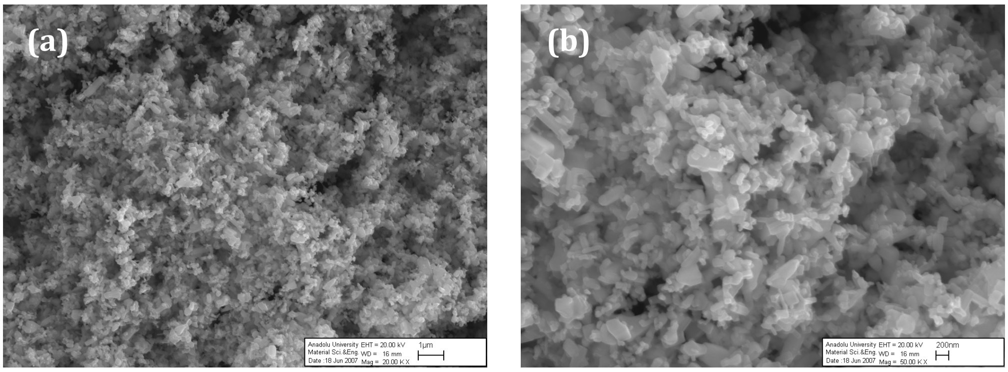

**Figure 4.29** SEM micrographs of < 1 µm ZnO (a) 20 000x, (b) 50 000x

For the determination of zinc borate crystal formation a series of experiment was performed for ZB6 sample. For the determination of ZnO and $B_2O_3$ content during the reaction, samples were taken from the reactor and analyzed. In a similar manner, samples were taken from the reactor starting from 20th minute of the reaction and after that time in every 20 minutes, samples were acquired and then SEM analysis were performed to determine the formation of zinc borate and determine how the crystals were formed and to support the logistic model. In Figure 4.30, SEM micrographs of the samples taken from the reactor at the 20th and the 40th minutes are given. The SEM micrographs conclude that the crystals are still like ZnO crystals, thus formation of zinc borate did not start yet in the reactor.

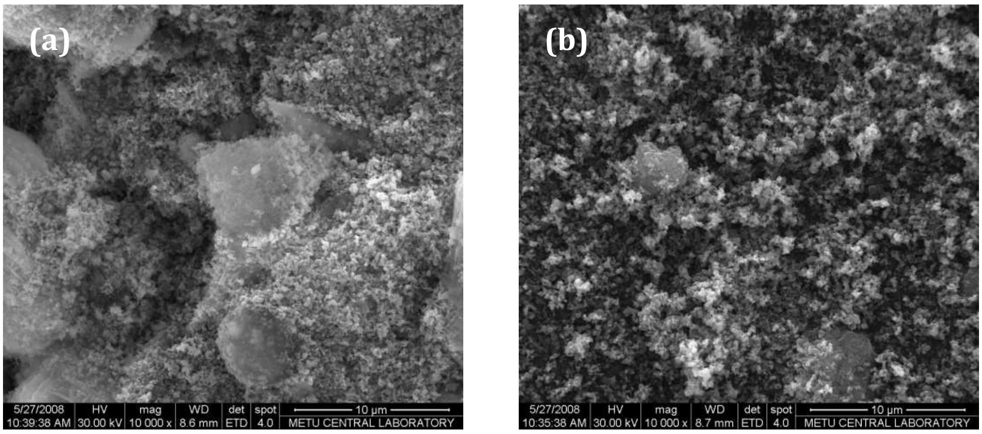

**Figure 4.30** SEM micrographs of ZB6 sample. (a) 20 min. After reaction initiates, (b) 40 min after reaction initiates (temperature 85°C, seed amount 1.5%, initial reactants mole ratio ($H_3BO_3$:ZnO ratio of 5:1), stirring rate 580 rpm, and average particle size of zinc oxide particles were < 1 μm)

In Figure 4.31, SEM pictures of the samples at 80th and 120th minute are given. It could be seen that, while at 80 minutes after the initiation of reaction the crystal structures are like zinc oxide crystals, at 120 minutes after reaction starts, the crystalline structures tend to change for the formation of zinc borate. It is observed that small budlike crystals were formed on the surfaces of zinc borates which would not be seen on letter SEM micrographs. Between 80 and 120 minutes time interval, zinc borate formation occurs and then crystal growth continues after that time interval.

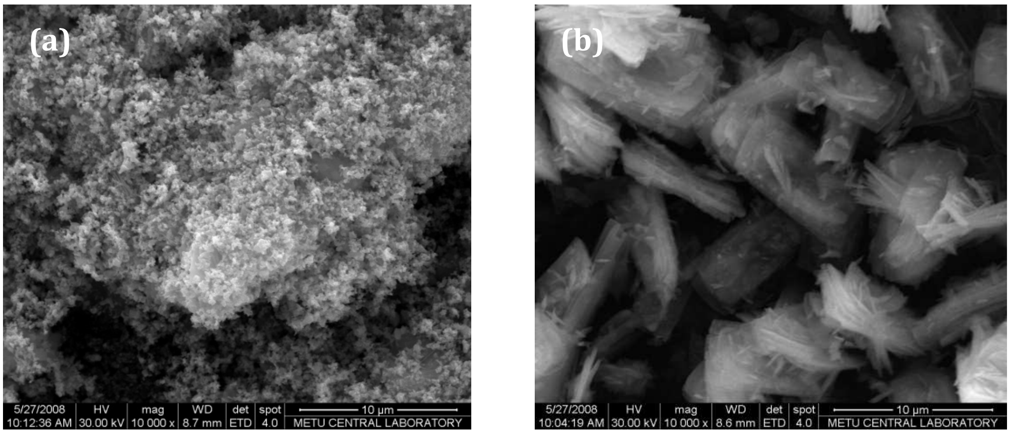

**Figure 4.31** SEM micrographs of ZB6 sample. (a) 80 min. After reaction initiates, (b) 120 min. after reaction initiates (temperature 85°C, seed amount 1.5%, initial reactants mole ratio ($H_3BO_3$:ZnO ratio of 5:1), stirring rate 580 rpm, and average particle size of zinc oxide particles were < 1 µm)

SEM images of the samples at the 160th and 200th minutes are given in Figure 4.32. After 120 minutes from the beginning of the reaction zinc borate crystals were formed and started to grow. Beyond 160 minutes the morphology of the zinc borate crystals did not change noticeably.

SEM micrographs showed that zinc borate formation occurs between the 80th and 120th minutes time interval from the beginning of the reaction and support the proposed logistic model for the reaction kinetics which was proposing that the zinc borate formation was occurring on the zinc oxide crystals with the diffusion of boric acid and then the formed zinc borate crystals left the zinc oxide crystals and continued to grow.

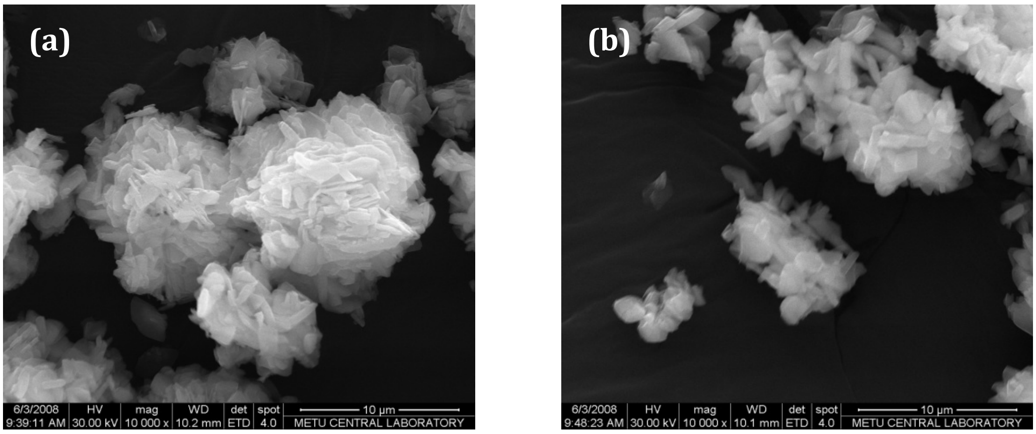

**Figure 4.32** SEM micrographs of ZB6 sample. (a) 160 min. After reaction initiates, (b) 240 min. after reaction initiates (temperature 85°C, seed amount 1.5%, initial reactants mole ratio ($H_3BO_3$:ZnO ratio of 5:1), stirring rate 580 rpm, and average particle size of zinc oxide particles were < 1 µm)

In the laboratory scale synthesis of zinc borate, for the determination of effect of zinc oxide average particle size on final product average particle size distribution SEM micrographs of ZB7 in which 50-70 nm ZnO was used for the synthesis are given in Figure 4.33. It can be concluded that when the reaction was performed with smaller particle sized zinc oxide, the final product has smaller mean particle size distribution. It was expected that according to the proposed kinetic model, when the reaction was initiated with bigger ZnO particles, due to the higher surface area there would be more sites available for the zinc borate formation. When the reaction was initiated with nano sized zinc oxide it was observed that the final products had smaller particle size distribution as if the crystals were formed by the growth of the ZnO crystals which could be assumed spherical, thus they had smaller average particle size.

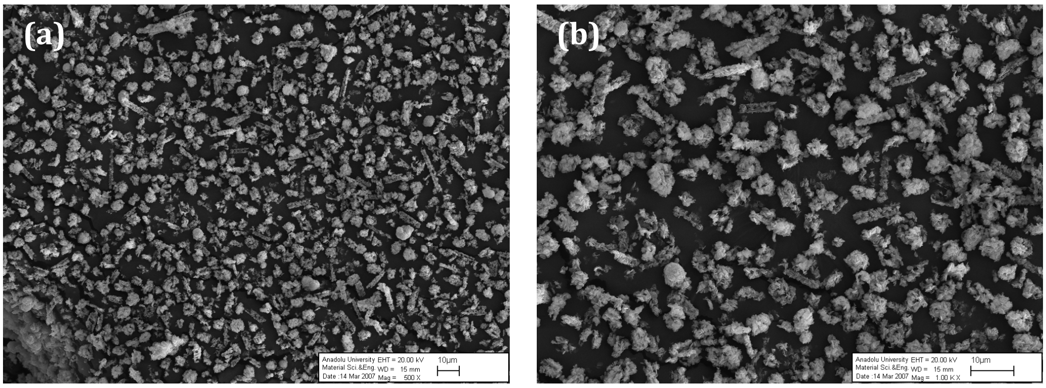

**Figure 4.33** SEM micrographs of ZB7 sample. (a) 500x, (b) 1000x (temperature 85°C, seed amount 1.5%, initial reactants mole ratio ($H_3BO_3$:ZnO ratio of 5:1), stirring rate 580 rpm, and average particle size of zinc oxide particles were 50-70 nm)

### 4.1.13 SEM Analysis of Pilot Scale Produced 3.5 Hydrated Zinc Borate

SEM analysis was also performed for the pilot scale production of zinc borate. ZBP1 is the pilot scale synthesized zinc borate, which was used in the formulations of flame retardant PET composites. In Figure 4.34, 500x and 1000x magnified zinc borate crystals can be seen. Zinc borate crystals formed agglomerates and they had a random direction growth tendency. Pilot scale produced zinc borate have particles which are smaller in terms of average particle size when compared to the commercial 3.5 hydrated zinc borate Firebrake ZB, of which particle size analysis results are given by the manufacturere's data sheet and measured by particle size analysis, and this could be designated in the SEM micrographs (Figures 4.34 and 4.35). Effective mixing and the increase of stirring rate caused decrease on the average particle size distribution of zinc borates.

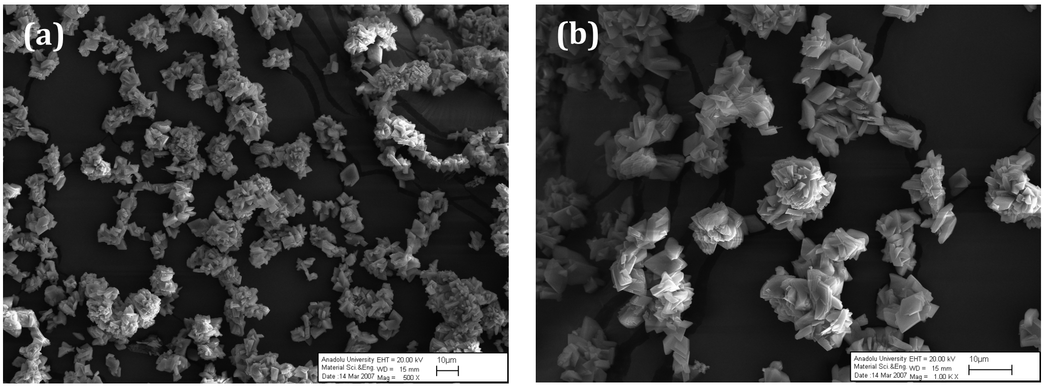

**Figure 4.34** SEM micrographs of ZBP1 sample. (a) 500x, (b) 1000x (temperature 85°C, seed amount 1.5%, initial reactants mole ratio ($H_3BO_3$:ZnO ratio of 5:1), stirring rate 96 rpm, 98% ZnO purity, and average particle size of zinc oxide particles were 25 µm)

In Figure 4.35, 5000x magnification of a zinc borate crystal is given which is ZBP1 sample.

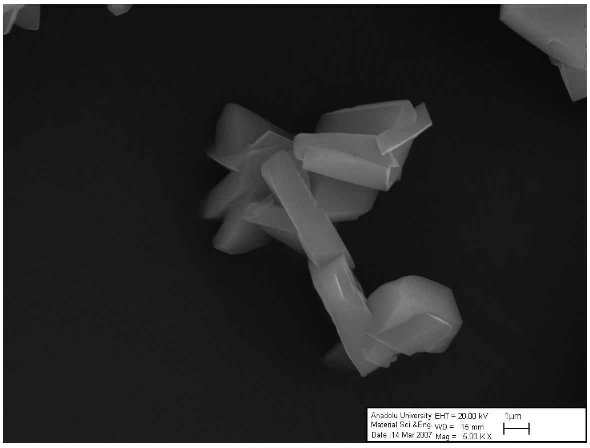

**Figure 4.35** SEM micrograph of ZBP1 sample. 5000x (temperature 85°C, seed amount 1.5%, initial reactants mole ratio ($H_3BO_3$:ZnO ratio of 5:1), stirring rate 96 rpm, 98% ZnO purity, and average particle size of zinc oxide particles were 25 µm)

## 4.2 Synthesis and Characterization of Boron Phosphate

Boron phosphate, ($BPO_4$), is an important catalyst, especially for organic reactions [149]. The other importance of $BPO_4$ is its usage as a phosphating agent. Vasovic et al. [150] investigated the phosphating feature of $BPO_4$ to obtain Mg, Ca, Zn and Pb phosphates through solid state reactions of $BPO_4$ with the corresponding oxides. The strength of porcelain can be considerably improved by the addition of $BPO_4$ [151]. It is also used as an insulator [152]. Furthermore, in electronic packaging substrate technology, borophosphosilicate glass ceramics have been used in recent years [153, 154].

The structure of boron phosphate is isomorphous with β-cristtoballite. High pressure form isomorphous with α-quartz can also be obtained.

In this study, three different methods were tried in boron phosphate synthesis, dry method, wet method and microwave method, respectively which were described in detail before. Among those, microwave technique produced zinc borate was chosen for the usage in production of flame retardant PET composites, as the overall reaction time for the production is shorter in microwave technique compared to wet and dry technique and in general smaller average particle size is obtained when microwave technique is applied.

### 4.2.1 XRD Analysis of Produced Boron Phosphates

XRD is again a powerful and suitable technique to characterize the produced samples whether they are boron phosphate or not as each inorganic compound has its unique XRD plot. The XRD patterns of the boron phosphates are given in Figure 4.36. The three attempts to produce boron phosphate were successful in terms of $BPO_4$ formation. The peaks match with each other perfectly and also with the previous studies in the literature [155-157].

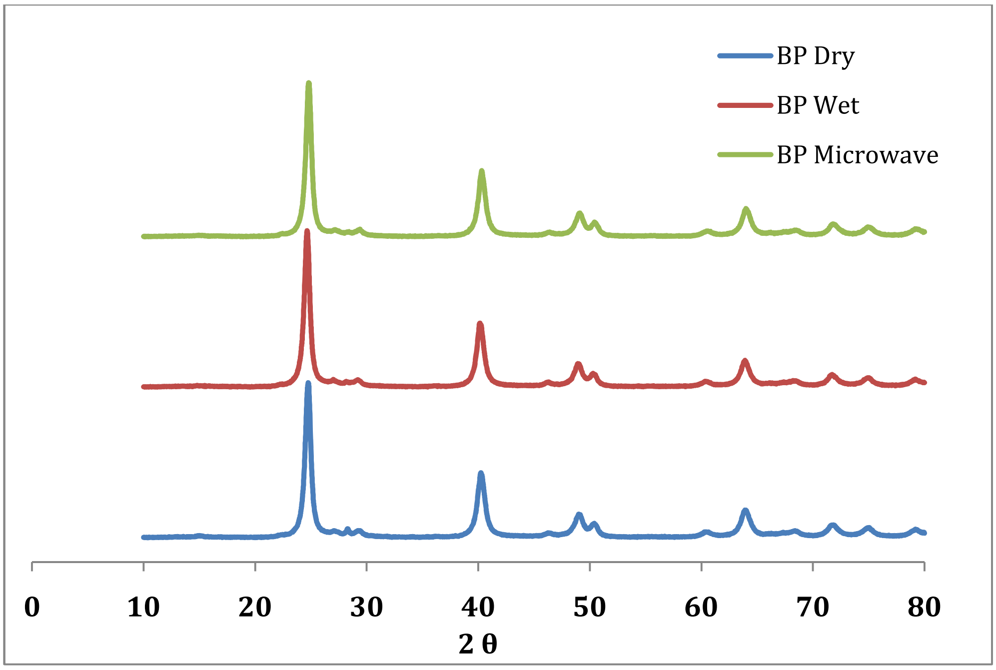

**Figure 4.36** XRD patterns of boron phosphates produced by different techniques

The characteristic peaks of boron phosphate are in between 20-70° 2 theta values range.

### 4.2.2 TGA Analysis of Boron Phosphate

Boron phosphate is a very stable inorganic substance and has a melting point over 1200°C. TGA analysis proved this data as when heated in the TGA instrument up to 1000°C, microwave technique produced boron phosphate lost only about 2.5% of its initial weight and did not show any degradation peak (Figure 4.37). That little amount of weight loss is related to the loss of water which could be absorbed as moisture on boron phosphate or other volatile impurities. The high thermal stability of boron phosphate makes it a suitable flame retardant additive.

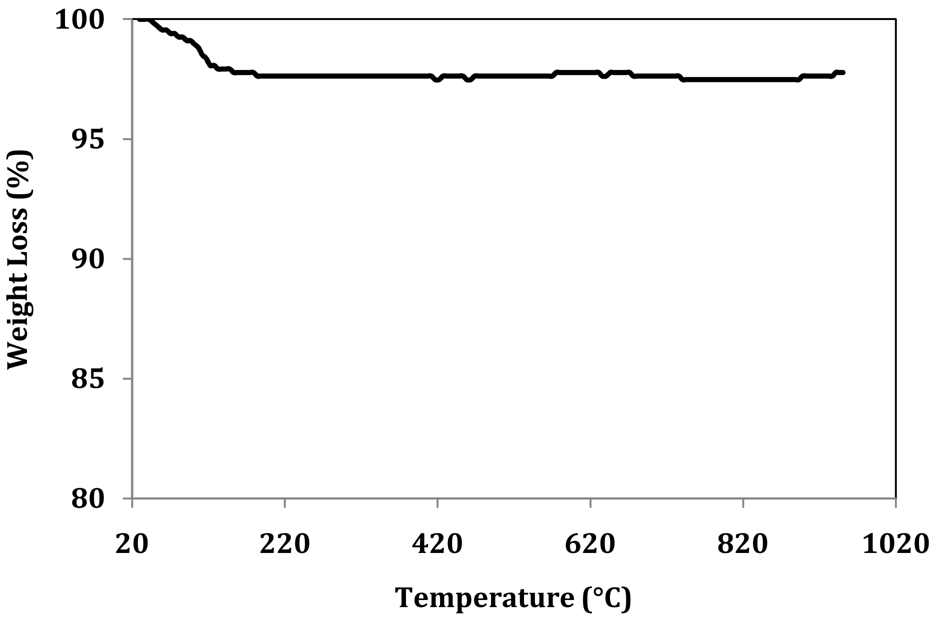

**Figure 4.37** TGA diagram of microwave technique produced $BPO_4$

### 4.2.3 Particle Size Distribution of Boron Phosphate

BET surface characterization is a widely used technique for the characterization of porous materials especially catalysts. BET technique uses the principle of the physical inert gas adsorption (nitrogen) and analyzes the relationship between the partial pressure of nitrogen and its vapor pressure to the temperature of liquid nitrogen. With this technique surface areas of investigated materials could be determined per gram. Assuming the boron phosphate crystals as spheres, this technique is adopted for the average particle size distribution of boron phosphate. Once the surface area is determined, the radius of the boron phosphate sphere could be determined as it is a non-porous material and the surface area of a sphere is equal to $4\pi r^2$ where r is the radius. In this case, the following formula was used to calculate the diameter of the boron phosphate particles.

$$A = \frac{6}{\rho \, x \, D} \tag{4.6}$$

In this equation A is the BET surface area ($m^2/g$), $\rho$ is the density of the material ($g/cm^3$) and D is the diameter of the material (m). The BET surface area of microwave produced boron phosphate was determined as 5.3928 $m^2/g$. By using Equation 4.6 the average particle size of the boron phosphate crystals were determined as 397 nm. The small mean particle size of $BPO_4$ is a big advantage for the homogeneous distribution of the material in polymer matrix when distributed as a flame retardant additive.

### 4.2.4 SEM Analysis of Boron Phosphate

The determination of the crystal structure of boron phosphate was performed by SEM analysis. SEM analysis also gave an idea about the particle size distribution of the boron phosphate crystals. In Figure 4.38, SEM micrographs of boron phosphate crystals which were produced via microwave technique are given. From the SEM micrographs it is seen that $BPO_4$ produced by microwave technique had a broad distribution of particle size distribution. This could be the result of the finishing step of boron phosphate production as in this step the sintered powder was ground by agate mortar and as a result some of the particles could not be ground enough while some of them were ground highly. As a result, a more effective technique may be proposed for the finishing step of $BPO_4$ synthesis in order to break up the agglomerates.

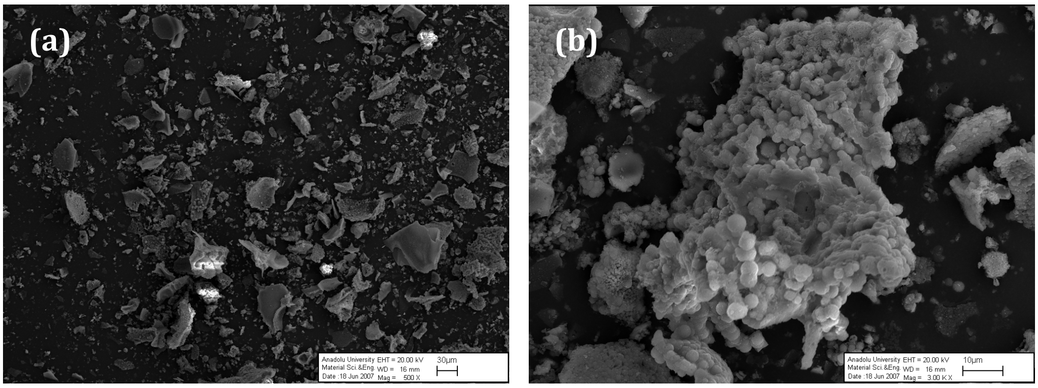

**Figure 4.38** SEM micrographs of microwave technique produced boron phosphate, (a) 500x (b) 3000x magnification

In Figure 4.39, SEM pictures of boron phosphate at 7500 and 50 000 magnifications are given. It could be seen that the $BPO_4$ crystals are in the form of nearly spherical crystals and are connected to each other forming agglomerates which shows the effect of grinding on the final step of the synthesis.

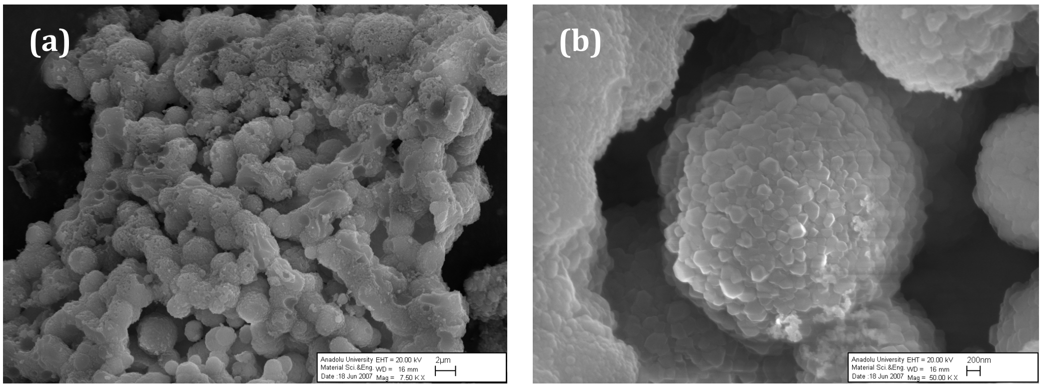

**Figure 4.39** SEM micrographs of microwave technique produced boron phosphate, (a) 7500x (b) 50 000x magnification

### 4.3 Production and Characterization of Flame Retardant PET Composites

As mentioned before, zinc borate and boron phosphate were synthesized and characterized prior to the flame retardant composites production. Poly(ethylene terephthalate) (PET), which is a widely used polyester, was chosen as the polymer matrix. In addition to the synthesized flame retardant additives, commercially available flame retardant additives were chosen and obtained after literature survey.

Experiments were planned to be performed in two stages. In the first stage, recycled PET was chosen as the polymer matrix and all flame retardant additives were added in equal weight percent amount in order to determine their effectiveness in PET matrix. Only anhydrous borax could not be added in equal amount due to the process limitations. Those composites were the first stage flame retardant additives.

After determining the effect of each flame retardant additive, the most effective four additives were chosen to be used in the second stage experiments. While this decision was made their performances to increase flame retardancy, mechanical properties and decrease smoke density were also considered. Different combinations of these additives were prepared by changing their weight percent in the composites and characterized. Further characterization was performed to determine the act mechanisms of those additives. In the production of second stage flame retardant composites, crystalline PET was chosen as the polymer matrix. Crsytalline PET was chosen in order to neutralize the effects of additives in the recycled PET, which could possibly interfere with the characterization test results and to use a virgin, additive free matrix.

In the following sections, flammability, thermal, mechanical, and morphological characterizations of the composites are given and discussed for both first stage and second stage flame retardant composites. Firstly, first stage flame retardant composites' characterization results are given. First stage composites were produced and characterized to determine the most effective flame retardant additives for the PET matrix in terms of both flammability and mechanical properties. Furthermore, smoke evolution during fire and transparency of the composites are also key parameters. Related to all these tests four flame retardant additives were determined and tried to be optimized to further improve results obtained in the first stage. So, secondly, second stage flame retardant composites' characterization results are given and finally the results of analyses which were performed to explain the detailed mechanism of flame retardant additives were mentioned.

### 4.3.1 Flammability Analysis of PET Based First Stage FR Composites

To characterize the flammability of the composites, horizontal burning rate test and limiting oxygen index (LOI) tests were performed.

#### 4.3.1.1 Horizontal Burning Rate Test of PET Based First Stage FR Composites

Horizontal burning rate test is a common test performed for the characterization of the plastics. In this test, results are reported in two ways according to the specimens' behavior during the test. If the specimen burns completely, horizontal burning rate was reported only as mm/min. In case the sample self extinguishes then average burning time (s) and average burnt length (mm) are being reported. Averages of five specimens' results were reported.

In Tables 4.7-4.9 horizontal burning rate results of first stage flame retardant composites are reported. Neat recycled PET self extinguished in the horizontal burning rate test and its average burning time was determined as 32.5±3.2 s and average burnt length was measured as 51.7±9 mm It was seen that only PET4 composite; Cloisite 30B, which is organically modified clay, was burnt completely and the rest of the composites were self extinguished after some time from the ignition (Table 4.7). Addition of cloisite 30B had negatively affected the burning behavior of PET and this could be the results of the organic modifiers in its structure.

**Table 4.7** Horizontal burning test results of first stage FR composites PET1-PET4

| | **PET1** | **PET2** | **PET3** | **PET4** |
|---|---|---|---|---|
| Horizontal Burning Rate (mm/min) | --- | --- | --- | 26.3 ± 2.4 |
| Average Burning Time (s) | 76 ± 3.8 | 47.5 ± 4.3 | 35 ± 1.4 | --- |
| Average Burnt Length (mm) | 30.5 ± 3.5 | 24.0 ± 2.8 | 17.5 ± 2.1 | --- |

Average burning time gives a relative comparison of the flame spread speed of the composites. PET1 and PET2 have the highest average burning time values and contain zinc borate and dry method produced boron phosphate, respectively. Composites PET5-PET12 have nearly the same average burning time data (Table 4.8 and Table 4.9). The results are also almost the same as the result of neat recycled PET matrix.

**Table 4.8** Horizontal burning test results of first stage FR composites PET5-PET8

| | **PET5** | **PET6** | **PET7** | **PET8** |
|---|---|---|---|---|
| Horizontal Burning Rate (mm/min) | --- | --- | --- | --- |
| Average Burning Time (s) | 37.5 ± 4.2 | 39.5 ± 3.5 | 32.3 ± 2.8 | 33.5 ± 4.2 |
| Average Burnt Length (mm) | 23.0 ± 0.2 | 23.5 ± 0.7 | 22.8 ± 0.5 | 19.5 ± 0.6 |

Average burnt length is a measure of destruction on the material related to the flame. It was clear that with the addition of flame retardant additives, the average burning rate of PET was decreased significantly. This implies that except Cloisite 30B, all the flame retardants introduced flame retardancy to the PET matrix. Horizontal burning test is a good technique to compare the flammabilities of various composites, relatively. The results of this test give information about the flame spread rate and propagation of flame through the matrix.

**Table 4.9** Horizontal burning test results of first stage FR composites PET9-PET12

| | **PET9** | **PET10** | **PET11** | **PET12** |
|---|---|---|---|---|
| Horizontal Burning Rate (mm/min) | --- | --- | --- | --- |
| Average Burning Time (s) | 33.2 ± 3.7 | 38.8 ± 4.1 | 32.7 ± 2.2 | 33.2 ± 3.4 |
| Average Burnt Length (mm) | 26.0 ± 0.4 | 22.5 ± 0.3 | 25 ± 0.2 | 23 ± 0.5 |

Anhydrous borax (PET3) and combination of 2.5 weight percent of zinc borate and 2.5 weight percent of dry method produced boron phosphate (PET8) were the most effective additives to decrease the burnt amount of the material. This might be due to the inorganic character of the materials and their proposed mechanism of action is forming a glassy protective layer in the condensed phase.

#### 4.3.1.2 Limiting Oxygen Index Test of PET Based First Stage FR Composites

Limiting oxygen index is a worldwide accepted and accurate test method to characterize flammability of plastics. In this test, minimum oxygen concentration to achieve the continuous burning could be determined.

The LOI value of neat recycled PET was determined as 20.5% (Table 4.10). When the LOI test results were analyzed, Cloisite 30B, affects the flame retardancy of PET in a negative way and increases flammability. This result is also in accordance with the horizontal burning rate results. Addition of boron phosphate (dry produced, wet produced and microwave produced), triphenyl phosphate and triphenyl phosphine oxide increased the LOI value up to 25.0%, 25.5%, 25.5% and 26.0%, respectively. The highest increase in the LOI value was obtained with the addition of calcium sulfate dihydrate.

As mentioned before, the increase of flame retardancy related to the addition of boron phosphate and zinc borate are mainly due to the formation of protective glassy layer in the polymer matrix at high temperatures which protects the unburnt polymer from the flame. In addition zinc borate loses its crystalline water during fire which dilutes the flammable gases, and also the released water acts as a heat sink which decreases the temperature at the burning zone. Triphenyl phosphate is expected to increase the char formation of the polymer, because it has three phenyl groups and high carbon content so, its mechanism of action is in the condensed phase. It decomposes to firstly pyrophosphoric acid and that acid promotes the formation of char. Furthermore, the decomposition products of triphenyl phosphate acts in the gas phase like the act mechanism of halogenated flame retardant additives by inhibiting the $H^\bullet$ radicals. Thus the formation of phosphate based ions and radicals were proposed in the literature to inhibit the hydrogen cycle during fire [158-160]. Phosphate based flame retardants were found to be effective in the polymers that have oxygen in the main backbone by forming phosphorous oxides to interrupt radical formation [161], so triphenyl phosphate and triphenyl phosphine oxide are suitable additives for the PET matrix. Triphenyl phosphine oxide also acts similar to triphenyl phosphate in the PET matrix as their structures are very similar.

**Table 4.10** Limiting oxygen index test results of first stage FR composites

| Formulation | LOI Value (%) |
|---|---|
| Neat Recycled PET | 20.5 |
| 5% Zinc Borate – 95% Re-PET | 21.0 |
| 5% Boron Phosphate – 95% Re-PET | 23.0 |
| 10% Anhydrous Borax – 90% Re-PET | 26.0 |
| 5% Clay – 95 % Re-PET | 18.5 |
| 5% Phosphorus Based FR(R2000) – 95% Re-PET | 25.5 |
| 5% Metal Powder Synergist (SAZ-12) – 95% Re-PET | 23.5 |
| 5% Boron Phosphate (MW Produced) – 95% Re-PET | 25.0 |
| 2.5% Boron Phosphate – 2.5% Zinc Borate – 95% Re-PET | 23.5 |
| 5% Boron Phosphate (Wet Produced) – 95% Re-PET | 25.5 |
| 5% Calcium Sulfate Dihydrate – 95% Re-PET | 26.5 |
| 5% Triphenyl Phosphate – 95% Re-PET | 25.5 |
| 5% Triphenyl Phosphine Oxide – 95% Re-PET | 26.0 |

### 4.3.2 Smoke Density Measurement of PET Based First Stage FR Composites

Related to the previous studies and research reports, most of the casualties during fire are as a result of smoke formed during fire[22, 23, 25, 49, 50]. Smoke has stuffy effect on living beings. Thus, it causes humans not to breathe sufficiently. Most of the smokes are based on carbon monoxide and other unburnt hydrocarbons [162]. In some cases other poisonous gases are also formed, especially when halogenated compounds are used, HX where X is the halogen, are formed [163]. While the carbon monoxide forms a sooty black smoke, most of the other poisonous gases are colorless.

The scope of this study mainly focuses on the formation of sooty smoke during fire which is detectable by light transmittance test.

Polymers, which have aromatic groups in the structure, tend to release more smoke than linear chain polymers, due to their high carbon content. PET is also in this group of polymers. In Table 4.11 percent light transmittance analysis results of the first stage flame retardant additives are given.

**Table 4.11** Smoke density test results of first stage FR composites

| Formulation | Light Transmittance (%) |
|---|---|
| Neat Recycled PET | 83 |
| 5% Zinc Borate – 95% Re-PET | 84 |
| 5% Boron Phosphate – 95% Re-PET | 98 |
| 10% Anhydrous Borax – 90% Re-PET | 83 |
| 5% Clay – 95% Re-PET | 93 |
| 5% Phosphorus Based FR(R2000) – 95% Re-PET | 83 |
| 5% Metal Powder Synergist (SAZ-12) – 95% Re-PET | 62 |
| 5% Boron Phosphate (MW Produced) – 95% Re-PET | 98 |
| 2.5% Boron Phosphate–2.5% Zinc Borate – 95% Re-PET | 88 |
| 5% Boron Phosphate (Wet Produced) – 95% Re-PET | 98 |
| 5% Calcium Sulfate Dihydrate – 95% Re-PET | 98 |
| 5% Triphenyl Phosphate – 95% Re-PET | 70 |
| 5% Triphenyl Phosphine Oxide – 95% Re-PET | 95 |

As seen from the table, the highest transmittance values were detected when boron phosphate was used as flame retardant additive in the PET matrix followed by calcium sulfate dihydrate. When the flame retardant additives have high aromatic content, due to the high amounts of the carbon in the structure more carbon monoxide is formed during fire and smoke formation increases. Thus, composites containing triphenyl phosphate have lower light transmittance values. Boron phosphate was found to be a succesful smoke suppressant for the PET matrix. It is proposed that during formation of the glassy layer, $BPO_4$ turns into $BPO_3$ and the released oxygen atom combines with the carbon monoxide forming carbon dioxide. Elimination of CO is a sign that the unburnt species in the flame were decreasing thus the density of smoke is decreasing and it become less sooty. The proposed phenomenon will be proved in the upcoming sections.

### 4.3.3 Mechanical Properties of PET Based First Stage FR Composites

While improving flammability of the PET matrix is the main concern in this study, preserving or if possible improving the mechanical properties of the composites is also another important objective. In the literature, in most studies while the flammability of the composites were increased, the effect of flame retardant additives on the mechanical properties were disregarded. The amount of the flame retardant additive is an important parameter that affects the mechanical properties. Some additives must be added up to 40% to impart flame retardancy. Thus the mechanical properties decrease severely. In this study, the amount of flame retardant additives were kept constant at 5 weight percent for the first stage flame retardant additives and at 15 weight percent for the second stage flame retardant additives. Also, size of the flame retardant additives, the presence of the functional groups or their affinity to give reactions with the polymer matrix are important parameters to affect mechanical properties.

In this study, composites were characterized in terms of tensile properties; tensile strength, tensile modulus, elongation at break behavior; impact properties; and hardness properties.

#### 4.3.3.1 Tensile Properties of PET Based First Stage FR Composites

Tensile properties of first stage PET based flame retardant composites are given in Figure 4.40. Neat recycled PET has tensile strength value around 52 MPa. Addition of boron phosphate (wet method, microwave method produced), triphenyl phosphate, triphenyl phosphine oxide increased the tensile strength of the PET matrix. Triphenyl phosphate caused the highest increase in the tensile strength which is about 63 MPa. It is proposed in the literature that triphenyl phosphate acts as a chain extender in the polyester matrices [164, 165]. Molecular weight determinations, which will be mentioned in the upcoming parts, proved this phenomenon. Microwave produced boron phosphate has an average particle size of 397 nm, so it could be mentioned as nanofiller. Small particle size of microwave produced boron phosphate introduces an advantage of homogeneous distribution in the polymer matrix and this distribution causes the dissipation of the impact energy in the matrix via crack propagation theory, thus causes an increase in impact strength. Introduction of dry method produced boron phosphate, anhydrous borax, Reogard 2000 decreased the tensile strength of the composites significantly. Reogard 2000 is an intumescent flame retardant additive, that means the additive transforms to a porous morphology when exposed to heat, thus forms a protective layer. During the processing of the polymer matrix with the flame retardant additives some portion of the Reogard 2000 could be turned to porous structure and those porous structures in the matrix could be stress concentrated areas that reduce the tensile strength of the polymer matrix. Anhydrous borax is an inorganic additive which does not have any functional groups in its structure and it has high hardness value as a result, it might not react with the PET matrix and so will not be bound to the polymer backbone, as a result it will give rise to stress concentration areas which reduces the tensile strength of the polymer matrix. In terms of tensile strength, triphenyl phosphate, triphenyl phosphine oxide, microwave produced boron phosphate, are successful additives for the PET matrix.

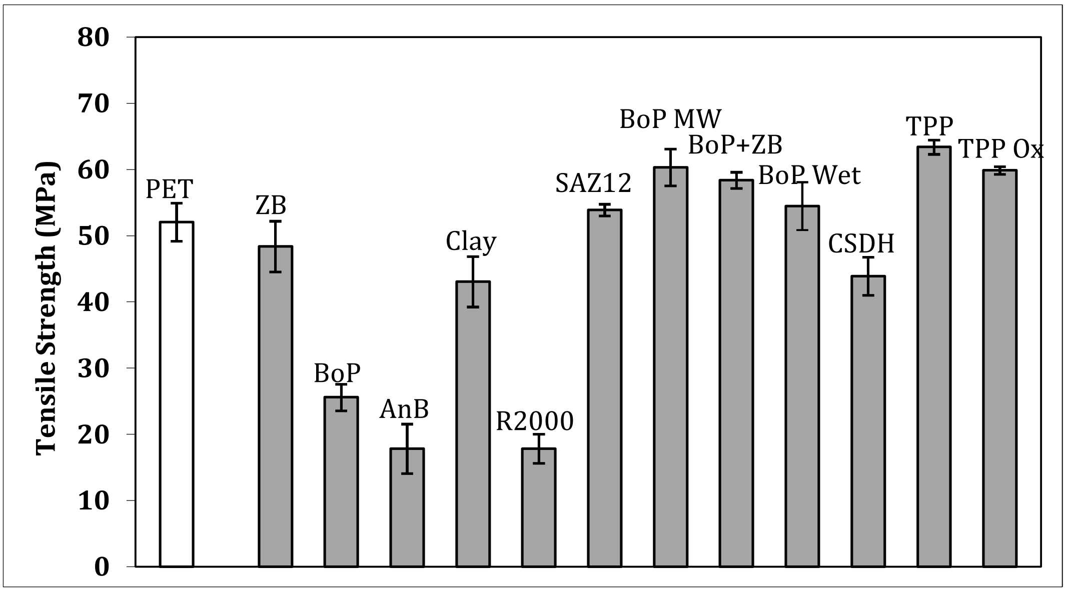

**Figure 4.40** Tensile strength data of first stage PET based flame retardant composites

In Figure 4.41 tensile modulus data of the first stage flame retardant composites are given. Neat recycled PET has a tensile modulus value around 1450 MPa. Most of the flame retardant additives decreased the tensile modulus value of PET matrix. The most noticeable decrease was observed with the addition of dry method produced boron phosphate, which could be the result of non-homogeneous distribution of the crystals in the matrix due to the relatively larger particle size distribution in the matrix. So those crystals could form agglomerates and form stress concentrated regions in the matrix and could increase the crystallinity to affect the tensile properties in a negative manner. Calcium sulfate dihydrate, microwave produced boron phosphate increased the tensile modulus of the matrix and, anhydrous borax and triphenyl phosphate slightly decreased the tensile modulus of the matrix. Calcium sulfate dihydrate is a crystalline additive mainly acting as a char former. Boron phosphate and calcium sulfate dehydrate have high hardness values, thus they introduce stiffness to the polymer matrix that causes increase in tensile modulus.

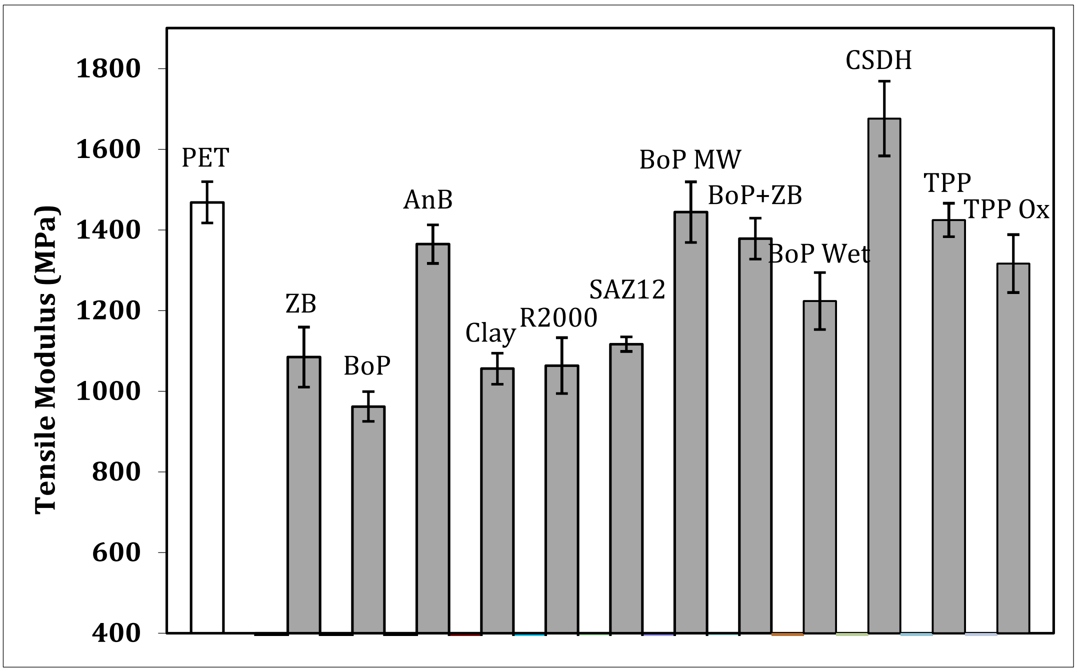

**Figure 4.41** Tensile modulus data of first stage PET based flame retardant composites

When elongation at break values of flame retardant composites were considered (Figure 4.42), addition of triphenyl phosphate and triphenyl phosphine oxide increased the elongation at break values of the composites significantly; while the elongation at break value of PET was around 30%, triphenyl phosphate addition to the matrix increased it up to 300%. This huge increase in the elongation could be the result of plasticizing effect of triphenyl phosphate on the PET matrix combined with the chain extension effect. As the molecular structure of triphenyl phosphine oxide is similar to the triphenyl phosphate it behaves in the same manner with triphenyl phosphate. These two triaryl phosphate type additives may also decrease the crystallinity of the matrix, which also increases their tolerance to deformation, thus elongation. It can also be concluded that introduction of stiffer and harder additives to the PET matrix decreased the elongation at break values of the PET matrix.

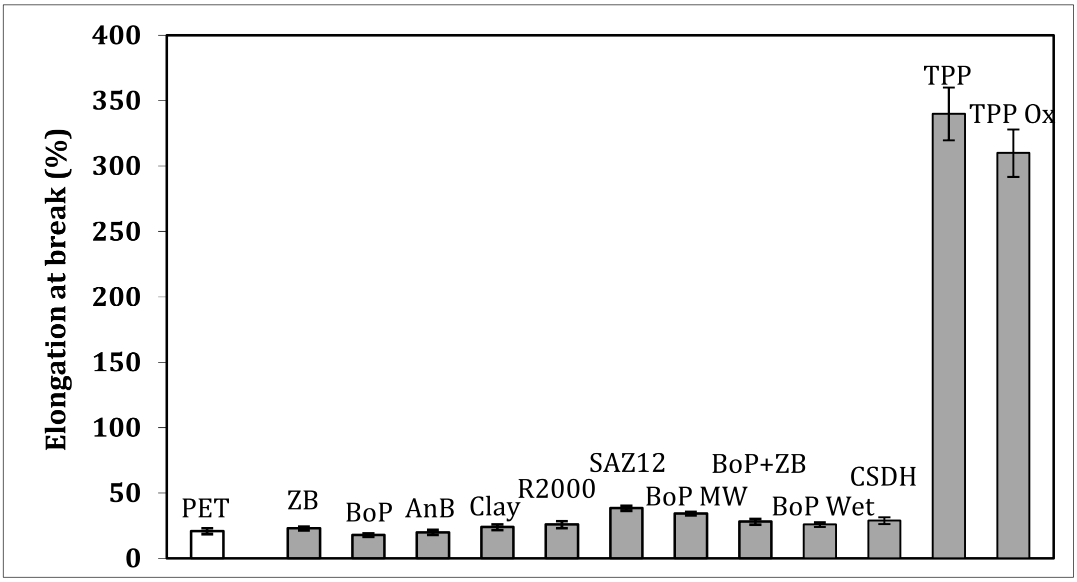

**Figure 4.42** Elongation at break data of first stage PET based flame retardant composites

### 4.3.3.2 Impact Properties of PET Based First Stage FR Composites

Impact strength test is used to characterize the responses of the materials to a sudden impact and energy. One of the main drawbacks of the PET matrix is its relatively low impact resistance when compared to the other thermoplastic polymers like, polyethylene, propylene, nylon 6, etc. Elastomers are widely used to improve the mechanical properties of the polymers. The impact strength values of the first stage flame retardant composites are given in Figure 4.43. Neat recycled PET had an impact strength value of 13 kJ/m$^2$. Introduction of highly hard and stiff materials decreased the impact resistance of the polymer matrix, like boron phosphate, anhydrous borax and calcium sulfate dihydrate. The increase in the impact strength with the addition of triphenyl phosphate and phosphine oxide were due to the plasticizing effects of the additives which was also mentioned in the explanation of the drastic increase in the elongation behavior of the composites. Another important parameter is the homogeneous distribution of the inorganic fillers in the matrix; as a result the additives would not affect the distribution of the impact energy in the polymer matrix when the specimen is exposed to impact. Thus it is expected that the more homogeneous distribution of the inorganic filler in the matrix, the less interference with the energy dissipation of the polymer matrix.

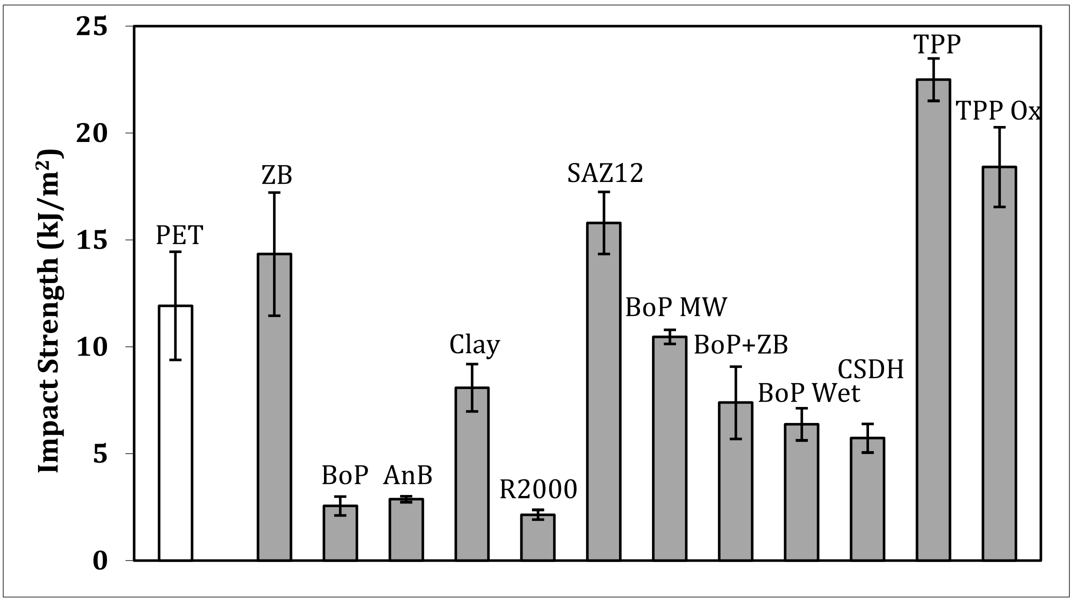

**Figure 4.43**Impact strength data of first stage PET based flame retardant composites

Although they were inorganic additives and they were not expected to give reactions with the PET matrix, zinc borate and metal powder synergist Smokebloc AZ-12 caused an increase in the impact strength of the composites. Also, the smaller the particle size of the additive, the impact energy would be more dissipated in the matrix with the direction change when the crack faces with a particle in the matrix known as crack propagation theory.

#### 4.3.3.3 Hardness Test Results of PET Based First Stage FR Composites

Hardness values of the composites were evaluated by using a Shore D durometer and the results are given in Table 4.12.

**Table 4.12** Hardness test results of first stage FR composites

| Sample | Shore Hardness Value (Shore D) |
|---|---|
| Neat Recycled PET | 70.4 ± 1.3 |
| PET1 | 74.3 ± 2.1 |
| PET2 | 76.5 ± 1.6 |
| PET3 | 78.7 ± 1.7 |
| PET4 | 69.0 ± 1.4 |
| PET5 | 66.3 ± 3.1 |
| PET6 | 72.5 ± 1.5 |
| PET7 | 81.2 ± 2.4 |
| PET8 | 75.4 ± 0.8 |
| PET9 | 79.5 ± 1.1 |
| PET10 | 77.3 ± 1.5 |
| PET11 | 61.2 ± 1.3 |
| PET12 | 62.3 ± 0.7 |

Hardness values showed that the triphenyl phosphate and triphenyl phosphine oxide acts as plasticizer on PET matrix, as the hardness values were decreased when compared with neat crystalline PET. Addition of stiffer additives like boron phosphate also increased the hardness of the polymer composites.

### 4.3.4 Thermal Analysis of PET Based First Stage FR Composites

Thermal analyses of the flame retardant composites were performed by using differential scanning calorimeter (DSC) and thermogravimetric analyzer (TGA). DSC gives information about the glass transition temperature, degree of crystallinity of the composites and melting temperatures of the composites. TGA analysis indicates the thermal decomposition range of the composite and also the remaining char after burning and the char yield (char yield is the remaining amount of char at 800°C). TGA is a complementary analysis to characterize the flame retardancy of the composites especially used to determine the mechanism of action of the additives in the condensed phase.

#### 4.3.4.1 DSC Analysis of PET Based First Stage FR Composites

DSC analyses of the first stage flame retardant composites are given in Table 4.13. Percent crystallinity values were calculated using the equation given below [162]:

$$X_c = \frac{(\Delta H_m - \Delta H_c)}{\Delta H_m^0} x \frac{1}{w_{PET}} x 100 \tag{4.7}$$

where; $\Delta H_m$ is heat of melting, $\Delta H_c$ is heat of crystallization, $\Delta H_m^0$ is the heat of crystallization assuming 100% crystallinity of polymer and $w_{PET}$ represents the weight fraction of PET in the blend/composite. $\Delta H_m^0$ of a 100% crystalline PET was taken as 138 J/g [167].

From DSC analyses results, it can be concluded that, the melting point of the composites did not change with the type of the flame retardant additive and around 250°C. Glass transition temperature of the PET matrix decreased with the addition of triphenyl phosphate (PET11) and triphenyl phosphine oxide (PET12), which confirms the plasticizing effect of the both additives. Crystallinity is an important parameter that affects both the mechanical properties and the transparency of the composites. Crystallinity at least to some extent introduces stiffness and strength to polymers when compared to amorphous polymers, however amorphous regions in polymers contribute to the toughness and flexibility of the polymers. PET11 and PET12 composite also have relatively low crystallinity thus the mechanical properties were affected in increasing manner. Inorganic additives usually acts as nucleation zones in the PET matrix, thus composites containing inorganic additives had relatively high crystallinities. Crystallization temperature of the composites vary between 88-113°C.

**Table 4.13** DSC analyses results of first stage FR composites

| Sample | $T_g$ (°C) | $T_c$ (°C) | $X_c$ (%) | $T_m$ (°C) | $T_D$ (°C) |
|---|---|---|---|---|---|
| Neat PET | 74.3 | --- | --- | 255.3 | 425.1 |
| PET1 | 70.2 | 93.4 | 17.2 | 249.2 | 410.9 |
| PET2 | 68.2 | 107.5 | 19.4 | 258.6 | 434.2 |
| PET3 | 73.4 | 115.6 | 16.4 | 260.1 | 425.6 |
| PET4 | 75.1 | 98.7 | 19.4 | 256.3 | 421.8 |
| PET5 | 69.4 | 84.5 | 17.8 | 251.2 | 390.3 |
| PET6 | 67.2 | --- | --- | 262.3 | 440.4 |
| PET7 | 66.1 | 105.4 | 19.8 | 256.8 | 423.3 |
| PET8 | 68.4 | 95.3 | 17.2 | 255.3 | 395.2 |
| PET9 | 69.7 | 112.3 | 13.2 | 250.2 | 450.2 |
| PET10 | 63.2 | 88.4 | 22.4 | 253.2 | 442.9 |
| PET11 | 58.4 | 92.4 | 13.4 | 257.2 | 419.2 |
| PET12 | 53.2 | 95.6 | 11.2 | 254.3 | 423.5 |

#### 4.3.4.2 TGA Analysis of PET Based First Stage FR Composites

TGA analyses of the first stage flame retardant composites are given in Table 4.14. From TGA thermograms, decomposition start and end temperatures, as well as average decomposition temperatures were determined. Char yields of the composites were also evaluated at the weight loss of the samples at 800°C.

Addition of Cloisite 30B clay (PET4), mixture of zinc borate and boron phosphate (PET8), triphenyl phosphate (PET11) and triphenyl phosphine oxide (PET12) increased the average decomposition temperature of the composites. It was expected that the addition of triphenyl phosphate and triphenyl phosphine oxide would increase the char yield of the composites related to the aromatic groups in their structure and the char yield calculations confirmed this expectation. Results of the thermogravimetric analysis confirmed the effect of the triaryl phosphates (triphenyl phosphate and triphenyl phosphine oxide) in the condensed phase by char formation [168].

**Table 4.14** TGA analyses results of first stage FR composites

| **Sample** | **Decomposition Temperatures** | | | **Weight Loss (%)** |
|---|---|---|---|---|
| | Start (°C) | End (°C) | Average (°C) | @ 800°C |
| Neat PET | 345.0 | 483.0 | 440.0 | 91.4 |
| PET1 | 375.0 | 485.0 | 435.0 | 92.6 |
| PET2 | 360.0 | 520.0 | 432.0 | 89.7 |
| PET3 | 375.0 | 507.0 | 445.0 | 87.5 |
| PET4 | 381.0 | 490.0 | 451.0 | 86.4 |
| PET5 | 372.0 | 484.0 | 427.0 | 89.1 |
| PET6 | 395.0 | 528.0 | 434.0 | 90.4 |
| PET7 | 392.0 | 512.0 | 442.0 | 87.5 |
| PET8 | 385.0 | 495.0 | 453.0 | 88.4 |
| PET9 | 350.0 | 465.0 | 420.0 | 83.5 |
| PET10 | 380.0 | 515.0 | 439.0 | 79.5 |
| PET11 | 374.0 | 525.0 | 458.0 | 75.5 |
| PET12 | 370.0 | 530.0 | 460.0 | 77.2 |

### 4.3.5 Summary of Characterizations of First Stage FR Composites

The first stage flame retardant additives were formulated in order to evaluate the effects of different flame retardant additives on PET matrix. Composites were characterized in terms of flammability behavior, mechanical and thermal properties. Those characterizations were helpful for determining the pathway for the second stage flame retardant composite characterization. In the second stage, four flame retardant additives were chosen among 12 of the first stage additives. Microwave technique produced boron phosphate, 3.5 hydrated zinc borate, triphenyl phosphate and triphenyl phosphine oxide were chosen as the flame retardant additives. Additives were chosen after evaluating both the flammability improvement introduced to the composite and the improvement in the mechanical properties. Microwave technique produced boron phosphate had an average particle size of 397 nm which helps the uniform distribution in the polymer matrix. It increased the LOI value of PET up to 25%. In addition, it was a very effective smoke suppressant for the PET matrix. Due to the nanometer sized crystals, it increased the tensile strength of the polymer matrix without decreasing the tensile modulus values. While zinc borate did not significantly improve the flammability properties, it increased the impact properties of the flame retardant composites. Triphenyl phosphate and triphenyl phosphine oxide have very similar chemical structures. Both were very effective flame retardant additives as they had increased the LOI value of the matrix up to 25.5% and 26.0%, respectively. While they were effective flame retardant additives, due to the presence of phenyl groups and high carbon content they tend to increase the smoke emission especially the carbon monoxide emissions. In addition, they not only improve the flammability of the composites but also increased the composites mechanical properties; especially the tensile strength, elongation at break and impact strength of the composites. As a result of these mentioned effects of the additives they were chosen for the production of second stage flame retardant composites in the study.

### 4.3.6 Flammability Analysis of PET Based Second Stage Composites

In the second stage flame retardant PET based composites, 13 different composites were produced containing four of the successive flame retardant additives of the first stage flame retardant composites. Different amounts and combinations of the flame retardant additives were produced. Total additive amount was limited to 20 weight percent. Same analyses were performed for the characterization of the composites, and in addition further characterizations were done to understand the mechanism of action of flame retardant additives. In the second stage of the experiments, crystalline PET was used rather than recycled PET in order to eliminate the possible interactions or effects coming from the previous additives that were found in the recycled PET.

#### 4.3.6.1 Horizontal Burning Rate Test of PET Based Second Stage FR Composites

All second stage flame retardant composites were self extinguished after the ignition of the samples, thus average burning time and average burnt length were reported. Average burning time of crystalline PET was, 38.4±2.3 s, and average burnt length was 61.4±7 mm. Test results are given in Tables 4.15 to 4.18.

Average burning time of the composites did not change significantly with the addition of flame retardant additives. When triphenyl phosphate was used with boron phosphate average burning time decreased to 31 second (Table 4.17).

**Table 4.15** Horizontal burning test results of second stage FR composites PT1-PT3

| | **PT1** | **PT2** | **PT3** |
|---|---|---|---|
| Horizontal Burning Rate (mm/min) | --- | --- | --- |
| Average Burning Time (s) | 34.1 ± 0.4 | 33.4 ± 0.6 | 32.3 ± 0.2 |
| Average Burnt Length (mm) | 24.0 ± 1.4 | 25.5 ± 0.7 | 26.5 ± 0.7 |

With the addition of flame retardant additives the average burnt length of the composites decreased significantly and in some formulations more than twice.

Combination of triphenyl phosphate and boron phosphate decreased the burnt length below 30 mm (PT6, PT8).

**Table 4.16** Horizontal burning test results of second stage FR composites PT4-PT6

| | **PT4** | **PT5** | **PT6** |
|---|---|---|---|
| Horizontal Burning Rate (mm/min) | --- | --- | --- |
| Average Burning Time (s) | 31.8 ± 0.4 | 31.6 ± 0.4 | 31.2 ± 0.6 |
| Average Burnt Length (mm) | 28.5 ± 0.7 | 32.5 ± 0.8 | 27.5 ± 2.1 |

**Table 4.17** Horizontal burning test results of second stage FR composites PT7-PT9

| | **PT7** | **PT8** | **PT9** |
|---|---|---|---|
| Horizontal Burning Rate (mm/min) | --- | --- | --- |
| Average Burning Time (s) | 31.7 ± 0.2 | 31.5 ± 0.1 | 32.2 ± 0.8 |
| Average Burnt Length (mm) | 30.0 ± 2.8 | 25.5 ± 3.5 | 28.6 ± 2.2 |

When both the results of the first stage and second stage flame retardant additives were considered together, it can be concluded that triphenyl phosphate and triphenyl phosphine oxide were more effective when used together with boron phosphate rather than their stand alone usage.

**Table 4.18** Horizontal burning test results of second stage FR composites PT10-PT13

| | PT10 | PT11 | PT12 | PT13 |
|---|---|---|---|---|
| Horizontal Burning Rate (mm/min) | --- | --- | --- | --- |
| Average Burning Time (s) | 32.1 ± 0.4 | 33.4 ± 0.3 | 33.3 ± 0.5 | 31.9 ± 0.8 |
| Average Burnt Length (mm) | 31.5 ± 0.9 | 31.0 ± 2.8 | 27.0 ± 1.3 | 23.8 ± 1.2 |

#### 4.3.6.2 Limiting Oxygen Index Test Results of PET Based Second Stage FR Composites

LOI value of crystalline PET was determined as 21.0%. When the triphenyl phosphate content in the matrix was increased to 15%, LOI was reduced to 29.5%. 8 weight percent of microwave technique produced boron phosphate resulted in a LOI value of 30.5%, while the same amount of zinc borate caused a slight increase in LOI, which is 23.5%. Highest LOI values were obtained when triphenyl phosphate was combined with boron phosphate. When 2 weight percent triphenyl phosphate was combined with 5 weight percent of boron phosphate, LOI value of 33.0% was obtained; further increase of triphenyl phosphate content to 5 weight percent increases LOI value to 36.0%. Similar to the horizontal burning rate test results, according to the LOI results, boron phosphate and triphenyl phosphate were the two most successive flame retardants for the PET matrix. The mechanism of action for boron phosphate is in the condensed phase, and for triphenyl phosphate, it is in both condensed and gas phase. Test results also implied that when they were used together they showed a synergestic effect. Further addition of the additives beyond 15 weight percent was avoided because of the efforts to preserve or increase the mechanical properties and to achieve the highest flame retardancy with less additive usage.

**Table 4.19** Limiting oxygen index test results of second stage FR composites

| Formulation | LOI Value (%) |
|---|---|
| Neat PET | 21.0 |
| TPP (2) + PET (98) | 24.0 |
| TPP (10) + PET (90) | 26.5 |
| TPP (15) + PET (85) | 29.5 |
| TPP (5) + TPP Ox (5) + PET (90) | 30.5 |
| TPP (10) + TPP Ox (10) + PET (80) | 31.0 |
| TPP (5) + BoP MW (5) + PET (90) | 36.0 |
| TPP (10) + BoP MW (10) + PET (80) | 32.5 |
| TPP (2) + BoP MW (5) + PET (93) | 33.0 |
| TPP (5) + ZB (5) + PET (90) | 29.0 |
| TPP (5) + BoP MW (5) + ZB (5) + PET (85) | 29.5 |
| ZB (8) + PET (92) | 23.5 |
| BoP MW (8) + PET (92) | 30.5 |
| BoP MW (5) + ZB (5) + PET (90) | 25.5 |

### 4.3.7 Smoke Density Measurement of PET Based Second Stage FR Composites

Smoke density evolution tests were done similarly to the previous first stage flame retardant composites tests. Results of the smoke density of second stage flame retardants are given in Table 4.20.

As mentioned before, both boron phosphate and triphenyl phosphate were effective flame retardant additives, but triphenyl phosphate has a drawback of releasing high amount of smoke during fire due to the aromatic groups in its structure.

**Table 4.20** Smoke density test results of second stage FR composites

| Formulation | Light Transmittance (%) |
|---|---|
| Neat PET | 78 |
| TPP (2) + PET (98) | 75 |
| TPP (10) + PET (90) | 67 |
| TPP (15) + PET (85) | 62 |
| TPP (5) + TPP Ox (5) + PET (90) | 83 |
| TPP (10) + TPP Ox (10) + PET (80) | 76 |
| TPP (5) + BoP MW (5) + PET (90) | 85 |
| TPP (10) + BoP MW (10) + PET (80) | 87 |
| TPP (2) + BoP MW (5) + PET (93) | 90 |
| TPP (5) + ZB (5) + PET (90) | 78 |
| TPP (5) + BoP MW (5) + ZB (5) + PET (85) | 84 |
| ZB (8) + PET (92) | 81 |
| BoP MW (8) + PET (92) | 99 |
| BoP MW (5) + ZB (5) + PET (90) | 92 |

In contrast, boron phosphate is a very effective smoke suppressant for the PET matrix. Thus when they were combined together the composite’s smoke density value was in between both of the additives which is 85%. When 8 percent of boron phosphate was added to the PET matrix, light transmittance value of 99% was obtained which is a significant improvement as the smoke density of neat crystalline PET is 78%.

### 4.3.8 Mechanical Properties of PET Based Second Stage FR Composites

Mechanical properties of the second stage flame retardant composites were characterized in terms of tensile, impact and hardness properties of the composites. As mentioned before, to preserve or increase the mechanical properties of flame retardant composites is one of the aims of this study, to increase the field of applications of flame retardant composites.

### 4.3.8.1 Tensile Properties of PET Based Second Stage FR Composites

In Figure 4.44 tensile strength data of the second stage flame retardant composites are given. Tensile strength of neat crystalline PET was determined as 57 MPa. Composites PT1; which has 2 percent of triphenyl phosphate, PT6; which has 5 percent of triphenyl phosphate and boron phosphate and PT8; which has two percent of triphenyl phosphate and 5 percent of boron phosphate had higher tensile strength values than crystalline PET.

Triphenyl phosphate has a twofold effect in the PET matrix. Firstly, it acts as a chain extender in the polymer matrix that causes an increase in the tensile strength value of the composites and secondly acts as a plasticizer which helps to improve the elongation and impact properties of the composite.

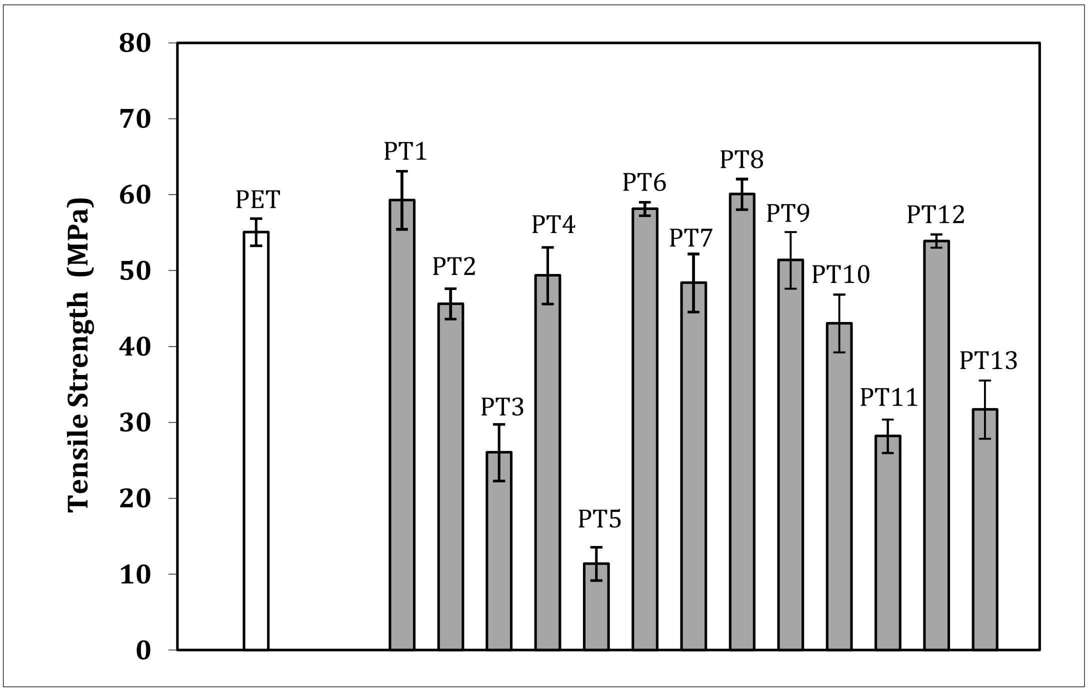

**Figure 4.44** Tensile strength data of second stage PET based flame retardant composites

It is claimed that addition of triphenyl phosphate increases the molecular weight of the PET in the literature [164, 173]. Increase in mechanical properties can be related to this increase in molecular weight due to the formation of copolymers with triphenyl phosphate.

To examine whether the molecular weight of the polymer matrix was increased or not, intrinsic viscosity measurements and by using the Mark-Houwink constants for PET an estimated viscosity average molecular weight calculations were performed.

**Table 4.21** Intrinsic viscosity analysis & MW determination of PET+TPP composites

| | Intrinsic Viscosity (dl/g) | Viscosity Average MW (g/gmol) |
|---|---|---|
| PET | 0.77 | 16 441 |
| PET + 2 % TPP | 0.78 | 16 771 |
| PET + 5 % TPP | 0.95 | 22 714 |
| PET + 10 % TPP | 0.70 | 14 199 |
| PET + 15 % TPP | 0.59 | 10 915 |

Results of these analyses are given in Table 4.21. With the increase of triphenyl phosphate content in PET up to 5 weight percent, intrinsic viscosities and estimated molecular weights of the composites were increased as proposed in the literature [164, 173]. Increase in intrinsic viscosity is a sign of formation of new groups in the matrix and a possible increase in molecular weight due to chain extension reactions. Beyond 5 weight percent the intrinsic viscosity of the matrix tends to decrease. This phenomenon implies that beyond certain load, plasticizing effect of triphenyl phosphate is dominant and it could not act as a chain extender in the matrix.

In Figure 4.45 tensile modulus analysis of the composites are given. Composites either containing zinc borate or boron phosphate have higher tensile modulus value than neat PET.

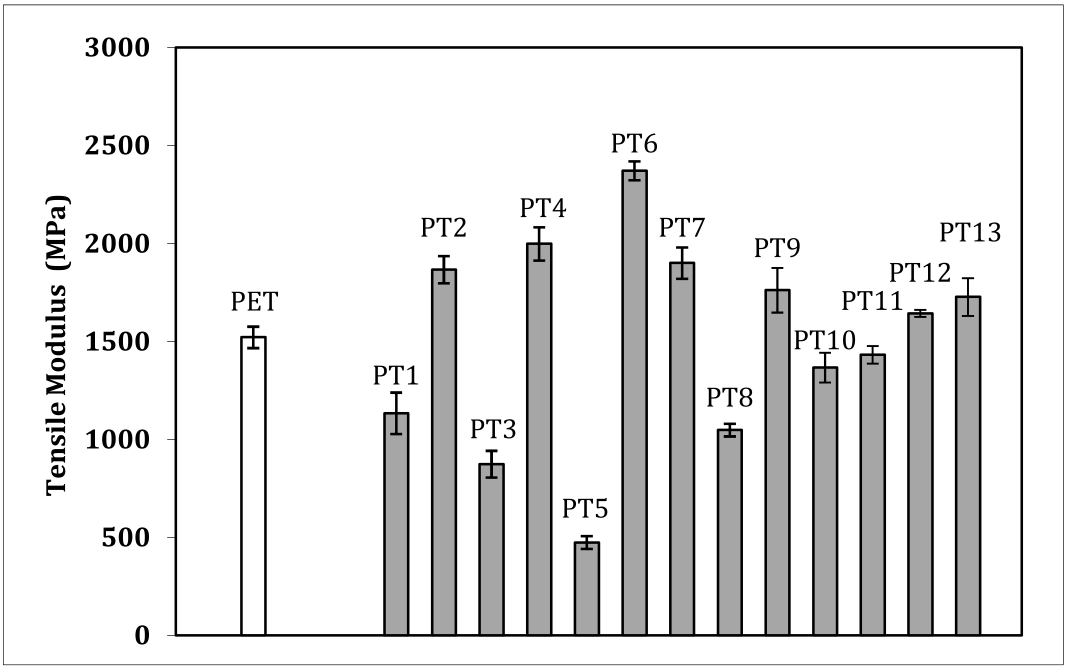

**Figure 4.45** Tensile modulus data of second stage PET based flame retardant composites

Combination of the two organic phosphate based additives, drastically reduced the tensile modulus value of the matrix.

In Figure 4.46, elongation at break data of the composites were mentioned. Inorganic flame retardant additives decreased the elongation at break of the composites. Addition of triphenyl phosphate and triphneyl phosphine oxide increased the elongation behavior of the composites as in the first stage flame retardant composites.

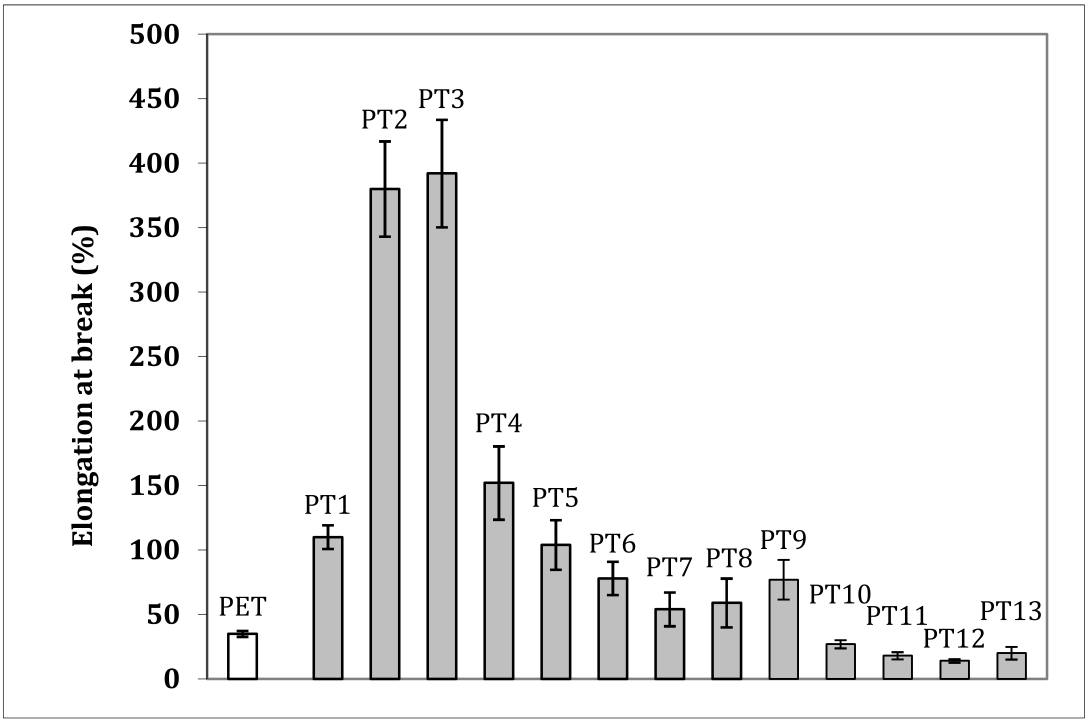

**Figure 4.46** Elongation at break data of second stage PET based flame retardant composites

### 4.3.8.2 Impact Properties of PET Based Second Stage FR Composites

Impact properties of the neat PET, which is around 11 kJ/m$^2$, was tripled with the addition of 10 percent triphenyl phosphate (Figure 4.47). Also, when the two successful impact strength additives of the first stage flame retardant additives were combined (PT9), impact strength was nearly doubled. Besides its plasticizing effect, triphenyl phosphate has effect on the crystallinity of the PET matrix in decreasing the crystallinity and increasing the amorph content of the matrix, which will be mentioned in the upcoming section.

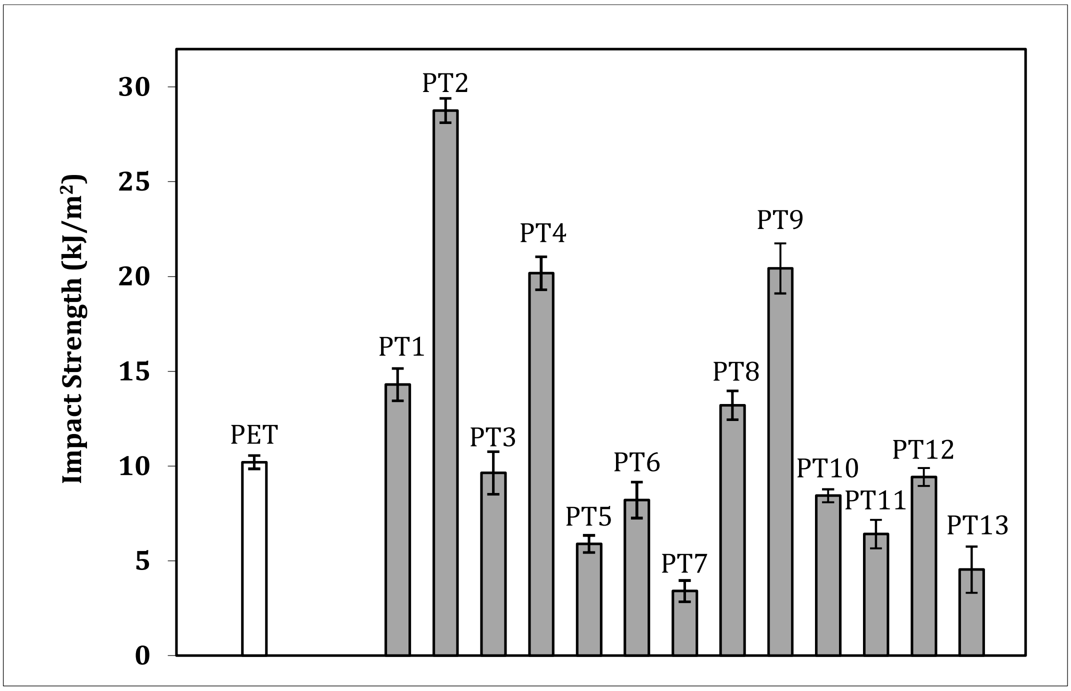

**Figure 4.47** Impact strength data of second stage PET based flame retardant composites

### 4.3.8.3 Hardness Test Results of PET Based Second Stage FR Composites

Hardness is a measure of the resistance of a plastic to permanent (plastic) deformation. Shore D hardness test results of the second stage flame retardant composites are given in Table 4.22. Addition of inorganic flame retardant additives increased the hardness values of the polymer matrix when compared with the organic flame retardant additives as the hardness of inorganic additives are higher. Decrease in the hardness of the composites with the addition of triphenyl phosphate and triphenyl phosphine oxide supports the proposed plasticizing effect of the additive as the material softens when it is plasticized.

**Table 4.22** Hardness test results of second stage FR composites

| Sample | Shore Hardness Value (Shore D) |
|---|---|
| Neat Crystalline PET | 73.2 ± 1.4 |
| PT1 | 74.0 ± 2.4 |
| PT2 | 78.5 ± 2.6 |
| PT3 | 71.7 ± 2.5 |
| PT4 | 68.0 ± 1.1 |
| PT5 | 64.0 ± 2.9 |
| PT6 | 76.5 ± 1.2 |
| PT7 | 77.0 ± 1.4 |
| PT8 | 74.7 ± 0.9 |
| PT9 | 69.5 ± 1.2 |
| PT10 | 80.0 ± 1.8 |
| PT11 | 77.5 ± 1.0 |
| PT12 | 76.7 ± 0.9 |
| PT13 | 70.5 ± 2.8 |

### 4.3.9 Thermal Analyses of PET Based Second Stage FR Composites

DSC analyses, TGA analyses and DTA analyses were performed for the thermal stability and decomposition behavior of the composites. The experimental procedure was same as the first stage flame retardant composites.

#### 4.3.9.1 DSC Analysis of PET Based Second Stage FR Composites

Table 4.23 summarizes the DSC analyses test results. It can be concluded that the melting points of the composites were around 250°C. The increase of the triphenyl phosphate content (PT1-PT3) decreased the glass transition temperature of the matrix. Percent crystallinities of the composites were around 15%, which indicated that the polymer matrix has high amorphous phase, thus the mechanical properties, especially the impact strength of the composites were affected in positive manner.

**Table 4.23** DSC analyses results of second stage FR composites

| Sample | $T_g$ (°C) | $T_c$ (°C) | $X_c$ (%) | $T_m$ (°C) | $T_D$ (°C) |
|---|---|---|---|---|---|
| Neat PET | 75.5 | --- | --- | 254.2 | 423.1 |
| PT1 | 64.5 | 111.5 | 13.9 | 252.3 | 418.7 |
| PT2 | 46.5 | 94.3 | 19.5 | 254.1 | 426.0 |
| PT3 | 35.2 | 81.6 | 26.8 | 251.0 | 387.5 |
| PT4 | 55.2 | 100.9 | 19.4 | 249.2 | 380.3 |
| PT5 | --- | 71.6 | 24.8 | 245.7 | --- |
| PT6 | 58.3 | 102.7 | 19.7 | 251.9 | 433.2 |
| PT7 | 47.1 | 92.8 | 16.3 | 252.5 | 386.2 |
| PT8 | 50.4 | 101.7 | 15.6 | 250.9 | 432.0 |
| PT9 | 59.4 | 105.6 | 14.6 | 255.0 | 421.9 |
| PT10 | 52.4 | 100.5 | 18.2 | 256.7 | 421.2 |
| PT11 | 70.5 | 121.5 | 17.1 | 253.3 | 440.7 |
| PT12 | 72.0 | 122.1 | 17.9 | 255.5 | 441.0 |
| PT13 | 67.4 | 116.2 | 10.8 | 255.0 | 320.0 |

### 4.3.9.2 TGA and DTA Analyses of PET Based Second Stage FR Composites

TGA analyses outputs supported that the usage of triaryl phosphates had increased the char formation of the polymer matrix during decomposition.

**Table 4.24** TGA analyses results of second stage FR composites

| **Sample** | **Decomposition Temperatures** | | | **Weight Loss (%)** |
|---|---|---|---|---|
| | Start (°C) | End (°C) | Average (°C) | @ 800°C |
| Neat PET | 340.0 | 480.0 | 445.0 | 92.3 |
| PT1 | 320.0 | 470.0 | 441.0 | 90.7 |
| PT2 | 230.0 | 500.0 | 444.0 | 88.7 |
| PT3 | 230.0 | 500.0 | 445.0 | 88.3 |
| PT4 | 250.0 | 500.0 | 444.0 | 89.5 |
| PT5 | 200.0 | 480.0 | 440.0 | 92.0 |
| PT6 | 250.0 | 500.0 | 447.0 | 84.7 |
| PT7 | 230.0 | 500.0 | 444.0 | 89.5 |
| PT8 | 280.0 | 500.0 | 446.0 | 85.3 |
| PT9 | 250.0 | 480.0 | 437.0 | 84.5 |
| PT10 | 250.0 | 500.0 | 434.0 | 78.5 |
| PT11 | 240.0 | 500.0 | 435.0 | 75.8 |
| PT12 | 370.0 | 520.0 | 441.0 | 85.7 |
| PT13 | 370.0 | 520.0 | 435.0 | 80.1 |

In Table 4.25 differential thermal analyses (DTA) results of the composites are given. Differential thermal analysis (or DTA) is a thermoanalytic technique, similar to differential scanning calorimetry. In DTA, the material under study and an inert reference are heated under identical conditions, while recording any temperature difference between sample and reference this differential temperature is then plotted against time, or against temperature. Changes in the sample, either exothermic or endothermic, can be detected relative to the inert reference. Thus, a DTA curve provides data on the transformations that have occurred. DTA analyses was performed by the TGA equipment. DTA analyses gave information about the crystallization, melting and decomposition temperatures of the samples. With the help of this experiment DSC analyses results could be double checked. Decomposition temperature of the composites ranged in between 420-460°C and melting temperature of the composites were around 255°C.

**Table 4.25** DTA analyses results of second stage FR composites

| **Sample** | **$T_c$ (°C)** | **$T_m$ (°C)** | **$T_D$ (°C)** |
|---|---|---|---|
| Neat PET | --- | 239.1 | 423.6 |
| PT1 | 120.1 | 255.4 | 429.5 |
| PT2 | 108.0 | 253.8 | 436.1 |
| PT3 | 94.8 | 252.6 | 435.5 |
| PT4 | 110.4 | 250.5 | 441.0 |
| PT5 | 82.3 | 245.4 | 439.4 |
| PT6 | 117.5 | 255.5 | 438.0 |
| PT7 | 98.8 | 252.9 | 462.0 |
| PT8 | 121.3 | 252.8 | 443.1 |
| PT9 | 116.6 | 251.3 | 437.7 |
| PT10 | 122.6 | 250.0 | 414.7 |
| PT11 | 111.7 | 252.0 | 436.9 |
| PT12 | 128.2 | 251.0 | 439.4 |
| PT13 | 135.6 | 255.0 | 456.2 |

Not only the flame retardant composites, but also the additives used in the production of second stage flame retardant composites were analyzed via TGA (Table 4.26). Triaryl phosphates were completely decomposed at 800°C. Microwave produced boron phosphate lost only 2.3 weight percent of its original weight at 800°C, while 3.5 hydrated zinc borate lost 12.9 percent of its initial weight.

**Table 4.26** TGA analyses results of selected flame retardant additives

| **Sample** | **Decomposition Temperatures** | | | **Weight Loss (%)** |
|---|---|---|---|---|
| | Start (°C) | End (°C) | Average (°C) | @ 800°C |
| TPP | 180.0 | 320.0 | 303.0 | 100.0 |
| TPP Ox | 200.0 | 350.0 | 331.0 | 99.7 |
| BoP MW | --- | --- | --- | 2.3 |
| ZB | 280.0 | 450.0 | 396.0 | 12.9 |

Weight loss of zinc borate was the loss of the crystalline water in its structure and its decomposition range was 280-450°C.

## 4.4 Further Characterization for Determination of the Act Mechanisms of FR Additives

Flame retardant composites were characterized in terms of flammability behavior, mechanical behavior and thermal properties. Results of these characterizations indicated that zinc borate, boron phosphate, triphenyl phosphate and triphenyl phosphine oxide were successive flame retardant additives for the PET matrix. With the additon of these additives, flammability resistance of the matrix was increased, smoke evolution during burning was decreased and also mechanical properties of the composites were improved. Improvements for the mechanical properties were mentioned in the former sections. From now on the improvements on the flame retardancy will be considered and explained with different characterization techniques. In the literature [169], the mechanism of action of the inorganic additives boron phosphate and zinc borate were proposed to act in the condensed phase. Zinc borate forms a glassy amorphous protective layer in the matrix and thus prevents the flame spread. Furthermore, it releases its crystalline water during burning, which dilutes the fuel gases and also cools the burning media. Boron phosphate also forms a glassy layer during decomposition by turning into amorphous structure. Triaryl phosphates both act in the condensed phase and in the gas phase. In the condensed phase, char promotion is the main effect and was proved by TGA analysis. In the gas phase, it was suggested that the decomposition products act like the halogenated flame retardant additives that interrupts the hydrogen cycle. Pyrolysis MS technique was chosen to analyze the products formed in the gas phase during fire. Proposed and predicted radicals and ions were tried to be detected with this technique.

### 4.4.1 Morphological Analysis for Determination of the Act Mechanisms of FR Additives

For the determination of machanism of action of inorganic flame retardant additives, additives were analyzed by XRD after heat treatment was applied to the additives, which was simulating the heat exposed during fire. This analysis was performed for both boron phosphate and zinc borate to examine the crystal structure change and whether the amorphous protective layer was formed or not, after heat exposure similar to the technique in the literature [170].

Protective layer formation was not only tried to be determined by XRD analyses, but also scanning electron microscopy technique was used to examine the proposed protective layer formed at the outside perimeter of the polymer matrix during fire.

#### 4.4.1.1 XRD Analysis of Inorganic Flame Retardant Additives

XRD analyses were performed to characterize the crystal structure change of the inorganic flame retardant additives with respect to heat during fire. Prior to the analyses, small amounts of inorganic additive was put in porcelain crucible and then placed into the oven. Each sample was kept in the oven for one hour at 100, 200, 300, 350, 400, 450, 500, 600, 700, 880, 940°C. From the TGA analyses, it was conluded that the average decomposition temperature of the PET matrix was around 450°C, so around that temperature; temperature difference rate was chosen as 50°C to characterize the phenomenon on more precisely. After the sintering procedure, the samples were kept in desicator till the XRD analysis. Samples were analyzed in between 1 to 80° 2 theta region to characterize the crystal structure change related to heat.

In Figure 4.48 crystal structure change with respect to heat for boron phosphate is given. It is clear from the figure that with the increase of temperature crystal structure of boron phosphate did not change up to 940°C. Temperature above 940°C were not considered, as in general fires, the highest temperature is not more than 800°C. XRD patterns showed that the 2 theta values of the crystals did not change, but the intensities of the peaks were increased after sintering beyond 700°C, which indicates the increase of the crystallinities of the crystals.

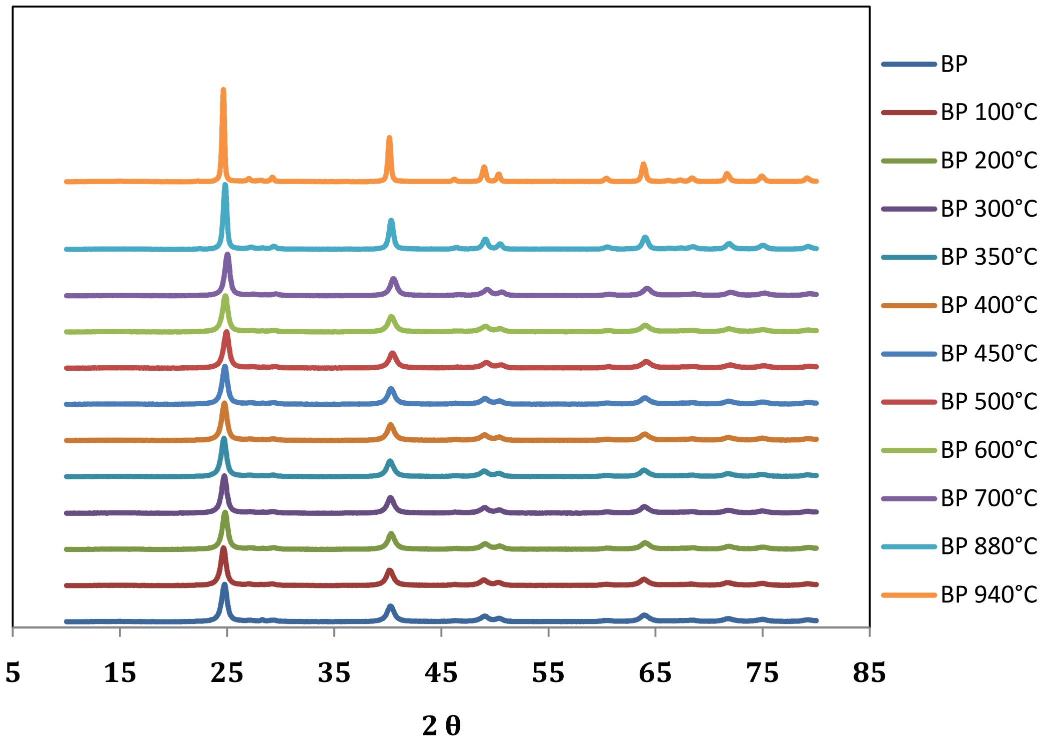

**Figure 4.48** XRD patterns of boron phosphate, which was sintered in oven up to 940°C for crystal structure shift detection (BP represents original non sintered boron phosphate)

It was expected to observe a low crystalline structure after the sintering as the proposed mechanism of action of boron phosphate is the formation of a glassy protective layer. The opposite behavior might be the result of the peak hinderance effect of $BPO_4$ over $BPO_3$ and $BPO_2$, which are in the glassy amorphous form. To characterize this phenomenon more deeply, FTIR analysis were also performed.

In Figure 4.49, XRD patterns of sintered zinc borates were given. The proposed mechanism of action of zinc borate is the formation of glassy protective layer and the release of crystalline water in its structure. The relase of crystalline water was proven with thermogravimetric analysis. XRD analysis indicated that up to 400°C, the crystal structure of zinc borate did not change. From 300°C to 400°C the intensities of the crystals started to decrease which was the sign of increasing amorphous structure.

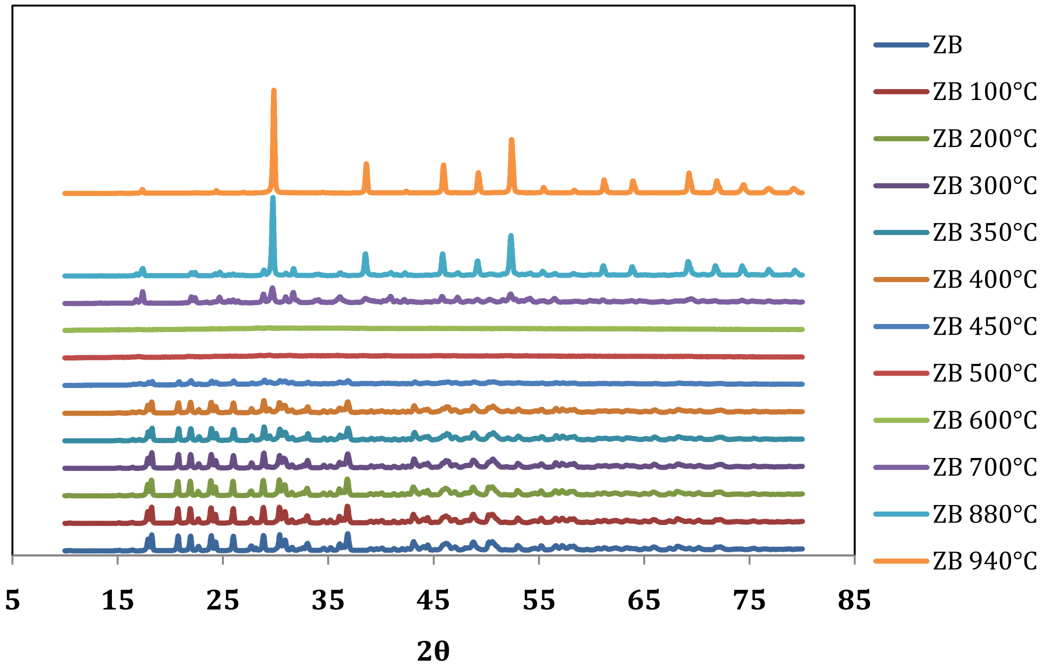

**Figure 4.49** XRD patterns of zinc borate, which was sintered in oven up to 940°C for crystal structure shift detection (ZB represents original non sintered zinc borate)

After 400°C the peaks were very broadened which is the evidence of the amorphous structure up to 700°C. Between 400°C and 700°C zinc borate formed a glassy layer that is the proposed layer for the flame retardancy. The decomposition range of PET was between 340°C to 450°C in which zinc borate was transformed to the amorphous phase. After 700°C a new crystalline form of zinc borate was formed as the 2 theta peaks were shifted. In conclusion, XRD analysis confirmed the formation of the glassy layer and the proposed mechanism of action of the flame retardant additive in the condensed phase.

#### 4.4.1.2 SEM Analysis of Inorganic Flame Retardant Additives

SEM analysis were performed to further investigate whether there was formation of glassy protective layer during fire. For this purpose, specimens burnt in the LOI test were cut by using a razor blade with sudden impact to get a cross section of the burnt sample. Specimens were analyzed both investigating the center and the edges of the cut cross sections. The specimens were burnt during the LOI test, thus if a protective layer was formed, it should be visible via SEM analysis.

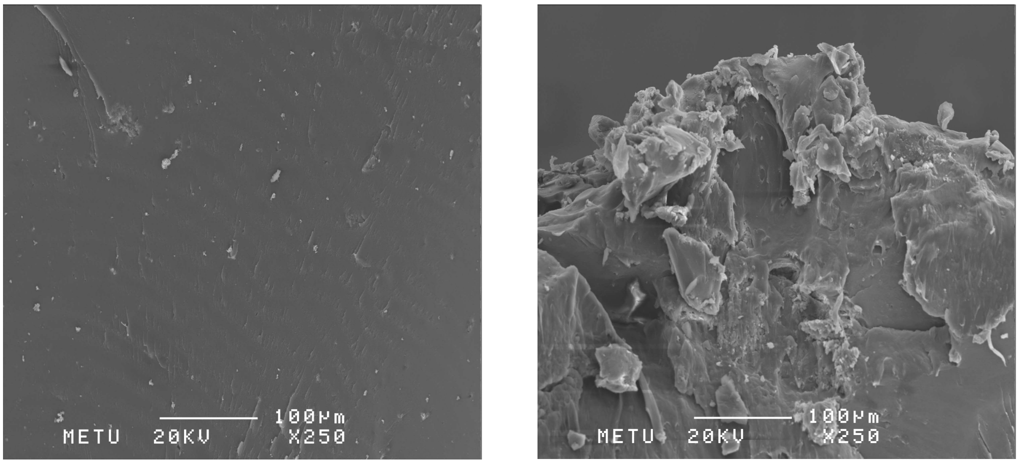

**Figure 4.50** SEM analysis of sample containing 8% boron phosphate 92% PET.(a) center of cross-section 250x (b) edge of the cross-section 250x

In Figure 4.50, SEM micrographs of composites containing 8% boron phosphate are given. When the center of the composites were examined, which was unburnt, the morphology was as expected showing the distrubed boron phosphate particles in the matrix. Unlike the morphology of center part, the SEM photograph which was taken near the edge of the specimen, showed a second phase rather then the polymer matrix. This section was exposed to fire during burning. The additional phase seems to have an amorphous structure which supports the formation of the glassy protective layer. These results seem to be in contradiction with the XRD analysis, thus further characterization was done by performing FTIR analysis to get more proof about glassy layer formation when boron phosphate was used as flame retardant additive.

SEM micrographs, belonging to composites that had 8% zinc borate are given in Figure 4.51. Similar to the boron phosphate contianing composites, while the center of the specimens were normal and has only one phase, the edge of the specimens has a differentr phase which could be related to the glassy layer formation in the condensed phase during burning. SEM observations for zinc borate samples are supporting the XRD analysis performed to proof the formation of glassy layer.

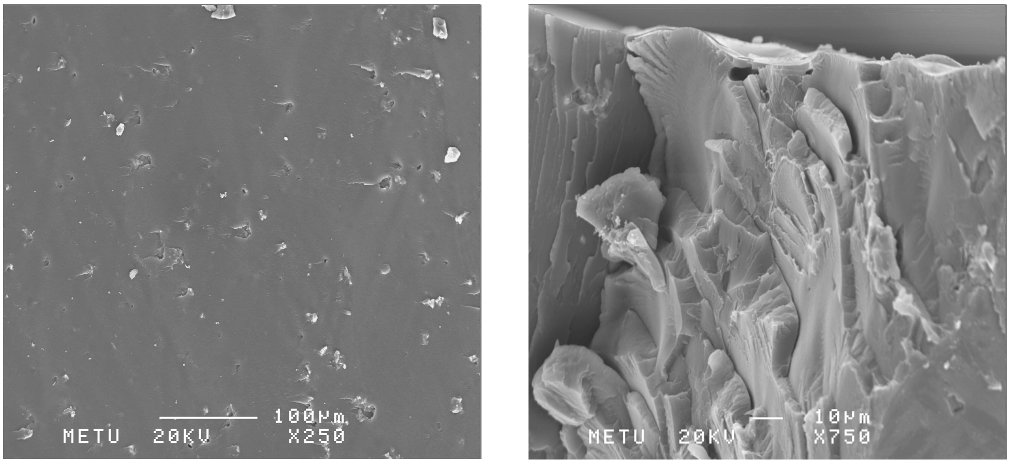

**Figure 4.51** SEM analysis of sample containing 8% zinc borate 92% PET.(a) center of cross-section 250x (b) edge of the cross-section 750x

Amorphous protective layer is expected to be formed at the outer surface of the polymer matrix which was exposed to fire directly. Formation of this layer is not expected to the interior of the specimen as less heat is diffused and the presence of the layer is directly related to the presence of the heat. The thickness of the layer seems to be less than 20 μm.

In Figure 4.52, SEM micrographs of composites containing 10 weight percent of zinc borate and 10 weight percent of boron phosphate are given. The glassy amorphous layer which was observed when the additives were used stand alone, was again observed, when both of the additives were used together.

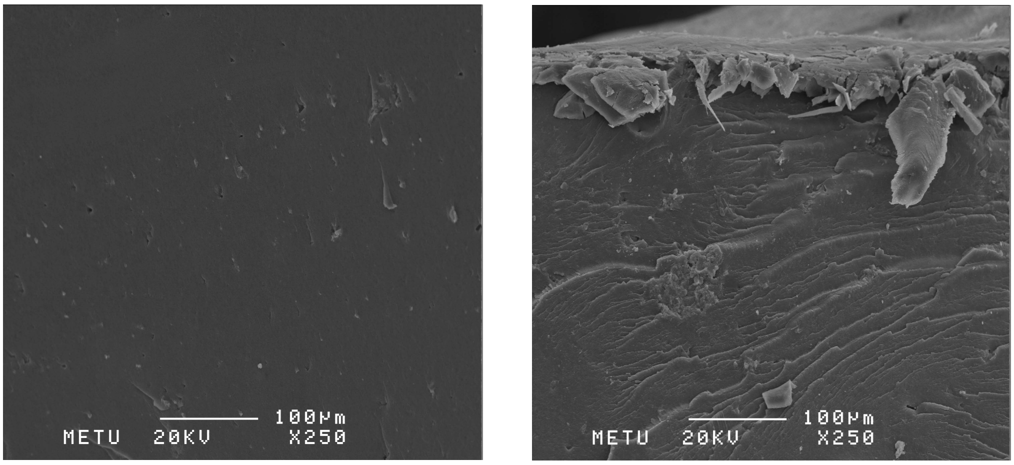

**Figure 4.52** SEM analysis of sample containing 10% boron phosphate 10% triphenyl phosphate 80% PET (a) center of cross-section 250x (b) edge of the cross-section 250x

### 4.4.2 FTIR Analyses of Inorganic Flame Retardant Additives

FTIR analysis were performed in order to track the changes in the chemical structure of boron phosphate to get information whether the amorphous layer was formed during fire. FTIR analysis were perfomed for the boron phosphate samples of non sintered $BPO_4$ (Figure 4.53), firstly. FTIR spectra of boron phosphate, 1 h sintered at 500°C $BPO_4$, 1 h sintered at 940°C $BPO_4$, 3 h sintered at 940°C $BPO_4$ and 6 h sintered at 940°C $BPO_4$ were taken (Figures 4.54-4.57). In previous SEM analysis, formation of a second phase in the polymer matrix was observed at the edges of the specimens that contained boron phosphate which were prepared after LOI test. Although in XRD analysis no evidence of formation of glassy structure, SEM analysis implied a secondary phase. In XRD the formed amorphous phase could be hindered by the XRD pattern of original $BPO_4$ as the amorphous layer could be $BO_3$ and $BO_2$ which have

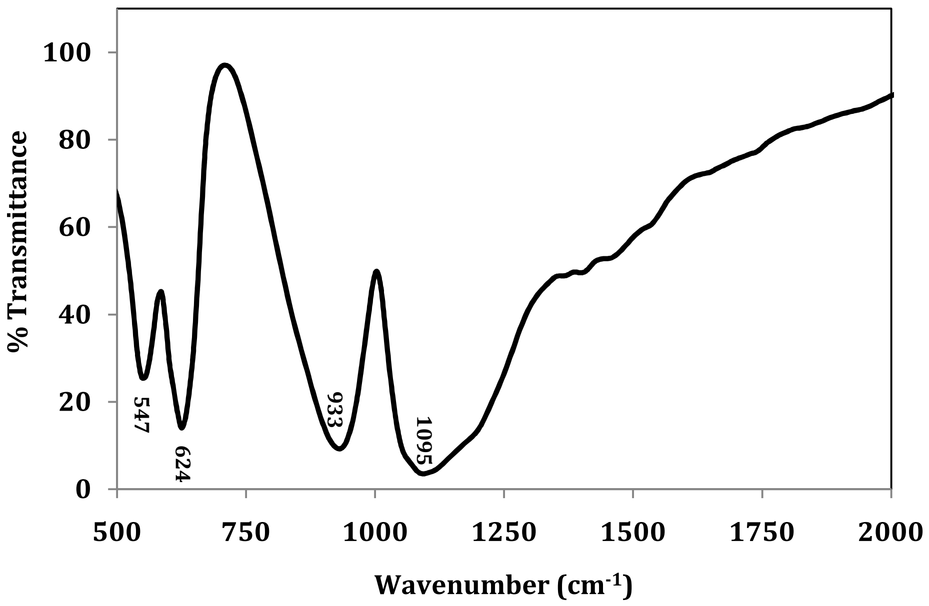

**Figure 4.53** FTIR pattern of microwave technique produced boron phosphate thermally not treated

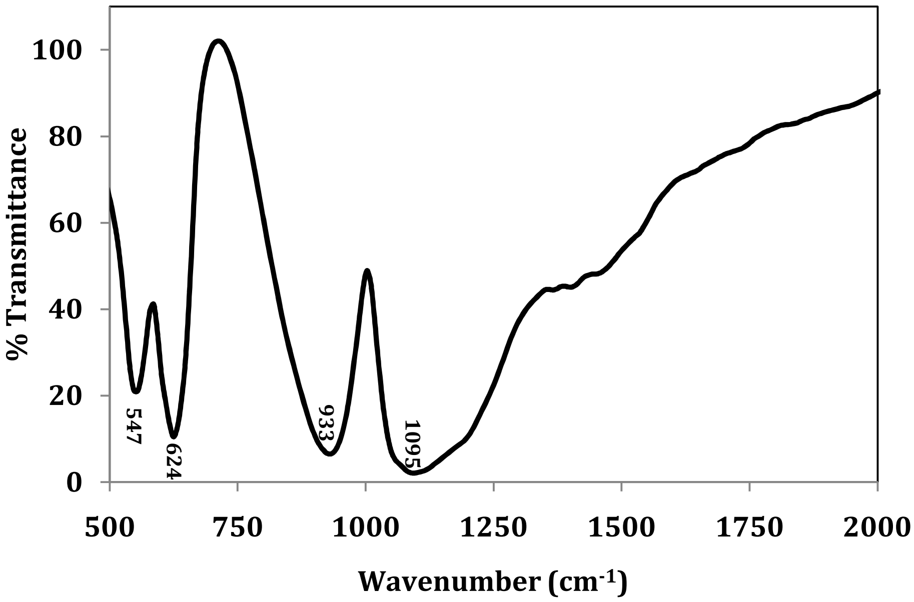

**Figure 4.54** FTIR pattern of microwave technique produced boron phosphate sintered at 500°C for 1 hour

similar structures to $BPO_4$. There was a good agreement between the IR spectrum of microwave produced $BPO_4$, and tetragonal $BPO_4$ given in the literature [155]. The IR spectrum of boron phosphate contains four strong, rather broad bands at 550, 615, 925, and 1085 $cm^{-1}$, which can be seen in Fig. 4.54. P-O-P link was not present in boron phosphate.

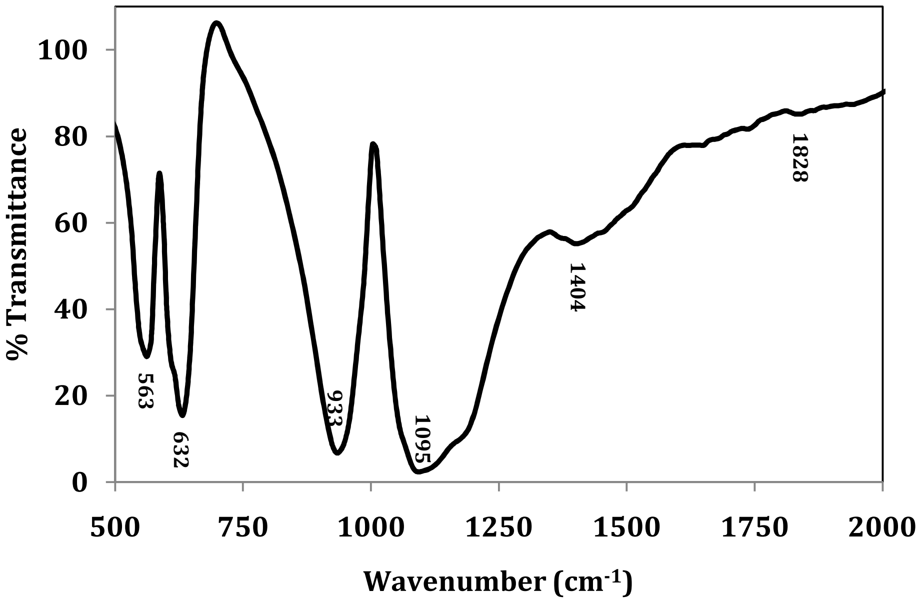

**Figure 4.55** FTIR pattern of microwave technique produced boron phosphate sintered at 940°C for 1 hour

The band at 550 cm$^{-1}$ is due to bending vibrations of B–O bond. The band around 918 cm-$^{1}$ is assigned to the strecthing B-O bond vibrations in $BO_4$ [171] tetrahedron. The band at 1323 cm$^{-1}$ can be assigned to a double P=O bond vibration. This band is not observed in crystalline $BPO_4$, where the excess of negative charge in the $BO_4$ unit is compensated by the excess of positive charge in the $PO_4$ unit [172].

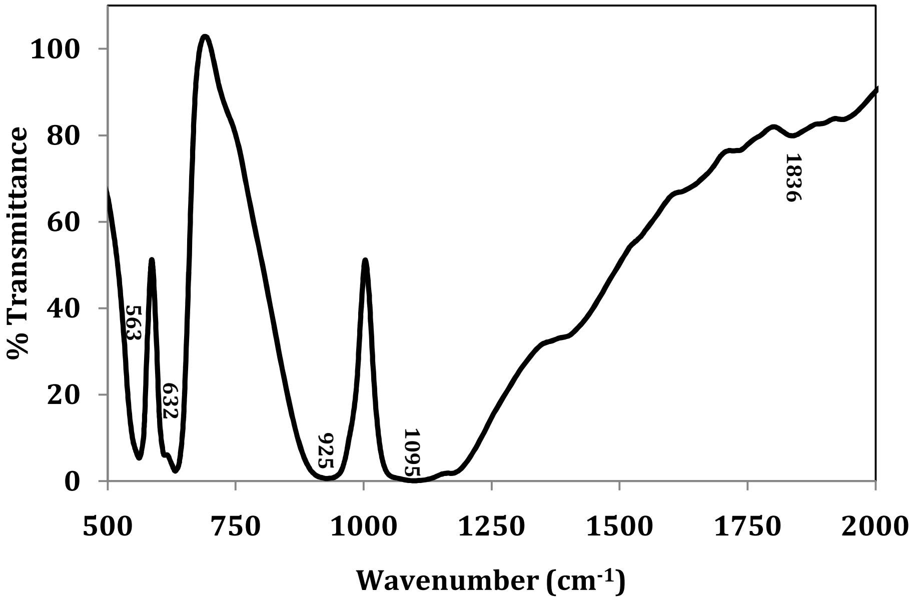

**Figure 4.56** FTIR pattern of microwave technique produced boron phosphate sintered at 940°C for 3 hour

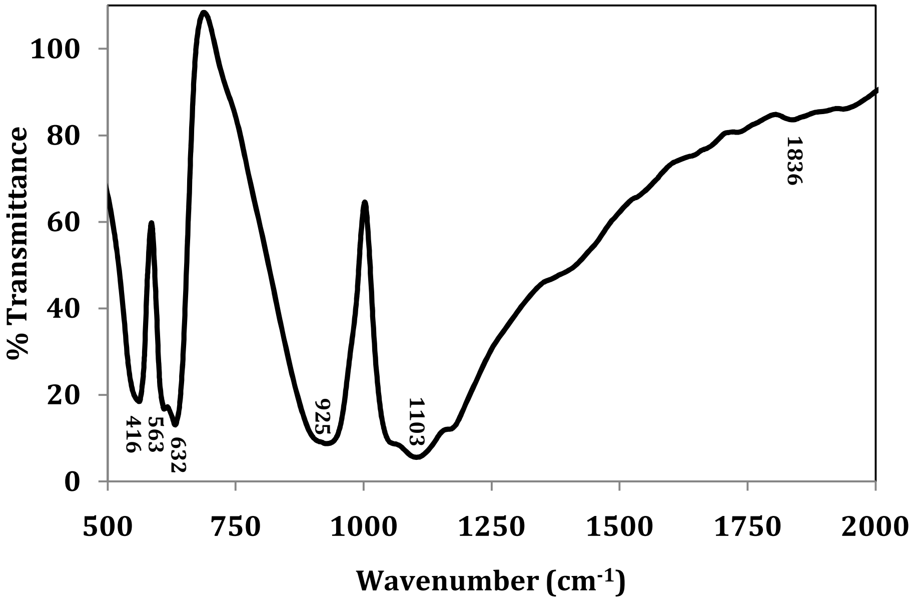

**Figure 4.57** FTIR pattern of microwave technique produced boron phosphate sintered at 940°C for 6 hour

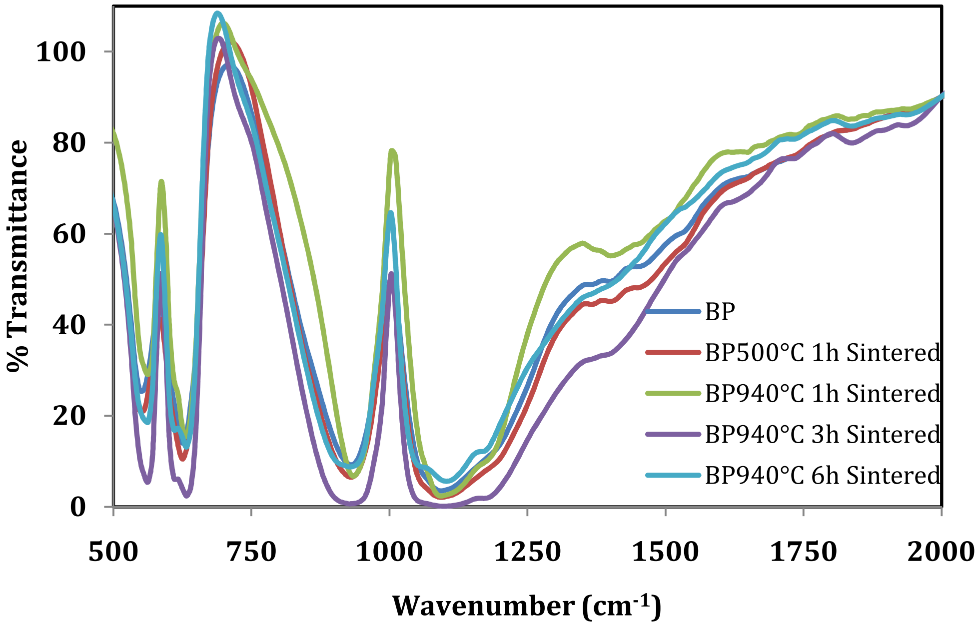

**Figure 4.58** FTIR pattern comparison of non treated and sintered boron phosphate samples

The band at about 673 $cm^{-1}$ results from B–O bond vibrations in boroxyl rings, the band in the range 917–920 $cm^{-1}$ can be assigned to B–O bond vibrations in $BO_4$ units, while the last band at about 1404 $cm^{-1}$ originates from the vibrations of B–O bond in $BO_3$ groups. A broad but low intensity band at about 1390 $cm^{-1}$ is due to the B–O bond vibrations in $BO_3$ units [173] and its intensity decreases with increasing $BPO_4$ content which is caused by changes of boron coordination from trigonal to tetragonal.

In Figure 4.58, FTIR patterns of the all samples are given for comparison. The band at around 1323 $cm^{-1}$ was visible in the samples which were sintered at 940°C. The presence of this band implies the transformation from crystalline phase to amorphous phase after exposure to heat. In addition, peak around 1390 $cm^{-1}$ that was present in the samples sintered at 500°C for 1 hour, and 940°C for 1 hour, represents the B-O bond vibrations in $BO_3$ units which are amorphous. Formation of amorphous layer when $BPO_4$ was exposed to heat was not only seen in SEM micrographs, but also detected in the FTIR analysis.

### 4.4.3 Py-MS Analysis of PET Based FR Composites

Pyrolysis MS is a powerful technique to characterize the gas phase mechanism of action of flame retardant additives. The volatile and non-volatile decomposition products of the desired matrix could easily be determined with the help of this technique. In this series of experiments, matrix polymer PET, composite containing 10% of triphenyl phosphate-90% of PET, 10% of boron phosphate-90% of PET and 10% of triphenyl phosphate-10% of boron phosphate-80% of PET were analyzed with Py-MS technique. In Figure 4.59 total ion current pyrogramme of PET was given.

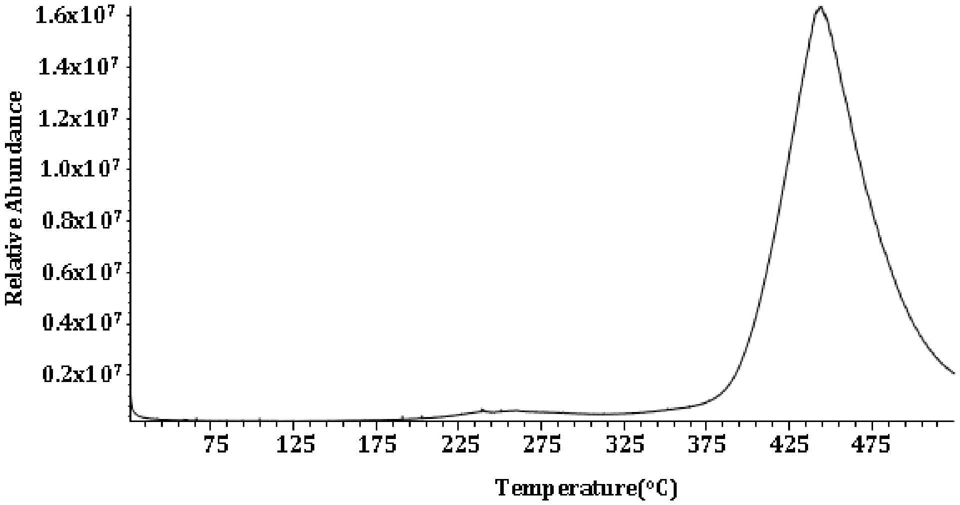

**Figure 4.59** Total ion current pyrogramme of PET

This pyrogramme indicated that the decomposition of PET was started around 375°C and ended around 500°C and the average decomposition temperature was around 450°C. In Figure 4.60, pyrolysis products of PET were designated at the top point of the total ion current pyrogramme of PET which was at 443°C.

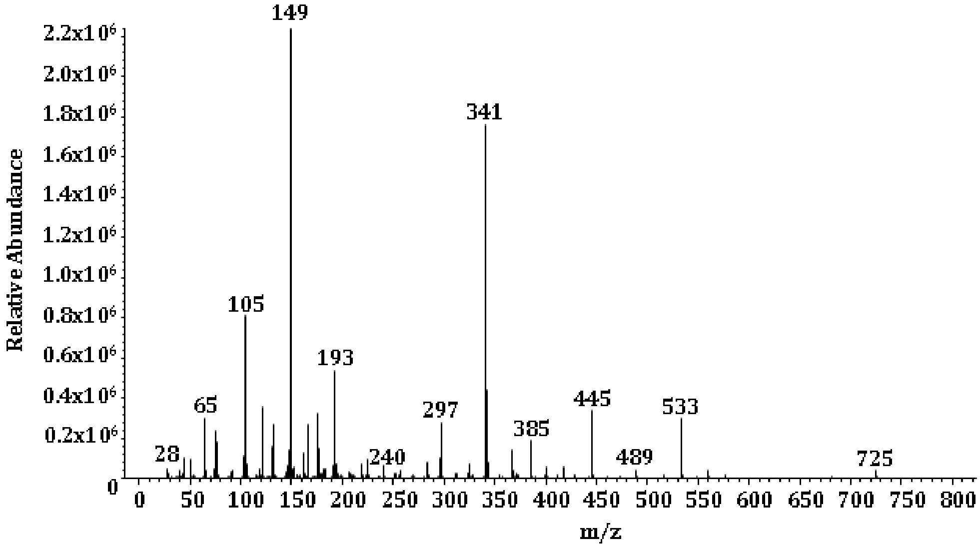

**Figure 4.60** Pyrolysis mass spectrum of poly(ethylene terephthalate) at 443°C

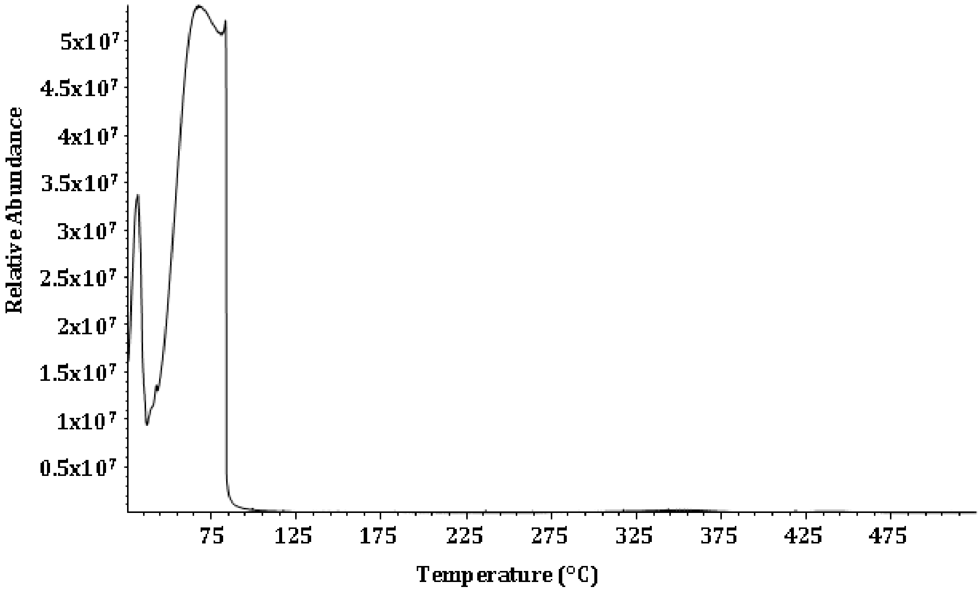

**Figure 4.61** Total ion current pyrogramme of triphenyl phosphate

The fragment m/z 149 is assigned as the carboxonium ion of the terephthalic acid. Since in previous studies terephthalic acid was identified as one pyrolysis product of

PET [174, 175], it can be deduced that the series of m/z 149-917 corresponds to oligomers with a thermally formed carboxyl end group. Pyrolysis of neat PET are benzene, benzoic acid, acetophenone, toluene, styrene, vinyl terephthalate, divinyl terephthalate, vinyl benzoate, methyl benzoate, biphenyl, diacetyl benzene.

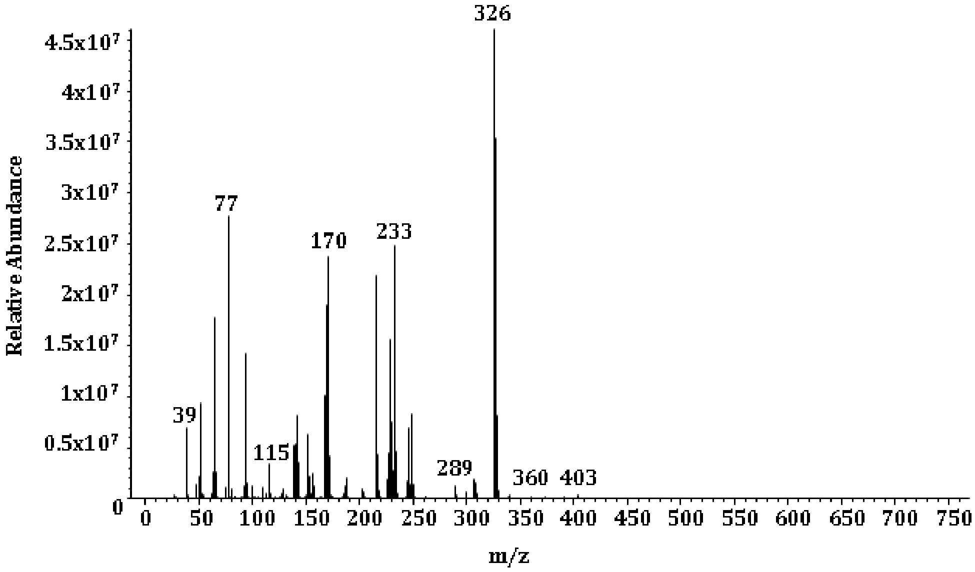

**Figure 4.62** Pyrolysis mass spectrum of triphenyl phosphate at 81°C

In Figure 4.61, total ion current pyrogramme of triphenyl phosphate is shown. TPP degrades around 80°C and after that temperature no decomposition could be observed. The mass spectrum of TPP was gathered at the peak point of decomposition which was 81°C (Figure 4.62). As mentioned before, phosphate based flame retardants' gas phase mechanism of action by forming radicals and ions which interrupt the hydrogen radical cycle. When the decomposition products was examined for the chemical species, desired decomposition products; [176] $PO_4$, $PO_2$, $P_2$, $PO^\bullet$ were determined. In addition $P_2O_2$ and $P_2O_5$ were also detected. In Figure 4.63, relative abundance comparison of these products is also given. When the products abundance was compared, $P_2O_2 > P_2O_5 > PO_2 > PO_4 > PO^\bullet > P_2$ was observed.

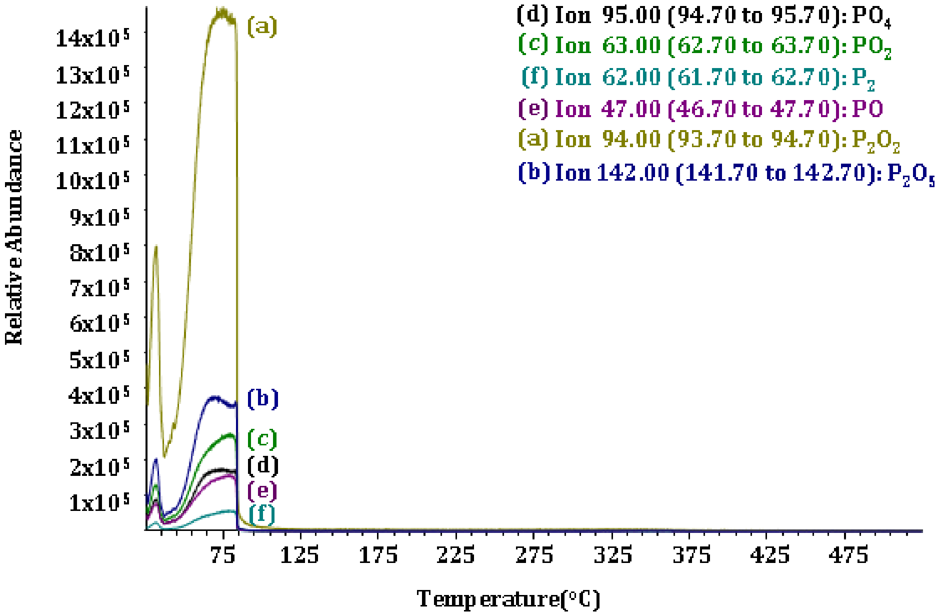

**Figure 4.63** Comparison of single ion current pyrogrammes of triphenyl phosphate decomposition products

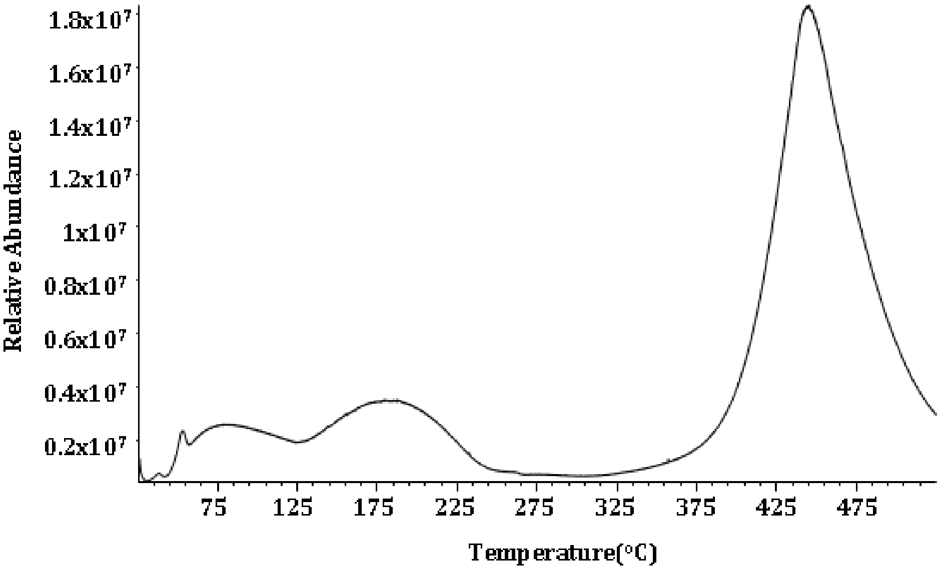

**Figure 4.64** Total ion current pyrogramme of 10% triphenyl phosphate-90% PET composite

In Figure 4.64, total ion current pyrogramme of composite consisting of 10% triphenyl phosphate and 90% percent of PET is given. Two different decomposition regions are observed from the pyrogramme. The first region between 30-250°C resembles the decomposition of TPP, Differing from Figure 4.61, the decomposition peak is broadened and intensity was decreased. This is due to the reactions especially the chain extension reactions that occurred between TPP and PET and thus the thermal stability was also increased. The second decomposition peak belonged to the PET decomposition and the top of the peak was shifted to 453°C that also implied the increase of thermal stability. Mass spectra, belonging to the two decomposition zones are given in Figure 4.65 and 4.66.

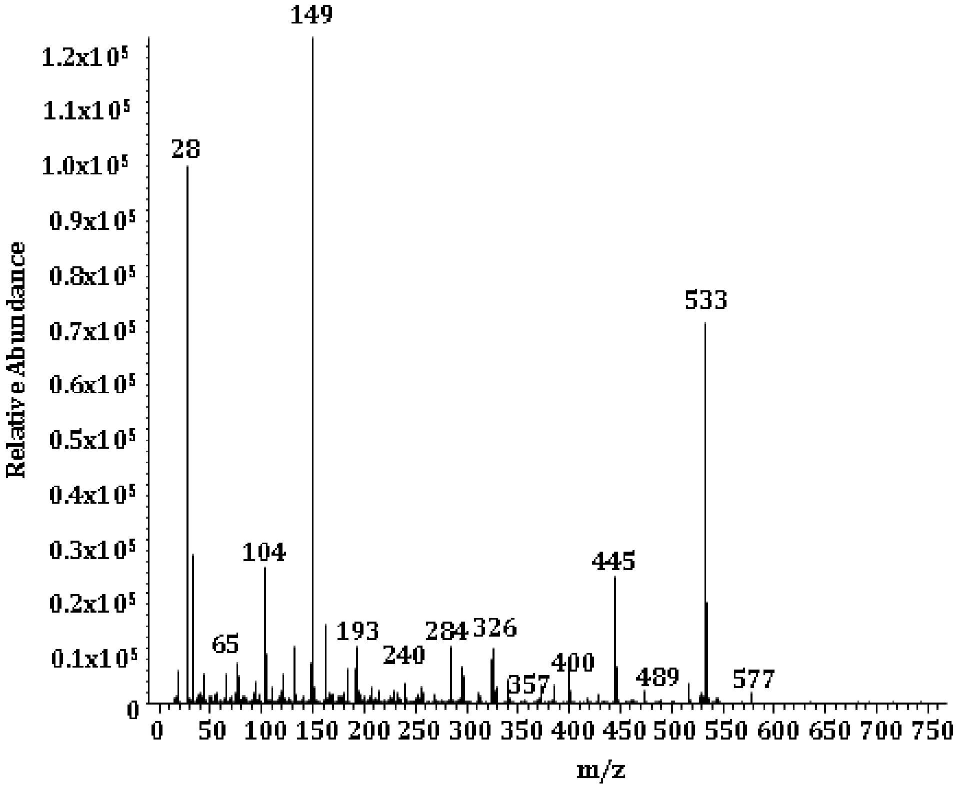

**Figure 4.65** Pyrolysis mass spectrum of 10% triphenyl phosphate-90% PET composite at 182°C

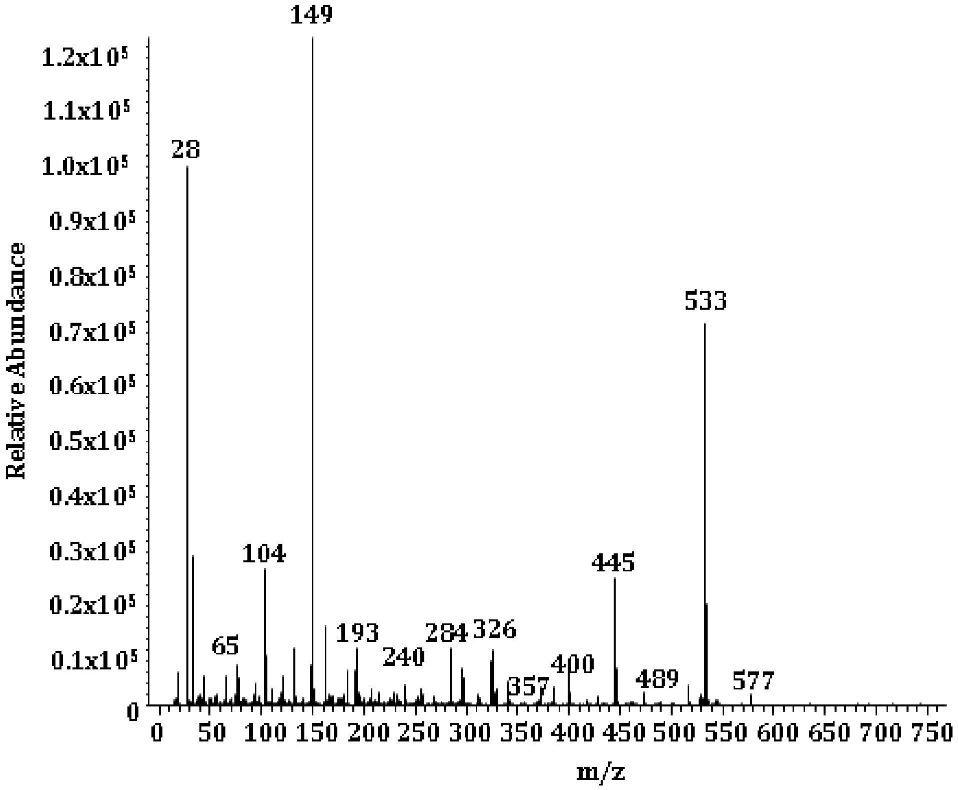

**Figure 4.66** Pyrolysis mass spectrum of 10% triphenyl phosphate-90% PET composite at 453°C

It was seen that $PO_4$, $PO^•$, $P_2$, $P_2O_2$, $P_2O_5$, $PO_2$ could be determined in the gaseous decomposition products. In the TPP decomposition products, the products' abundance were decrease in the order of $P_2O_2 > P_2O_5 > PO_2 > PO^• = PO_4 > P_2$ and in the decomposition products of PET, $PO_2 > P_2O_2 > P_2 > P_2O_5 > PO_4 > PO^•$. $P_2O_2$ and $P_2O_5$ were expected to decompose further to inherit the radical formation cycle. $P_2$ and $PO_2$, which were the smallest radicals and that can easily combine with $H^•$, were formed more in the PET decomposition range and as a result triphenyl phosphate is an effective flame retardant acting in the gas phase.

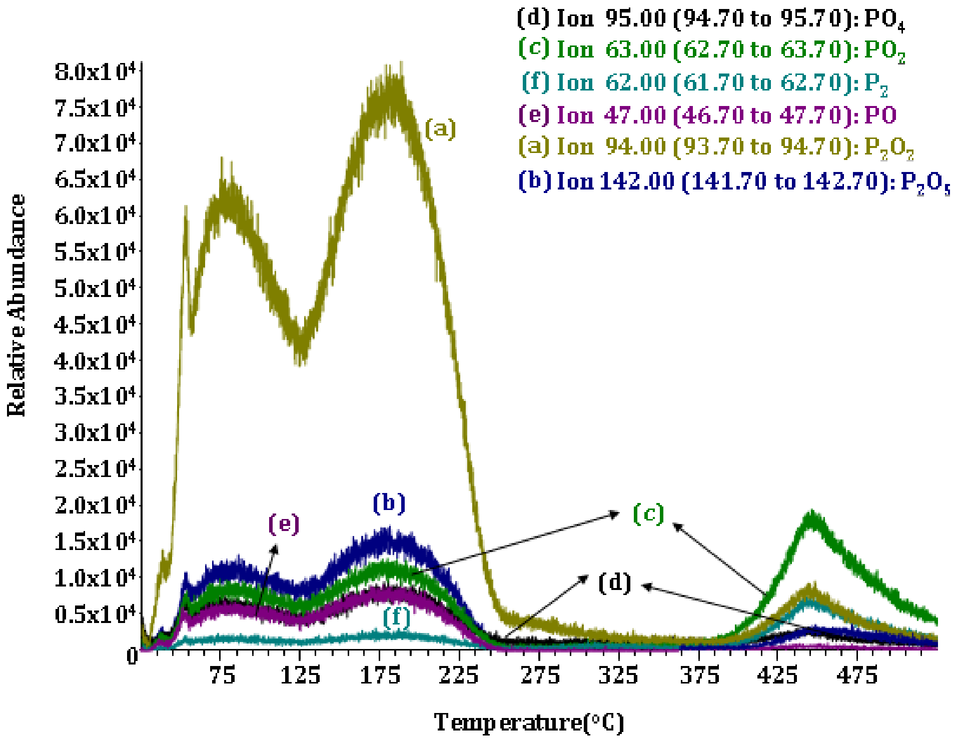

**Figure 4.67** Comparison of single ion current pyrogrammes of 10% triphenyl phosphate-90% PET decomposition products

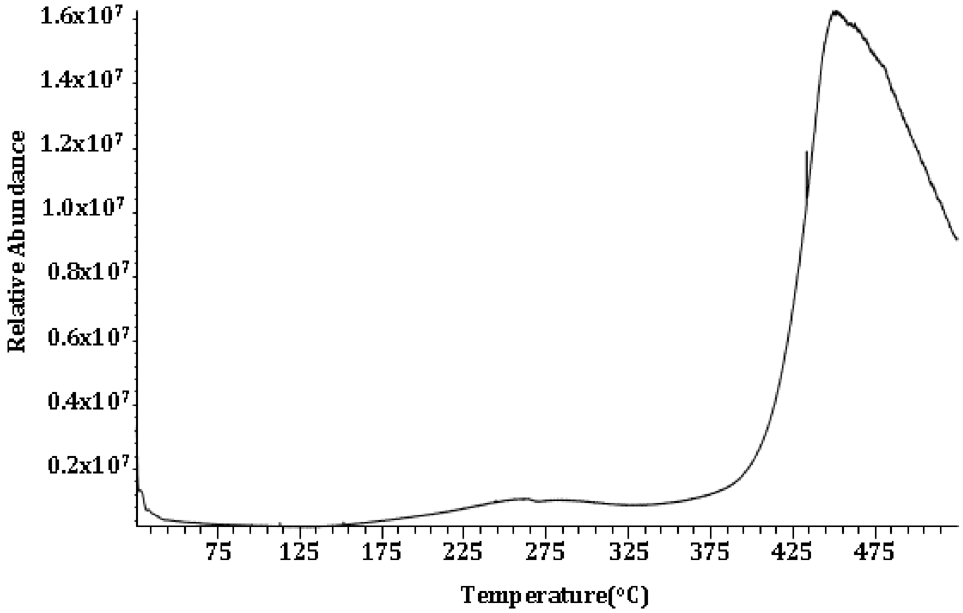

**Figure 4.68** Total ion current pyrogramme of 8% boron phosphate-92% PET composite

In Figure 4.68, total ion current program of 8% BoP MW + 92% PET are given. In the figure, one sharp peak for the decomposition of PET could be seen around 450°C. Unlike TPP, BoP MW decomposition could not be seen in the scanned temperature range as it is an inorganic additive and could not be completely decomposed in the range. There is a broad peak around 275°C, which could be the result of the volatile decomposition products of boron phosphate. In Figure 4.69, mass spectrum of the same composite's decomposition products is also given.

It is expected that the only mechanism of action of boron phosphate in the condensed phase is formation of glassy protective layer. In Figure 4.70, single ion current pyrogramme of the 8% boron phosphate-92% PET is given. It can be figured out that the decomposition products were $BPO_4$, $BPO_3$, $BPO^{\bullet}$, $PO_4$, $O_2$. Presence of decomposition products were in the order of $BPO_4 > BPO_2 > BPO_3 > PO_4 > O_2 > BPO^{\bullet}$. Those decomposition products indicate that boron phosphate could also act in

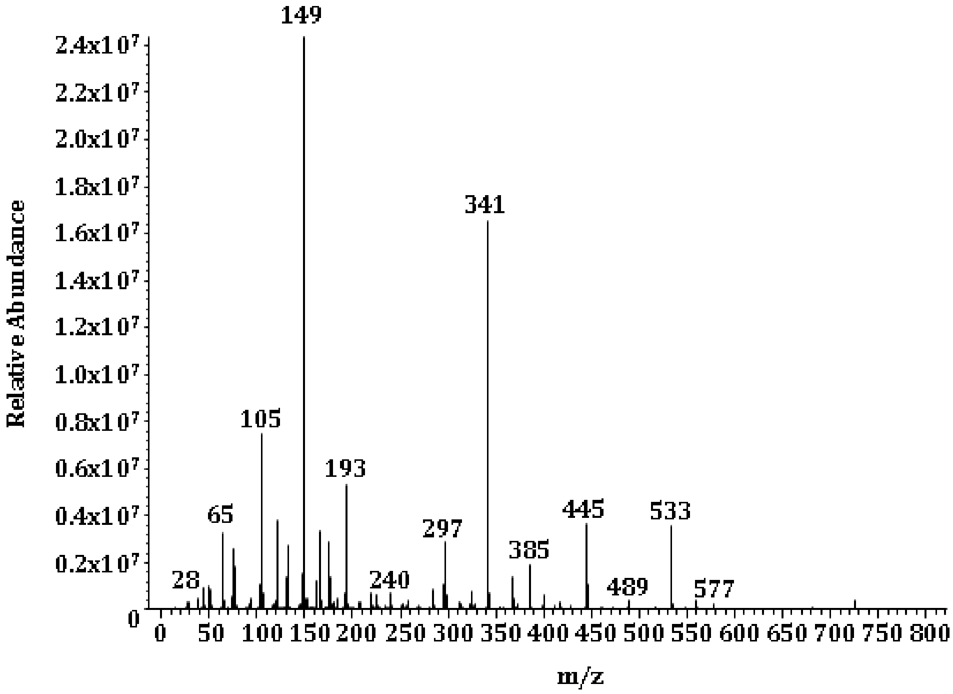

**Figure 4.69** Pyrolysis mass spectrum of 8% boron phosphate-92% PET composite at 450°C

the gas phase and could interrupt the burning cycle like triphenyl phosphate. Also, the formation of $BPO_3$ and $BPO_2$ supports the formation of the glassy layer when $BPO_4$

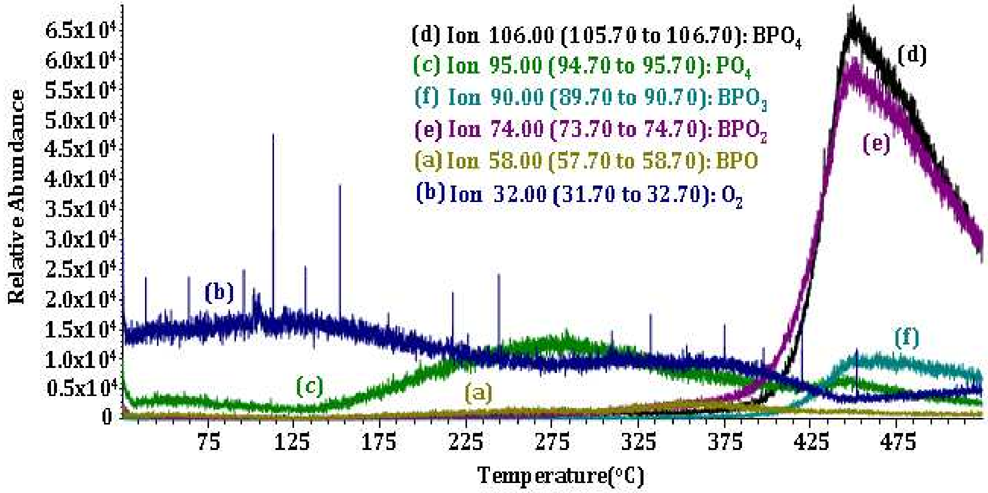

**Figure 4.70** Comparison of single ion current pyrogrammes of 8% boron phosphate-92% PET decomposition products

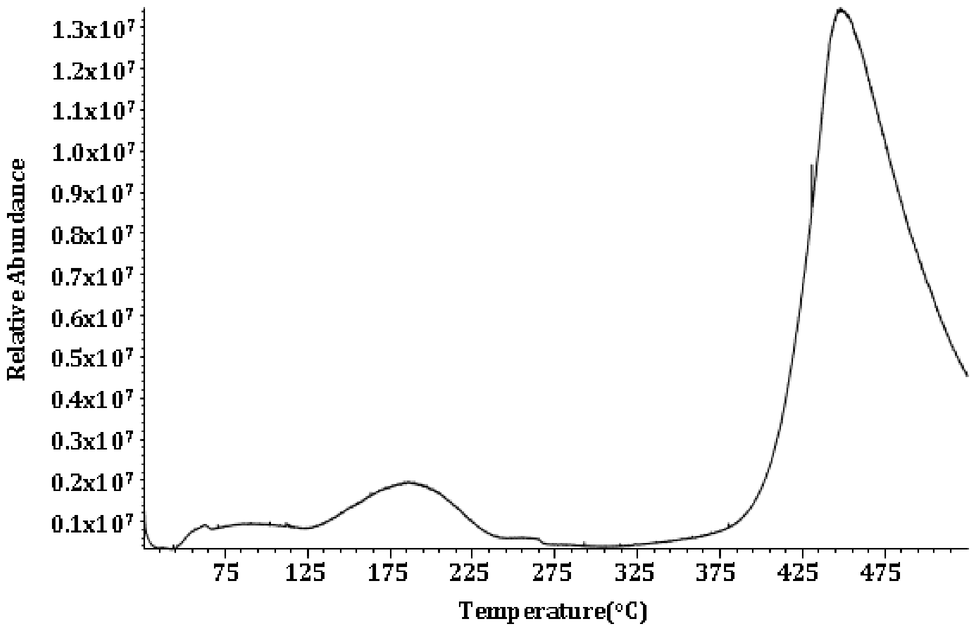

**Figure 4.71** Total ion current pyrogramme of 5% triphenyl-phosphate-5% boron phosphate-90% PET composite

was exposed to heat as those species have triangular structure and have more amorphous character.

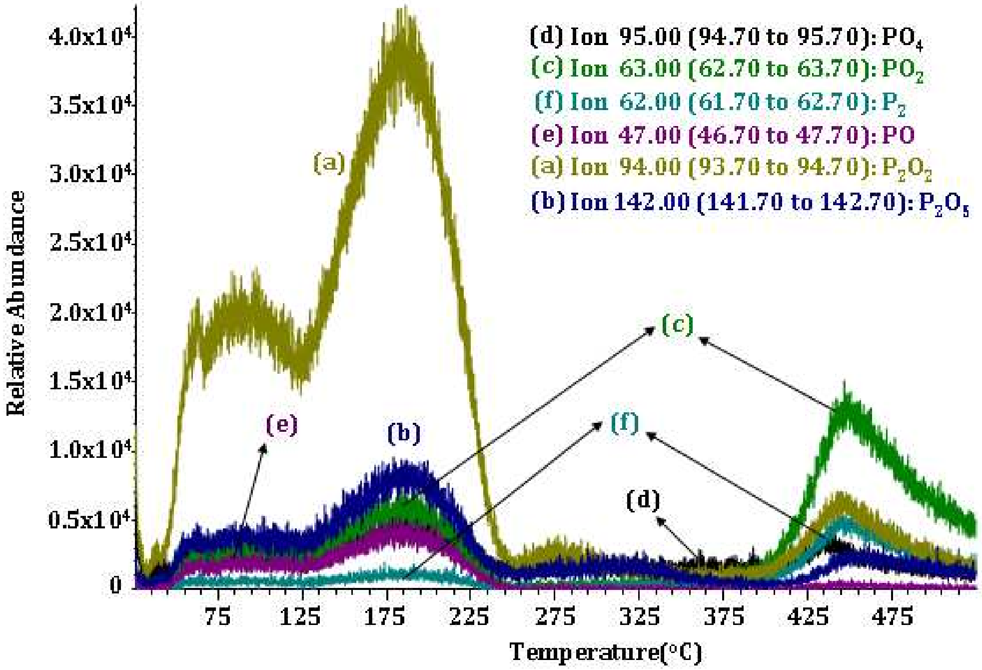

**Figure 4.72** Comparison of single ion current pyrogrammes of 5% triphenyl phosphate-5% boron phosphate-90% PET decomposition products in terms of triphenyl phosphate decompostion products

In order to examine the combined effect of triphenyl phosphate and boron phosphate together, composite containing 5% triphenyl phosphate and 5% boron phosphate was also examined by Py-MS technique (Figure 4.71). When the decomposition of the composite containing both TPP and BoP MW is considered, triphenyl phosphate decomposition products, are decreasing in the order of $P_2O_2 > P_2O_5 > PO_2 > PO^\bullet > PO_4 > P_2$, in triphenyl phosphate decomposition temperature range, and in the order of $PO_2 > P_2O_2 > P_2 > P_2O_5 = PO_4 > PO^\bullet$ (Figure 4.72), in the decomposition temperature of PET.

When the decomposition of the composite was examined on the side of boron phosphate decomposition (Figure 4.73), decomposition products were present at the PET decomposition temperature and decreased in the order of $BPO_4$ > $BPO_2$ > $BPO_3$ > $PO_3$ > $PO_4$ > $BPO^\bullet$ in terms of abundance.

It can be concluded that triphenyl phosphate and boron phosphate were both acting in the gas phase as a flame retardant similar to the mechanisms of action of halogenated flame retardant additives.

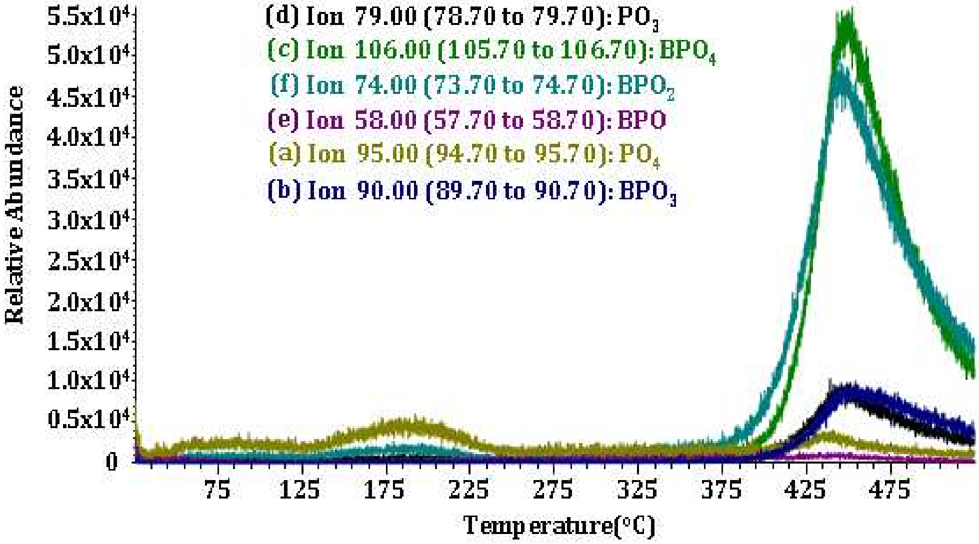

**Figure 4.73** Comparison of single ion current pyrogrammes of 5% triphenyl phosphate-5% boron phosphate-90% PET decomposition products in terms of boron phosphate decompostion products

One of the main aspects of flame retardancy is the prevention of smoke release during fire as most of the casualties during fire are directly related to the poisonings related to smoke. From the previous experiments in this study, it can be concluded that microwave technique produced boron phosphate is an effective smoke suppressant for PET matrix. Unlike $BPO_4$, triphenyl phosphate is not a smoke suppressant for PET due to the phenyl groups in its structure and high carbon content. Analysis confirmed that triphenyl phosphate increased the smoke formation during fire. In general one way of acquiring smoke suppression is to convert CO to $CO_2$ as much as possible as the more CO present, the more soot would be present as the CO is the sign of presence of unburnt species in the media [177]. For the smoke suppressant effect of boron phosphate, it is proposed that BP releases $O^{\bullet}$ and $O_2$ during fire and these could be combined with CO, and oxygen would help to complete the burning of unburnt species which are poisonous to humans and have black sooty smoke, and turns it them to $CO_2$ which is less harmful and colorless.

A series of experiments were performed to prove this phenomenon by using Py-MS. During PET decomposition the evolved decomposition products were examined in terms of CO and $CO_2$ presence (Figure 4.74). It was identified that the amount of $CO_2$ evolved was higher (around 50%) than CO evolved in the PET decomposition temperature range.

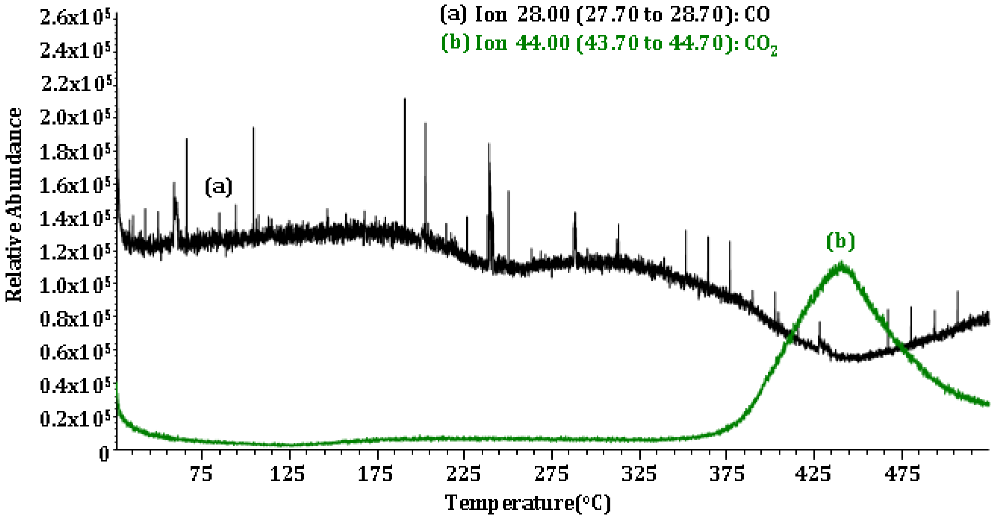

**Figure 4.74** Single ion current pyrogramme of CO and $CO_2$ during PET decomposition

To figure out the effect of presence of boron phosphate, the composite containing 8% $BPO_4$ was investigated with the same method (Figure 4.74). There was a significant increase in the amount of $CO_2$ formed at the PET decomposition range

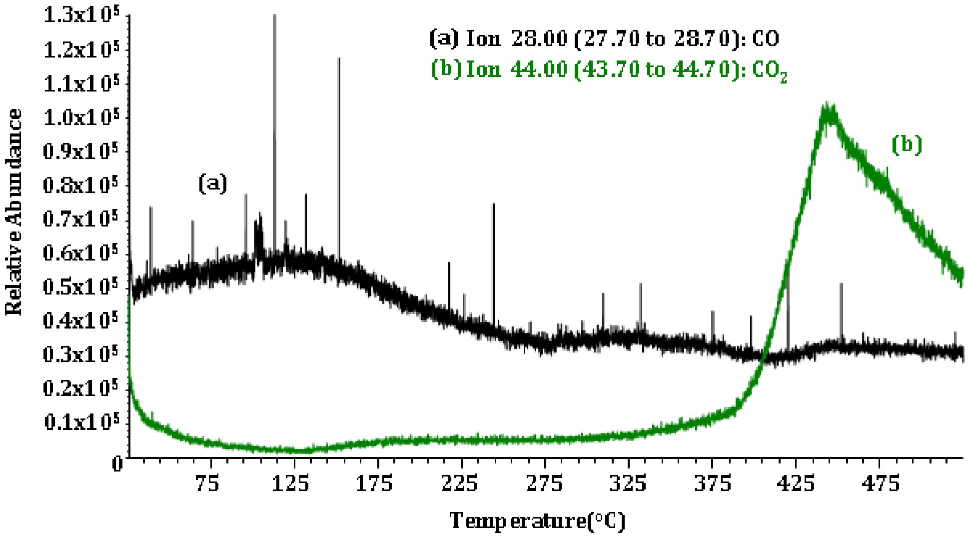

**Figure 4.75** Single ion current pyrogramme of CO and $CO_2$ during 8% boron phosphate-92% PET composite decomposition

when compared to the case of neat PET decomposition. The $CO_2$ amount formed is around 300% higher than the CO amount evolved. Thus, the light transmittance value of 8% boron phosphate containing composite was 99%, while the transmittance value for neat PET was 78%, supporting the results of the Py-MS analysis.

For the transformation of carbon monoxide to the carbon dioxide, $O^{\bullet}$ and $O_2$ must be present in the combustion media. Analyses were performed to characterize the formation of radicalic and gaseous oxygen (Figure 4.76). Supporting the claim, $O^{*}$ and $O_2$ were formed during decomposition of 8% boron phosphate-92 % PET composite at the PET decomposition temperature range. The $O^{\bullet}$ radical formation was only observed at the decomposition of PET. The evolved $O_2$ is 250% higher than $O^{\bullet}$ evolved.

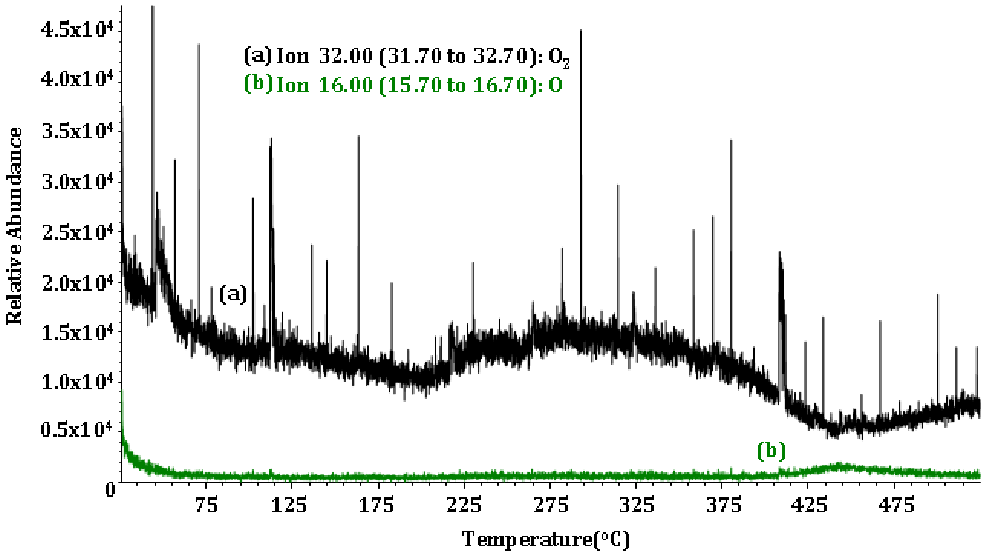

**Figure 4.76** Single ion current pyrogramme of $O^*$ and $O_2$ during 8% boron phosphate-92% PET composite decomposition

Lastly, in Figure 4.77, formation of CO and $CO_2$ was determined in the ternary composite of triphenyl phosphate-boron phosphate-PET.

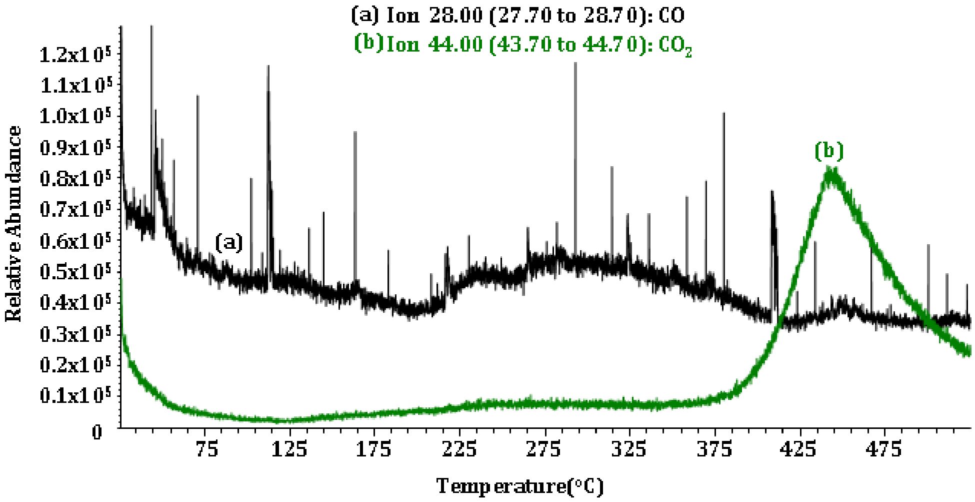

**Figure 4.77** Single ion current pyrogramme of CO and $CO_2$ during 5% triphenyl phosphate-5% boron phosphate-90% PET composite decomposition

Similar increase on the formation of $CO_2$ was clear as the evolved $CO_2$ was 100% higher than CO evolved. The evolved $CO_2$ amount is still higher than the decomposition of neat PET, but not as much as decomposition of composite containing only boron phosphate as a result of the negative effect of triphenyl phosphate, which is to increase the formation of CO due to the aromatic groups.

### 4.5 Additional Analysis Performed on PET Based FR Composites

Up to here, flame retardant composites were characterized in terms of flammability behaviour, mechanical properties and thermal properties. Further characterizations were performed to investigate the mechanisms of action of flame retardant additives. PET is a widely used thermoplastic polymer which makes it important. For different applications mechanical properties are as important as the flammability properties.

In addition to the previous characterization experiments, the two important parameters for the usage of PET in film form especially for packaging applications and construction material; UV transmittance and transparency analysis were performed finally.

#### 4.5.1 UV Transmittance Analysis of PET Based Second Stage FR Composites

UV transmittance analyses were performed by using an UV spectrophotometer and specimens were prepared in the form of thin films by compression molding technique, which have an average thickness of 20 µm.

Many polymers used in consumer products degrade by UV light, and need addition of UV absorbers to inhibit attack, especially if the products are used outdoors and so exposed to sunlight. The problem appears as discoloration or fading, cracking and sometimes, total product disintegration if cracking has proceeded far enough. The rate of attack increases with exposure time and sunlight intensity. It is known as UV degradation, and is one form of polymer degradation. UV-A (315-400 nm wavelength) and UV-B (280-315 nm wavelength) are the most harmful UV ranges that affect the humans, thus the transmittances of the composites were investigated in those ranges. Incorporation of the flame retardant additives decreased both UV-A and UV-B transmittance of the PET matrix in both first and second stage flame retardant composites Table 4.27 and 4.28).

**Table 4.27** UV transmittance analysis of first stage FR composites

| | Average Transmittance (%) | |
|---|---|---|
| | 315-400 nm (UV-A) | 280-315 nm (UV-B) |
| Neat PET | 40.8 | 3.8 |
| PET1 | 22.4 | 3.2 |
| PET2 | 23.5 | 2.9 |
| PET3 | 30.4 | 2.5 |
| PET4 | 35.4 | 3.1 |
| PET5 | 21.8 | 1.7 |
| PET6 | 27.4 | 2.0 |
| PET7 | 23.2 | 1.1 |
| PET8 | 21.4 | 1.3 |
| PET9 | 29.5 | 1.9 |
| PET10 | 25.6 | 0.9 |
| PET11 | 12.3 | 0.3 |
| PET12 | 11.5 | 0.2 |

Triaryl phosphates, which were triphenyl phosphate and triphenyl phosphine oxide, in this study, have three aromatic phenyl groups in their structures. Aromatic rings are known as good UV light absorbers due to the delocalized electron in the aromatic ring. Thus, it was expected that the addition triaryl phosphates would decrease the UV transmittance. Composites PET11 and PET12 had lower UV-A and UV-B transmittances confiming the proposal.

Similar results were obtained from the UV analyses of the second stage flame retardant composites. The increase of the triaryl phosphate content resulted in the decrease in the UV transmittance of the composites. As a result triphenyl phosphate is not only a good flame retardant additive and mechanical property improver, but also a successful UV stabilizer for the PET matrix.

**Table 4.28** UV transmittance analysis of second stage FR composites

| | Average Transmittance (%) | |
|---|---|---|
| | 315-400 nm (UV-A) | 280-315 nm (UV-B) |
| Neat PET | 41.2 | 3.8 |
| PT1 | 7.1 | 0.4 |
| PT2 | 3.2 | 0.2 |
| PT3 | 1.1 | 0.1 |
| PT4 | 0.2 | 0.1 |
| PT5 | 0.2 | 0.1 |
| PT6 | 5.6 | 0.2 |
| PT7 | 3.1 | 0.1 |
| PT8 | 6.3 | 0.3 |
| PT9 | 4.1 | 0.2 |
| PT10 | 3.9 | 0.1 |
| PT11 | 20.3 | 2.6 |
| PT12 | 27.1 | 2.9 |
| PT13 | 21.3 | 2.7 |

### 4.5.2 Transparency Analysis of PET Based Second Stage FR Composites

One of the main drawback of the flame retardant additives is that the refractive indices of them are not close to those of most thermoplastic polymers. Most of the additives are in white powder form. Also most of the additives, especially the inorganic ones have particle sizes around microns, thus they scatter the incoming light to the matrix. Lastly, they could possibly act as crystallization promoters when they are above certain average particle size. These points mentioned affect the polymer matrix and make it opaque.

**Figure 4.78** Transparency comparison of second stage flame retardant composites

In Figure 4.78, transparencies of the second stage flame retardant composites were compared. Analysis were done by placing the specimens on a written manuscript and then taking their photos by a digital camera to compare the readability of the manuscript behind the samples. Triphenyl phosphate and triphenyl phosphine oxide are organic flame retardant additives. Belonging to the triaryl phosphate group, they tend to give chain extension reactions with the PET matrix and also decrease the crystallization of the PET matrix. Zinc borate scatters the light passing to through the PET matrix, as it has average particle diameter around 4 µm. As a result, composites containing zinc borate have lower transparency. Microwave technique produced boron phosphate has an average particle size around 400 nm. Due to this relatively small particle diameter compared to the zinc borate, it scatters less light than zinc borate and makes the matrix more transparent, but not as transparent as triphenyl phosphate. It is observed that when the triphenyl phosphate content exceeds 5%, the matrix becomes more opaque. Composites containing both triphenyl phosphate-zinc borate (PT9) or triphenyl phosphate-boron phosphate (PT6) are more transparent than the ones that contain only zinc borate (PT11) or boron phosphate (PT12).

# CHAPTER 5

# CONCLUSIONS

The first part of this study mainly focuses on the production of the inorganic boron based flame retardant additives, 3.5 hydrated zinc borate and boron phosphate. It is aimed to produce 3.5 hydrated zinc borate in laboratory scale and then to scale up the production to 80 liter reactor. Reaction parameters such as effect of seed amount, presence of baffle, stirring rate, zinc oxide particle size for laboratory scale production; stirring rate, zinc oxide particle size, zinc oxide purity $H_3BO_3$:ZnO mole ratio are examined in pilot scale production. Another flame retardant additive, boron phosphate is synthesized via three different techniques, dry, wet and and microwave techniques. Microwave technique is decided to be used in the flame retardant composite production as a result of the achievement of synthesis of submicron sized boron phosphate. The following conclusions can be drawn for the first part of the study:

- 3.5 hydrated zinc borate is synthesized both in laboratory and pilot scale and effects of reaction parameters are evaluated.
- Stirring rate, ZnO average particle size, presence of baffle are effective on final products' particle size distribution and the size of the zinc borate.
- The amount of seed does not interfere with the either reaction speed or final products particle size, but presence of seed is essential for a succesful synthesis.
- Analysis in pilot scale production shows that excess amount of boric acid and purity of zinc oxide are important for the successful synthesis of zinc borate.

- To examine throughly the zinc borate formation, a kinetic model, namely logistic model, is proposed and checked whether it fits with the experimental data.
- The crystal growth rate of the model is increased with the increase of stirring rate in both laboratory and pilot scale production of zinc borate.
- The average particle size distribution of the laboratory scale produced zinc borates is smaller than the commercially available 3.5 hydrated zinc borate, Firebrake ZB.
- After filtration and drying procedure, zinc borates are obtained between 72-82% yield in laboratory scale and 75-80% yield in pilot scale. These results show an acceptable scale-up of production of zinc borate.
- Boron phosphate is synthesized via dry, wet, and microwave techniques.
- Microwave technique produced boron phosphate has an average particle size of 397 nm according to the result of BET analysis.

After synthesis of the boron based flame reatardant additives is completed, production of flame retardant composites are made. To determine the successive flame retardant additive for the PET matrix, besides the synthesized additives, Cloisite 30B, anhydrous borax, calcium sulfate dihydrate, metal powder synergist Smokebloc AZ-12, phosphorus based intumescent additive, Reogard 2000, triphenyl phosphate and triphenyl phosphine oxide are used and composites are produced and characterized as the first stage flame retardant composites.

Owing to the results of flammability, thermal and mechanical characterizations of the first stage flame retardant composites; zinc borate, microwave produced boron phosphate, triphenyl phosphate and triphenyl phosphine oxide are found to be the successful flame retardant additives for the PET matrix and in the second stage production of flame retardant composites, different amounts and combinations of these four additives are evaluated as the second stage PET based flame retardant composites.

From the characterization experiments of the second stage flame retardant composites, the following conclusions can be drawn:

- Boron phosphate, which is synthesized by micro-wave technique, is the most effective additive for PET among boron phosphates produced with different techniques.
- While triphenyl phosphate containing composites have a LOI of 29.5, they have an average smoke density regarding the phenyl groups in the chemical structure.
- When triphenyl phosphate is combined with boron phosphate; it is found that not only the LOI value of the composites increases up to 36.0, but also the smoke evolution of the composites decreases significantly.
- Py-MS analysis shows the formation of $P_2$, PO, $PO_2$, etc. species which act as scavengers of $H^{\bullet}$ and $OH^{\bullet}$ radicals and this explains the mechanism of triphenyl phosphate and triphenyl phosphine oxide in the gas phase.
- TGA analysis shows the increase of char formation, which gives the mechanism of action of triphenyl phosphate and triphenyl phosphine oxide in the condensed phase.
- XRD and SEM analyses show the formation of vitreous protective layer in the condensed phase when 3.5 hydrated zinc borate and boron phosphate are used as flame retardant additives.
- Boron phosphate is an efficient smoke suppressant for PET. It releases $O^{\bullet}$ radical during the decomposition, which combines with carbon monoxide and the other partially burnt decomposition products to transform them to the less sooty carbon dioxide.
- Triphenyl phosphate and triphenyl phosphine oxide have noticeably increased the impact properties of PET.
- Up to 10 weight percent loading, triphenyl phosphate acts as chain extender and beyond this percent it acts as plasticizer.
- Addition of the flame retardant additives decreases the degree of crystallization of the composites significantly.
- According to TGA analysis char formation of the composites after fire increases noticeably with the addition of triphenyl phosphate, and zinc borate.
- According to the TGA results PET tends to decompose around 450°C.
- The addition of triphenyl phosphate severely decreases the glass transition temperature of the polymer matrix.

- Melting point of the composites do not change significantly compared with the PET matrix.
- Addition of triphenyl phosphate and triphenyl phosphine oxide decreases the UV transmittance of the composites due to the their phenyl groups.
- Almost all flame retardant additives tend to turn the PET matrix to opaque. Unlike the others, triphenyl phosphate protects the transparency of the matrix.
- As the concentration of zinc borate and/or boron phosphate in the flame retardant composites increases, the transparency of the PET matrix decreases.

# REFERENCES

**[1]** Schubert, D. M., U.S. Patent 5,342,533, 1994.

**[2]** Choudhury, A., Neeraj, S., Natarajan, S., Rao, C. N., J. Chem. Soc., Dalton Trans., 7, 2002.

**[3]** Lehmann, H. A., Sperscheider, K., Kessler, G. Z. Anorg. Allg. Chem., 354, 1967.

**[4]** Ozols, J., Tetere, I., Levins, A., Izv. Akad. Latv. Nauk. SSSR, Ser. Kim., 1, 1973.

**[5]** Putnins, J., Levins, A. Latv., Valsts Univ. Kim. Fak. Zinat. Raksti., 22, 1958.

**[6]** Lyday, P. A., End uses of boron other than glass. In Borates: Economic Geology and Production, Ch. 7, Soc. Min. Eng., AIMMPE, New York, 1985.

**[7]** Giúdice, C. A., Benitez, J .C., Prog. Org. Coat., 42, 2001.

**[8]** Garba, B., Polym. Degrad. Stab., 64, 1999.

**[9]** Wen, Y. C. and Hu, C. H., Eur. Polym. J., 32, 1996.

**[10]** Samyn, F., Bourbigot, S., Duquesne, S., Delobel, R., Thermochem. Acta, 456, 2007.

**[11]** Dong, J. X. and Hu, Z. S., Tribol. Int., 31, 1998.

**[12]** Nies, N. P., Beach, L., Hulbert, R. W., U.S. Patent 3,549,316, 1970.

**[13]** Shete, A. V., Sawant, S. B., Pangarkar, V. G., J. Chem. Technol. Biot., 79, 2004.

**[14]** Eltepe, H. E., Balköse, D., Ülkü, S., Ind. Eng. Chem. Res., 46, 2007.

**[15]** Gürhan, D., Çakal, G. Ö, Eroğlu, İ, Özkar, S., J. Cryst. Growth., 311, 2009.

**[16]** Schubert, D. M., Alam, F., Mandana, Z. V., Knobler, C., Chem. Mater., 15, 2003.

**[17]** Brandrub, J. and Immergut, E. H., Polymer Handbuch, John Wiley & Sons, Berlin, 1991.

**[18]** Brossas, G. J., Polym. Degrad. Stab., 23, 1989.

**[19]** Hawkins, W. L., Polymer Degradation and Stabilization, Springer Verlag, Berlin, 1984.

**[20]** Laoutid, F., Ferry, L., Lopez-Cuesta, J. M., Crespy, A., Polym. Degrad. Stab., 82, 2003.

**[21]** Cusack, P. A., Heer, M. S., Monk, A. W., Polym. Degrad. Stab., 58, 1997.

**[22]** Horrocks, A.R., and Price, D., Fire Retardant Materials, CRC Press, Cambridge, 2001.

**[23]** Innes, J and Innes A., Plastic Flame Retardants: Technology and Current Developments, Woodhead Publishing, Cambridge, 2004.

**[24]** Dias, M.L.; Nascimento, C.R., J. of Therm. Analy. and Cal., 69, 2002.

**[25]** Grand, A. F. and Wilkie, C. A., Fire Retardancy of Polymeric Materials, Marcel Dekker, New York, 2000.

**[26]** Hastie, C, W. and McBee, C. L., National Bureau of Standards IR, 1975.

**[27]** Ullmann's Encyclopedia of Industrial Chemistry, Vol. A11, 5th ed., VCH Publication, Weinherm, 1988.

**[28]** Eti Maden İşletmeleri http://www.etimaden.gov.tr/tr/0_sayfa_ortakSayfa.asp?hangisayfa=4_sayfa_a_1, last accessible 20 January 2009.

**[29]** Kirk-Othmer Encyclopedia of Chemical Technology, Vol.10 & Vol.4, 4th ed., John Wiley and Sons, New York, 1994.

**[30]** Nies, N. P., Campbell, G. W., Adams, M. R., Boron, Metallo-Boron Compounds, and Boranes, New York, Interscience Publishers, 1964.

**[31]** Woods, W. G. and Bhatnager, V. M., Advances in Fire Retardants, Part 2, Technomic, Pa., 1973.

**[32]** Tektaş, E. and Mergen, A., Zinc Borate Production Feasibility Report, Etibank, May 2003.

**[33]** Nies, N. P., Beach, L., Hulbert, R. W., U.S. Patent 3,549,318, 1970.

**[34]** Dong, J. X. and Hu, Z. S., Tribol. Int., 31, 5, 1998.

**[35]** Ting, C., Cheng, D. J., Shuo, W. L., Fan, Y., Gang, F., Mater. Lett., 62, 2008.

**[36]** Yumei, T., Yi, H., Lianxiang, Y., Yanhui, D., Yunhui, Z., Fang, S., Zhihui, Li., Zichen, W., Colloid Surface A, 312, 2008.

**[37]** Polymer Science Learning Center http://www.psrc.usm.edu/macrog/index.htm, last accessible 25 January 2009.

**[38]** US Environmental Protection Agency Wastes http://www.epa.gov/epaoswer/nonhw/muncpl, last accessible 15 January 2009.

**[39]** Lyon, R. E., Fire and Polymers II, ACS Symposium Series 599, Ed. by O. Nelson, American Chemical Society, Washington, D.C., 1995.

**[40]** Sorathia, U., Lyon, R. E., Ohlemiller, T., Grenier, A., SAMPE Journal, 33, 1997.

**[41]** Sorathia, U., Lyon, R. E., Gann, R. G., Gritzo, L., Fire Technol., 33, 1997.

**[42]** Fire Safety Branch http://www.fire.tc.faa.gov/pdf/handbooklOO12_apC.pdf, last accessible 2 Febrauary 2009.

**[43]** Troitzsch, J., International Plastics Flammability Handbook; 2nd ed.; Hanser Publishing: New York, 1990.

**[44]** Lyons, J. W., The Chemistry and Uses of Fire Retardants; John Wiley and Sons Inc., New York, 1987.

**[45]** Landrock, A. H., Handbook of Plastics Flammability and Combustion Toxicology, Noyes Publication, Park Ridge, New Jersey, 1983.

**[46]** Cullis, C. F. and Hirschler, M., The Combustion of Organic Polymers, Clarendon Press, Oxford, 1981.

**[47]** Stevens, M. P., Polymer Chemistry: An Introduction, 3rd ed.; Oxford University Press: Oxford, 1999.

**[48]** Glassman, I., Combustion, 3rd ed.; Academic Press, New York, 1996.

**[49]** Nelson, G. L., Fire and Polymers II: Materials and Tests for Hazard Prevention, Washington, D.C., 1995.

**[50]** Hartzell, G. E., Fire Protection Handbook, 18th ed., National Fire Protection Association, Quincy, MA, 1997.

**[51]** Chien, J. C. W. and Kiang, J. K. Y., Adv. Chemn. Ser., 169, 1978.

**[52]** Chien, J. C. W. and Kiang, J. K. Y., J. Makromol. Chem., 181, 1980.

**[53]** Cullis, C. F. and Laver, H. S., Eur. Polym. J., 14, 1978.

**[54]** Fenimore, C. P. and Martin, F. J., Combust. Flame., 10, 1966.

**[55]** Mita, I., Effect of Structure on Degradation and Stability of Polymers, Elsevier, Amsterdam, 1978.

**[56]** Kelen, T., Polymer Degradation, Van Nostrand Reinhold, New York, 1983.

**[57]** Fristrom, R. M., Kinetic and Mechanism of Flame and Flame Suppression, NBS Spec. Publ., 357, 1972.

**[58]** Critchley, J.P., Knight, G. J., Wright, W., Heat-Resistant Polymers, Plenum Pres, New York, 1983.

**[59]** Pearce, E. M. and Weil, E. D., Fire and Polymers Materials and Solutions for Hazard Prevention, ACS Symposium Series, 797, Washington D.C., 2001.

**[60]** Dubois, A. B., Fire and Smoke: Understanding the Hazards, National Academy Press, Washington, D. C., 1986.

**[61]** Bolger, R., Ind. Minerals, 340, 1996.

**[62]** Hirschler, M. M., Flame Retardants, Interscience Communications: London, 1996.

**[63]** Hornsby, P. R., Fire Mater., 18, 1994.

**[64]** Hornsby, P. R. Macrol. Symp., 108, 1996.

**[65]** O'Driscoll, M., Ind. Minerals, 318, 1994.

**[66]** Hilado, C. L., Flammability Handbook for Plastics, 3rd ed., Technomic Publication, Westport, CT, 1982.

**[67]** Green, J., Fire Retardancy of Polymeric Materials, Marcel Dekker Inc, New York, 2000.

**[68]** Lee, F. T., Green, I., Gibilisco, R. D., J. Fire Retard. Chem., 9, 1982.

**[69]** Allen, C. W., J. Fire Sci., 11, 1993.

**[70]** Green, I., J. Fire Sci., 12, 1994.

**[71]** Inoue, K., Nakamura, H., Ariyoshi, S., Takagi, M., Tanigaki, T., Macromolecules, 22, 1989.

**[72]** Montaudo, G., Scamporrino, E., Vitalini, D., J. Polym. Sci. Part A: Polym. Chem., 21, 1983.

**[73]** Horacek, H. and Grabner, R., Polym. Degrad. Stab., 54, 1996.

**[74]** Horacek, H. and Grabner, W., Makromol. Chem. 74, 1993.

**[75]** Iji, M. and Serizawa, S., Polym. Adv. Technol., 9, 1998.

**[76]** Kambour, R. P., Klopper, H. I., Smith, S. A., J. Appl. Polym. Sci., 26, 1981.

**[77]** Zaikov, G. E. and Lomakin, S. M., Polym. Degrad. Stab., 54, 1996.

**[78]** Allen, N. S., Edge, M., Corrales, T., Polym. Degrad. Stab., 56, 1997.

**[79]** Chao, T. C., Sarmah, S. K., Boisvert, R. P., Burns, G. T., Katsoulis, D. E., Page, W. C., Proceedings of 43rd International SAMPE Symposium, Anaheim, 1998.

**[80]** Bolf, A. G. and Lichtenhan, I. D., Am. Chem. Soc. Polym. Prepr., 35, 1994.

**[81]** Allen, C. W., Trends in Polymer Science, 2, 1994.

**[82]** Mark, J. E., Allcock, H. R., West, R., Inorganic Polymers, Prentice Hall, New Jersey, 1992.

**[83]** Zingde, G., ANTEC Technical Conference Proceedings, 54, 3, 1996.

**[84]** Pritchard, G., Plastics Additives: An A-Z Reference, Chapman and Hall, 1998.

**[85]** Davis, J., J. Vinyl Addit. Techn., 2, 1, 1996.

**[86]** Hastie, J. W., J. Res. N.B.S., 77A, 1973.

**[87]** Petrella. R. V., J. Fire Flammability, 10, 1979.

**[88]** Hastie, J. W., McBee, C. L., Report NBSIR 75-741, National Bureau of Standards, Washington DC, 1975.

**[89]** Carpentier, F., Bourbigot, S., Bras, M. L., Delobel, R., Polym. Int., 49, 2000.

**[90]** Bonduel, D., Mainil, M., Alexandre, M., Monteverde, F., Dubois, P., Chem. Commun., 781, 2005.

**[91]** Laachachi, A., Cochez, M., Ferriol, M., Lopez-Cuesta, J. M., Leroy, E., Mater. Lett., 59, 2005.

**[92]** Hirschler, M. M., Carbon Monoxide and Human Lethality: Fire and Non-Fire Studies, Elsevier Applied Science, London, 1993.

**[93]** Calcote, H. F., Comb. Flame, 42, 1981.

**[94]** Hirschler, M. M., Heat Release in Fires, Elsevier Applied Science, London, 1992.

**[95]** Ahlstrom, D. A., Liebman, S. A., Quinn, E., J. Poly. Prep. Amer. Chem. Soc. Div. Poly. Chem., 14, 1973.

**[96]** Calcraft, A. M., Green, R. J. S., Mc Roberts, J. S., Plast. Polym., 42, 1974.

**[97]** Edgerley, R. G. and Pettett, K., Fire Mat., 2, 1978.

**[98]** Van Krevelen, D. W., Polymer, 16, 1975.

**[99]** Brown, S. C. and Herbert, M. J., Flame Retardants 92 Conference Paper, Elsevier Applied Science, London, 1992.

**[100]** Antia, F. K., Cullis, C. F., Hirschler, M. M., Eur Polym. J., 18, 1982.

**[101]** Hornsby, P., Inorganic Fire Retardants, RSC Conference Paper, London, 1993.

**[102]** Lawson, D. F., Kay, E. L., Roberts, D., Rubber Chem. Technol., 48, 1975.

**[103]** Kracklauer, J. J. and Sparks, C., J. Plast. Eng., 11, 1974.

**[104]** Lawson, D. F., J. Appl. Poly. Sci., 20, 1976.

**[105]** Carty, P. and White, S., Appl. Organometallic Chem., 10, 1996.

**[106]** Kroenke, W., J., J. Appl. Poly. Sci., 26, 1981.

**[107]** Mitchell, L. C., US Patent 3,845,001, 1974.

**[108]** Babrauskas, V., NBSIR 82-2611, U.S. Natl. Bur. Stand., 1982.

**[109]** Madorsky, S. L., Polymer Reviews Vol. 7, Interecience Publ., New York, 1964.

**[110]** Luderwald, I., Pure and Appl. Chem., 54, 1982.

**[111]** Ehrig, R. J., Plastics Recycling, Products & Processes, Hanser Publishers, New York, 1992.

**[112]** Granzow, A., Acct. Chem. Res., 11, 1978.

**[113]** Cooney, J. D., Day, M., Wiles, D. M., J. Appl. Polym. Sci., 28, 1983.

**[114]** Vijayakumar, C. T., Ponnusamy, E., Balakrishnan, T., Kothandaraman, H., J. Polym. Sci., 20, 1982.

**[115]** Cooney, J. D., Day, M., Wiles, D. M., J. Appl. Polym. Sci., 28, 1983.

**[116]** Marshell, I. and Todd, A., Trans. Faraday Soc., 49, 1953.

**[117]** Goodings, E. P., Soc. Chem. Ind., Sci. Monograph No. 13, 1961.

**[118]** Day, H., Ho, K.., Wiles, D. H., J. Appl. Polym Sci., 25, 1980.

**[119]** Bednas, M. E., Day, M., Ho, K., Sander, R., Wiles, D. M., J. Appl. Polym. Sci., 26, 1981.

**[120]** Sugimura, Y., J. Chromo Sci., 17, 1971.

**[121]** Carlsson, D. J., Day, H., Suprunchuk, T., Wiles, D. H., J. Appl. Polym. Sci. 28, 1983.

**[122]** Avondo, G., Vovelle, C., Delbourgo, R., Combust. Flame. 31, 1978.

**[123]** Zimmermann, H. and Leibnitz, E., Textiltech., 16, 1965.

**[124]** Zimmermann, H., Textiltech., 17, 1966.

**[125]** Yoda, K., Tsuboi, A., Hada, M., Yamadera, B., J. Appl. Polym. Sci., 14, 1970.

**[126]** Nealy, D. L. and Adams, L. J., J. Polym. Sci., 9, 1971.

**[127]** Spinninger, P. A., J. Polym. Sci., 12, 1974.

**[128]** Jones, C. E. R., and Cramers, C. A., Analytical pyrolysis, Elsevier Scientific Publishing Company, Amsterdam, 1977.

**[129]** Aguilera, C. and Luderwald, I., Makromol. Chem., 179, 1978.

**[130]** Morgan, A., Jurs, J., Tour, J., J. Appl. Polym. Sci., 76, 2000.

**[131]** Pape, P. and Romenesko, D., SPE Annual Technical Conference, 43, 1997.

**[132]** Sato, M., Kondo, H., Yokoyama, M., J. Appl. Polym. Sci., 29, 1984.

**[133]** Sato, M., Endo, S., Araki, Y., Matsuoka, G., Gyobu, S., Takeuchi, H., J. Appl. Polym. Sci., 78, 2000.

**[134]** Horrocks, A., Polym. Degrad. Stab., 54, 1996.

**[135]** Koch, J., Pearce, M., Lapham, A., Shalaby, W., J. Appl. Polym. Sci. 19, 1975.

**[136]** Bar-Yaacov, Y., Nir, Z., Nae, N., SPE Annual Technical Conference, 32, 1986.

**[137]** Cusack, P. A., Heer, M. S., Monk, A. W., Polym. Degrad. Stab., 58, 1997.

**[138]** Maspoch, M. L., Ferrando, H. E., Vega, D., Gordillo, A., Velasco, J. I., Martinez, A. B., Macromol. Symp., 221, 2005.

**[139]** Wang, M., Zhu, M., Sun, B., J. Macromol. Sci. Part A: Pure and Appl. Chem., 43, 2006.

**[140]** Swoboda, B., Buonomo, S., Leroy, E., Cuesta, J. M., Polym. Degrad. Stab., 93, 2008.

**[141]**Chemtura Corporation, Polymer Additives-Flame Retardants http://www.chemtura.com/bu/v/index.jsp?vgnextoid=f9a51dcc1d585110VgnVCM10000053d7010aRCRD&vgnextchannel=f9a51dcc1d585110VgnVCM10000053d7010aRCRD&vgnextfmt=default, last accessible 28 January 2009.

**[142]** Southern Clay Products http://www.scprod.com/product_bulletins/PB%20Cloisite%2030B.pdf, last accessible 12 January 2009.

**[143]** Eti Maden İşletmeleri http://www.etimaden.gov.tr/tr/0_sayfa_ortakSayfa.asp?hangisayfa=4_sayfa_a_5_7, last accessible 21 January 2009.

**[144]**Acros Organics http://www.acros.com/portal/alias__Rainbow/lang__en/tabID__28/DesktopDefault.aspx, last accessible 15 January 2009.

**[145]** Igarashi, H., Tatebe, A., Sakao, K., EP Patent 1,205,439A1, 2001.

**[146]** Nies, N. P., Beach, L., Hulbert, R. W., US Patent 3,549,320, 1970.

**[147]** Levenspiel, O., Fluid-particle reactions, in Chemical Reaction Engineering, 2nd ed., Wiley Interscience, Singapore, 1995.

**[148]** Eroğlu, İ., Tabanoğlu, A., Gündüz, U., Eroğlu, E., Yücel, M., Int. J. Hydrogen Energ., 33, 2, 2008.

**[149]** Hutchings, G. J., Hudson, I. D., Timms, D. G., J. Chem. Soc. Chem. Comm., 23, 1994.

**[150]** Vasovic, D. D., Stojakovic, D. R., Zec, S. P., Mat. Res. Bull., 32, 6, 1997.

**[151]** Schueller, K. H., Ber. Deu. Keram. Ges., 44, 6, 1967.

**[152]** Croop, E. J. and Vondracek, C.H., Westinghouse Electric Corp. Pat:Fr., 1965.

**[153]** Kumta, P. N. and Sriram, M. A., J. Mater. Sci., 28, 1993.

**[154]** Hsu, R., Kim, J. Y., Kumta, P.N., Feist, T. P., Chem. Mater., 8, 1996.

**[155]** Baykal. A., Kızılyalılı, M., Toprak, M., Kniep, R., Turk. J. Chem., 25, 2001.

**[156]** Palanichamy, K., Jin-Soo, P., Chang-Soo, K., J. Membrane Sci., 279, 2006.

**[157]** Achary, S. N. and Tyagi, A. K., J. Solid State Chem., 177, 2004.

**[158]** Xiao, J., Hu, Y., Yang, L., Cai, Y., Song, L., Chen, Z., Fan, W., Polym. Degrad. Stabil., 91, 2006.

**[159]** Kim, J., Loe, K., Lee, K., Bae, J., Yang, J., Hong, S., Polym. Degrad. Stab., 79, 2003.

**[160]** Laoutid, F., Ferry, L., Lopez-Cuesta, L. M., Crespy, A., Fire Mater., 30, 2005.

**[161]** Weil, E. and Levchik, S., J. Fire Sci., 22, 2004.

**[162]** Mouritz, A. P., Mathys, Z. B., Gibsin, A. G., Compos. Part A Appl. S., 37, 2006.

**[163]** Ning, Y. and Guo, S., J. Appl. Polym. Sci., 77, 2000.

**[164]** Ahoroni, S. M., Forbes, C. E., Hammond, W. B., Hindenlang, D. M., Mares, F., O'Brien, K., Sedgwick, R. D., J. Polym. Sci. Pol. Chem., 24, 1986.

**[165]** Chang, S., Shue, M. F., Chang, N. H., J. Polym. Sci. Pol. Chem., 20, 1986.

**[166]** Kang, Y. and Hay, N., Polymer, 43, 2002.

**[167]** Lee, D. and Shin, I., Polym. Composite, 33A, 2002.

**[168]** Lee, K., Kim, J., Bae, J., Yang, J., Hong, S., Kim, H. K., Polymer, 43, 2002.

**[169]** Yang, Y., Shi, X., Zhao, R., J. Fire Sci., 17, 1999.

**[170]** Levchik, S. V., Bright, D. A., Alessio, G. R., Dashevsky, S., Polym. Degrad. Stabil., 77, 2002.

**[171]** Adamczyk A., J. Mol. Struct., 614, 2002.

**[172]** Adamczyk, A. and Handke, M., J. Mol. Struct., 596, 2001.

**[173]** Adamczyk, A., Handke, M.; Mozgawa, W., J. Mol. Struct., 511, 1999.

**[174]** Du, X. H., Zhao, C. S., Wang, Y. Z., Zhou, Q., Deng, Y., Qu, M. H., Yang, B., Mater. Chem. Phys., 98, 2006.

**[175]** Zheng, J., Cui, P., Tian, X., Zheng, K., J. Appl. Polym. Sci., 104, 2007.

**[176]** Pawlowski, K. H. and Schartel, B., Polym. Int., 56, 2007.

**[177]** Kandare, E., Baljinder, K. K., Price, D., Nazare, S., Horrocks, A., Polym. Degrad. Stabil., 93, 11, 2008.

# APPENDIX A

# CHEMICAL ANALYSIS OF THE 3.5 HYDRATED ZINC BORATES

**Table A.1** Chemical analysis results of sample ZB1

| **Sample time (min)** | **ZnO in the sample (g)** | **EDTA used (ml)** | **ZnO in the sample %** | **$B_2O_3$ in the sample (g)** | **NaOH Used (ml)** | **$B_2O_3$ in the sample %** |
|---|---|---|---|---|---|---|
| 30 | 0.2025 | 41.26 | 82.9 | 0.2055 | 0.57 | 9.7 |
| 60 | 0.2015 | 23.41 | 47.3 | 0.2041 | 1.87 | 31.9 |
| 90 | 0.2077 | 20.14 | 39.5 | 0.2059 | 2.00 | 33.8 |
| 105 | 0.2041 | 19.45 | 38.8 | 0.2043 | 2.15 | 36.6 |
| 120 | 0.2082 | 19.80 | 38.7 | 0.2056 | 2.49 | 42.2 |
| 150 | 0.2036 | 19.15 | 38.3 | 0.2069 | 2.73 | 45.9 |
| 170 | 0.2074 | 19.44 | 38.1 | 0.2026 | 2.70 | 46.4 |
| 190 | 0.2050 | 19.55 | 38.8 | 0.2036 | 2.84 | 48.6 |
| 210 | 0.2042 | 18.95 | 37.8 | 0.2083 | 2.74 | 45.8 |
| 240 | 0.2030 | 19.09 | 38.3 | 0.2009 | 2.64 | 45.7 |
| 240 | 0.2049 | 21.30 | 42.3 | 0.2031 | 2.74 | 47.0 |

**Table A.2** Chemical analysis results of sample ZB2

| **Sample time (min)** | **ZnO in the sample (g)** | **EDTA used (ml)** | **ZnO in the sample %** | **$B_2O_3$ in the sample (g)** | **NaOH Used (ml)** | **$B_2O_3$ in the sample %** |
|---|---|---|---|---|---|---|
| 30 | 0.2039 | 47.48 | 94.8 | - | - | - |
| 39 | 0.2022 | 45.84 | 92.2 | - | - | - |
| 60 | 0.2016 | 40.14 | 81.0 | 0.2023 | 0.59 | 10.2 |
| 90 | 0.2034 | 30.21 | 60.4 | 0.2013 | 1.31 | 22.7 |
| 120 | 0.2099 | 25.17 | 48.8 | 0.2016 | 1.79 | 30.9 |
| 150 | 0.2028 | 21.53 | 43.2 | 0.2058 | 2.38 | 40.3 |
| 180 | 0.2052 | 20.5 | 40.7 | 0.2079 | 2.73 | 45.7 |
| 210 | 0.2099 | 19.85 | 38.5 | 0.206 | 2.76 | 46.6 |
| 240 | 0.2016 | 19.67 | 39.7 | 0.2009 | 2.69 | 46.6 |
| 270 | 0.2034 | 19.61 | 39.2 | 0.2015 | 2.62 | 45.3 |

**Table A.3** Chemical analysis results of sample ZB3

| **Sample time (min)** | **ZnO in the sample (g)** | **EDTA used (ml)** | **ZnO in the sample %** | **$B_2O_3$ in the sample (g)** | **NaOH Used (ml)** | **$B_2O_3$ in the sample %** |
|---|---|---|---|---|---|---|
| 30 | 0.2093 | 47.31 | 92.0 | 0.2035 | 0.34 | 5.8 |
| 60 | 0.2091 | 40.12 | 78.1 | 0.2020 | 0.83 | 14.3 |
| 90 | 0.2030 | 28.76 | 57.6 | 0.2072 | 1.66 | 27.9 |
| 120 | 0.2024 | 22.10 | 44.4 | 0.2008 | 1.91 | 33.1 |
| 150 | 0.2074 | 22.36 | 43.9 | 0.2046 | 2.51 | 42.7 |
| 180 | 0.2077 | 22.15 | 43.4 | 0.2050 | 2.75 | 46.7 |
| 210 | 0.2016 | 21.79 | 44.0 | 0.2044 | 2.83 | 48.2 |
| 240 | 0.2099 | 21.60 | 41.9 | 0.2043 | 2.72 | 46.3 |
| 270 | 0.2093 | 20.99 | 40.8 | 0.2019 | 2.66 | 45.9 |

**Table A.4** Chemical analysis results of sample ZB4

| Sample time (min) | ZnO in the sample (g) | EDTA used (ml) | ZnO in the sample % | $B_2O_3$ in the sample (g) | NaOH Used (ml) | $B_2O_3$ in the sample % |
|---|---|---|---|---|---|---|
| 30 | 0.2089 | 48.59 | 94.6 | 0.2007 | 0.21 | 3.6 |
| 60 | 0.2019 | 47.2 | 95.1 | 0.2013 | 0.18 | 3.1 |
| 90 | 0.2033 | 47.81 | 95.7 | 0.2062 | 0.22 | 3.7 |
| 120 | 0.2019 | 44.79 | 90.3 | 0.2020 | 0.40 | 6.9 |
| 150 | 0.2048 | 34.99 | 69.5 | 0.2013 | 1.29 | 22.3 |
| 180 | 0.2070 | 22.20 | 43.6 | 0.2094 | 2.65 | 44.1 |
| 210 | 0.2028 | 20.78 | 41.7 | 0.2073 | 2.76 | 46.3 |
| 240 | 0.2044 | 19.86 | 39.5 | 0.2039 | 2.85 | 48.7 |
| 260 | 0.2074 | 19.62 | 38.5 | 0.2061 | 2.79 | 47.1 |

**Table A.5** Chemical analysis results of sample ZB5

| Sample time (min) | ZnO in the sample (g) | EDTA used (ml) | ZnO in the sample % | $B_2O_3$ in the sample (g) | NaOH Used (ml) | $B_2O_3$ in the sample % |
|---|---|---|---|---|---|---|
| 30 | 0.2011 | 47.08 | 95.3 | 0.2045 | 0.23 | 3.9 |
| 60 | 0.2087 | 47.53 | 92.7 | 0.2008 | 0.28 | 4.9 |
| 90 | 0.2062 | 47.61 | 94.0 | 0.2045 | 0.17 | 2.9 |
| 120 | 0.2081 | 43.50 | 85.1 | 0.2028 | 0.60 | 10.3 |
| 150 | 0.2088 | 25.10 | 48.9 | 0.2005 | 2.49 | 43.2 |
| 180 | 0.2044 | 19.78 | 39.4 | 0.2045 | 2.79 | 47.5 |
| 210 | 0.2021 | 19.10 | 38.5 | 0.2049 | 2.85 | 48.4 |
| 240 | 0.2076 | 19.56 | 38.3 | 0.2086 | 2.78 | 46.4 |
| 280 | 0.2045 | 19.01 | 37.8 | 0.2046 | 2.78 | 47.3 |

**Table A.6** Chemical Analysis Results of Sample ZB6

| Sample time (min) | ZnO in the sample (g) | EDTA used (ml) | ZnO in the sample % | $B_2O_3$ in the sample (g) | NaOH used (ml) | $B_2O_3$ in the sample % |
|---|---|---|---|---|---|---|
| 30 | 0.2057 | 49.06 | 97.0 | 0.2006 | 0.28 | 4.9 |
| 60 | 0.2035 | 47.75 | 95.5 | 0.2089 | 0.22 | 3.7 |
| 90 | 0.2056 | 47.15 | 93.3 | 0.2038 | 0.83 | 14.2 |
| 120 | 0.2037 | 43.18 | 86.3 | 0.2004 | 0.95 | 16.5 |
| 150 | 0.2080 | 33.7 | 65.9 | 0.2005 | 2.8 | 48.6 |
| 180 | 0.2062 | 29.7 | 58.6 | 0.2064 | 3.16 | 53.3 |
| 210 | 0.2037 | 23.88 | 47.7 | 0.2089 | 3.21 | 53.5 |
| 240 | 0.2021 | 20.58 | 41.4 | 0.2061 | 2.94 | 49.7 |
| 260 | 0.2028 | 19.87 | 39.9 | 0.2025 | 2.66 | 45.7 |

**Table A.7** Chemical analysis results of sample ZB7

| Sample time (min) | ZnO in the sample (g) | EDTA used (ml) | ZnO in the sample % | $B_2O_3$ in the sample (g) | NaOH Used (ml) | $B_2O_3$ in the sample % |
|---|---|---|---|---|---|---|
| 30 | 0.2077 | 48.12 | 94.3 | 0.2015 | 0.28 | 4.8 |
| 60 | 0.210 | 48.07 | 93.1 | 0.2011 | 0.17 | 2.9 |
| 90 | 0.2042 | 35.57 | 70.9 | 0.2007 | 1.13 | 19.6 |
| 120 | 0.2045 | 22.91 | 45.6 | 0.2076 | 2.68 | 44.9 |
| 150 | 0.2024 | 19.70 | 39.6 | 0.2068 | 2.99 | 50.3 |
| 180 | 0.2020 | 19.33 | 38.9 | 0.2059 | 3.23 | 54.6 |
| 210 | 0.2017 | 18.81 | 37.9 | 0.2052 | 2.80 | 47.5 |
| 240 | 0.2059 | 20.98 | 41.5 | 0.2069 | 3.05 | 51.3 |
| 274 | 0.2067 | 19.99 | 39.4 | 0.2079 | 2.88 | 48.2 |

**Table A.8** Chemical analysis results of sample ZBP1

| Sample time (min) | ZnO in the sample (g) | EDTA used (ml) | ZnO in the sample % | $B_2O_3$ in the sample (g) | NaOH used (ml) | $B_2O_3$ in the sample % |
|---|---|---|---|---|---|---|
| 30 | 0.2065 | 49.14 | 96.8 | 0.2035 | 0.19 | 3.3 |
| 60 | 0.2072 | 48.4 | 95.0 | 0.203 | 0.22 | 3.8 |
| 90 | 0.2073 | 47.58 | 93.4 | 0.208 | 0.31 | 5.2 |
| 120 | 0.2066 | 43.78 | 86.2 | 0.2022 | 0.71 | 12.2 |
| 150 | 0.2073 | 27.43 | 53.8 | 0.2088 | 1.87 | 31.2 |
| 180 | 0.2005 | 20.62 | 41.8 | 0.2047 | 2.7 | 45.9 |
| 210 | 0.2052 | 20.12 | 39.9 | 0.2017 | 2.75 | 47.5 |
| 240 | 0.2027 | 19.24 | 38.6 | 0.2 | 2.76 | 48.0 |
| 250 | 0.2014 | 19.2 | 38.8 | 0.2028 | 2.7 | 46.3 |

**Table A.9** Chemical analysis results of sample ZBP2

| Sample time (min) | ZnO in the sample (g) | EDTA used (ml) | ZnO in the sample % | $B_2O_3$ in the sample (g) | NaOH used (ml) | $B_2O_3$ in the sample % |
|---|---|---|---|---|---|---|
| 30 | 0.2024 | 49.85 | 100.2 | 0.2045 | 0.2 | 3.4 |
| 60 | 0.2008 | 47.77 | 96.8 | 0.2078 | 0.2 | 3.4 |
| 90 | 0.2044 | 48.74 | 97.0 | 0.206 | 0.17 | 2.9 |
| 120 | 0.2082 | 44.89 | 87.7 | 0.2001 | 0.58 | 10.1 |
| 150 | 0.2085 | 30.72 | 60.0 | 0.2034 | 1.42 | 24.3 |
| 180 | 0.2025 | 22.74 | 45.7 | 0.2006 | 2.45 | 42.5 |
| 210 | 0.2021 | 21.38 | 43.0 | 0.2007 | 2.25 | 39.0 |
| 240 | 0.2045 | 18.7 | 37.2 | 0.2043 | 2.45 | 41.7 |
| 270 | 0.2006 | 18.87 | 38.3 | 0.2075 | 2.26 | 37.9 |
| 300 | 0.2061 | 20.14 | 39.8 | 0.208 | 2.45 | 41.0 |
| 330 | 0.2059 | 20.75 | 41.0 | 0.2047 | 2.5 | 42.5 |
| 370 | 0.205 | 20.04 | 39.8 | 0.2075 | 2.55 | 42.8 |

**Table A.10** Chemical analysis results of sample ZBP3

| Sample time (min) | ZnO in the sample (g) | EDTA used (ml) | ZnO in the sample % | $B_2O_3$ in the sample (g) | NaOH used (ml) | $B_2O_3$ in the sample % |
|---|---|---|---|---|---|---|
| 30 | 0.2039 | 56.1 | 99.0 | 0.208 | 0.22 | 3.7 |
| 60 | 0.2079 | 48.86 | 95.6 | 0.2079 | 0.26 | 4.4 |
| 90 | 0.2024 | 40.55 | 81.5 | 0.2008 | 0.81 | 14.0 |
| 120 | 0.2006 | 29.06 | 58.9 | 0.2053 | 1.78 | 30.2 |
| 150 | 0.2060 | 21.14 | 41.8 | 0.2021 | 2.69 | 46.3 |
| 180 | 0.2028 | 19.78 | 39.7 | 0.2038 | 2.53 | 43.2 |
| 210 | 0.2018 | 19.47 | 39.3 | 0.2036 | 2.65 | 45.3 |
| 240 | 0.2035 | 19.69 | 39.4 | 0.2023 | 2.75 | 47.3 |
| 270 | 0.2021 | 19.69 | 39.6 | 0.2072 | 2.78 | 46.7 |
| 300 | 0.2046 | 19.33 | 38.4 | 0.202 | 2.77 | 47.7 |

**Table A.11** Chemical analysis results of sample ZBP4

| Sample time (min) | ZnO in the sample (g) | EDTA used (ml) | ZnO in the sample % | $B_2O_3$ in the sample (g) | NaOH used (ml) | $B_2O_3$ in the sample % |
|---|---|---|---|---|---|---|
| 30 | 0.2019 | 51.93 | 100.0 | 0.2032 | 0.29 | 5.0 |
| 60 | 0.2028 | 44.13 | 88.5 | 0.2031 | 0.45 | 7.7 |
| 90 | 0.2039 | 27.92 | 55.7 | 0.2053 | 1.84 | 31.2 |
| 120 | 0.2042 | 22.12 | 44.1 | 0.2005 | 2.54 | 44.1 |
| 150 | 0.2000 | 20.32 | 41.3 | 0.2017 | 2.69 | 46.4 |
| 180 | 0.2006 | 18.02 | 36.6 | 0.2063 | 2.8 | 47.2 |
| 210 | 0.2054 | 17.95 | 35.6 | 0.2003 | 2.74 | 47.6 |
| 240 | 0.2047 | 18.71 | 37.2 | 0.2038 | 2.89 | 49.4 |
| 270 | 0.2006 | 18.46 | 37.4 | 0.2031 | 2.79 | 47.8 |
| 300 | 0.2022 | 19.42 | 39.1 | 0.2078 | 2.81 | 47.1 |

**Table A.12** Chemical analysis results of sample ZBP5

| Sample time (min) | ZnO in the sample (g) | EDTA used (ml) | ZnO in the sample % | $B_2O_3$ in the sample (g) | NaOH used (ml) | $B_2O_3$ in the sample % |
|---|---|---|---|---|---|---|
| 30 | 0.2043 | 51 | 101.6 | 0.2086 | 0.21 | 3.5 |
| 60 | 0.2089 | 48.2 | 93.9 | 0.2044 | 0.23 | 3.9 |
| 90 | 0.2001 | 47.92 | 97.4 | 0.2058 | 0.38 | 6.4 |
| 120 | 0.2089 | 40.94 | 79.7 | 0.2075 | 0.64 | 10.7 |
| 150 | 0.2070 | 35.31 | 69.4 | 0.2029 | 0.82 | 14.1 |
| 180 | 0.2008 | 29.95 | 60.7 | 0.2058 | 1.66 | 28.1 |
| 210 | 0.2012 | 27.41 | 55.4 | 0.202 | 2.08 | 35.8 |
| 240 | 0.2029 | 25.89 | 51.9 | 0.2007 | 2.2 | 38.2 |
| 270 | 0.2008 | 21.01 | 42.6 | 0.2031 | 2.21 | 37.9 |
| 300 | 0.2046 | 20.77 | 41.3 | 0.2001 | 2.18 | 37.9 |
| 320 | 0.2067 | 21.12 | 41.6 | 0.2045 | 2.5 | 42.6 |
| 320 | 0.2076 | 21.430 | 42.0 | 0.2087 | 2.58 | 43.0 |

**Table A.13** Chemical analysis results of sample ZBP6

| Sample time (min) | ZnO in the sample (g) | EDTA used (ml) | ZnO in the sample % | $B_2O_3$ in the sample (g) | NaOH used (ml) | $B_2O_3$ in the sample % |
|---|---|---|---|---|---|---|
| 30 | 0.2037 | 59.82 | 100.0 | 0.2059 | 0.41 | 6.9 |
| 60 | 0.2065 | 59.41 | 100.0 | 0.2041 | 0.27 | 4.6 |
| 90 | 0.2025 | 55.21 | 100.0 | 0.2008 | 0.42 | 7.3 |
| 120 | 0.2022 | 40.04 | 80.6 | 0.2059 | 0.7 | 11.8 |
| 150 | 0.2060 | 37.31 | 73.7 | 0.2098 | 1.43 | 23.7 |
| 180 | 0.205 | 46.71 | 92.7 | 0.2053 | 2.05 | 34.8 |
| 210 | 0.2036 | 48.58 | 97.1 | 0.2045 | 2.44 | 41.5 |
| 240 | 0.2059 | 50.15 | 99.1 | 0.2094 | 2.48 | 41.2 |
| 270 | 0.2039 | 53.71 | 94.2 | 0.2047 | 2.07 | 35.2 |
| 300 | 0.2067 | 33.75 | 66.4 | 0.2022 | 2.12 | 36.5 |

# APPENDIX B

# ESTIMATED and OBTAINED PRODUCTION AMOUNTS of ZINC BORATE

**Table B.1** Estimated and obtained production amounts of zinc borate in laboratory scale

| Sample | Estimated Zinc Borate Production (kg) | Realized Zinc Borate Production (kg) |
|---|---|---|
| ZB1 | 0.566 | 0.454 |
| ZB2 | 0.566 | 0.408 |
| ZB3 | 0.566 | 0.415 |
| ZB4 | 0.566 | 0.464 |
| ZB5 | 0.566 | 0.459 |
| ZB6 | 0.566 | 0.423 |
| ZB7 | 0.566 | 0.447 |

**Table B.2** Estimated and obtained production amounts of zinc borate in pilot scale

| Sample | Estimated Zinc Borate Production (kg) | Realized Zinc Borate Production (kg) |
|---|---|---|
| ZBP1 | 17.55 | 14.04 |
| ZBP2 | 17.55 | 13.16 |
| ZBP3 | 17.55 | 13.56 |
| ZBP4 | 17.55 | 13.80 |
| ZBP5 | 17.55 | 13.23 |
| ZBP6 | 17.55 | 13.92 |

# APPENDIX C

## TGA RESULTS of THE 3.5 HYDRATED ZINC BORATES

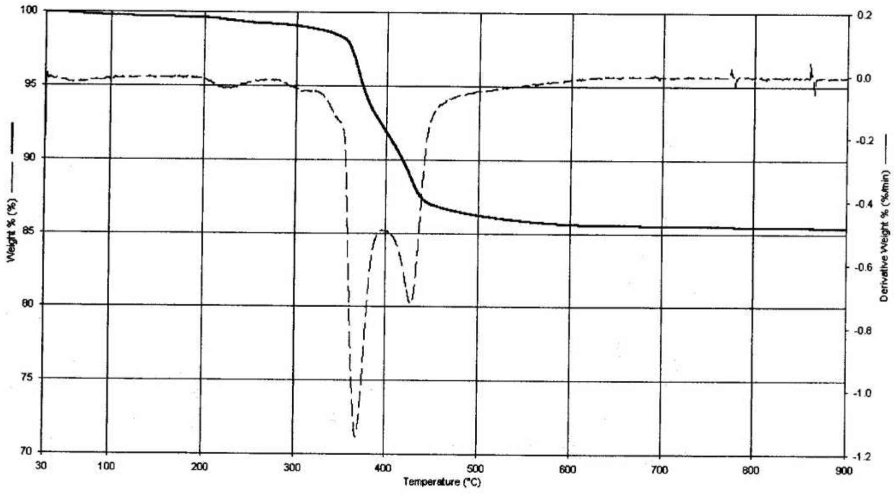

**Figure C.1** TGA thermogram of Firebrake ZB 3.5 hydrated zinc borate

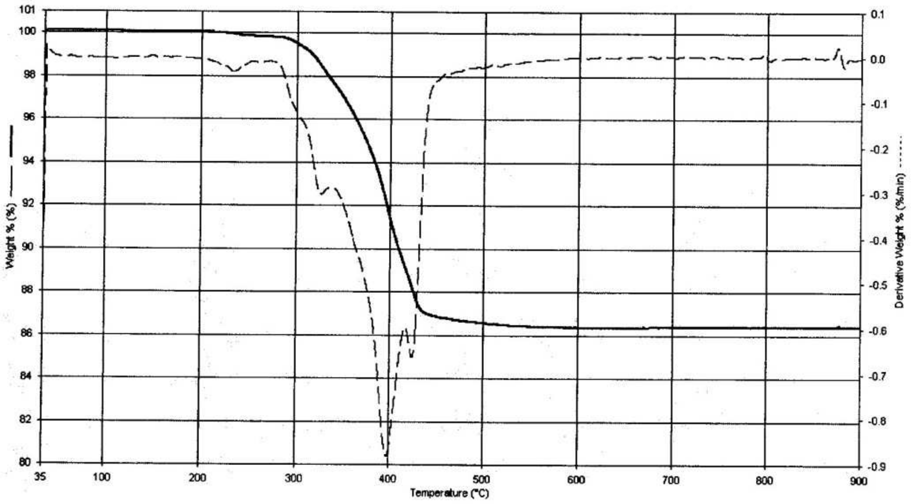

**Figure C.2** TGA thermogram of ZBP1 zinc borate (zinc borate used in flame retardant composite production)

# APPENDIX D

# XRD RESULTS of THE 3.5 HYDRATED ZINC BORATES

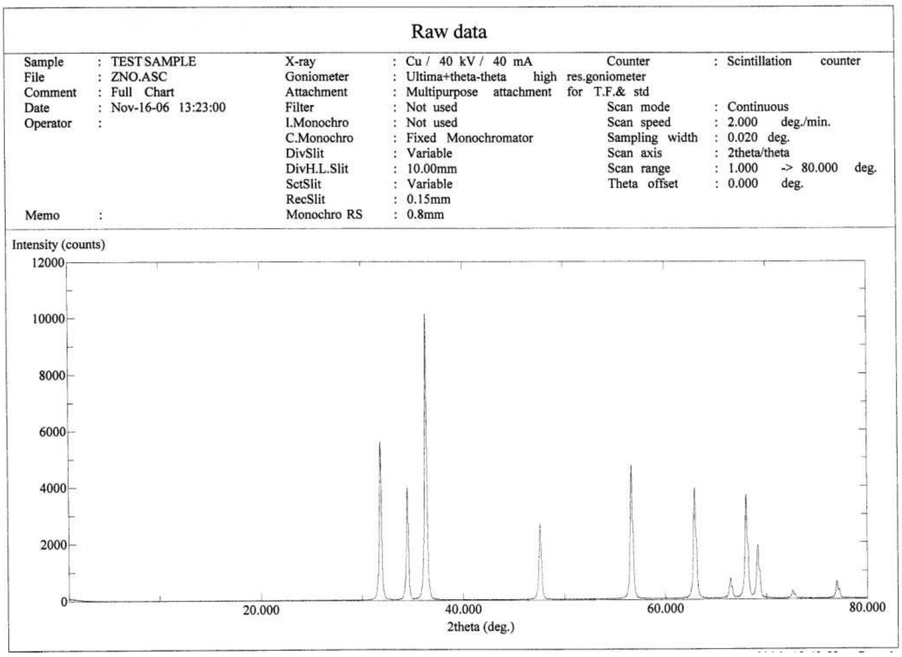

```
                                              Raw data
Sample     : TEST SAMPLE          X-ray        : Cu /  40 kV /  40 mA           Counter         : Scintillation    counter
File       : ZNO.ASC              Goniometer   : Ultima+theta-theta    high  res.goniometer
Comment    : Full   Chart         Attachment   : Multipurpose   attachment   for  T.F.&  std
Date       : Nov-16-06  13:23:00  Filter       : Not  used                      Scan  mode      : Continuous
Operator   :                      I.Monochro   : Not  used                      Scan  speed     : 2.000    deg./min.
                                  C.Monochro   : Fixed  Monochromator           Sampling  width : 0.020  deg.
                                  DivSlit      : Variable                       Scan  axis      : 2theta/theta
                                  DivH.L.Slit  : 10.00mm                        Scan  range     : 1.000    -> 80.000    deg.
                                  SctSlit      : Variable                       Theta  offset   : 0.000    deg.
                                  RecSlit      : 0.15mm
Memo       :                      Monochro RS  : 0.8mm
```

**Figure D.1** XRD plot of 25 μm average particle sized zinc oxide

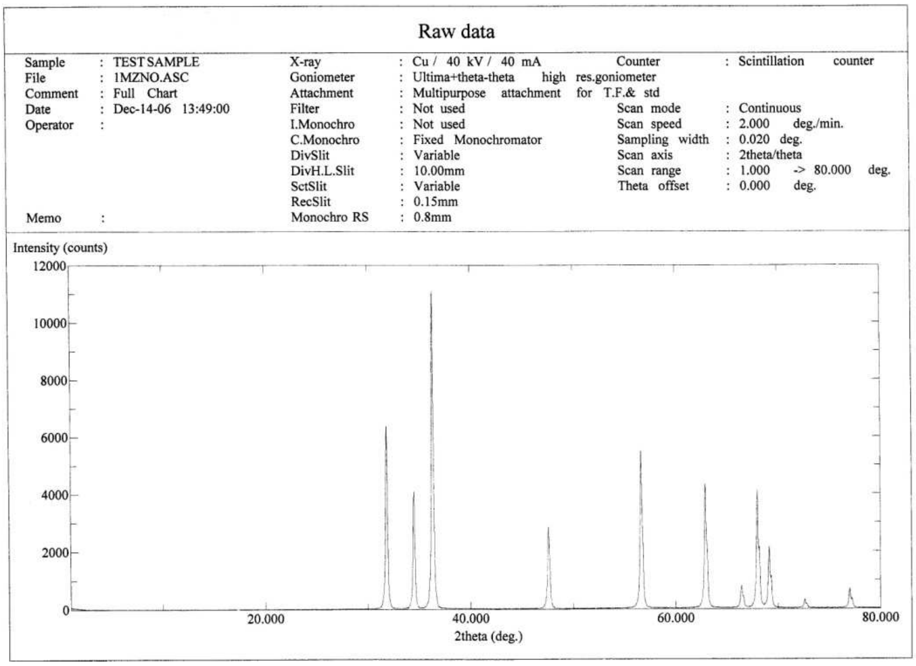
Raw data

Sample : TEST SAMPLE
File : 1MZNO.ASC
Comment : Full Chart
Date : Dec-14-06 13:49:00
Operator :
Memo :

X-ray : Cu / 40 kV / 40 mA
Goniometer : Ultima+theta-theta high res.goniometer
Attachment : Multipurpose attachment for T.F.& std
Filter : Not used
I.Monochro : Not used
C.Monochro : Fixed Monochromator
DivSlit : Variable
DivH.L.Slit : 10.00mm
SctSlit : Variable
RecSlit : 0.15mm
Monochro RS : 0.8mm

Counter : Scintillation counter
Scan mode : Continuous
Scan speed : 2.000 deg./min.
Sampling width : 0.020 deg.
Scan axis : 2theta/theta
Scan range : 1.000 -> 80.000 deg.
Theta offset : 0.000 deg.

**Figure D.2** XRD plot of < 1 μm average particle sized zinc oxide

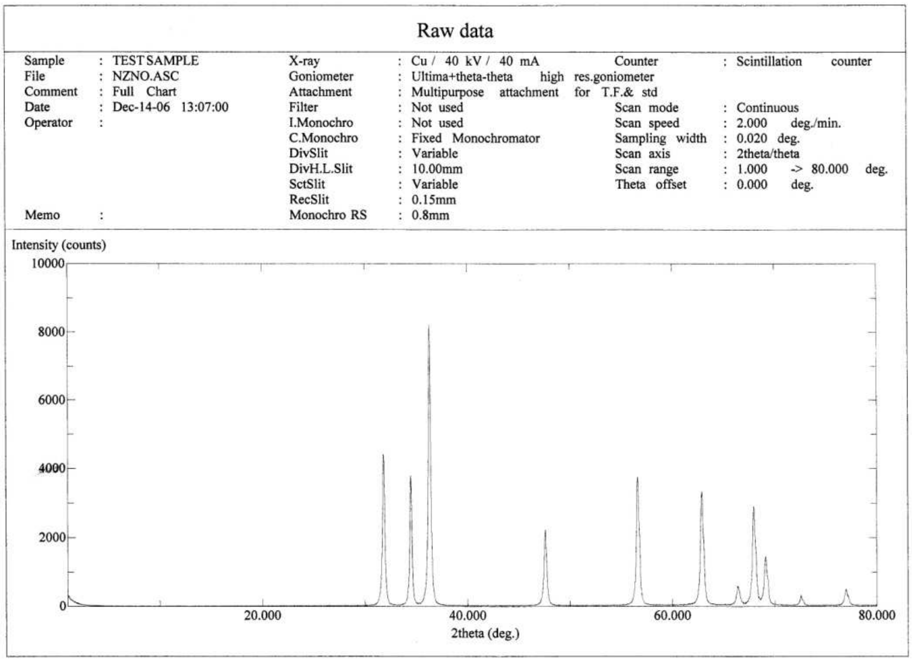
Raw data

Sample : TEST SAMPLE
File : NZNO.ASC
Comment : Full Chart
Date : Dec-14-06 13:07:00
Operator :
Memo :

X-ray : Cu / 40 kV / 40 mA
Goniometer : Ultima+theta-theta high res.goniometer
Attachment : Multipurpose attachment for T.F.& std
Filter : Not used
I.Monochro : Not used
C.Monochro : Fixed Monochromator
DivSlit : Variable
DivH.L.Slit : 10.00mm
SctSlit : Variable
RecSlit : 0.15mm
Monochro RS : 0.8mm

Counter : Scintillation counter
Scan mode : Continuous
Scan speed : 2.000 deg./min.
Sampling width : 0.020 deg.
Scan axis : 2theta/theta
Scan range : 1.000 -> 80.000 deg.
Theta offset : 0.000 deg.

**Figure D.3** XRD plot of 50-70 nm average particle sized zinc oxide

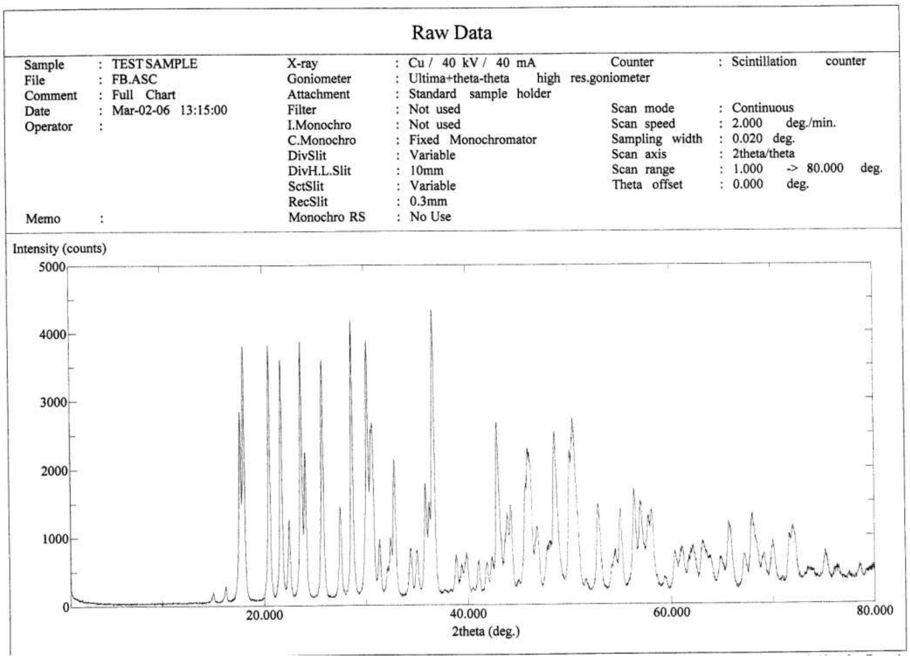
Raw Data

Sample : TEST SAMPLE
File : FB.ASC
Comment : Full Chart
Date : Mar-02-06 13:15:00
Operator :
Memo :
X-ray : Cu / 40 kV / 40 mA
Goniometer : Ultima+theta-theta high res.goniometer
Attachment : Standard sample holder
Filter : Not used
I.Monochro : Not used
C.Monochro : Fixed Monochromator
DivSlit : Variable
DivH.L.Slit : 10mm
SctSlit : Variable
RecSlit : 0.3mm
Monochro RS : No Use
Counter : Scintillation counter
Scan mode : Continuous
Scan speed : 2.000 deg./min.
Sampling width : 0.020 deg.
Scan axis : 2theta/theta
Scan range : 1.000 -> 80.000 deg.
Theta offset : 0.000 deg.

**Figure D.4** XRD plot of commercial 3.5 hydrated zinc borate Firebrake ZB

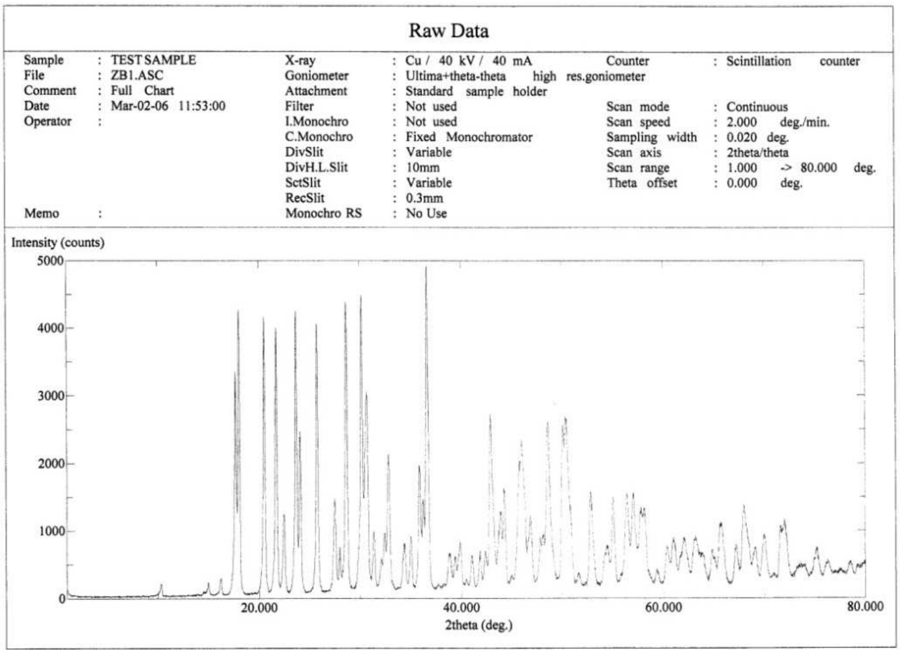
Raw Data

Sample : TEST SAMPLE
File : ZB1.ASC
Comment : Full Chart
Date : Mar-02-06 11:53:00
Operator :
Memo :
X-ray : Cu / 40 kV / 40 mA
Goniometer : Ultima+theta-theta high res.goniometer
Attachment : Standard sample holder
Filter : Not used
I.Monochro : Not used
C.Monochro : Fixed Monochromator
DivSlit : Variable
DivH.L.Slit : 10mm
SctSlit : Variable
RecSlit : 0.3mm
Monochro RS : No Use
Counter : Scintillation counter
Scan mode : Continuous
Scan speed : 2.000 deg./min.
Sampling width : 0.020 deg.
Scan axis : 2theta/theta
Scan range : 1.000 -> 80.000 deg.
Theta offset : 0.000 deg.

**Figure D.5** XRD plot of ZBP1 zinc borate, used in flame retardant composite production

# APPENDIX E

# BET RESULTS of THE 3.5 HYDRATED ZINC BORATES and MICROWAVE TECHNIQUE PRODUCED BORON PHOSPHATE

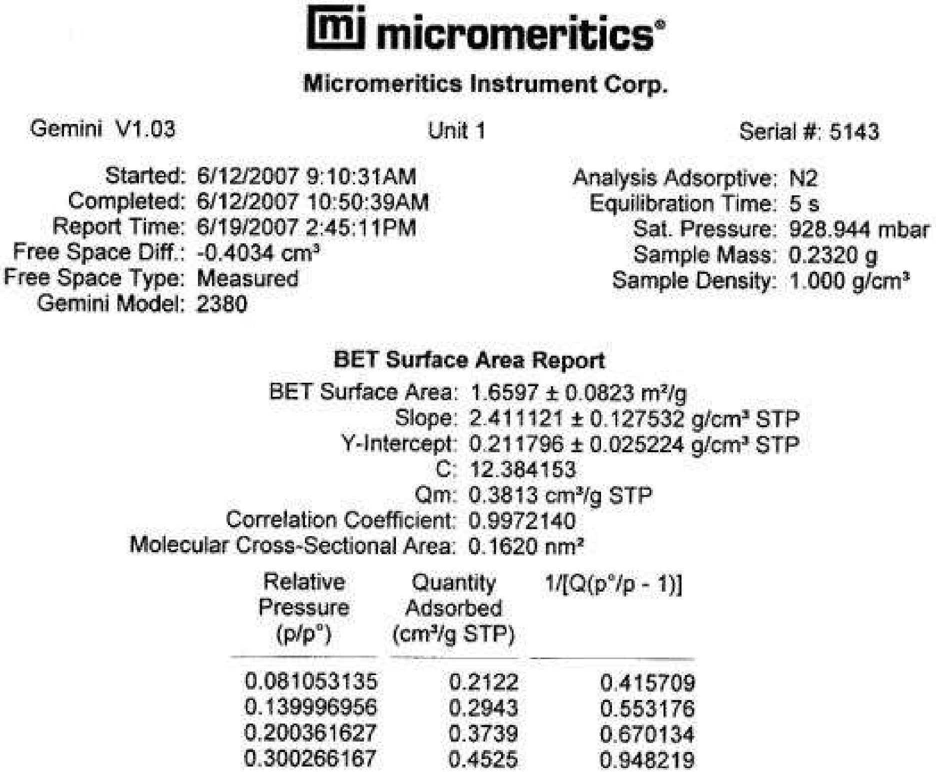

micromeritics®

Micromeritics Instrument Corp.

Gemini V1.03 Unit 1 Serial #: 5143

Started: 6/12/2007 9:10:31AM
Completed: 6/12/2007 10:50:39AM
Report Time: 6/19/2007 2:45:11PM
Free Space Diff.: -0.4034 $cm^3$
Free Space Type: Measured
Gemini Model: 2380

Analysis Adsorptive: N2
Equilibration Time: 5 s
Sat. Pressure: 928.944 mbar
Sample Mass: 0.2320 g
Sample Density: 1.000 $g/cm^3$

**BET Surface Area Report**

BET Surface Area: 1.6597 ± 0.0823 $m^2/g$
Slope: 2.411121 ± 0.127532 $g/cm^3$ STP
Y-Intercept: 0.211796 ± 0.025224 $g/cm^3$ STP
C: 12.384153
Qm: 0.3813 $cm^3/g$ STP
Correlation Coefficient: 0.9972140
Molecular Cross-Sectional Area: 0.1620 $nm^2$

| Relative Pressure ($p/p^\circ$) | Quantity Adsorbed ($cm^3/g$ STP) | $1/[Q(p^\circ/p - 1)]$ |
|---|---|---|
| 0.081053135 | 0.2122 | 0.415709 |
| 0.139996956 | 0.2943 | 0.553176 |
| 0.200361627 | 0.3739 | 0.670134 |
| 0.300266167 | 0.4525 | 0.948219 |

**Figure E.1** BET analysis report of 3.5 hydrated zinc borate sample ZBP1

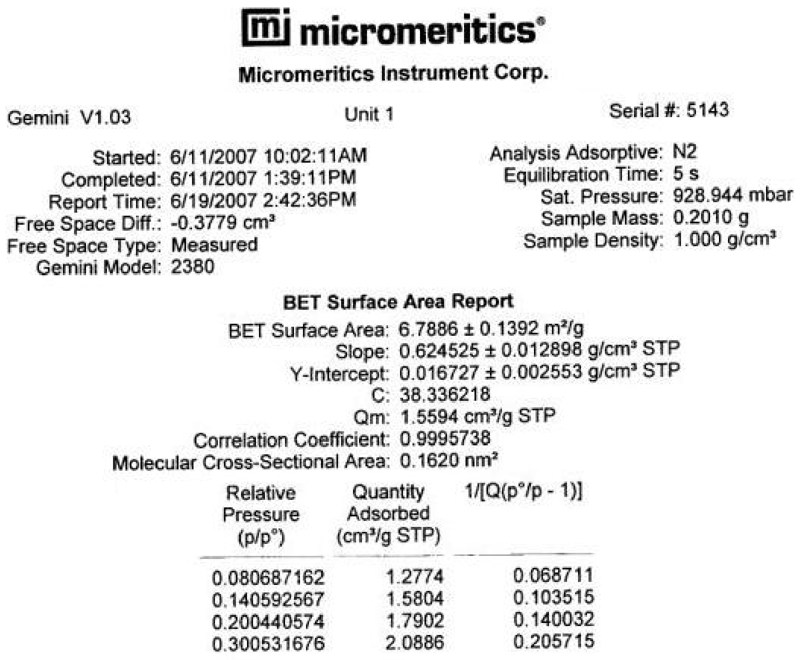

**micromeritics®**

**Micromeritics Instrument Corp.**

Gemini V1.03 Unit 1 Serial #: 5143

Started: 6/11/2007 10:02:11AM
Completed: 6/11/2007 1:39:11PM
Report Time: 6/19/2007 2:42:36PM
Free Space Diff.: -0.3779 cm³
Free Space Type: Measured
Gemini Model: 2380

Analysis Adsorptive: N2
Equilibration Time: 5 s
Sat. Pressure: 928.944 mbar
Sample Mass: 0.2010 g
Sample Density: 1.000 g/cm³

**BET Surface Area Report**

BET Surface Area: 6.7886 ± 0.1392 m²/g
Slope: 0.624525 ± 0.012898 g/cm³ STP
Y-Intercept: 0.016727 ± 0.002553 g/cm³ STP
C: 38.336218
Qm: 1.5594 cm³/g STP
Correlation Coefficient: 0.9995738
Molecular Cross-Sectional Area: 0.1620 nm²

| Relative Pressure (p/p°) | Quantity Adsorbed (cm³/g STP) | 1/[Q(p°/p - 1)] |
|---|---|---|
| 0.080687162 | 1.2774 | 0.068711 |
| 0.140592567 | 1.5804 | 0.103515 |
| 0.200440574 | 1.7902 | 0.140032 |
| 0.300531676 | 2.0886 | 0.205715 |

**Figure E.2** BET analysis report of 3.5 hydrated zinc borate ZB7

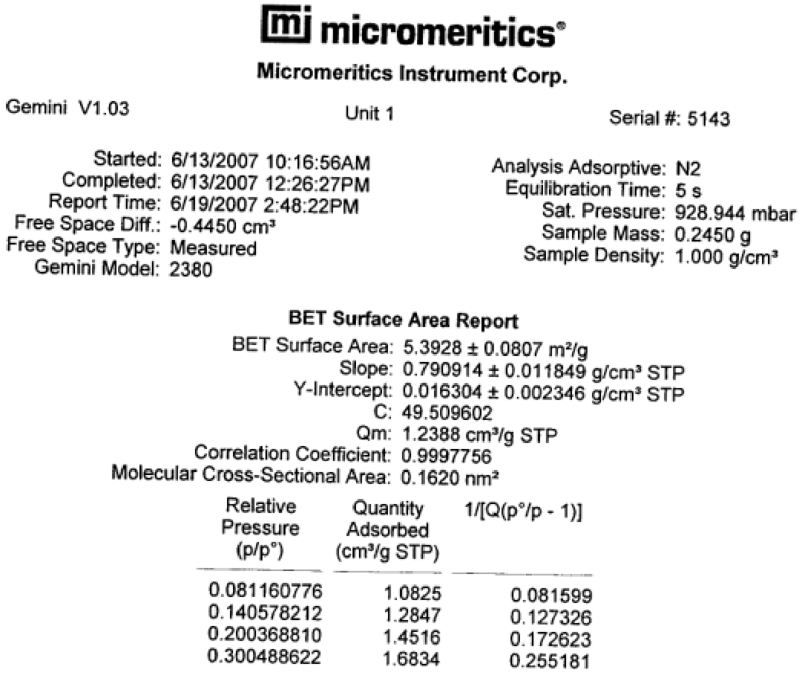

**micromeritics®**

**Micromeritics Instrument Corp.**

Gemini V1.03 Unit 1 Serial #: 5143

Started: 6/13/2007 10:16:56AM
Completed: 6/13/2007 12:26:27PM
Report Time: 6/19/2007 2:48:22PM
Free Space Diff.: -0.4450 cm³
Free Space Type: Measured
Gemini Model: 2380

Analysis Adsorptive: N2
Equilibration Time: 5 s
Sat. Pressure: 928.944 mbar
Sample Mass: 0.2450 g
Sample Density: 1.000 g/cm³

**BET Surface Area Report**

BET Surface Area: 5.3928 ± 0.0807 m²/g
Slope: 0.790914 ± 0.011849 g/cm³ STP
Y-Intercept: 0.016304 ± 0.002346 g/cm³ STP
C: 49.509602
Qm: 1.2388 cm³/g STP
Correlation Coefficient: 0.9997756
Molecular Cross-Sectional Area: 0.1620 nm²

| Relative Pressure (p/p°) | Quantity Adsorbed (cm³/g STP) | 1/[Q(p°/p - 1)] |
|---|---|---|
| 0.081160776 | 1.0825 | 0.081599 |
| 0.140578212 | 1.2847 | 0.127326 |
| 0.200368810 | 1.4516 | 0.172623 |
| 0.300488622 | 1.6834 | 0.255181 |

**Figure E.3** BET analysis report of microwave technique produced boron phosphate

# APPENDIX F

# SAMPLE CONVERSION CALCULATION for the SUGGESTED KINETIC MODEL for THE 3.5 HYDRATED ZINC BORATES

A sample calculation for the logistic model for the zinc borate produced at the reaction conditions of 580 rpm stirring rate, with the presence of baffle, seed amount of 1.5%, $B_2O_3$:ZnO mole ratio of 5:1 (ZB3) were given below as sample calculation.

The crystal growth of zinc borate from the reaction of zinc oxide and boric acid can be modeled by adopting the logistic model, which has been used for growth in biological system [149]. In contrast to the biological system, the extent of reaction in crystallization is limited to the complete conversion of reactant to the product. Data for the conversion of zinc oxide versus time was fit to the logistic model. In this model, the rate law is given by Equation F.1 where the rate of crystal growth for zinc borate

$$\text{rate} = \frac{dX}{dt} = k\left(1 - \frac{X}{X^*}\right)X \tag{F.1}$$

in M/min is equal to dX/dt in the case of batch reactor, X is the zinc borate concentration (M) in the slurry reactor, X* is the maximum zinc borate concentration (M), k is the specific growth rate (1/min). When X is equal to the X* the crystal growth rate is zero. The integrated form of the rate law is where $X_0$ is the critical initial

$$X = \frac{X^*}{1 + (\frac{X^*}{X_o} - 1)e^{-kt}} \tag{F.2}$$

concentration of zinc borate. Using the normalized concentrations ($\chi$ = X/X* and $\chi_o$= $X_o$/X*) will reduce the number of parameters to two, k and $\chi_o$ in the integrated form of rate equation:

$$\chi = \frac{1}{1+(\frac{1}{\chi_o}-1)e^{-kt}} \tag{F.3}$$

This equation can be rearranged into linear form:

$$\ln\left(\frac{1}{\chi}-1\right) = -kt+\ln\left(\frac{1}{\chi_o}-1\right) \tag{F.4}$$

Either using the curve fitting software, Microsoft Excel, the experimental data were fit to the integrated rate law (Eq. F.3) or the linear regression of the data with Equation F.4, the values of two model parameters k and $\chi_o$ were obtained. It is worth to mention that the normalized concentration is nothing else the conversion of zinc oxide since the X* is the maximum concentration of zinc borate at complete conversion. $X_o$ values are related to the seed concentration, added to the solution at the beginning of reaction. Since zinc borate is initially added as seed to the solution, the initial normalized concentration $\chi_o$ are nonzero in all experiments but smaller than the experimental value $\chi_o$(exp) = 0.0213.

For the sample calculation, first of all amount of ZnO and $B_2O_3$ in the samples were determined by using the results of chemical analysis which were performed for the ZB3 sample. Results were summarized in Table F.1

**Table F.1** Conversion calculations for ZB3 zinc borate sample based on ZnO consumption

| Sample Time (min.) | Amount of ZnO in the sample (g) | Amount of $B_2O_3$ in the sample (g) | Consumed ZnO amount (g) | Conversion |
|---|---|---|---|---|
| 30 | 0.19250439 | 0.011835 | 0.010986 | 0.05707 |
| 60 | 0.16324828 | 0.028892 | 0.026819 | 0.164287 |
| 90 | 0.11702444 | 0.057785 | 0.053639 | 0.458357 |
| 120 | 0.0899249 | 0.066487 | 0.061717 | 0.686319 |
| 150 | 0.09098284 | 0.087373 | 0.081105 | 0.891429 |
| 180 | 0.09012835 | 0.095728 | 0.08886 | 0.985925 |
| 210 | 0.08866351 | 0.098512 | 0.091445 | 1.031369 |
| 240 | 0.0878904 | 0.094683 | 0.08789 | 1 |

For the determination of consumed ZnO, a constant was needed to be calculated which was found as the ratio of the $B_2O_3$ content to ZnO content at the final product which was at 240 minutes. For the ZB3 sample it was 1.0772. Thus the consumed ZnO amounts were calculated dividing the final ZnO amounts at the samples by this constant. Finally ZnO conversion was calculated dividing the consumed ZnO amounts to the ZnO amounts in the samples for each time interval.

After that the left part of the Equation F.4 was calculated for ZB3 sample as the linear column in Table F.2. $\chi_o = X_o/X^*$, was calculated as 0.0134 for this case.

**Table F.2** Data used to calculate conversion from the logistic model

| Sample Time (min.) | X Calculated | Linear | X Model |
|---|---|---|---|
| 30 | 0.057 | 2.806015 | 0.0495 |
| 60 | 0.164 | 1.628762 | 0.166448 |
| 90 | 0.458 | 0.168397 | 0.433641 |
| 120 | 0.686 | -0.78148 | 0.745924 |
| 150 | 0.891 | -2.101 | 0.918414 |
| 180 | 0.985 | -4.18459 | 0.977357 |

k was needed for the calculation of conversion from the model. Thus time vs. linear graph was drawn as in Figure F.1, the slope of which was the k value.

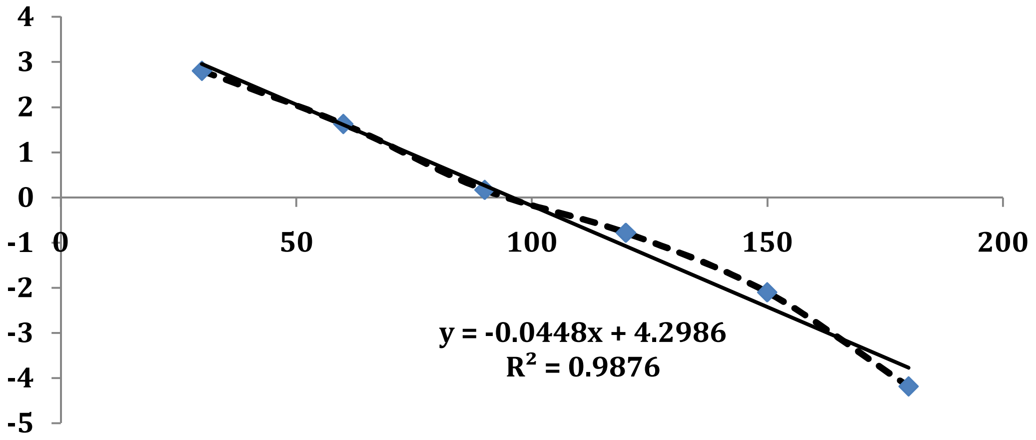

**Figure F.1** Time vs. linear graph for the determination of k and $R^2$

After calculating all the unknowns in Equation F.2, conversion from the model can be calculated and comparison graphs for the conversion calculated from experimental data and conversion from the logistic model were drawn and the degree of fit of the model to the experimental data was discussed previously in the results and discussion part of the thesis.

# APPENDIX G

# XRD RESULTS of THE BORON PHOSPHATES

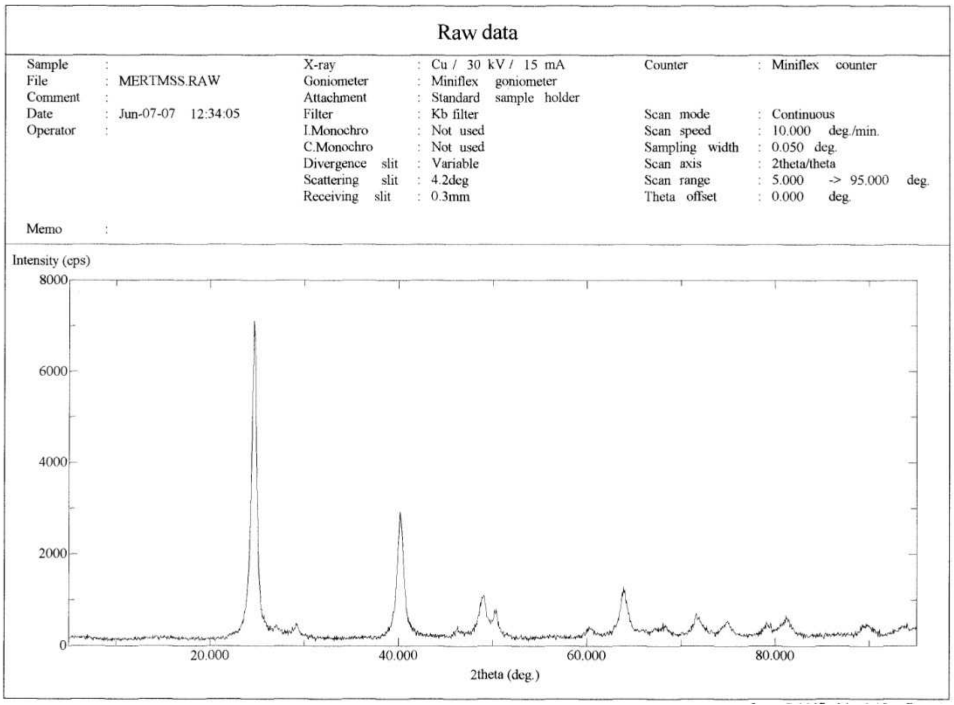

Raw data

Sample :
File : MERTMSS.RAW
Comment :
Date : Jun-07-07 12:34:05
Operator :

X-ray : Cu / 30 kV / 15 mA
Goniometer : Miniflex goniometer
Attachment : Standard sample holder
Filter : Kb filter
I.Monochro : Not used
C.Monochro : Not used
Divergence slit : Variable
Scattering slit : 4.2deg
Receiving slit : 0.3mm

Counter : Miniflex counter
Scan mode : Continuous
Scan speed : 10.000 deg./min.
Sampling width : 0.050 deg.
Scan axis : 2theta/theta
Scan range : 5.000 -> 95.000 deg.
Theta offset : 0.000 deg.

Memo :

**Figure G.1** XRD plot of microwave technique produced boron phosphate

# APPENDIX H

# MECHANICAL TEST RESULTS of FLAME RETARDANT COMPOSITES

**Table H.1** Tensile strength data for first stage FR composites

| Composite | Tensile Strength (MPa) | Stand. Dev. |
|---|---|---|
| Neat Recycled PET | 52.3 | 2.2 |
| PET1 | 48.4 | 3.8 |
| PET2 | 25.6 | 2.0 |
| PET3 | 17.8 | 3.7 |
| PET4 | 43.1 | 3.8 |
| PET5 | 17.8 | 2.2 |
| PET6 | 53.9 | 0.9 |
| PET7 | 60.3 | 1.5 |
| PET8 | 58.4 | 1.8 |
| PET9 | 54.5 | 2.3 |
| PET10 | 43.9 | 3.2 |
| PET11 | 63.4 | 3.8 |
| PET12 | 59.9 | 1.4 |

**Table H.2** Tensile strength data for second stage FR composites

| Composite | Tensile Strength (MPa) | Stand. Dev. |
|---|---|---|
| Neat Crystalline PET | 55.1 | 1.8 |
| PT1 | 59.3 | 3.8 |
| PT2 | 45.6 | 2.0 |
| PT3 | 26.0 | 3.7 |
| PT4 | 49.4 | 3.8 |
| PT5 | 11.4 | 2.2 |
| PT6 | 58.1 | 0.9 |
| PT7 | 48.4 | 1.3 |
| PT8 | 60.1 | 1.7 |
| PT9 | 51.4 | 2.6 |
| PT10 | 43.1 | 1.9 |
| PT11 | 28.2 | 2.1 |
| PT12 | 53.9 | 0.9 |
| PT13 | 31.7 | 0.7 |

**Table H.3** Tensile modulus data for first stage FR composites

| Composite | Tensile Modulus (MPa) | Stand. Dev. |
|---|---|---|
| Neat Recycled PET | 1303 | 62.8 |
| PET1 | 891 | 16.9 |
| PET2 | 1048 | 32.3 |
| PET3 | 2354 | 35.1 |
| PET4 | 1316 | 58.5 |
| PET5 | 1090 | 89.2 |
| PET6 | 1644 | 17.9 |
| PET7 | 1444 | 76.3 |
| PET8 | 1378 | 44.7 |
| PET9 | 1224 | 67.4 |
| PET10 | 1676 | 95.4 |
| PET11 | 1425 | 56.7 |
| PET12 | 1316 | 71.3 |

**Table H.4** Tensile modulus data for second stage FR composites

| Composite | Tensile Modulus (MPa) | Stand. Dev. |
|---|---|---|
| Neat Crystalline PET | 1522 | 54.7 |
| PT1 | 1134 | 105.9 |
| PT2 | 1867 | 69.3 |
| PT3 | 874 | 68.2 |
| PT4 | 1999 | 85.5 |
| PT5 | 474 | 32.5 |
| PT6 | 2372 | 47.9 |
| PT7 | 1901 | 79.8 |
| PT8 | 1048 | 32.2 |
| PT9 | 1762 | 114.1 |
| PT10 | 1367 | 75.5 |
| PT11 | 1432 | 45.2 |
| PT12 | 1644 | 17.9 |
| PT13 | 1728 | 96.3 |

**Table H.5** Elongation at break data for first stage FR composites

| Composite | Elongation at Break (%) | Stand. Dev. |
|---|---|---|
| Neat Recycled PET | 21.1 | 0.4 |
| PET1 | 23.2 | 0.3 |
| PET2 | 18.5 | 0.6 |
| PET3 | 20.4 | 0.8 |
| PET4 | 24.5 | 0.7 |
| PET5 | 26.3 | 0.6 |
| PET6 | 38.2 | 0.9 |
| PET7 | 34.1 | 1.1 |
| PET8 | 28.9 | 0.8 |
| PET9 | 26.2 | 0.5 |
| PET10 | 29.2 | 0.7 |
| PET11 | 340.4 | 14.3 |
| PET12 | 310.8 | 16.5 |

**Table H.6** Elongation at break data for second stage FR composites

| Composite | Elongation at Break (%) | Stand. Dev. |
|---|---|---|
| Neat Crystalline PET | 35.1 | 2.3 |
| PT1 | 110.3 | 9.2 |
| PT2 | 380.4 | 36.9 |
| PT3 | 392.4 | 41.7 |
| PT4 | 152.3 | 28.4 |
| PT5 | 104.9 | 19.2 |
| PT6 | 78.6 | 12.9 |
| PT7 | 54.3 | 13.1 |
| PT8 | 59.7 | 18.9 |
| PT9 | 77.3 | 15.4 |
| PT10 | 27.2 | 3.2 |
| PT11 | 18.9 | 2.8 |
| PT12 | 14.6 | 1.4 |
| PT13 | 20.2 | 4.9 |

**Table H.7** Impact strength data for first stage FR composites

| Composite | Impact Strength (kj/m$^2$) | Stand. Dev. |
|---|---|---|
| Neat Recycled PET | 11.92 | 0.57 |
| PET1 | 19.95 | 4.10 |
| PET2 | 24.38 | 1.42 |
| PET3 | 19.76 | 2.59 |
| PET4 | 20.18 | 0.87 |
| PET5 | 22.65 | 1.61 |
| PET6 | 20.31 | 2.37 |
| PET7 | 10.47 | 2.12 |
| PET8 | 7.39 | 1.34 |
| PET9 | 6.38 | 1.59 |
| PET10 | 5.73 | 0.64 |
| PET11 | 22.50 | 1.34 |
| PET12 | 18.40 | 0.96 |

**Table H.8** Impact strength data for second stage FR composites

| Composite | Impact Strength (kj/m$^2$) | Stand. Dev. |
|---|---|---|
| Neat Crystalline PET | 10.21 | 0.81 |
| PT1 | 14.30 | 1.23 |
| PT2 | 28.76 | 1.34 |
| PT3 | 9.64 | 0.92 |
| PT4 | 20.18 | 1.34 |
| PT5 | 5.90 | 0.32 |
| PT6 | 8.21 | 0.78 |
| PT7 | 3.41 | 0.23 |
| PT8 | 13.21 | 1.34 |
| PT9 | 20.43 | 2.12 |
| PT10 | 8.44 | 1.45 |
| PT11 | 6.42 | 1.56 |
| PT12 | 9.43 | 1.22 |
| PT13 | 4.54 | 1.68 |

# APPENDIX I

# DSC RESULTS of THE FLAME RETARDANT COMPOSITES

In the following DSC figures, for the first run, samples were heated beyond their melting points to erase their thermal history. In the second run samples were analyzed to figure out the melting and decomposition peaks. To clarify the temperature where glass transition of the samples occured, the temperature scale was zoomed between 40-180°C temperature range and only that region was reported in the first runs.

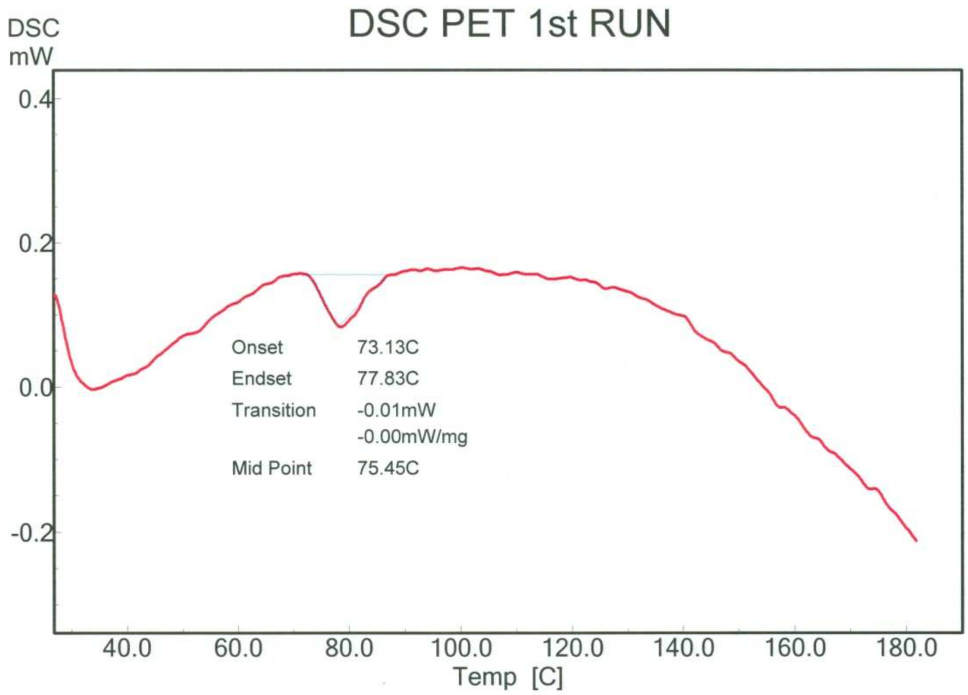

**Figure I.1** First run of DSC thermogram of crystalline PET

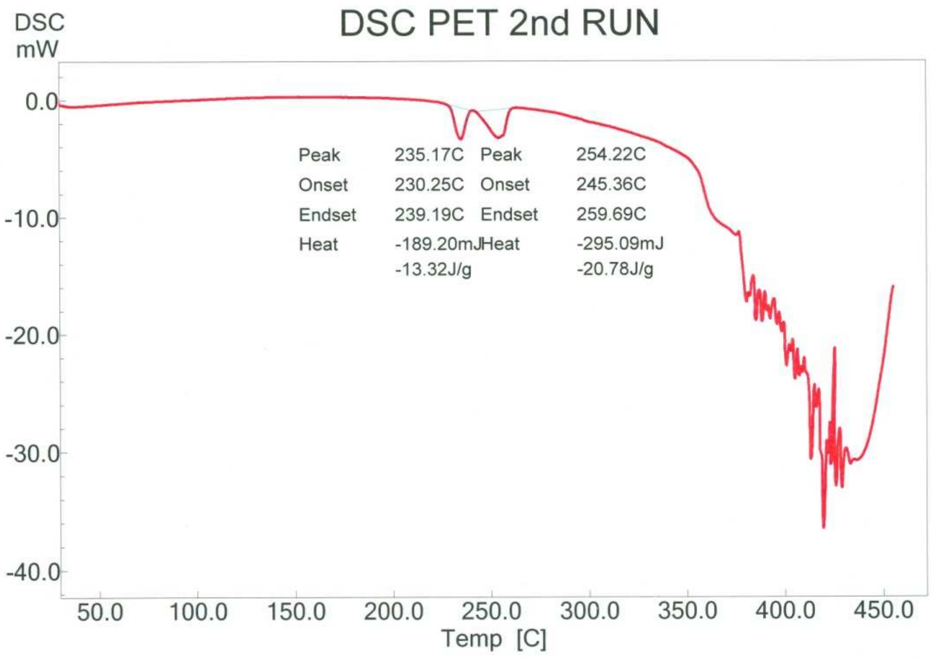

**Figure I.2** Second run of DSC thermogram of crystalline PET

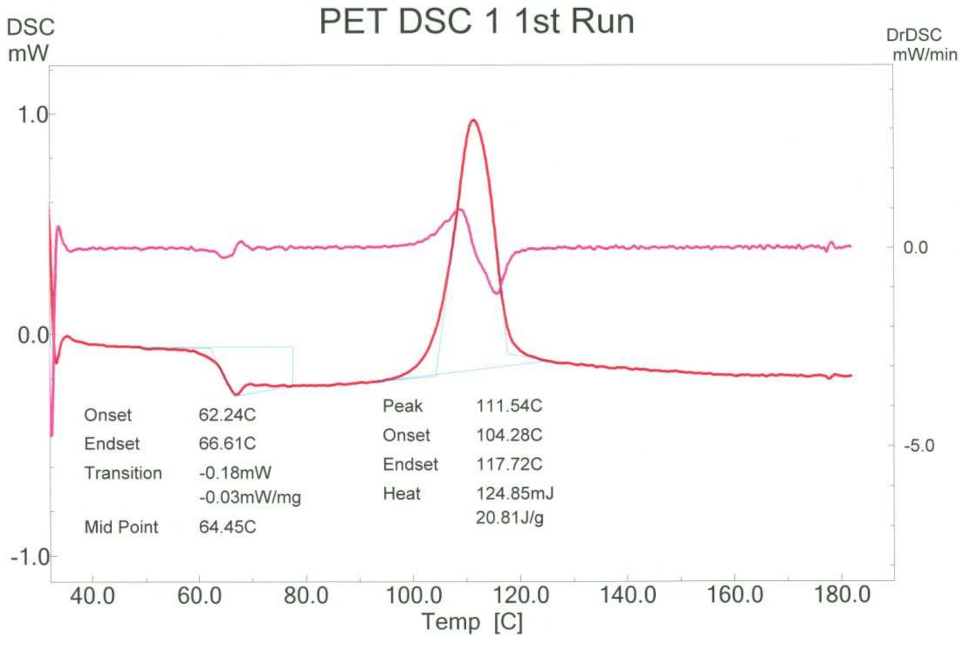

**Figure I.3** First run of DSC thermogram of second stage flame retardant composite PT1

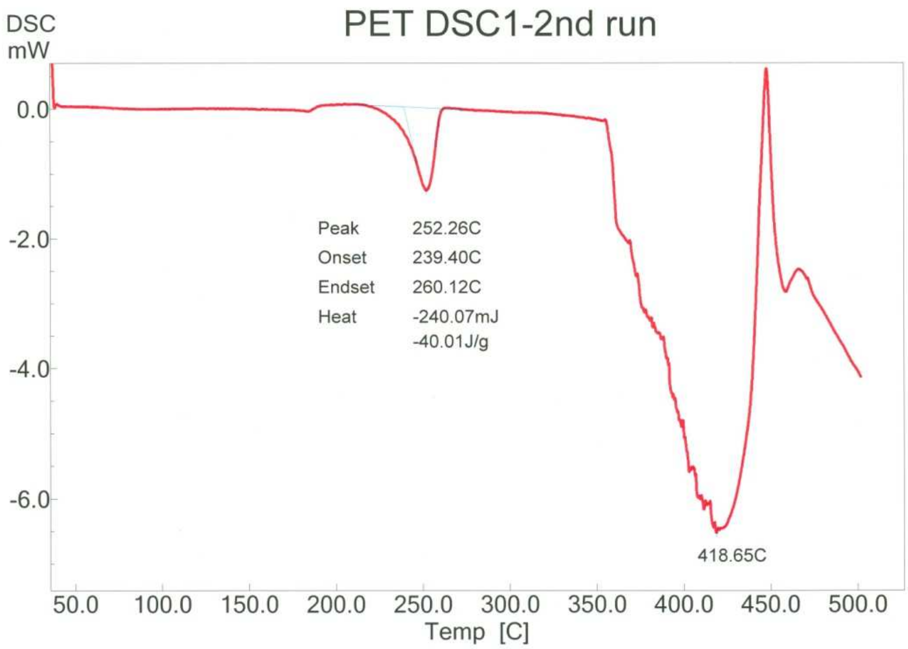

**Figure I.4** Second run of DSC thermogram of second stage flame retardant composite PT1

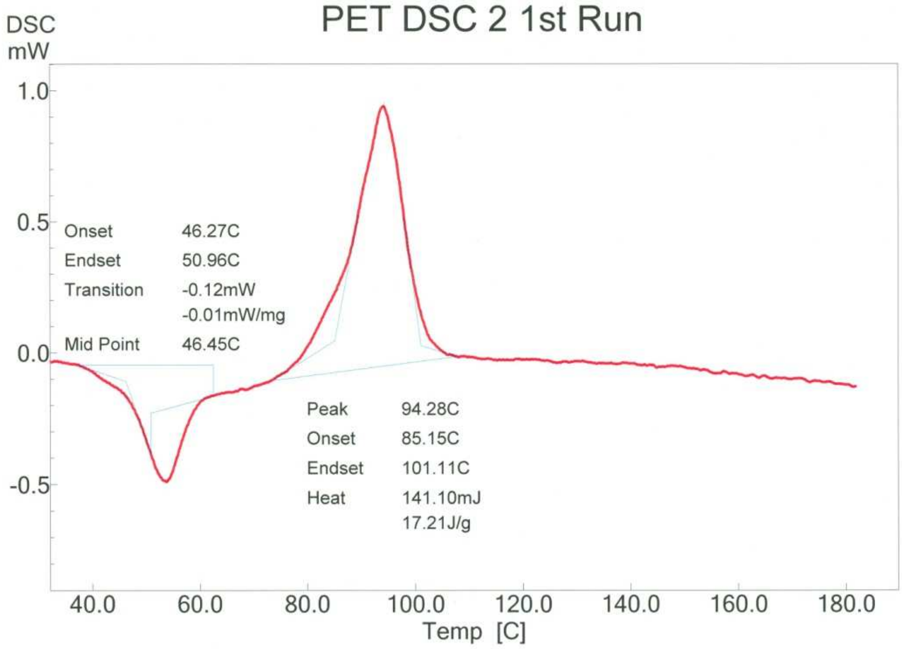

**Figure I.5** First run of DSC thermogram of second stage flame retardant composite PT2

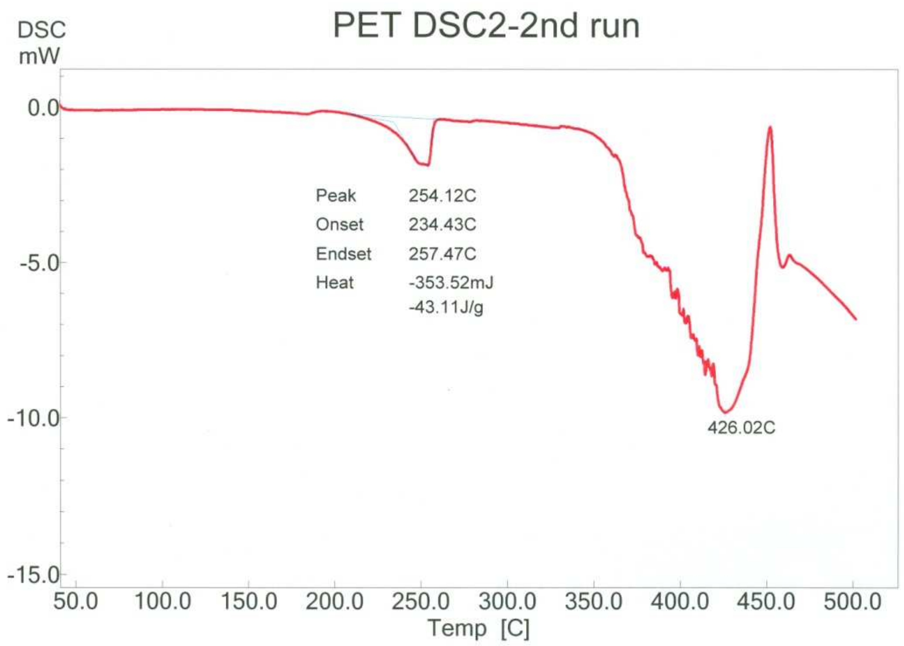

**Figure I.6** Second run of DSC thermogram of second stage flame retardant composite PT2

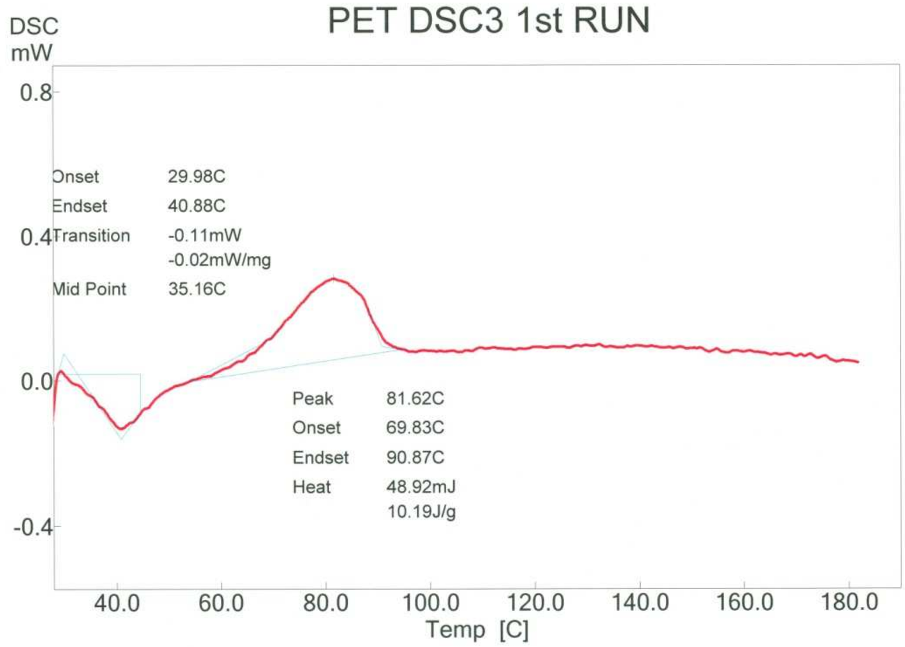

**Figure I.7** First run of DSC thermogram of second stage flame retardant composite PT3

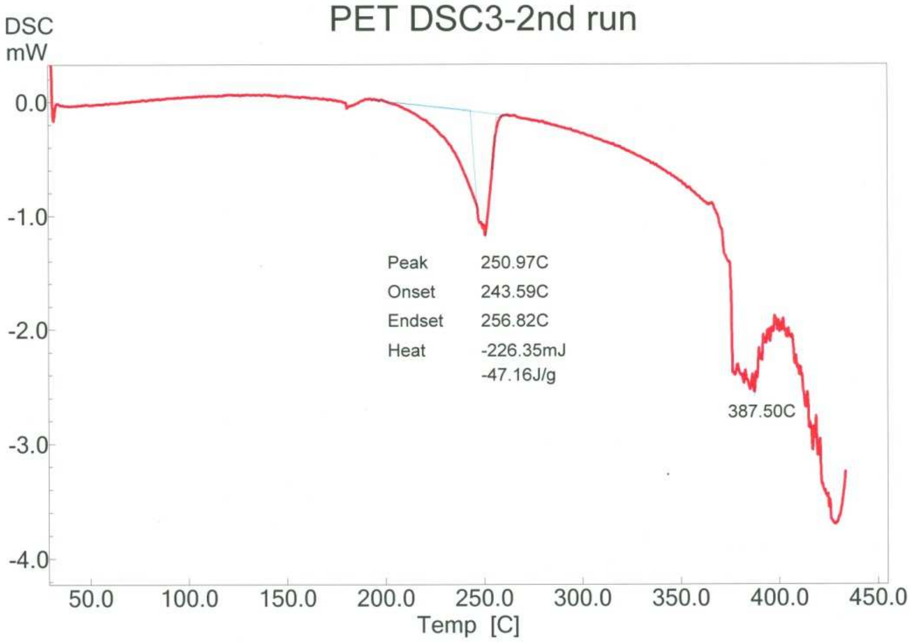

**Figure I.8** Second run of DSC thermogram of second stage flame retardant composite PT3

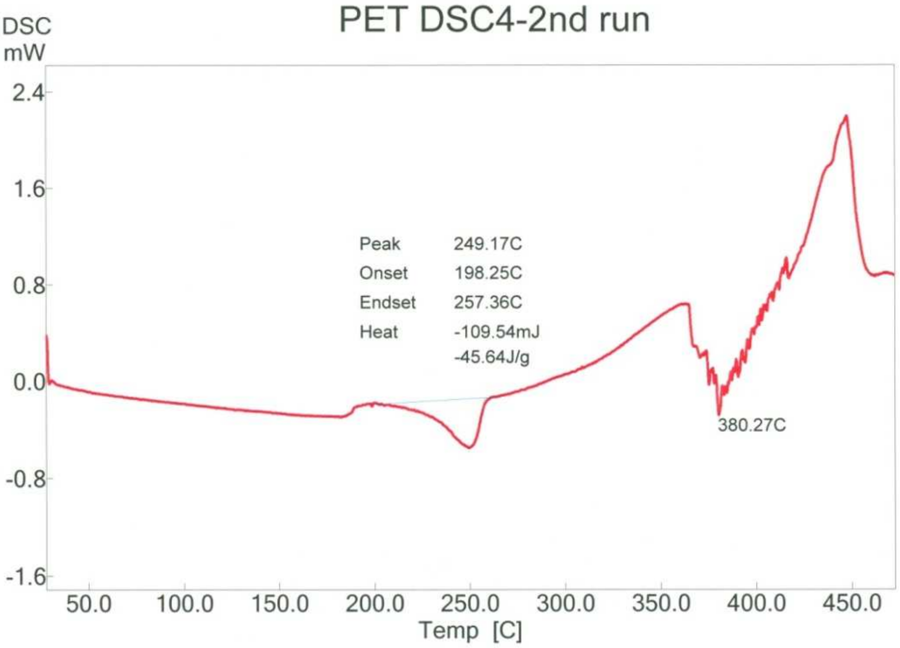

**Figure I.9** Second run of DSC thermogram of second stage flame retardant composite PT4

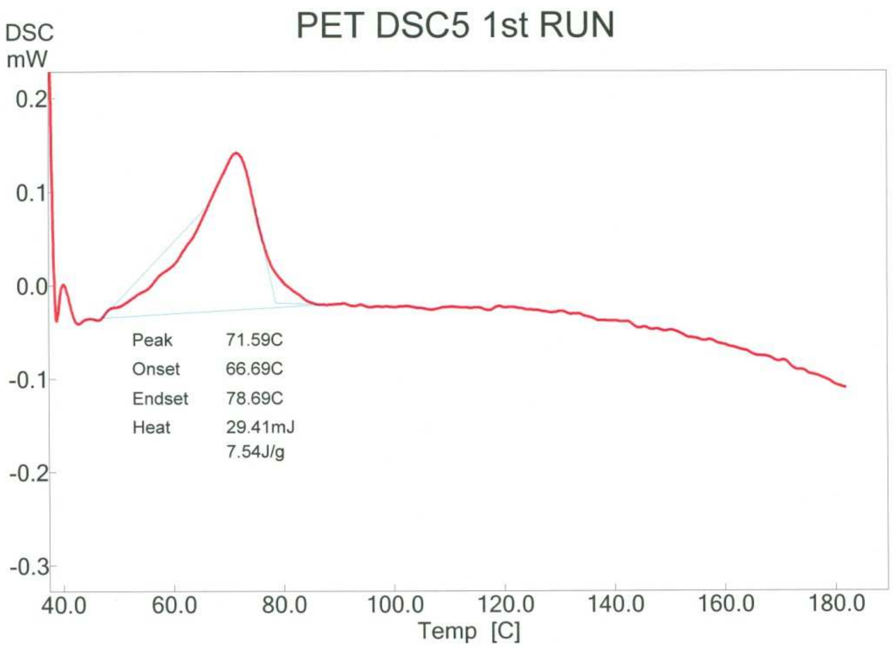

**Figure I.10** First run of DSC thermogram of second stage flame retardant composite PT5

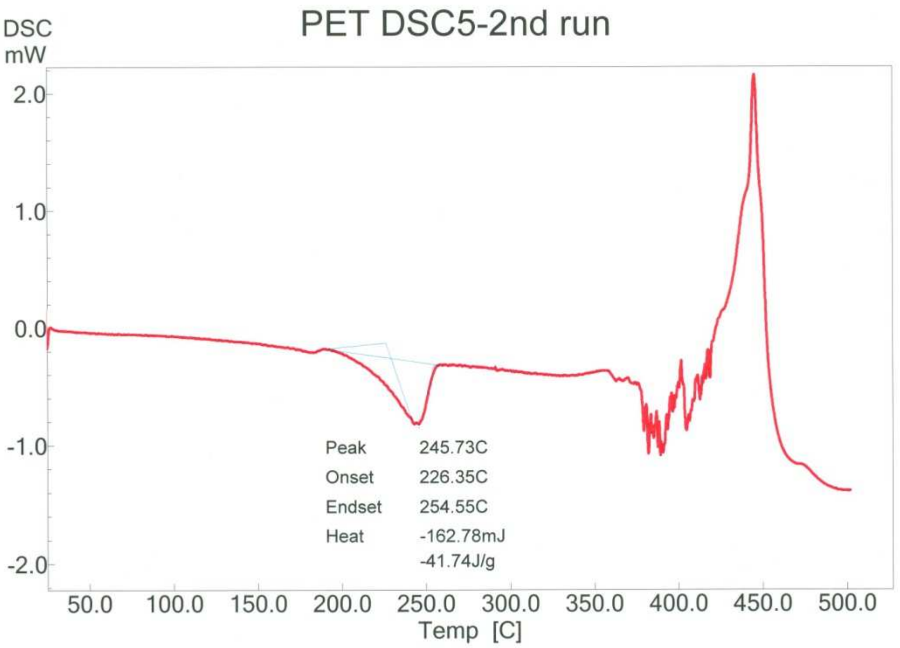

**Figure I.11** Second run of DSC thermogram of second stage flame retardant composite PT5

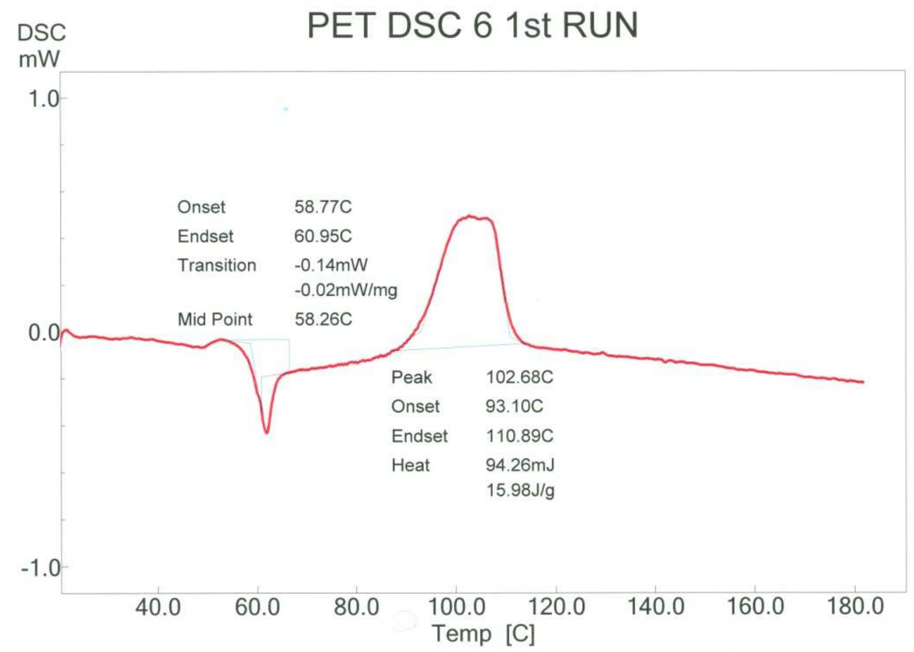

**Figure I.12** First run of DSC thermogram of second stage flame retardant composite PT6

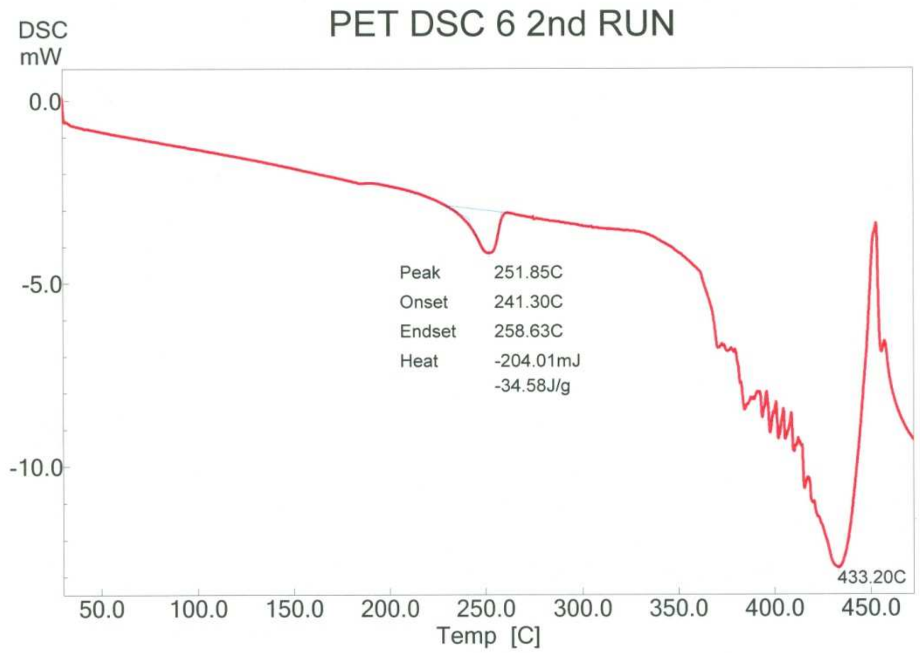

**Figure I.13** Second run of DSC thermogram of second stage flame retardant composite PT6

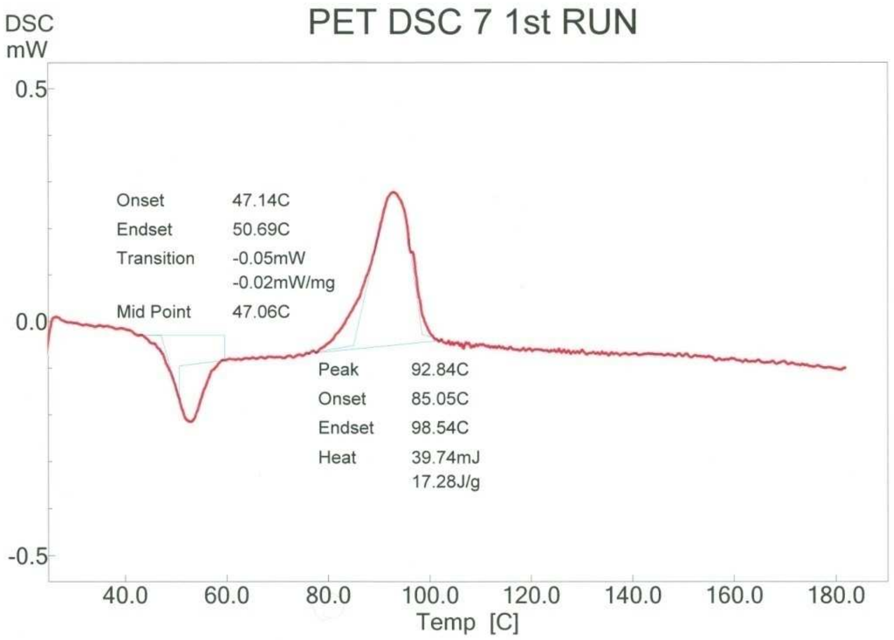

**Figure I.14** First run of DSC thermogram of second stage flame retardant composite PT7

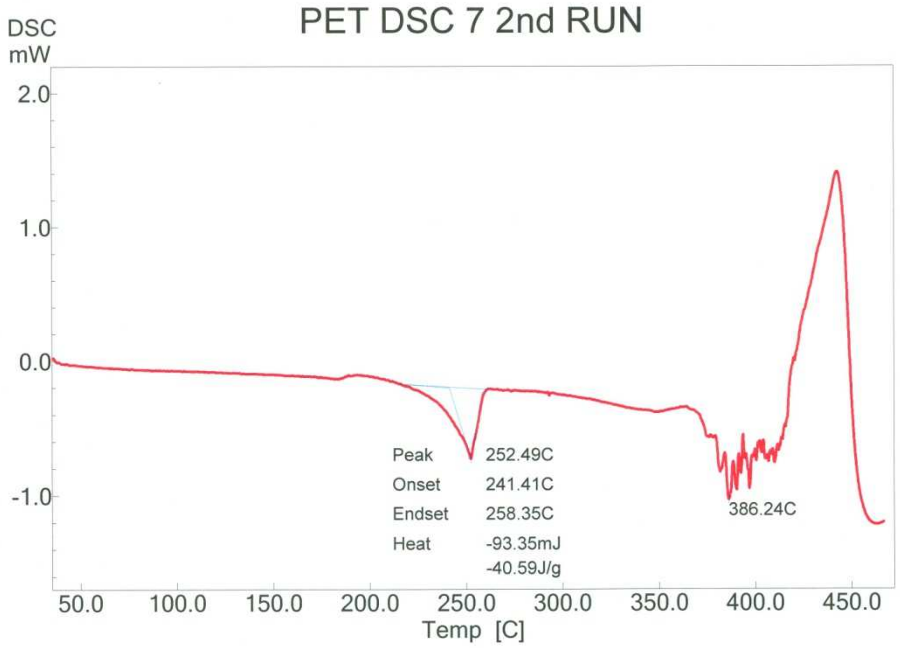

**Figure I.15** Second run of DSC thermogram of second stage flame retardant composite PT7

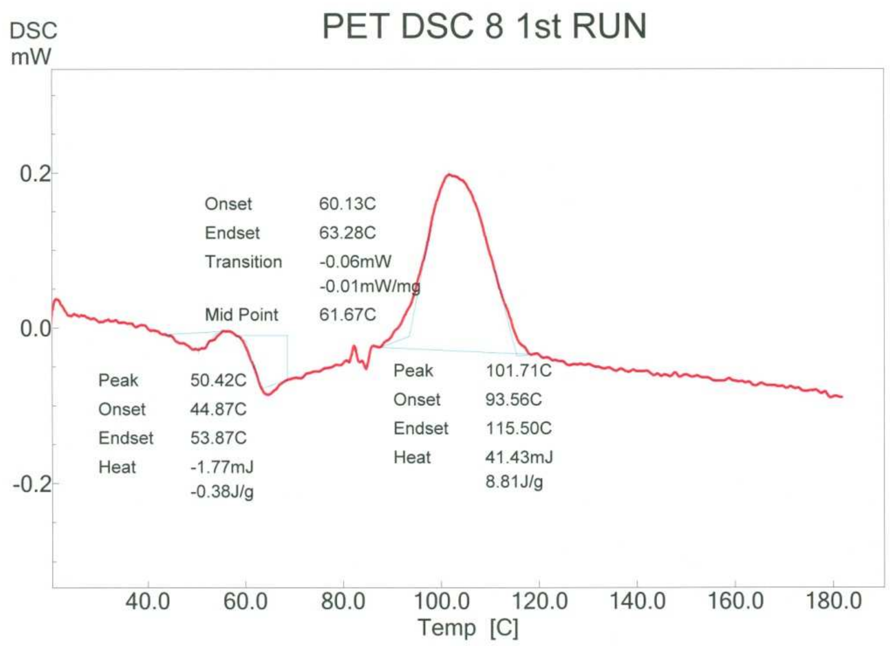

**Figure I.16** First run of DSC thermogram of second stage flame retardant composite PT8

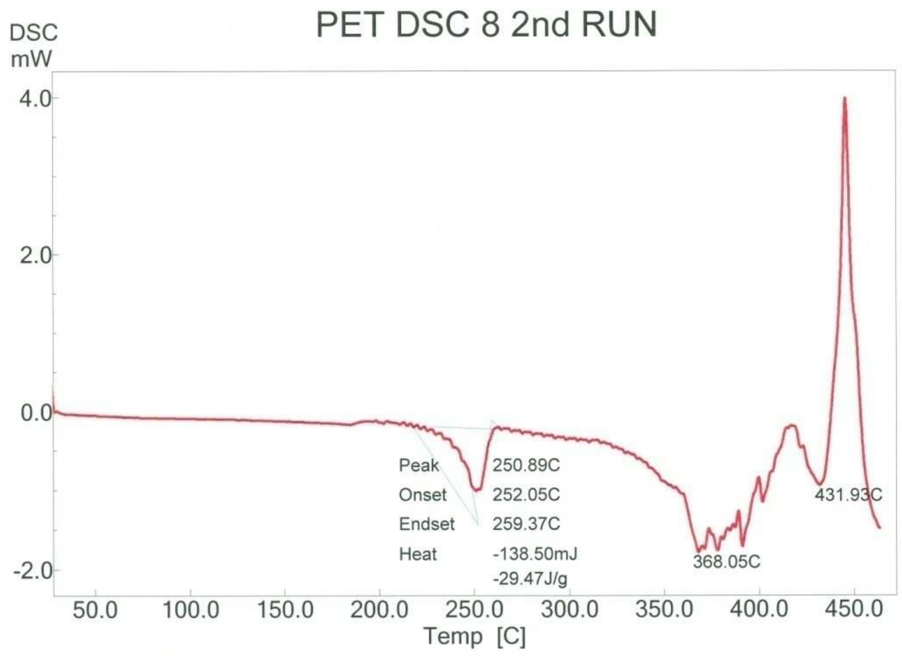

**Figure I.17** Second run of DSC thermogram of second stage flame retardant composite PT8

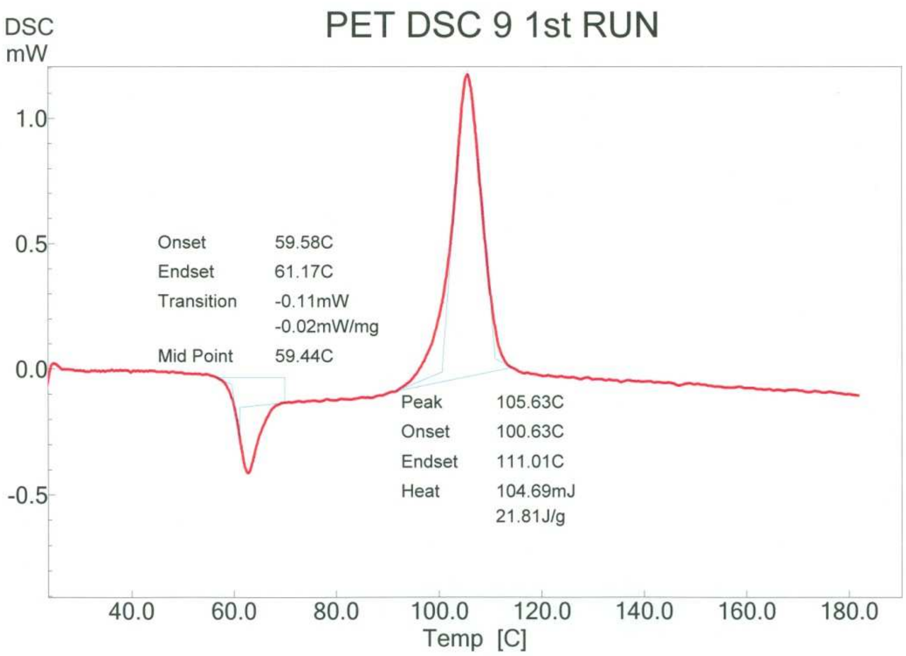

**Figure I.18** First run of DSC thermogram of second stage flame retardant composite PT9

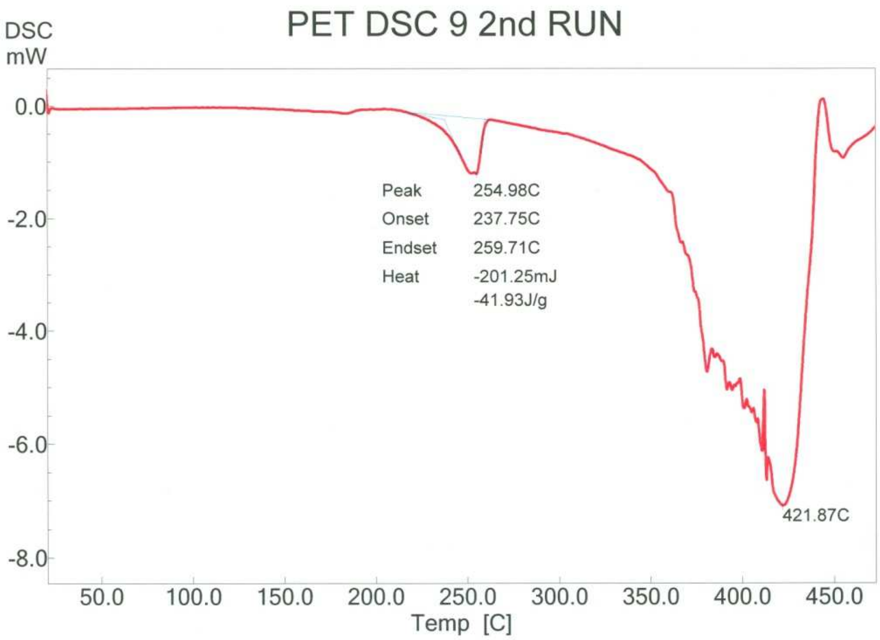

**Figure I.19** Second run of DSC thermogram of second stage flame retardant composite PT9

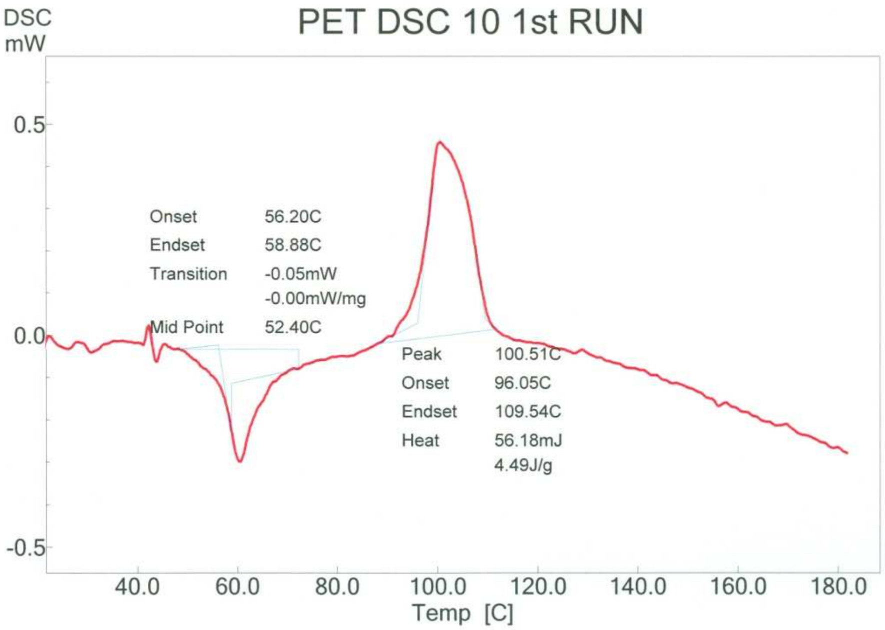

**Figure I.20** First run of DSC thermogram of second stage flame retardant composite PT10

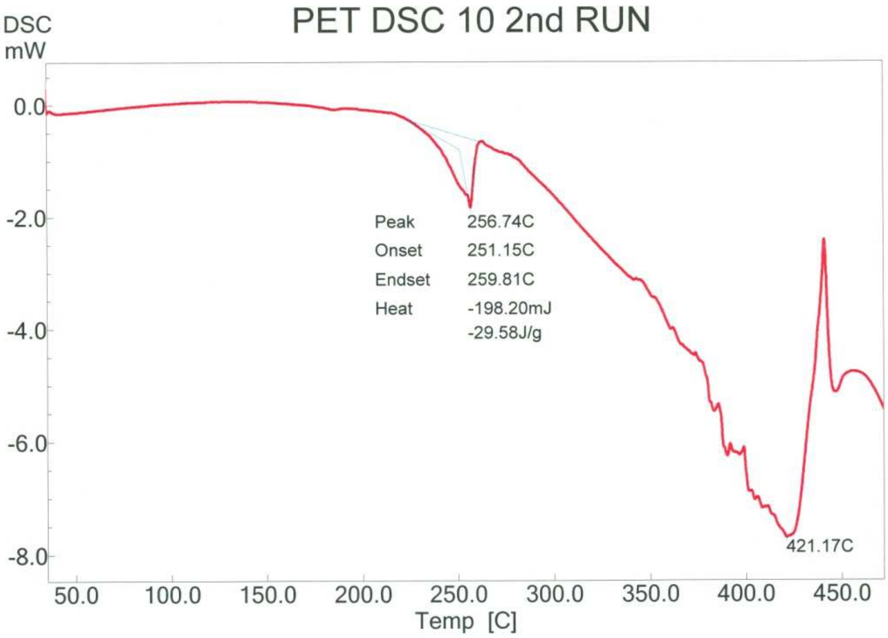

**Figure I.21** Second run of DSC thermogram of second stage flame retardant composite PT10

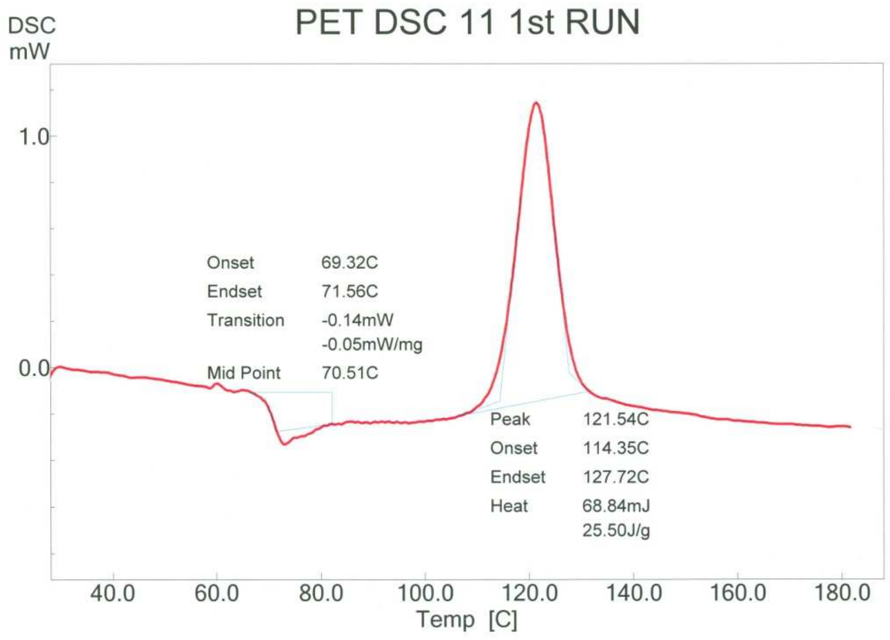

**Figure I.22** First run of DSC thermogram of second stage flame retardant composite PT11

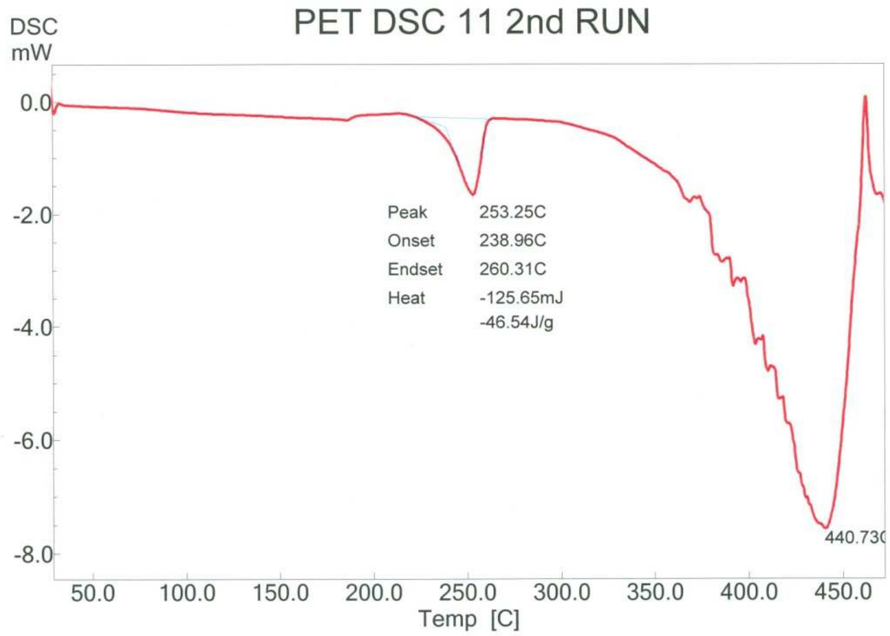

**Figure I.23** Second run of DSC thermogram of second stage flame retardant composite PT11

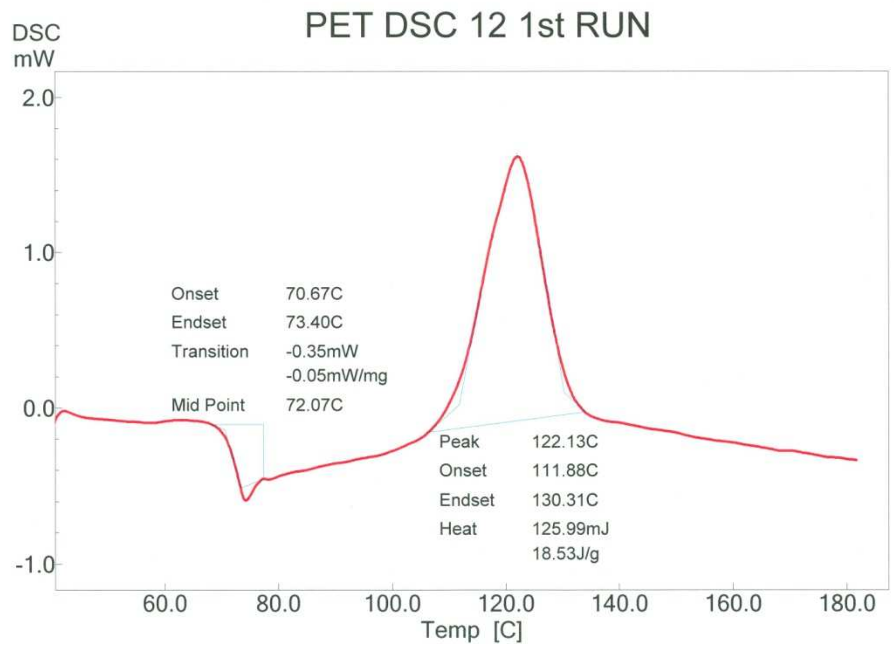

**Figure I.24** First run of DSC thermogram of second stage flame retardant composite PT12

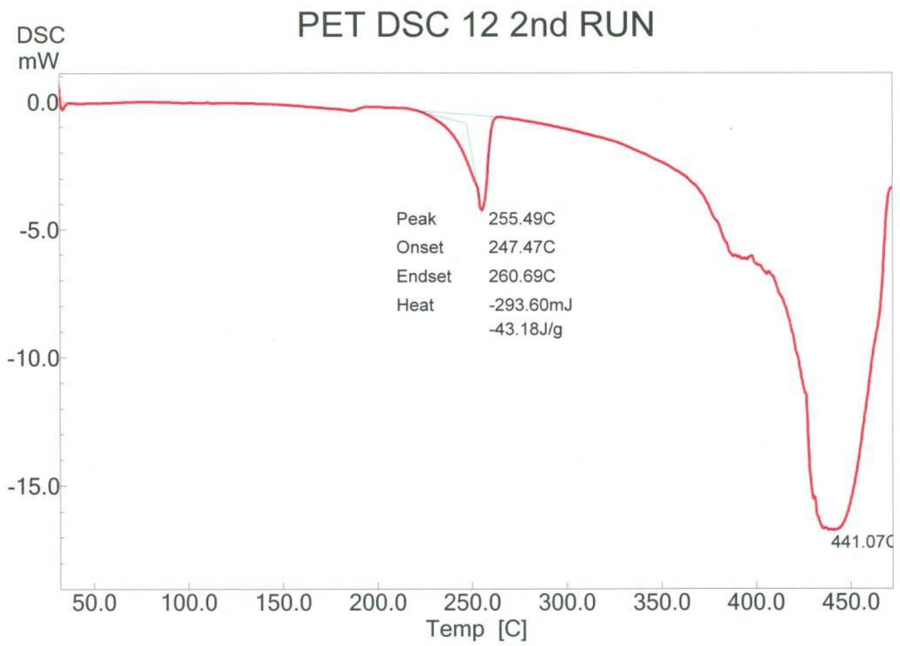

**Figure I.25** Second run of DSC thermogram of second stage flame retardant composite PT12

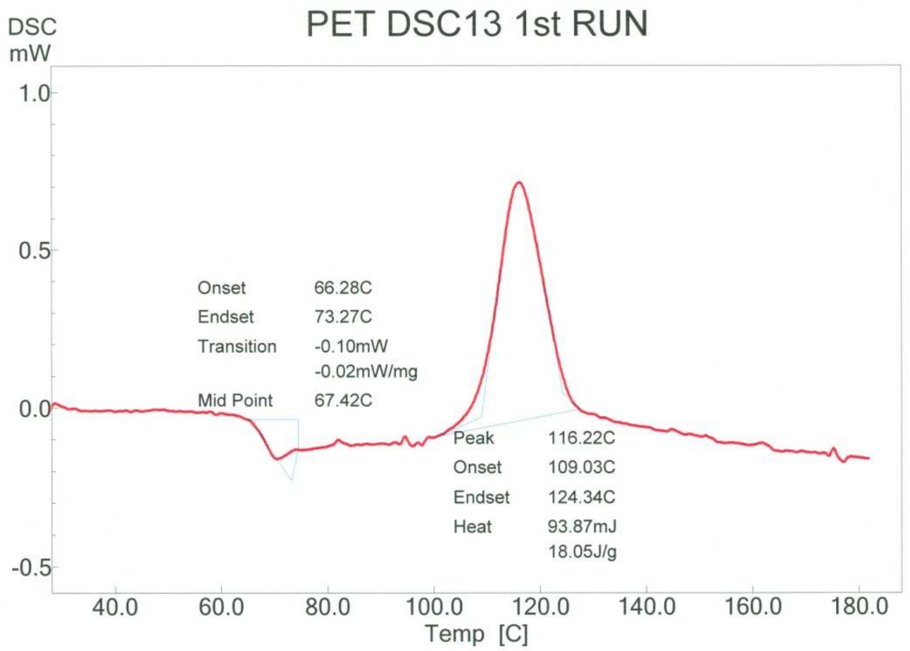

**Figure I.26** First run of DSC thermogram of second stage flame retardant composite PT13

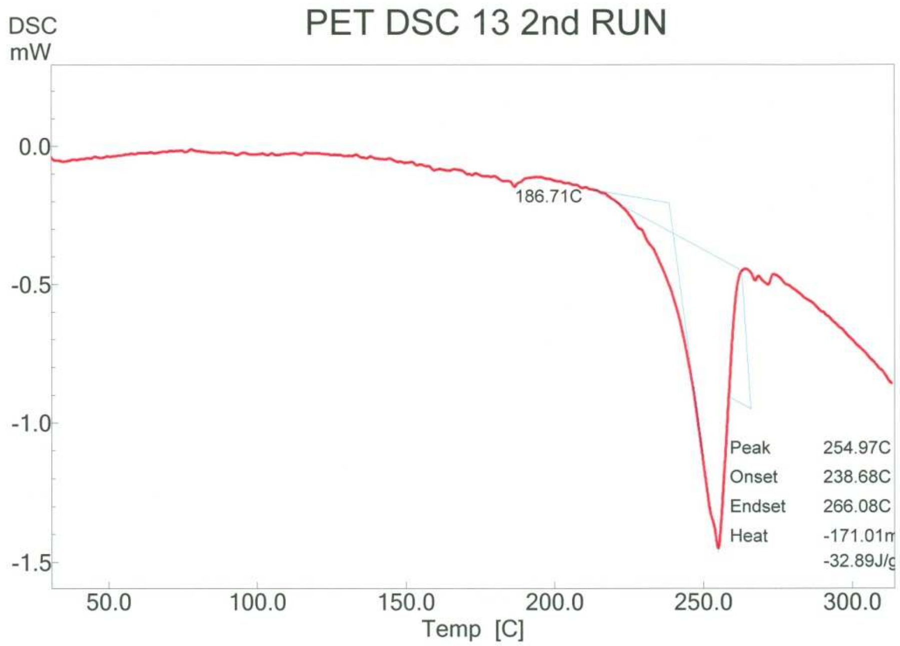

**Figure I.27** Second run of DSC thermogram of second stage flame retardant composite PT13

# APPENDIX J

# TGA RESULTS of THE FLAME RETARDANT ADDITIVES

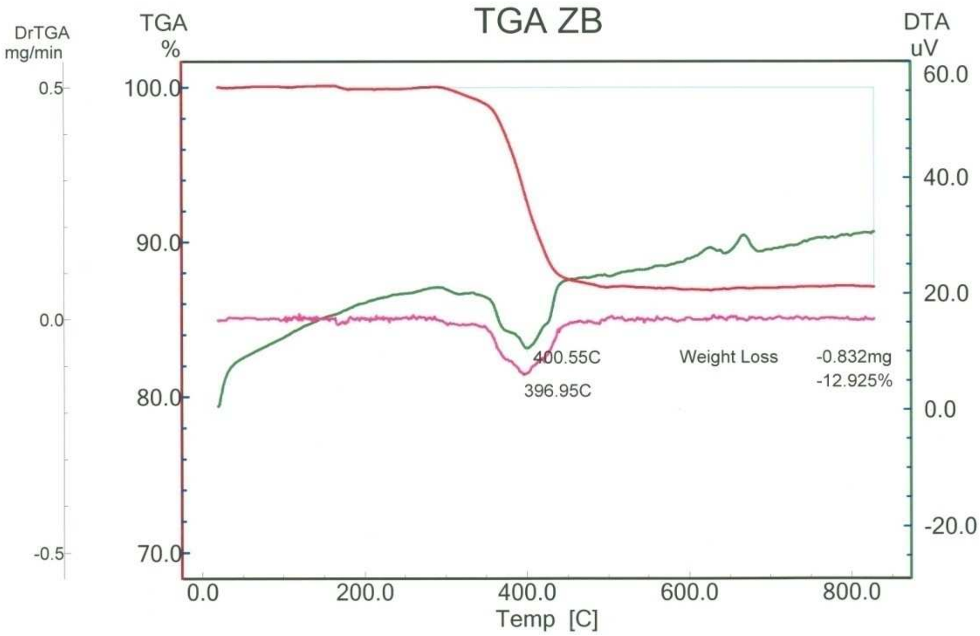

**Figure J.1** TGA thermogram of flame retardant additive 3.5 hydrated zinc borate ZBP1

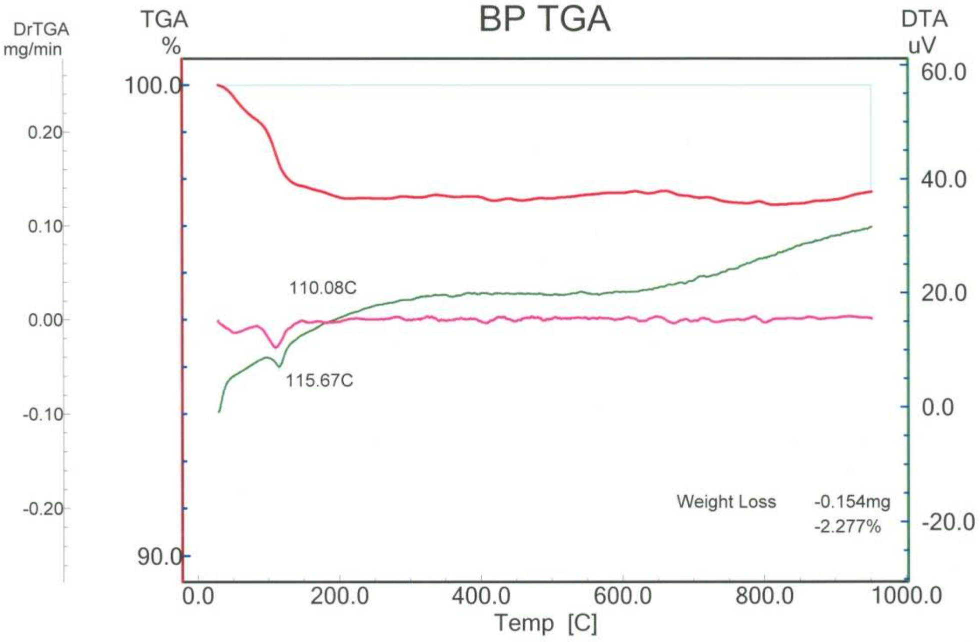

**Figure J.2** TGA thermogram of flame retardant additive microwave technique produced boron phosphate

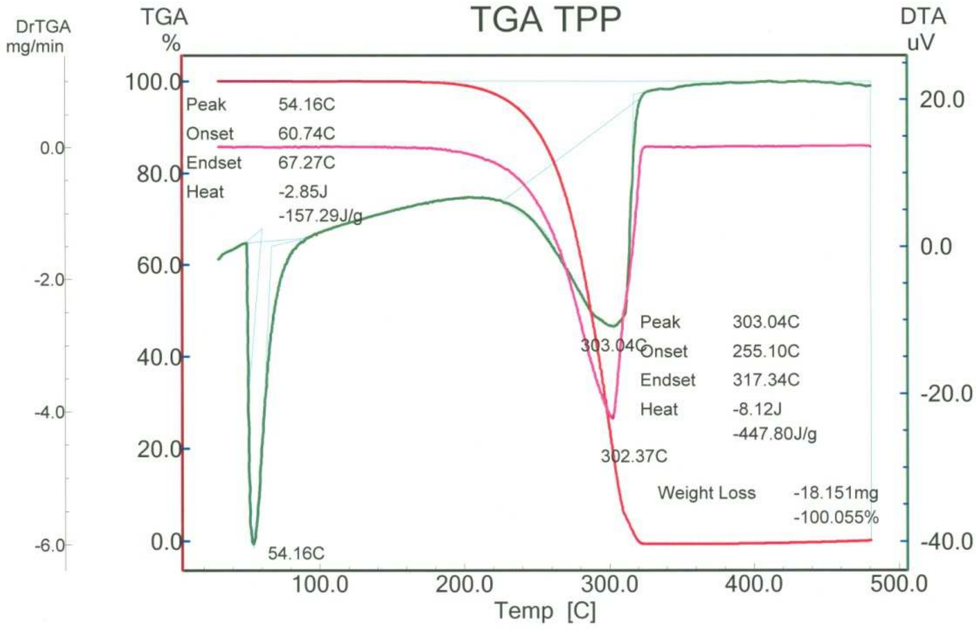

**Figure J.3** TGA thermogram of flame retardant additive triphenyl phosphate

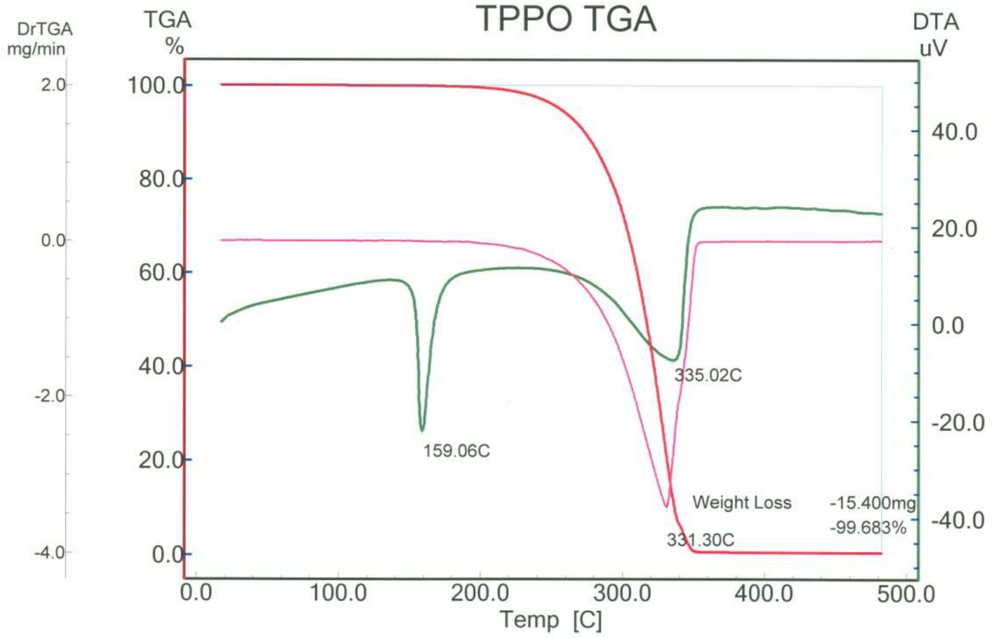

**Figure J.4** TGA thermogram of flame retardant additive triphenyl phosphine oxide

# APPENDIX K

# TGA RESULTS of THE FLAME RETARDANT COMPOSITES

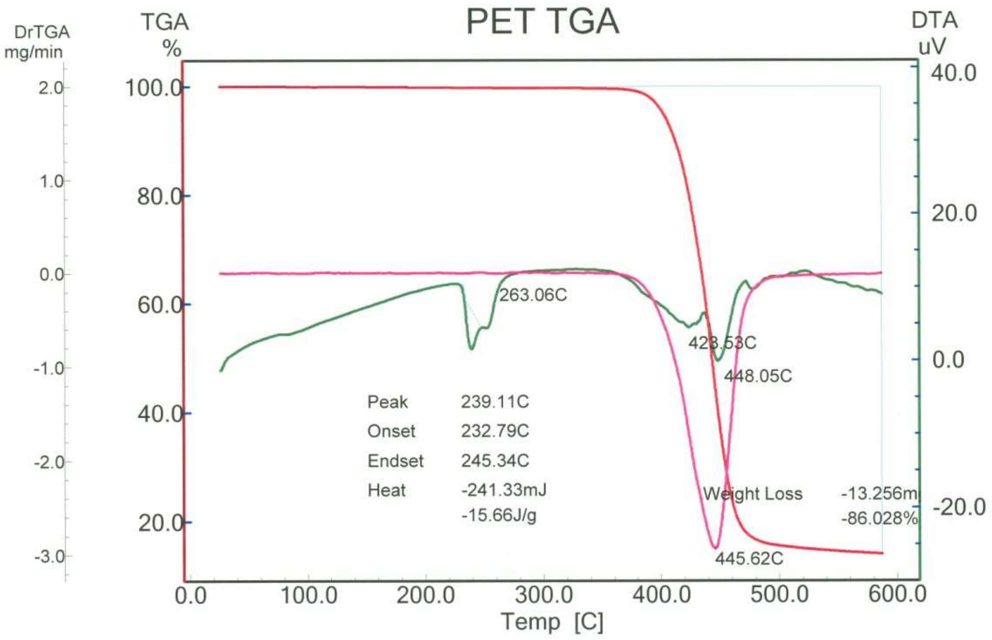

**Figure K.1** TGA thermogram of crystalline PET

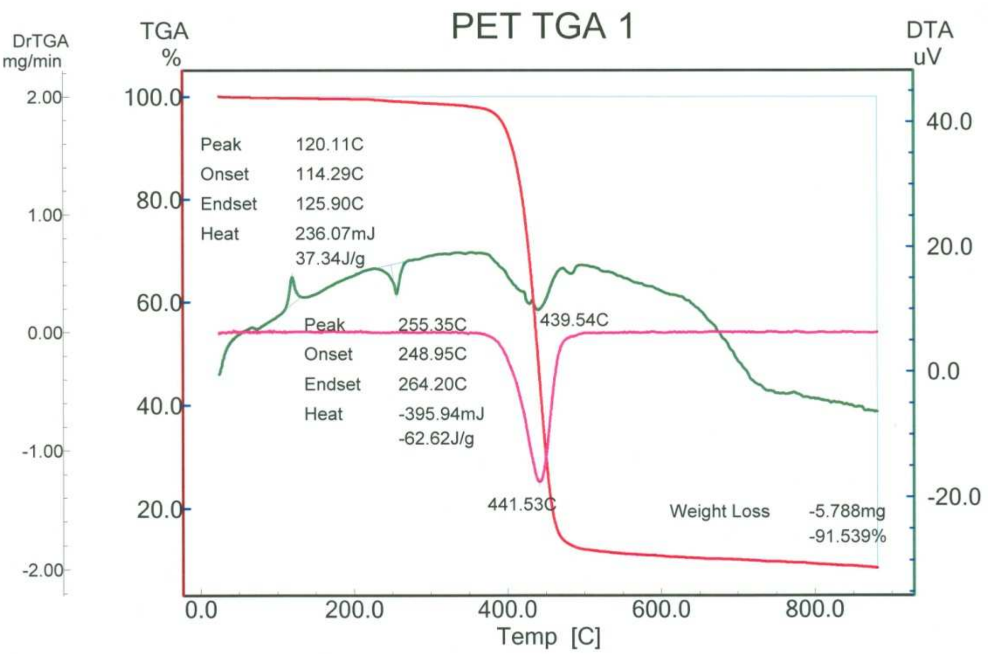

**Figure K.2** TGA thermogram of second stage flame retardant composite PT1

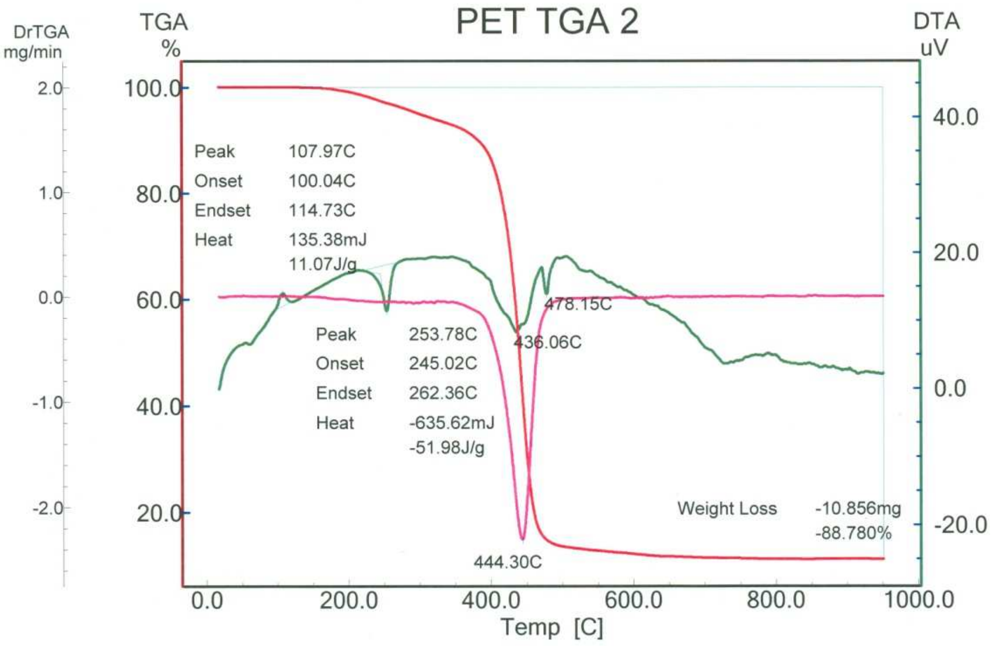

**Figure K.3** TGA thermogram of second stage flame retardant composite PT2

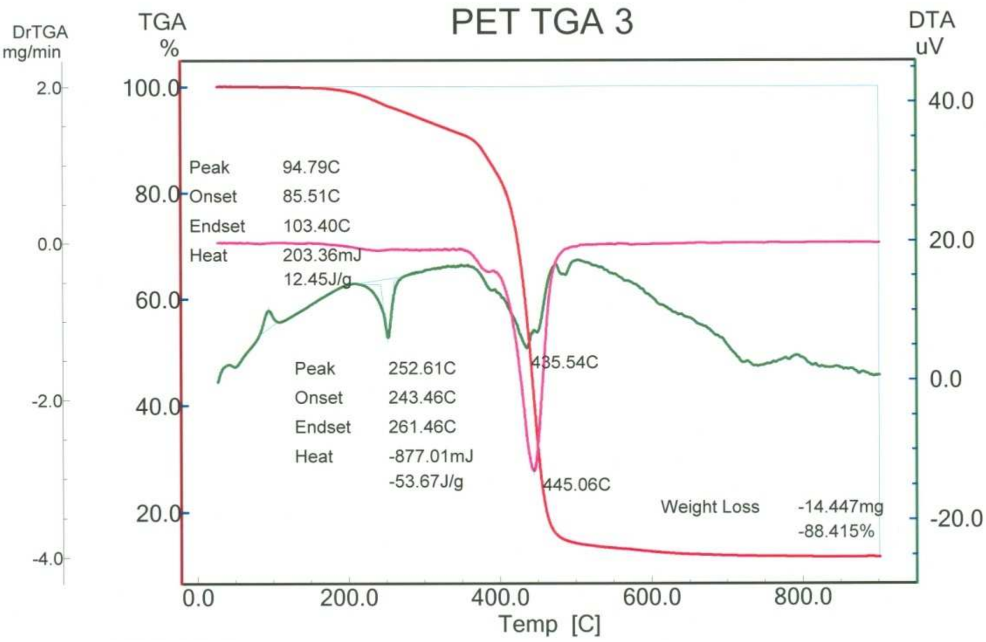

**Figure K.4** TGA thermogram of second stage flame retardant composite PT3

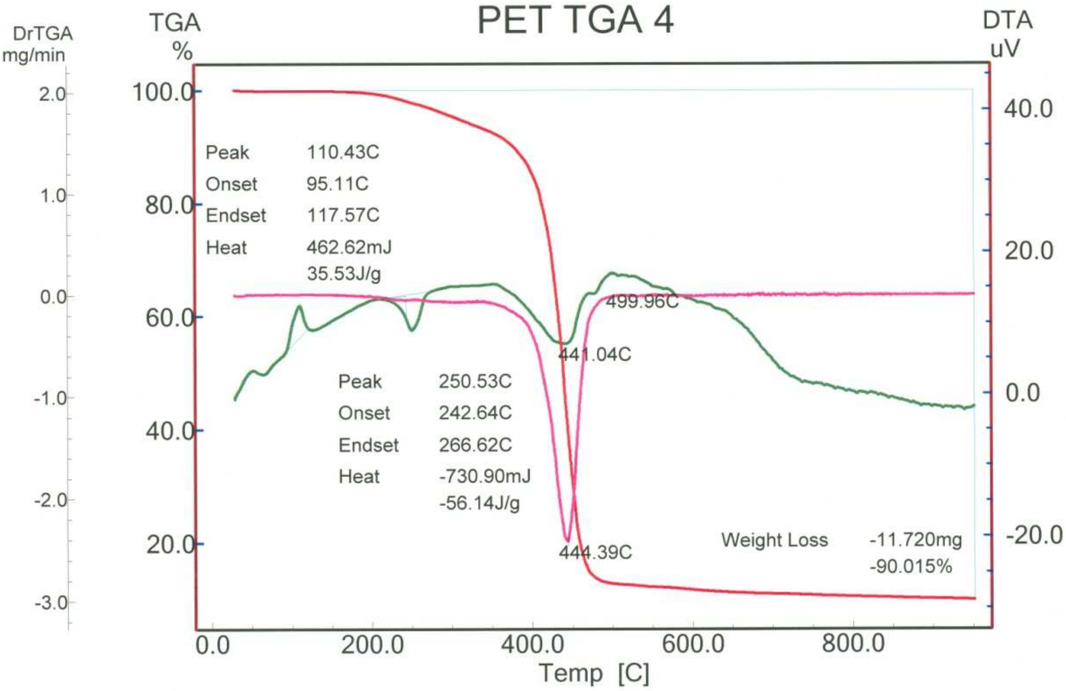

**Figure K.5** TGA thermogram of second stage flame retardant composite PT4

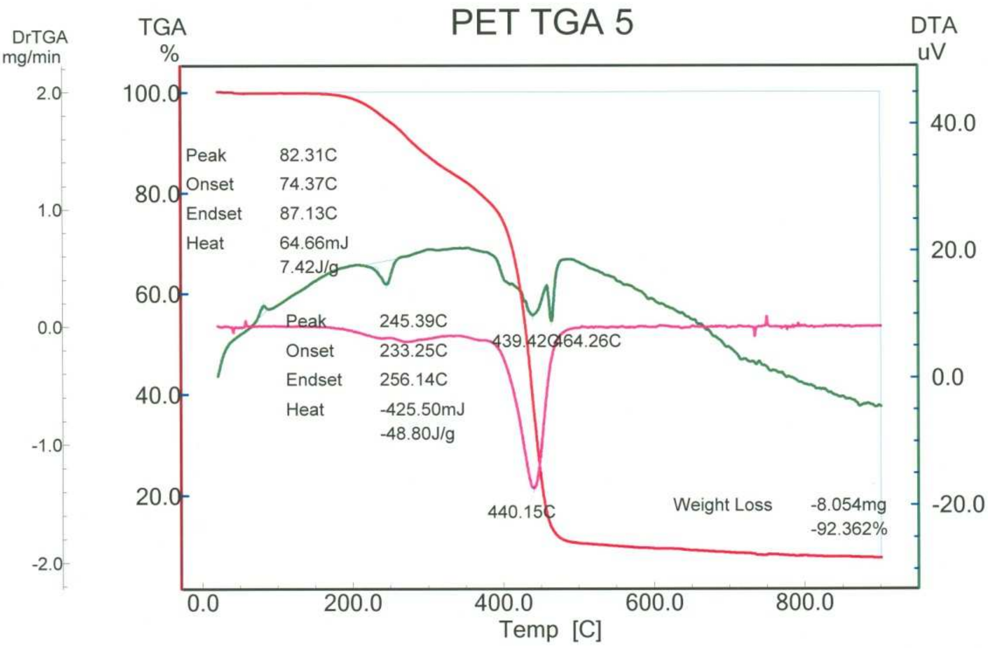

**Figure K.6** TGA thermogram of second stage flame retardant composite PT5

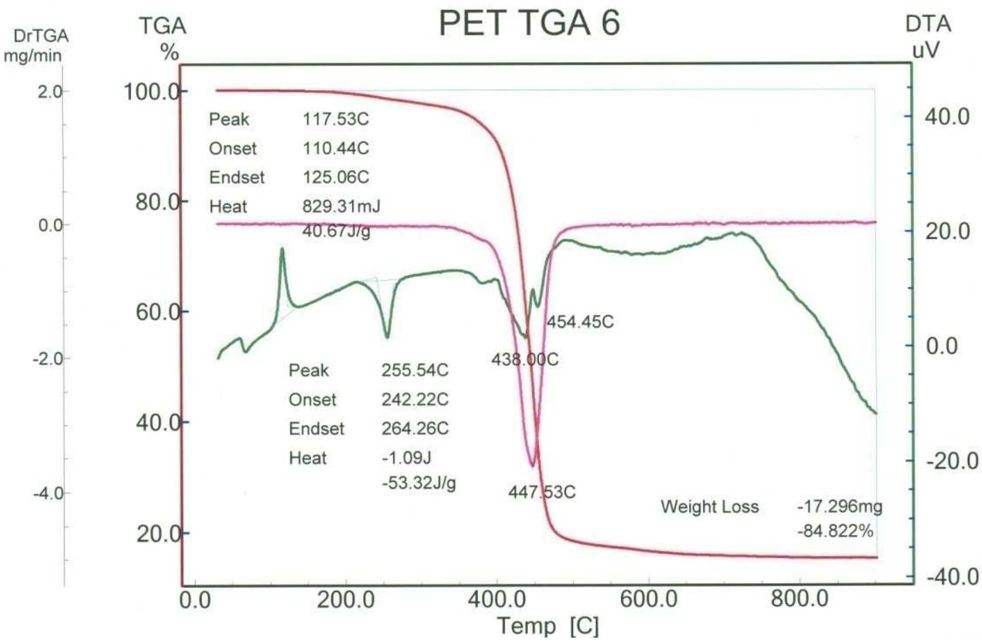

**Figure K.7** TGA thermogram of second stage flame retardant composite PT6

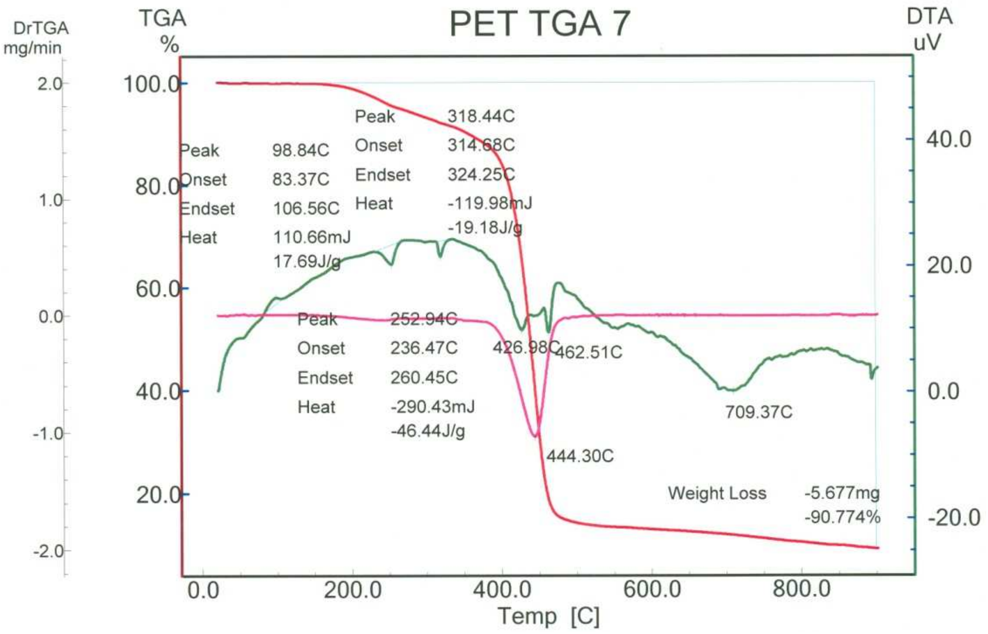

**Figure K.8** TGA thermogram of second stage flame retardant composite PT7

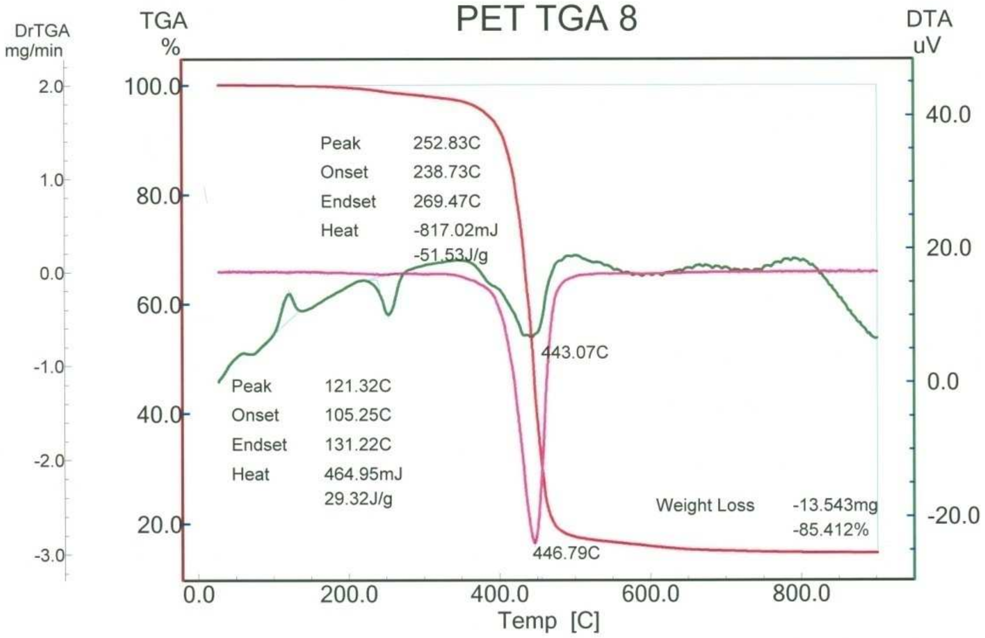

**Figure K.9** TGA thermogram of second stage flame retardant composite PT8

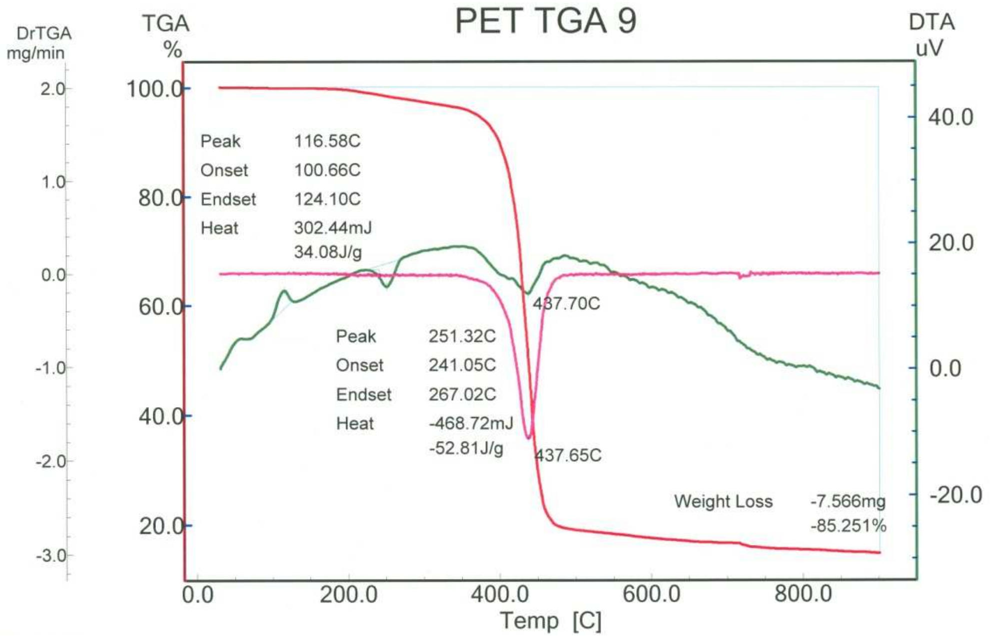

**Figure K.10** TGA thermogram of second stage flame retardant composite PT9

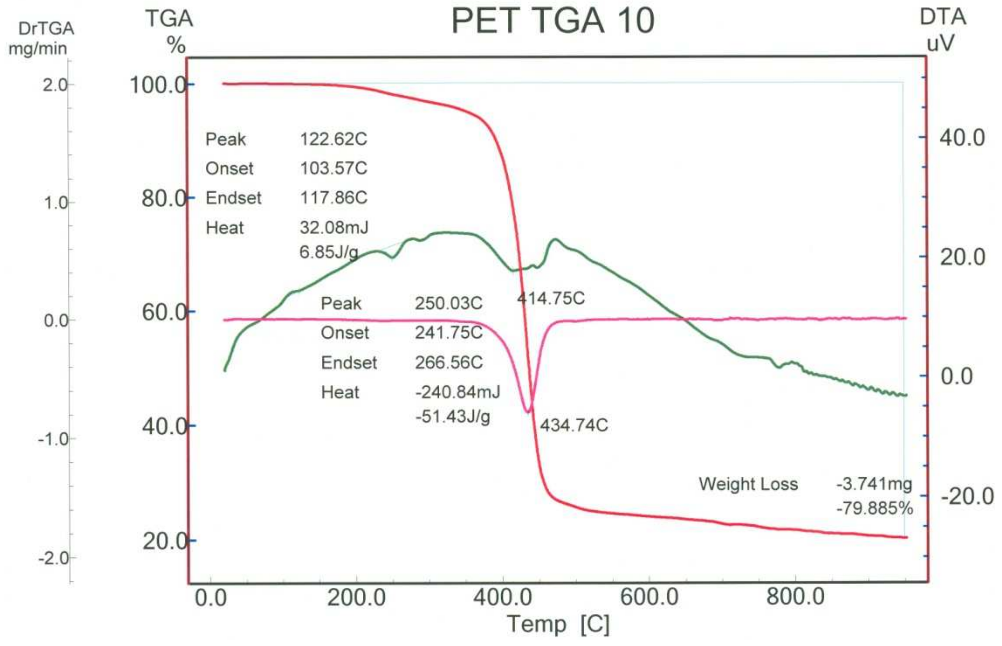

**Figure K.11** TGA thermogram of second stage flame retardant composite PT10

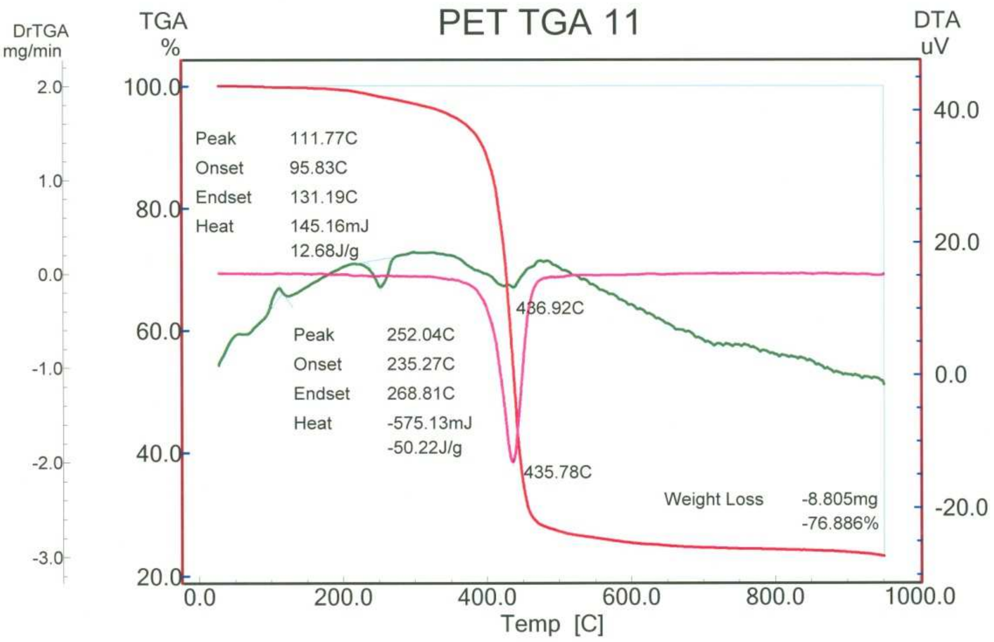

**Figure K.12** TGA thermogram of second stage flame retardant composite PT11

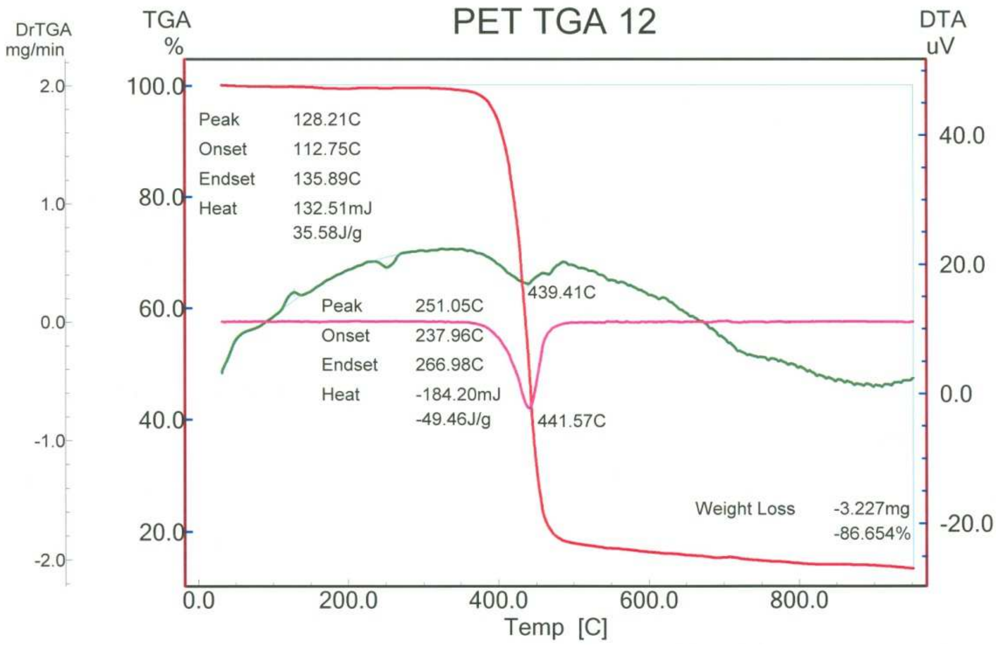

**Figure K.13** TGA thermogram of second stage flame retardant composite PT12

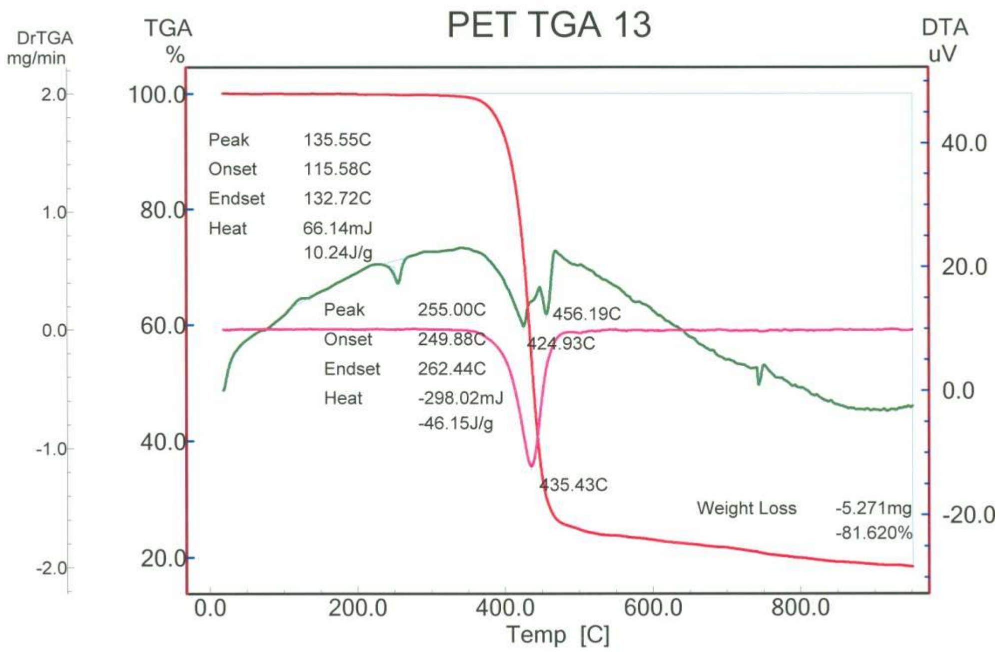

**Figure K.14** TGA thermogram of second stage flame retardant composite PT13

# APPENDIX L

# FTIR RESULTS RELATED to THE CALCINATION of FLAME RETARDANT ADDITIVE BORON PHOSPHATE

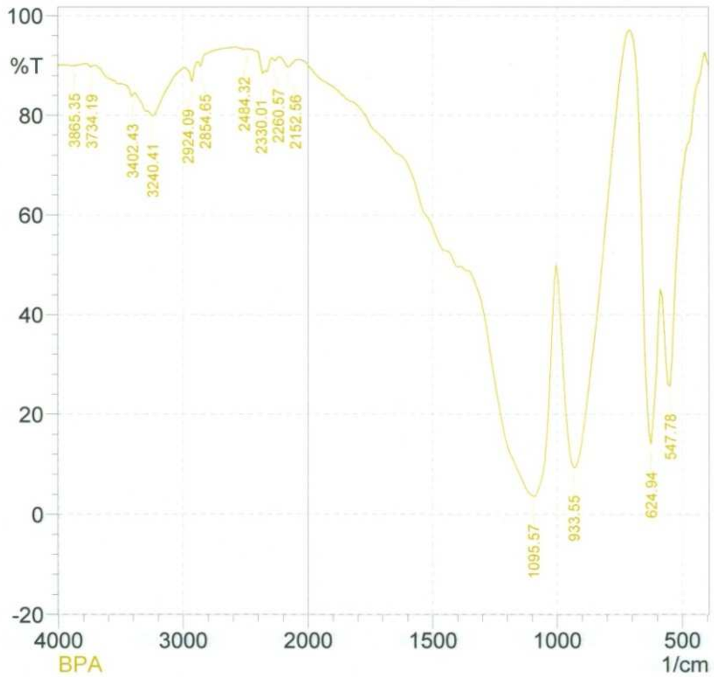

**Figure L.1** FTIR plot of non-sintered microwave technique produced boron phosphate

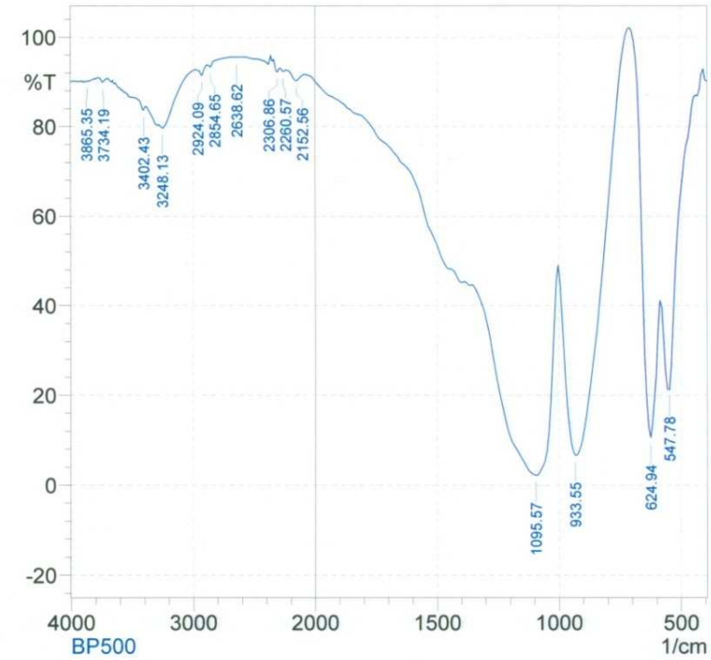

**Figure L.2** FTIR plot of 1 h at 500°C sintered microwave technique produced boron phosphate

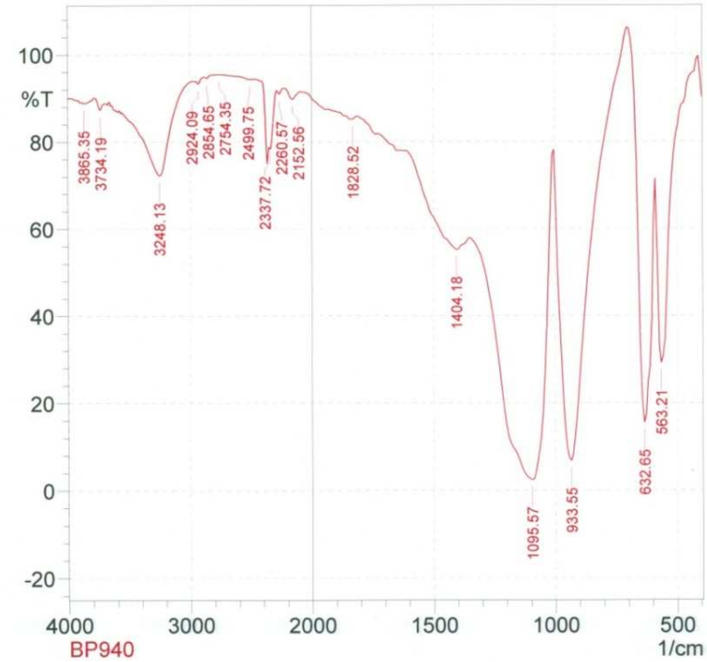

**Figure L.3** FTIR plot of 1 h at 940°C sintered microwave technique produced boron phosphate

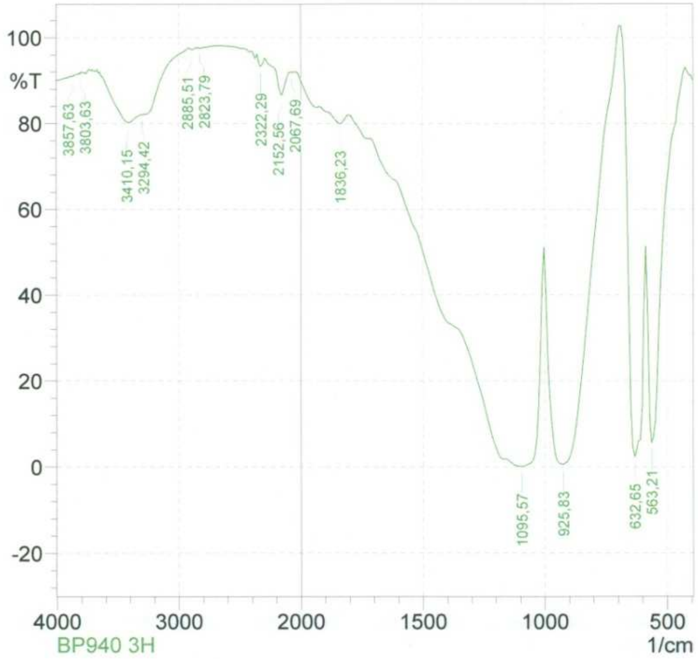

**Figure L.4** FTIR plot of 3 h at 940°C sintered microwave technique produced boron phosphate

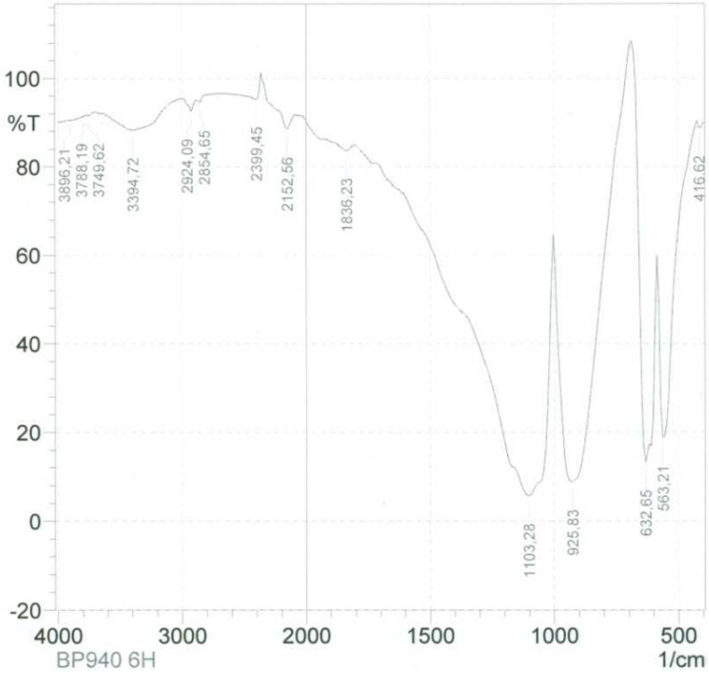

**Figure L.5** FTIR plot of 6 h at 940°C sintered microwave technique produced boron phosphate

# CURRICULUM VITAE

## Personal Information

**Birth:** 1979, İzmir, Turkey.
**Nationality:** Turkish.
**Marital Status:** Single.
**Military Service:** Deferred till 2011.

**Adress:** Ileri Sok. Anit Apt. 20/7 Anittepe
Ankara, TURKEY
**E-mail:** mert.kilinc@mam.gov.tr
**Mobile:** + 90 532 376 51 10

## Education

**Ph.D.** (Chemical Engineering)
**[September 2004 – June 2009]**
**Middle East Technical University**, Department of Chemical Engineering, Ankara, Turkey
**Dissertation Title:** Production and Characterization of Boron Based Flame Retardant Additives, and the Effect of Flame Retardant Additives on PET-Based Composites
**Thesis Advisor:** Associate Professor Goknur Bayram

**M.Sc.** (Chemical Engineering)
**[September 2002 - July 2004]**
**Middle East Technical University**, Department of Chemical Engineering, Ankara, Turkey
**Dissertation Title:** Processing & Characterization of Poly(ethylene terephthalate) Based Composites

**Thesis Advisor:** Associate Professor Goknur Bayram
**B.Sc.** (Chemical Engineering)
**[September 1998 - June 2002]**
**Gazi University**, Department of Chemical Engineering, Ankara, Turkey

**High School**
**[September 1990 – February 1997]**
**Ankara Ataturk Anatolian High School**, Ankara, Turkey

## Additional Educational Activities

- Reactor Design Project for Sulfuric Acid Production in Reactor Design Course, Gazi University, Ankara, Turkey.
- Equipment Design Project for Phthalic Anhydride Production Plant in Chemical Engineering Design I Course, Gazi University, Ankara, Turkey.
- Plant Design for Solvent Recovery Section of Siloxane Plant in Chemical Engineering Design II Course, Gazi University, Ankara, Turkey.
- Kinetic Studies of Oxygenated Unleaded Gasoline Additives in Graduation Project Course, Gazi University, Ankara, Turkey.
- Kinetic Study and Kinetic Model Development for Oxygenated Unleaded Gasoline Additive ETBE in Undergraduate Research Project Course Gazi University, Ankara, Turkey.
- Computational Reactor Design of Ethane Cracking Reactor, Middle East Technical University, Ankara, Turkey.

## Professional Experience

**Researcher**
**[September 2008 – to date]**
**The Scientific and Technological Research Council of Turkey (TUBITAK), Marmara Research Center**, Chemistry Institute, Kocaeli, Turkey

**Research Assistant** (Chemical Engineering)
**[October 2002 – September 2008]**
**Middle East Technical University**, Department of Chemical Engineering, Ankara, Turkey

**Intern Chemical Engineer** (Summer Practice)
**[July 2001 – August 2001]**
**TUPRAS Middle Anatolia Refinery**, Process III (Hydro-cracking Unit) & Process IV (Asphalt and Sulphur Production Unit), Kirikkale, Turkey

**Intern Chemical Engineer** (Summer Practice)
**[June 2000 – July 2000]**
**TUPRAS Middle Anatolia Refinery**, Process I (Atmospheric Distillation Unit) & Process II (Vacuum Distillation Unit), Kirikkale, Turkey

## Academic Experience

- Assistantship to some undergraduate courses namely, Introduction to Chemical Engineering, Heat & Mass Transfer Operations, Chemical Engineering Laboratory I, Chemical Engineering Laboratory II, and Computer Aided Graphical Design.

## Laboratory Skills

- Various Analytical Chemical Analysis
- Pilot Scale Chemical Synthesis
- Twin Screw Extruder
- Polymer Blends and Composites
- Polymeric Nanocomposites
- Injection Molding
- Compression Molding
- Mechanical Testing Device
- LOI Device

- Impact Testing Device
- DSC, TGA, DTA
- FT-IR
- Shore Hardness Test
- Melt Flow Index
- UV-Spectrophotometer
- Gas Chromatography
- Karl-Fischer, KF-Coulemeter, Acid-Base Number Titrations

## Publications

- M. Kilinc and G. Bayram, "Effect of Process Parameters and Glass Fiber Content on the Mechanical, Thermal Properties and Morphologies of the Recycled PET/Glass Fiber Composites", Book of Abstracts of UKMK-6, UKMK-6, Poster presentation, September 7 - 10, İzmir, Turkey, 2004.

- M. Kilinc and G. Bayram, "Morphological, Mechanical and Thermal Properties of Ternary Composites with Poly(ethylene terephthalate) Matrix", Book of Abstracts of MRS-2004 Fall Meeting, MRS-2004 Fall Meeting, Poster presentation, November 29 - December 3, Boston, USA, 2004.

- M. Kilinc and G. Bayram, "Mechanical Properties and Morphologies of PET-Based Ternary Composites", Book of Abstracts of ANTEC-2005 Meeting, ANTEC-2005, Poster presentation, May 1 - 5, Boston, USA, 2005.

- M. Kilinc and G. Bayram, "Effect of Elastomer Type on Mechanical and Morphological Properties of PET Based Ternary Composites", Book of Abstracts of PPS-21 Meeting, PPS-21, Oral presentation, June 19 - 23, Leipzig, Germany, 2005.

- S. Yesil, M. Kilinc and G. Bayram, "Production & Characterization of PET/PEN Based Composites", Book of Abstracts of 1st Polymer Science & Technology Congress & Exhibition, 1st Polymer Science & Technology Congress & Exhibition, Oral presentation, June 21 – 23, Ankara, Turkey, 2006.

- M. Kilinc, S. Yesil and G. Bayram, "Effect of Elastomer Type on Mechanical and Morphological Properties of PEN/PET Blend Based Composites", Book of Abstracts of PPS-22 Meeting, PPS-22, Oral presentation, July 02 - 06, Yamagata, Japan, 2006.

- M. Kilinc and G. Bayram, "Fire Behavior and Mechanical Properties of Zinc Borate Containing Flame Retardant Polypropylene Based Composites", Book of Proceedings of 3th International Boron Symposia, 3th International Boron Symposia, Oral presentation, November 02 - 04, Ankara, Turkey 2006.

- M. Kilinc and G. Bayram, "Flame Retardancy & Mechanical Properties of Polypropylene Based Composites", Book of Proceedings of SOMER Symposium Series I, SOMER Symposium Series I, Poster presentation, May 14 - 17, Ankara, Turkey 2007.

- M. Kilinc, S. Yesil, G. Cakal, G. Bayram, S. Ozkar, and I. Eroglu "Production and Characterization of Hydrated Zinc Borate", Book of Proceedings of SOMER Symposium Series I, SOMER Symposium Series I, Poster presentation, May 14 - 17, Ankara, Turkey 2007.

- M. Kilinc, S. Yesil, G. Cakal, G. Bayram, I. Eroglu, and S. Ozkar "Production and Characterization of 3.5 Mol Crystal Water Containing Zinc Borate on Pilot Scale", Book of Proceedings of 2nd National Boron Workshop, 2nd National Boron Workshop, Oral presentation, April 17 - 18, Ankara, Turkey 2008.

- M. Kilinc, G. Bayram, A. Yilmaz, G. Cakal, I, Eroglu, and S. Ozkar "Characterization of Flame Retardancy and Effect of Synergism on PET based composites via Phosphate Based Flame Retardant Additives", Book of Proceedings of PPS-24 Meeting, PPS-24, Oral presentation, June 15 - 19, Salerno, Italy, 2008.

## Research Projects

- "Processing and Characterization of Recycled PET with Elastomer and Short Glass Fiber Reinforcement", G. Bayram, M. Kilinc, TUBITAK (The Scientific & Technological Research Council of Turkey, MISAG-197, METU, Ankara, Turkey, March 2002-May 2004, Researcher.

- "Processing and Characterization of PET Based Composites", G. Bayram, M. Kilinc, BAP-2003-07-02-00-04, METU, Ankara, Turkey, May 2003-April 2004, Researcher.

- "Processing of PET/Elastomer Blends and Improvement of Their Impact Properties", G. Bayram, M. Kilinc, BAP-2003-03-04-01, METU, Ankara, Turkey, May 2003-December 2004, Researcher.

- "Development of Production Techniques of Zinc Borate and Investigation of Its Uses as Flame Retardant Additive", G. Bayram, M. Kilinc, G. Cakal, I. Eroglu, S. Ozkar, D. Gurhan, S. Yesil, BOREN (National Boron Research Foundation) BOREN-2005-07-G10-10, METU, Ankara, Turkey, July 2005-July 2007, Researcher.

- "Improvement of Flame Retardancy in Polymeric Compsites Using Silicon Containing Polymers", G. Bayram, D. Eroglu, M. Pitcher, L. K. Toppare, M. Kilinc, TUBITAK (The Scientific & Technological Research Council of Turkey, 107M031, METU, Ankara, Turkey, September 2007 (On Progress), Scholarship Holder.

- "Production of Submicron Size Zinc Borate & Its Usage as Flame Retardant in Polymers", G. Bayram, M. Kilinc, G. Cakal, İ. Eroglu, S. Ozkar, S. Yesil, BOREN (National Boron Research Foundation) BOREN-2008.Ç0179, METU, Ankara, Turkey, January 2008 (On Progress), Researcher.

- "Settlement and Monitoring of Waste Mineral Oil Project", TUBITAK (The Scientific & Technological Research Council of Turkey, 107G007, TUBITAK Marmara Research Center, Gebze, Kocaeli, September 2008 (On Progress), Researcher.

- "Development of Pilot Plant for Sodium Metal for Production for Sodium Boronhydride", BOREN (National Boron Research Foundation) 508G108, TUBITAK Marmara Research Center, Gebze, Kocaeli, January 2009 (On Progress), Researcher.

- "Monitoring of Greenhouse Gases Emissions of TÜPRAŞ (Turkish Petroleum Refineries Corporation) Refineries", TÜPRAŞ, 508G114 TUBITAK Marmara Research Center, Gebze, Kocaeli, January 2009 (On Progress), Researcher.

## Patents

- M. Kilinc, G. Bayram, G. Cakal, A. Yilmaz, I. Eroglu, and S. Ozkar, "Production of Flame Retardant PET Based Composite Construction Materials via Phosphorus and Boron Based Additives", National Patent Application, Ankara, Turkey, 2008 (On Evaluation).

## Courses, Trainings

- Attended to "Polymer Processing on Micro-Compounders" scientific program in DSM Xplore Company, Geleen, Netherlands in January 2005.

- Attended to “Innovations in Micro Fiber Spinning & Hot Stretching Combined with Micro-Compounding Environment” scientific program in DSM Xplore Company, Geleen, Netherlands in July 2007.

- Attended to “Basic Principles of Extrusion and Rheology and Their Applications on Polymer Technology” training program at Anamed-Thermo Companies, Hacettepe University, Ankara, Turkey at November 2007.

- Attended to “Advanced Materials Characterization by Thermal Analysis, Calorimetry and Rheometers” training program at Likrom-TA Instruments Companies, Ankara University, Ankara, Turkey at January 2008.

- Attended to “Applied Research & Development Engineering” program at Turkish Institute for Industrial Management, Gebze, Turkey at November 2008.

- Attended to “ISO 9001:2008 Quality Management System” training at Turkish Scientific and Technological Research Instittue Marmara Research Center, Gebze, Turkey at March 2009.

- Attended to “ISO 14001 Environment Management System” training at Turkish Scientific and Technological Research Instittue Marmara Research Center, Gebze, Turkey at March 2009.

## Honors, Prizes, and Awards

- The Thesis of the Year Award, M.Sc Thesis, “Processing & Characterization of Poly(ethylene terephthalate) Based Composites”, Middle East Technical University Prof. Dr. Mustafa N. Parlar Education and Research Foundation, December 2004.

## Computer Related Experience and Skills

- **Programming Languages:** FORTRAN 77/90
- **Operating Systems:** Windows 9X/2000/XP/Vista
- **Commercial and Research Software Packages:** ChemCAD, MathCAD, Visio, Sigma Plot, Sigma Scan, Paint Shop Pro, Adobe Photoshop, Microsoft Office XP/2003/2007 (Word, Excel, Power Point, Outlook)

## Languages

**Turkish:** Native speaker
**English:** Good in reading and writing, fluent in speaking
**French:** Beginner
**German:** Beginner